Naval Surface Warfare Center

Carderock Division

West Bethesda, MD 20817-5700

NSWCCD-80-TR-2024/003 **May 2024**

Naval Architecture and Engineering Department

Technical Report

MEASUREMENTS OF SECONDARY LOADS USING THE GENERIC PRISMATIC PLANING HULL (GPPH)

by

Lawrence A. Snyder
Emily L. Harrison
Evan J. Lee
Ann Marie R. Powers
Maria L. Nadal
Andrew M. McCoy
Joel T. Park
NSWCCD

REPORT DOCUMENTATION PAGE

Form Approved
OMB No. 0704-0188

1. REPORT DATE *(DD-MM-YYYY)*	2. REPORT TYPE	3. DATES COVERED *(From - To)*
06-05-2024	Technical Report	2019 - 2021

4. TITLE AND SUBTITLE

Measurements of Secondary Loads Using the Generic Prismatic Planing Hull (GPPH)

5a. CONTRACT NUMBER
N0001419WX00393, et al.

5b. GRANT NUMBER

5c. PROGRAM ELEMENT NUMBER

6. AUTHOR(S)

Lawrence A. Snyder, Emily L Harrison, Evan J. Lee, Ann Marie R. Powers, Maria L. Nadal, Andrew M. McCoy and Joel T. Park

5d. PROJECT NUMBER

5e. TASK NUMBER

5f. WORK UNIT NUMBER

7. PERFORMING ORGANIZATION NAME(S) AND ADDRESS(ES)
NAVSEA Carderock
Naval Surface Warfare Center
Carderock Division (Codes 65,83,85,74,86)
9500 Macarthur Boulevard
West Bethesda, MD 20817-5700

8. PERFORMING ORGANIZATION REPORT NUMBER

NSWCCD-80-TR-2024/003

9. SPONSORING / MONITORING AGENCY NAME(S) AND ADDRESS(ES)
Office of Naval Research (ONR)
Division 331 – Ship Systems and Engineering Research
Dr. Robert Brizzolara – Program Officer
875 North Randolph Street, Suite 1425
Arlington, VA, 22203

10. SPONSOR/MONITOR'S ACRONYM(S)
xxxxxx
xxxxxx

11. SPONSOR/MONITOR'S REPORT NUMBER(S)
xxxxxx

12. DISTRIBUTION / AVAILABILITY STATEMENT
DISTRIBUTION STATEMENT (A). Approved for public release; distribution unlimited.

13. SUPPLEMENTARY NOTES

14. ABSTRACT
The Generic Prismatic Planing Hull, GPPH, a model with a 1:5.4 scale ratio, was tested in 2019 at NSWCCD in calm water and in waves. Motions and secondary loads measurements were collected and reduced to support future comparisons with calculations from numerical tools and design criteria. This technical report documents the effort.

15. SUBJECT TERMS
GPPH, Planing Hull, Planing Craft, FSI, Grillage Panel

16. SECURITY CLASSIFICATION OF:			17. LIMITATION OF ABSTRACT	18. NUMBER OF PAGES	19a. NAME OF RESPONSIBLE PERSON
a. REPORT	b. ABSTRACT	c. THIS PAGE			Lawrence A. Snyder
Unclassified	Unclassified	Unclassified	Unlimited	280	19b. TELEPHONE NUMBER *(include area code)* (301)227-2510

Standard Form 298 (Rev. 8-98)
Prescribed by ANSI Std. Z39.18

THIS PAGE INTENTIONALLY LEFT BLANK

CONTENTS

Administrative Information x
Acknowledgments x
Summary 1
Introduction 2
Objectives 3
Methods, Assumptions, and Procedures 4
Model Description 4
Table of Particulars 5
Model Measurement 5
Hull Modifications 9
Grillage Panels 10
Grillage Position 11
Grillage Design 12
Optimized Grillage 14
Grillage Fabrication 15
Grillage Installation 16
Sensor Layout 17
Model Ballasting 19
A Note on the Target LCG 24
Instrumentation 24
Instrumentation Locations 28
Polarity Convention 31
Data Acquisition 32
Test Details 32
Approach 32
Test Setup 32
Test Procedure 34
Test Matrix 35

Test Facility 37
Carriage 3 37
Wavemaker Description 39
Waves Achieved 40
Extended Tow Post 42
Methodology 46
Physical Variables 46
Zero Crossing Method for Peak Identification 46
Standard G Method for Peak Identification 47
Pressure and Grillage Peak Identification Method for Irregular Waves 49
Statistical Variables 49
Statistical Estimators and Confidence Intervals 51
Validation Metrics 51
Analysis 51
Results and Discussion 69
Calm Water Comparisons with Past Testing 69
Regular Waves 72
Irregular Waves 80
Extreme Value Analysis 88
Grillage and Pressure Measurements 88
Conclusions and Recommendations 102
Recommendations 102
References 103
Appendix A: Accura60 Coupon Test A-1
Appendix B: Stiffener Details for the Optimum Grillage B-1
Appendix C: Calibration of Grillages C-1
Appendix D: Instrument Calibration with Uncertainty Estimates D-1
Appendix E: Statistical Estimators and Confidence Intervals E-1
Appendix F: Analysis of Grillage and Pressure Events F-1
Appendix G: Maximum Strains on Single Strain Channels G-1
Appendix H: Tabulated results H-1
Appendix I: Weibull Analysis of Pressures and Grillage Loads I-1

FIGURES

Figure 1. Body Plan 4
Figure 2. Profile View....4
Figure 3. Comparison of Measured to Desired; Looking Aft (in) 6
Figure 4. Comparison of Measured to Desired; Hull Bottom (in)....7
Figure 5. Stem Aligned with Marking on Steel Table 8
Figure 6. Discrepancy at the Transom Shown 9
Figure 7. Traditional Grillage Panel Installed on GPPH Hull 11
Figure 8. GPPH Grillage location....12
Figure 9. Bottom View of GPPH Model and Grillage 13
Figure 10. Rendering of Traditional Grillage and Grillage with Backing Plate 13
Figure 11. Traditional Grillage Drawing 14
Figure 12. GPPH Optimized Grillage Design....15
Figure 13. GPPH Optimized (Design E) Grillage Stiffener Dimensions 15
Figure 14. Traditional Grillage and Backing Plate Made from Accura60....16
Figure 15. View of Traditional Grillage from Inside the Model 16
Figure 16. Grillage Strain Gage Diagram 18
Figure 17. Grillage Panel Location Relative to Pressure Transducers 18
Figure 18. Beam Used for Ballasting....22
Figure 19. Model Suspended from A-Frame During Ballasting....22
Figure 20. Inside of Model with Beam and Trim Weight Shown 23
Figure 21. Optimized Grillage Panel and Washers Shown....23
Figure 22. Wave Measurement Locations 31
Figure 23. GPPH Polarities (+ in Direction of Arrows) 31
Figure 24. Towing Apparatus 33
Figure 25. Tow Gear Stack-Up....34
Figure 26. Linear Towing Basin; Section View at East End. 38
Figure 27. Towing Carriage 3 39
Figure 28. NSWCCD High Speed Basin Pneumatic Wavemaker....40

Figure 29. Measured versus Desired during Wave Iterations 41
Figure 30. Measured Versus Desired during Testing 42
Figure 31. Schematic of Extended Tow Post 43
Figure 32. Photograph of the Extended Tow Post 44
Figure 33. Close-up of Extended Tow Post 44
Figure 34. Example of Peak Identification Methods 48
Figure 35. Example of the Pressure and Grillage Peak Identification 49
Figure 36. Traditional Grillage Strain Time History of Channel G16 at Spot 290, Displaying Peak Distortions 55
Figure 37. Traditional Grillage Filter Refinement for Peak 1 of Channel G16, Spot 290 56
Figure 38. Traditional Grillage Filter Refinement for Peak 2 of Channel G16, Spot 290 57
Figure 39. Maximum Event on Channel G7 (Traditional Grillage) 59
Figure 40. Maximum Event on Channel G18 (Traditional Grillage) 60
Figure 41. Maximum Event on Channel P11 (Traditional Grillage) 60
Figure 42. Largest Event on a Stiffener, Condition ID: 15 (Traditional Grillage) 62
Figure 43. Second Largest Event on a Stiffener, Condition ID: 15 (Traditional Grillage) 62
Figure 44. Third Largest Event on a Stiffener, Condition ID: 15 (Traditional Grillage) 63
Figure 45. Fourth Largest Event on a Stiffener, Condition ID: 15 (Traditional Grillage) 63
Figure 46. Fifth Largest Event on a Stiffener, Condition ID: 14 (Traditional Grillage) 64
Figure 47. Time History of Largest Event of Traditional Grillage (Left) and Layout of Channels 16-20 on Grillage (Right) 65
Figure 48. Spatial Distribution of Strains During Peak of Channel 18's Largest Measured Event, Traditional Grillage, Spot 276, t =17.6848 seconds 65
Figure 49. Resistance in Calm Water 70
Figure 50. Running Trim in Calm Water 71
Figure 51. Heave in Calm Water 71
Figure 52. LR3 and MM3 Weibull Plots of Channel G7 for Matrix ID 14 and 15 91
Figure 53. LR3 and MM3 Weibull Plots of Channel G15 for Matrix ID 14 and 15 93
Figure 54. LR3 and MM3 Weibull Plots of Channel G18 for Matrix ID 14 and 15 96
Figure 55. LR3 and MM3 Weibull Plots of Channel G23 for Matrix ID 14 and 15 99
Figure 56. LR3 and MM3 Weibull Plots of Channel P21 for Matrix ID 14 and 15 101

TABLES

Table 1. Particulars 5
Table 2. Target Mass Properties 21
Table 3. Desired Tolerances 21
Table 4. Mass Properties Achieved on A-Frame 21
Table 5. Table of Instrumentation.....25
Table 6. Pressure Transducer Locations 29
Table 7. Accelerometer Locations 30
Table 8. Prioritized Test Matrix.....36
Table 9. Limitations on Load.....45
Table 10. Typical Model Parameters 46
Table 11. Channel Quality Legend 53
Table 12. Summary of Data Quality for Matrix ID 14 of the Traditional Grillage 54
Table 13. Summary of Data Quality for Matrix ID 15 of the Traditional Grillage 54
Table 14. Summary Table of Extrema on Differential Bending Channels (Traditional Grillage) 57
Table 15. Summary Table of Positive Extrema on Single Strain Channels (Traditional Grillage) 58
Table 16. Summary Table of Negative Extrema on Single Strain Channels (Traditional Grillage) 58
Table 17. Summary Table of Extrema on Pressure Transducer Channels (Traditional Grillage) 59
Table 18. Maximum Strain on Channel 18 and Corresponding Stiffener Gage Strains (Traditional Grillage) 61
Table 19. Maximum Strain on Channel 23 and Corresponding Stiffener Gage Strains (Traditional Grillage) 61
Table 20. Maximum Strains on Each Channel for Largest Event (Traditional Grillage).....64
Table 21. Rate of Severe Events on Differential Bending Channels (Traditional Grillage) 66
Table 22. Rate of Severe Events on Single Strain Channels G11 - G18 (Traditional Grillage) 67
Table 23. Rate of Severe Events on Single Strain Channels G18 - G25 (Traditional Grillage) 67

Table 24. Rate of Severe Events on Pressure Transducer Channels (Traditional Grillage) 68
Table 25. Regular Wave Ensemble Results for H, Tp, $abow$, aCG, Fx, θ, and z 73
Table 26. Regular Wave Ensemble Results for $P11$-$P23$ 74
Table 27. Regular Wave Ensemble Results for $G1$-$G10$ 76
Table 28. Regular Wave Ensemble Results for $G11\ P$-$G15\ P$ and $G11\ N$-$G15\ N$ 77
Table 29. Regular Wave Ensemble Results for $G16\ P$-$G20\ P$ and $G16\ N$-$G20\ N$ 78
Table 30. Regular Wave Ensemble Results for $G21\ P$-$G25\ P$ and $G21\ N$-$G25\ N$ 79
Table 31. Contrast of Traditional to Optimized Grillage in Regular Waves 80
Table 32. Irregular Wave Ensemble Results for ς, $abow$, aCG, Fx, θ, and z 81
Table 33. Average of Largest 1/3rd Ensemble Values, $EV13,a$, for H, $abow$, aCG, Fx, θ, and z 82
Table 34. Average of Largest 1/3rd Ensemble Values, $EV13,a$, for $P11$-$P23$ 83
Table 35. Average of Largest 1/3rd Ensemble Values, $EV13,a$, for $G1$-$G10$ 84
Table 36. Average of Largest 1/3rd Ensemble Values, $EV13,a$, for $G11\ P$-$G15\ P$ 85
Table 37. Average of Largest 1/3rd Ensemble Values, $EV13,a$, for $G16\ P$-$G20\ P$ and $G16\ N$-$G20\ N$ 86
Table 38. Average of Largest 1/3rd Ensemble Values, $EV13,a$, for $G21\ P$-$G25\ P$ and $G21\ N$-$G25\ N$ 87
Table 39. Percent Difference $EV13,a$ between the Optimized and Traditional Grillage 88
Table 40. Multipliers to Estimate 36.8 % PNE Predictions 89
Table 41. Weibull Shape Parameters for Differential Bending Channels in Matrix ID 14 and 15 90
Table 42. Lifetime Extreme Estimates for Differential Bending Channels in Matrix ID 14 and 15 90
Table 43. Weibull Shape Parameters for Single Strain Channels G11 - G15 in Matrix ID 14 and 15 92
Table 44. Lifetime Extreme Estimates for Single Strain Channels G11 - G15 in Matrix ID 14 and 15 92
Table 45. Weibull Shape Parameters for Single Strain Channels G16 - G20 in Matrix ID 14 and 15 94
Table 46. Lifetime Extreme Estimates for Single Strain Channels G16 - G20 in Matrix ID 14 and 15 95
Table 47. Weibull Shape Parameters for Single Strain Channels G21 - G25 in Matrix ID 14 and 15 97
Table 48. Lifetime Extreme Estimates for Single Strain Channels G21 - G25 in Matrix ID 14 and 15 98

Table 49. Weibull Shape Parameters for Pressure Transducer Channels in Matrix ID 14 and 15.....100

Table 50. Lifetime Extreme Estimates for Pressure Transducer Channels in Matrix ID 14 and 15.....100

ADMINISTRATIVE INFORMATION

This test and analysis effort took place at the David Taylor Model Basin, Naval Surface Warfare Center, Carderock Division (NSWCCD) by a team of engineers spanning various divisions including Structures and Composites Division Code 65, Electromagnetic Signatures Technology Division Code 74, Combatant Craft Division Code 83, Surface Ship Hydromechanics Division Code 85, Submarine Maneuvering and Control Division Code 86, and Computational Fluid Dynamics and Propulsors Division Code 87. The work was funded by the Office of Naval Research (ONR) in Calendar Year (CY) 2019 and CY 2020 via Sales Order Numbers N0001419WX00393, N0001420WX01040, N0001420WX01041, N0001420WX01038, and N0001420WX01039.

ACKNOWLEDGMENTS

The authors would like to acknowledge a long list of folks who contributed to the overall test effort. The folks listed below made contributions towards the success of this project, and the authors would like to thank them for their assistance and expertise.

The authors would also like to thank the management team of Mike Brown and Martin Donnelly who together provided supplementary funding to support the development and fabrication of the extended tow post. The authors are confident that this test apparatus will be used again for future testing on Carriage 3, as appropriate. Finally, the authors would like to thank the Program Officer, Bob Brizzolara, for his participation and support, and the Office of Naval Research for funding the Generic Prismatic Planing Hull (GPPH) effort.

Contribution	Name
Development of the Extended Tow Post	John Hoyt
	Carl Baumann
Fabrication of the Extended Tow Post	Elbert Roberson
	Mounir Hadiji
	Don Seitz
	Alex Colon
	Keo Chum
	David Brown
Refurbishment of GPPH Hull	Mark Sawyer
Grillage Panel and Structural Instrumentation Support	Luke Karr
	Rich Lewis
	Dave Schwarzenberg
	Ivan Vu
	Nikia Perkins
Test Crew	Nathan Martin
	Tristan Wright
Data Acquisition Preparation and Support	Donnie Walker
Metrology Support	Brett Griffin
	Mike Hershaw
Technical Writing and Editing	Shane McCabe

SUMMARY

Current structural design methods for planing craft rely heavily on empiricism. If the dynamic response of a planing boat is understood and can be predicted using physics-based tools, the Navy will be able to design boat structures capable of withstanding impact loads and responding to seaway forces while minimizing the craft's structural weight and improving overall vessel performance.

The Office of Naval Research and Carderock have been collaborating for years to improve the capabilities of existing numerical tools. Most recently, a Distribution A planing craft called the Generic Prismatic Planing Hull (GPPH) was tested in the High Speed Basin at NSWCCD to generate motions, accelerations, and secondary load data required to support tool development.

This technical report documents the GPPH secondary loads testing conducted in calm water, and in regular and irregular wave conditions. The calm water data collected as part of this test effort demonstrated that the test was consistent with previous GPPH testing at NSWCCD and the United States Naval Academy (USNA). The measurements of drag, pitch and heave in calm water were the same within the calibration uncertainty.

The regular wave and irregular wave data were successfully collected, analyzed, and tabulated for future comparison with Computational Fluid Dynamics (CFD) / Computational Structural Dynamics (CSD) numerical tools. Ensemble analysis was used to reduce statistical uncertainty. For example, in regular waves, the uncertainties for an ensemble were approximately 35 % smaller than the uncertainties for a mean value for a given spot. For the irregular wave condition, the precision uncertainty was driven down through the collection of over 500 wave encounters for each grillage panel (two panels total) and for each speed (two target speeds total). Therefore, it is recommended that the ensemble mean values be used for any future validation effort.

The two grillage panels, referred to as the Traditional grillage and the Optimized grillage, produced statistically different results that were consistent for both regular and irregular waves. Due to an observed change in shape of the Optimized grillage with time, including prior to testing, it is recommended that data associated with the Optimized grillage be used with caution and with the change of shape in mind.

The fact that it was possible to test in the irregular wave condition was a fortunate outcome for the test effort since this was the first time that the GPPH model could be tested at NSWCCD in the irregular wave condition of interest due to past limitations of the carriage hardware. Prior to testing, a new tow post was designed and fabricated which enabled the GPPH model to be tested in a relatively large irregular wave condition which was not feasible during testing of the same hull years earlier.

The test matrix was completed and yielded a large amount of motion and structural data that will be used for future comparisons with CFD/CSD numerical tools. The model test data was analyzed and is presented within this technical report for future use. Two journal papers have been developed using the data contained in this report in combination with CFD/CSD numerical predictions.

INTRODUCTION

Current structural design methods for planing craft rely heavily on empiricism. If the dynamic response of a planing boat is understood and can be predicted using physics-based tools, the Navy will be able to design boat structures capable of withstanding impact loads and responding to seaway forces while minimizing the craft's structural weight and improving overall vessel performance.

Since 2013, the Office of Naval Research (ONR) has been funding Naval Surface Warfare Center Carderock Division to study fluid-structure interaction (FSI) of small craft in hopes of advancing our understanding, and to improve existing numerical tools. Numerous model tests have been conducted to generate test data to compare against numerical tools. A semi-planing hull, *Athena*, was tested in 2014, 2015, and 2017; and a planing hull, the Generic Prismatic Planing Hull (GPPH) was tested in March and November of 2015. GPPH was also tested at the United States Naval Academy (USNA) in May of 2014. The tests were designed to generate data to provide different comparisons to the numerical tools, with the level of complexity generally increasing with each test.

The GPPH was designed as a publically releasable hull that can be easily distributed to government contractors and universities. The hull design was chosen to mimic the physics and response to waves of planing hulls currently deployed by the Navy. The GPPH model, the test article for this assessment, was fabricated at the USNA and given to Carderock to support ONR.

The earlier portion of this multi-year project studied motions and localized (or nearly point) pressure measurements. For example, comparisons between experiments and Computational Fluid Dynamics (CFD) simulations were conducted for the semi-planing hull, Athena, in regular waves [1] [2] [3] and for the planing hull, GPPH, in both regular and irregular wave conditions [4] [5] [6] [7]. The extent to which the CFD results compare to the experiments is quantified in the form of forces, motions and pressure peaks for regular waves within these references.

To better study FSI of a semi-planing hull, structurally scaled flat-panels were mounted in the hull side in proximity to the free surface [1]. These panels, referred to as grillage panels, were instrumented with strain gages and calibrated to measure wave loading response on the model hull. They were structurally scaled representations of hull plating with adjacent stiffeners. The location of the grillages and the relatively small loads made the interpretation of the validation outcomes quite difficult, as the significant variables (such as pressure and strain) were characterized by small values with large uncertainties. Critical issues for proper validation of CFD/Computational Structural Dynamics (CSD) FSI studies were identified including the need for experimental structural dynamics characterization of material properties and boundary condition. In addition, differences between one- and two-way coupling FSI were not significant, highlighting the need for more significant/severe loads and larger/softer panels to better evaluate FSI predictions. Arising from the test data was a need for an experiment that was conducted on a planing craft using a grillage panel intentionally placed in a region with the highest expected slamming pressures.

The experiment was conducted using the GPPH planing hull on Carriage 3 at Naval Surface Warfare Center Carderock (NSWCCD). This technical report documents this experiment and associated data analysis.

Objectives

The focus of the model test and this test report was to obtain the motion and secondary load measurements of the GPPH hull form in a predetermined irregular wave condition to support two primary objectives. The first is to compare current design criteria to measured secondary loads and responses to examine the margin. The second is to compare grillage panel strain measurements with computational predictions of FSI.

These program objectives will ultimately be satisfied and documented in the form of a couple of journal papers. The first paper focused on the regular wave environment and was published by Marine Structures in September 2022 [8]. As of time of writing, the second paper focuses on the irregular wave environment and currently exists in the form of a complete document that is awaiting publication.

METHODS, ASSUMPTIONS, AND PROCEDURES

Model Description

The GPPH model is a hull that was fabricated by the USNA and tested numerous times at both the Naval Academy and NSWCCD. The hull form is shown in body plan view in Figure 1 and in profile view in Figure 2. The model was modified by replacing a portion of the starboard bow region with an instrumented panel, henceforth referred to as a "grillage panel" in order to collect measurements to study FSI.

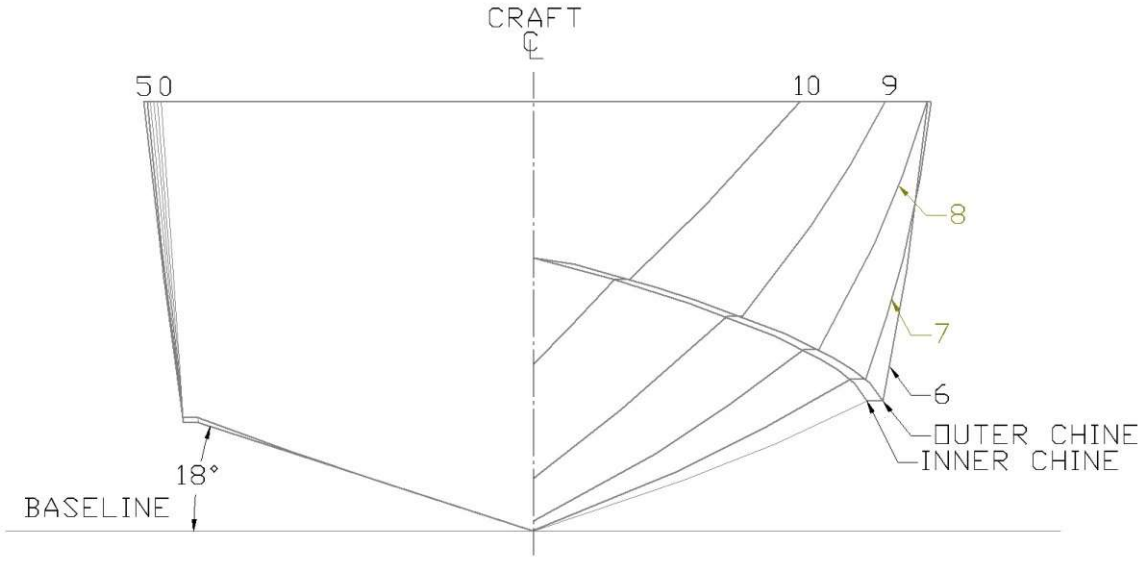

Figure 1. Body Plan

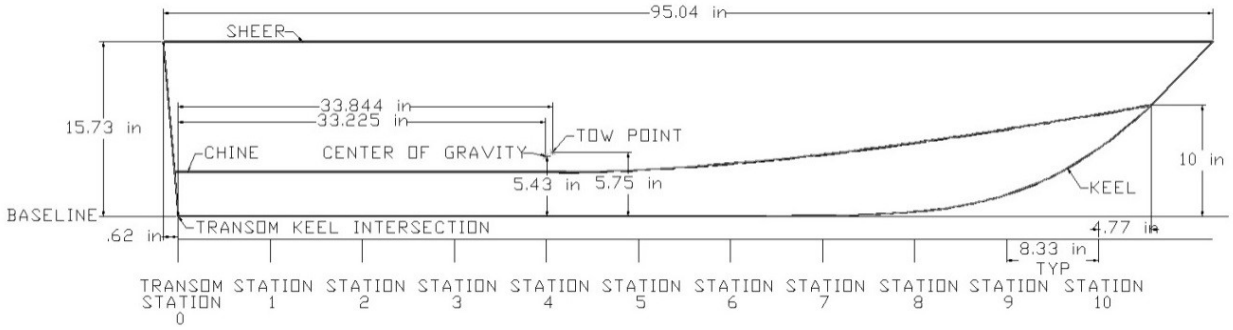

Figure 2. Profile View

Table of Particulars

The model particulars are shown in Table 1. Values are referenced relative to the origin unless otherwise noted. In the longitudinal, x, direction values are referenced forward of the transom-keel intersection (+FTK); in the transverse, y, direction values are referenced port of centerline (+PCL); and in the vertical, z, direction values are referenced above baseline (+ABL). Additional information can be found in the Polarity Convention subsection.

Table 1. Particulars

Parameter	Value (D)	
Degrees of Freedom	Heave, Trim	
Length Between Particulars, L_{PP}	95.04	(in)
Projected Chine Length, L_P	88.43	(in)
Projected Area of Hull Bottom, A_P	1954.11	(in^2)
Projected Chine Beam at the Transom, B_{PT}	24.70	(in)
Maximum Projected Chine Beam, B_{PX}	24.70	(in)
B_{PT} / B_{PX}	1	
Average Projected Chine Beam, $B_{PA}=A_P/L_P$	22.10	(in)
Deadrise Angle to Outer Chine, β	17.2	(deg)
Target Displacement, Δ	223.8	(lbs)
Loading Coefficient, $A_P/(Vol)^{2/3}$	5.78	
Target Longitudinal Center of Gravity, LCG (+FTK)	33.23	(in)
AP Centroid (+FTK)	38.42	(in)
Longitudinal Center of Gravity, LCG (%L_P Aft of A_P Centroid)	5.87	%
Target Vertical Center of Gravity, VCG (+ABL)	5.43	(in)
Target Pitch Mass Moment of Inertia, $I_{yy,CG}$ (About CG)	2,224	(in^4)
Target Pitch Gyradius, $k_{yy,CG}$ (About CG)	17.88	
Longitudinal Center of Tow Point, LTP (+FTK)	33.84	(in)
Vertical Center of Tow Point, VTP (+ABL)	5.75	(in)
Draft at Transom Above Baseline, $T_{Transom}$	5.81	(in)
Determined from Hydrostatics at Δ and LCG		
Draft at Transom Above Baseline, $T_{Transom}$	5.79	(in)
Static Trim Angle from Baseline (+bow↑), Θ_D	0.13	(deg)

Model Measurement

The GPPH model hull surfaces were measured by the Metrology group (Code 632) at NSWCCD using an existing laser scanner and standard practices. The laser scanner used was a MetraSCAN 750 elite. A report was generated on 15 May 2019 comparing the hull, as

measured, to the Official IGES file.[1] The model was deemed acceptable as the measurements fell within the desired tolerances set based on standard practices.

The comparison, measured relative to desired, is shown in Figure 3 and Figure 4, where a colormap is used to highlight regions where discrepancies exists. The colormap legend is shown in the right side of the figure and the units shown are in inches. In both figures, the region of the grillage panel is made apparent by the concentrated reddish area, indicating highest variation from the desired hull shape.

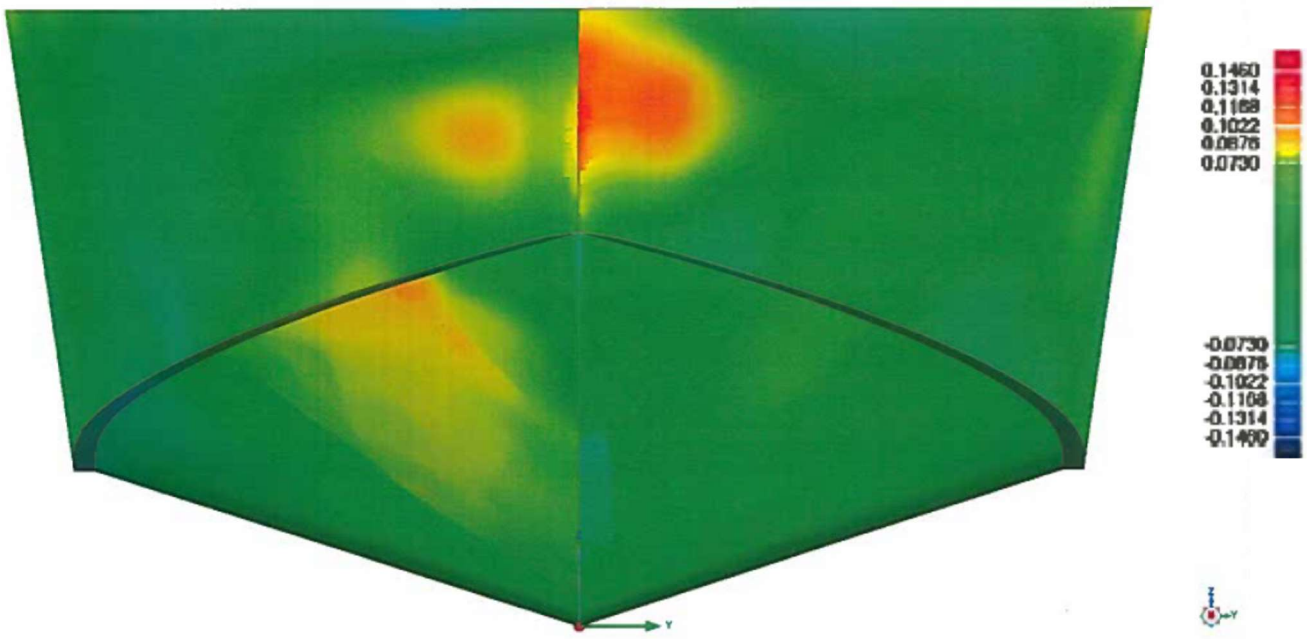

Figure 3. Comparison of Measured to Desired; Looking Aft (in)

[1] The Official IGES file is named "GPPH8 Official IGES" and was developed by NSWCCD Code 83, Combatant Craft Division. For those at NSWCCD with appropriate permissions, the file can be accessed at following network location: \\ccdprojects.nswccd.navy.mil\Projects\Data\Drawings\GPPH.

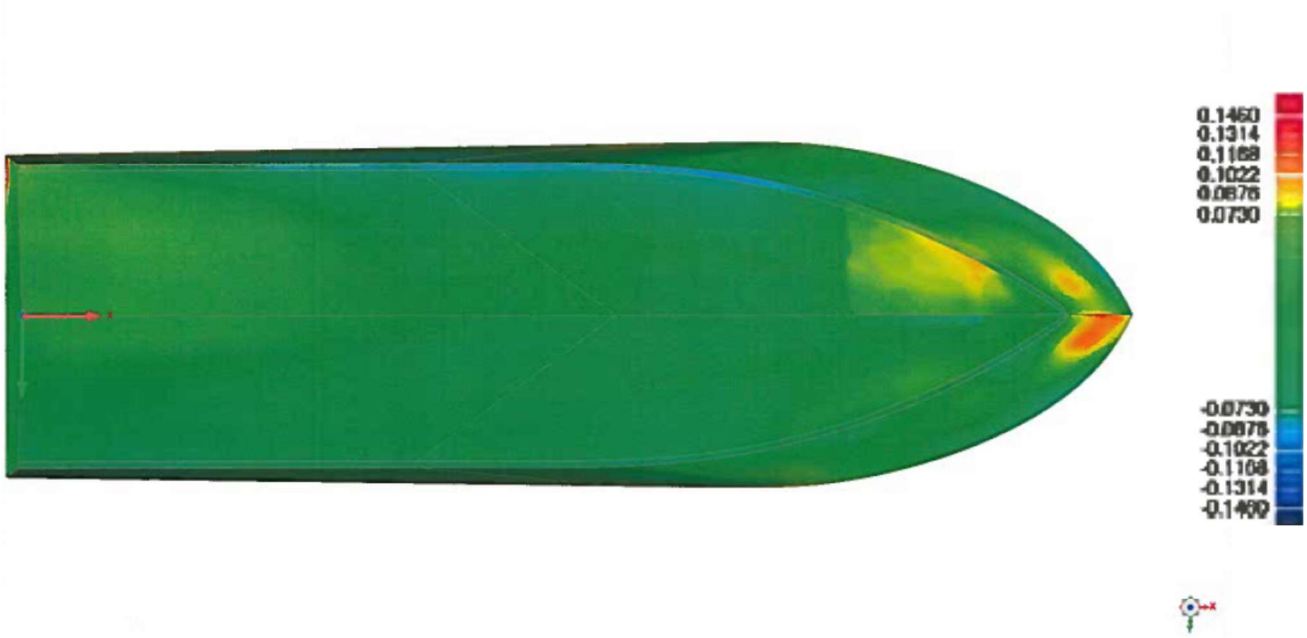

Figure 4. Comparison of Measured to Desired; Hull Bottom (in)

Additional Noted Differences in the Model

When placed upside down against a leveled metal table, as was done at the model shop, there are differences in hull shape that are visually apparent.

The two largest differences are as follows. First, the transom has a bowed shape, which is different than the desired hull form. It can be observed by placing a straight edge in the transverse direction across the transom at a fixed height. And second, when following the keel forward beginning at the transom, near the transom-keel-intersection (the origin of Figure 2), the keel deviates from the x-axis.

This difference is observed in Figure 5 and Figure 6. A line was marked parallel with the edge of the steel table. The stem of the model was aligned with the line on one end, as shown in Figure 5, and the centerline of the transom was placed in line with the other end of the marked line. When a perpendicular surface was placed against the transom using a straight edge, it was apparent that the transom was not perpendicular, as shown in Figure 6.

Despite these known differences, the hull form was found to be adequate for testing. The hull form satisfied the acceptance criteria for the laser measurement, the differences were presented to the team and appear in the test plan, and similar differences were also found in documentation from previous testing performed at NSWCCD. The acceptance criteria are summarized as follows.

- Tabulate the number of measured points that deviate from the target hull surface data by less than 0.5% and 1.0% of the maximum half-breadth of the model.

The values for allowable deviation are such that:

- At least 60% of the measured points deviate by less than 0.5% of maximum half-breadth of the target model
- At least 85% of the measured points deviate by less than 1.0% of the maximum half-breadth of the target model.

Figure 5. Stem Aligned with Marking on Steel Table

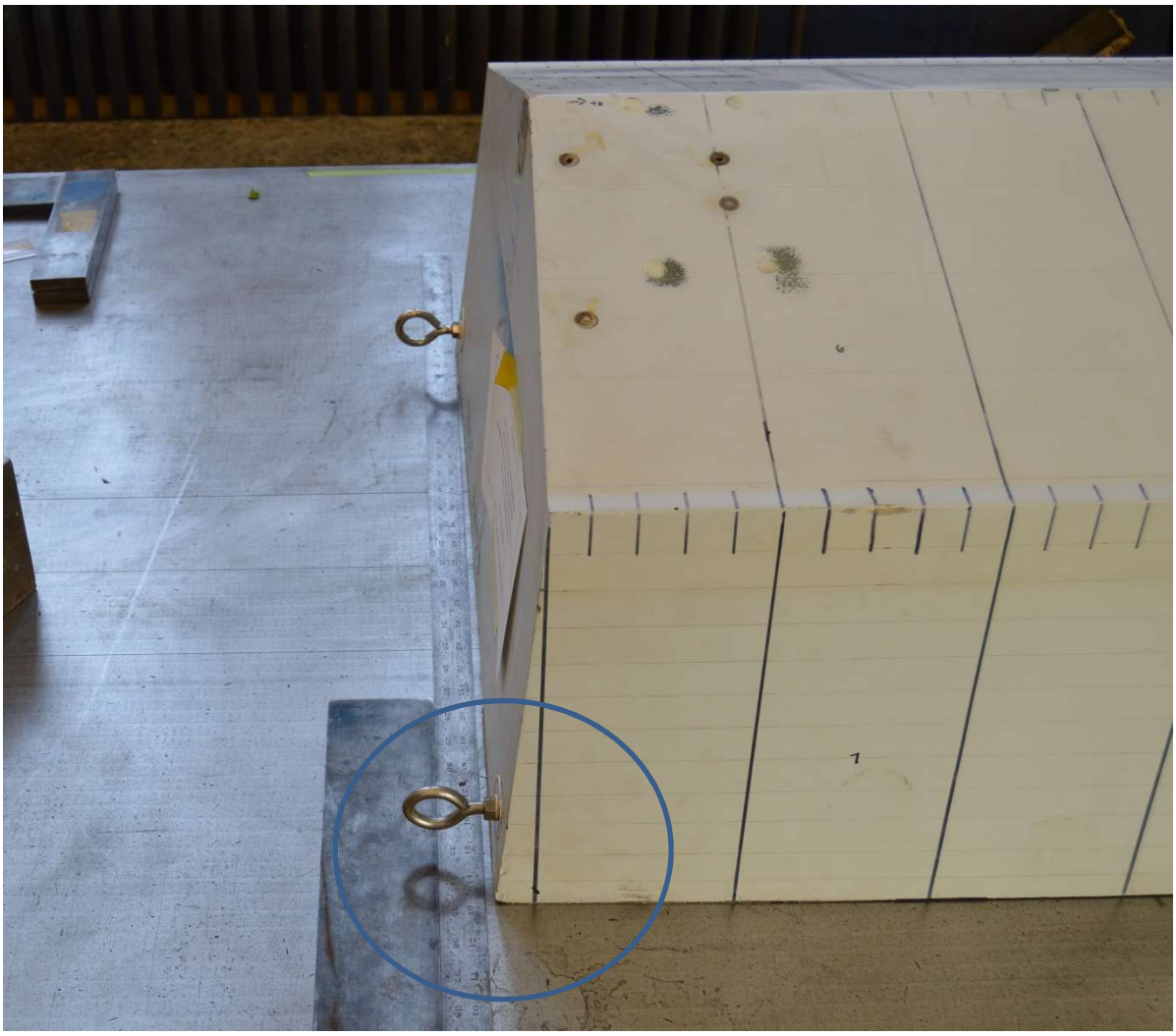

Figure 6. Discrepancy at the Transom Shown

Hull Modifications

The GPPH model was last tested in November of 2015 and required refurbishment prior to the most current test series. The hull modifications and repairs were made by NSWCCD's Model Shop.

The single largest modification to the model was the incorporation of the grillage panel. This modification involved cutting out a section of the hull near the bow, and bonding in a Stereolithography (SLA) frame. Heli-Coils were placed into the SLA frame to allow the grillage panel to fasten against the hull. More information on the grillage panel can be found in the next subsection. During this process, and due to interference, two pressure gage locations on the port side were relocated slightly further outboard. The locations of these gages are documented in the instrumentation section of this test report.

The hardwood block at the mounting interface was cracked and required repair. This hardwood bock was bonded to the inside of the hull at the desired tow location and serves as a flat surface that can be easily fastened into to facilitate attaching the model to the carriage. As

part of this repair, an aluminum mounting plate was bonded against the block using a blend of West System epoxy and filler and reinforced with fiberglass cloth. The height of the plate was adjusted so the location of the center-of-rotation of the pitch gimbal matched the target value based on testing from 2015. Please note that a different pitch gimbal was used for the current test series so that pitch angle could be measured in a more direct fashion, so the height of the top of the mounting plate itself is now different than it was in the model during 2015 testing.

There were also many nicks on the hull along the chines and keel where material was missing. These nicks were repaired and faired into the hull surface. The lifting location was changed for the current test series to ensure sufficient strength for lifting the hull out of waves while potentially traveling at high speed. Four swivel hoists were installed on the model by through-bolting them through the gunwale. The region around each lifting location was reinforced by bonding in an additional gusset. Finally, a foredeck and splash guard was then added in an effort to keep water out of the hull to the maximum extent possible during testing.

Grillage Panels

In order to measure secondary structural response, two custom grillage panels were fabricated, instrumented, and calibrated. The first grillage panel was built to NSWCCD Code 653's specification and is shown installed on the GPPH hull in Figure 7. This grillage panel was referred to as the "traditional" grillage or grillage panel. The panel is a scaled representative of a conventional structure for this type of planing craft.

The second grillage was a design that was built based on specifications from academia, a collaboration between the National Research Council-Institute of Marine Engineering (CNR-INM) and the University of Iowa. The goal of the second grillage was to reduce stiffener and plating sizes to reduce overall structural weight while preserving strength. This grillage was referred to as the "optimized" grillage.

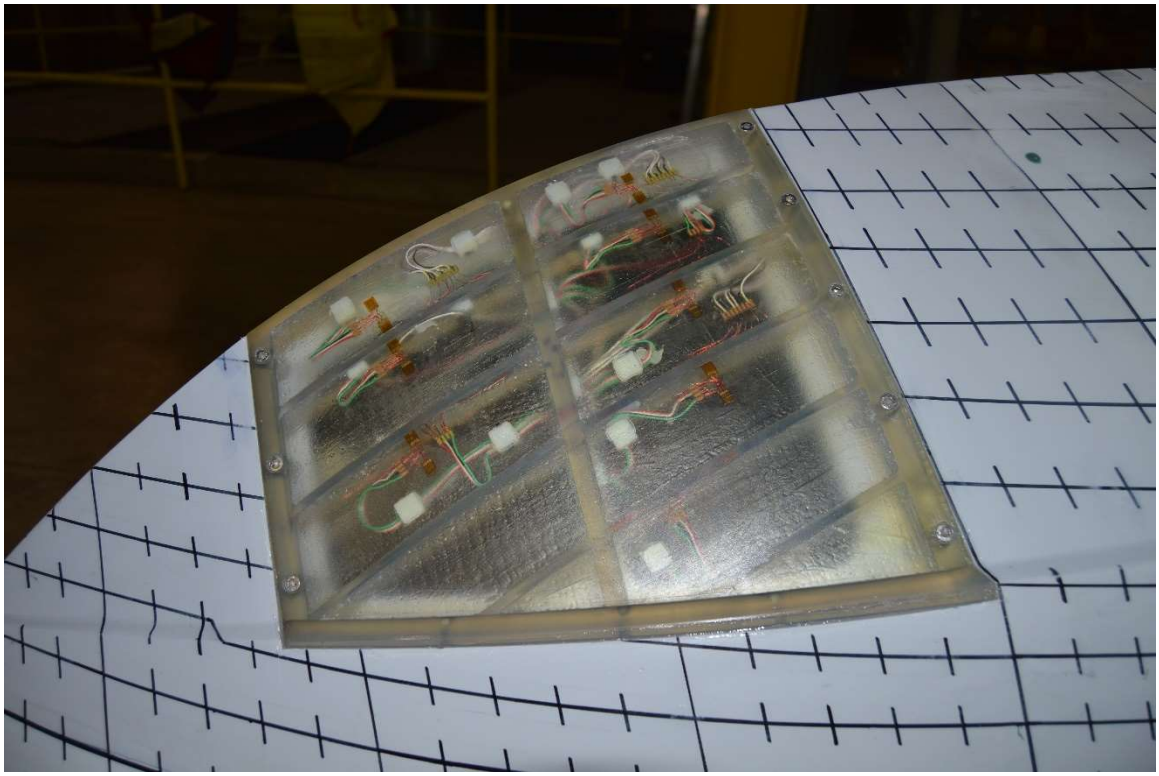

Figure 7. Traditional Grillage Panel Installed on GPPH Hull

Grillage Position

The Traditional and Optimized grillages were tested independently and occupy the same footprint on the model. Each grillage was positioned on the starboard side and covered two frame spacings from the keel to the chine as shown in blue in Figure 8. This region was selected since it lines up with the highest predicted wave impact pressures from the computational model, as seen by red in the figure.

Both grillages had longitudinal stiffeners and a transverse frame built into them. The transverse frame represents a watertight bulkhead. Although the transverse frame does not model the stiffness of the watertight bulkhead, it is significantly stiffer than the surrounding structure, so it was expected to provide an adequate boundary condition.

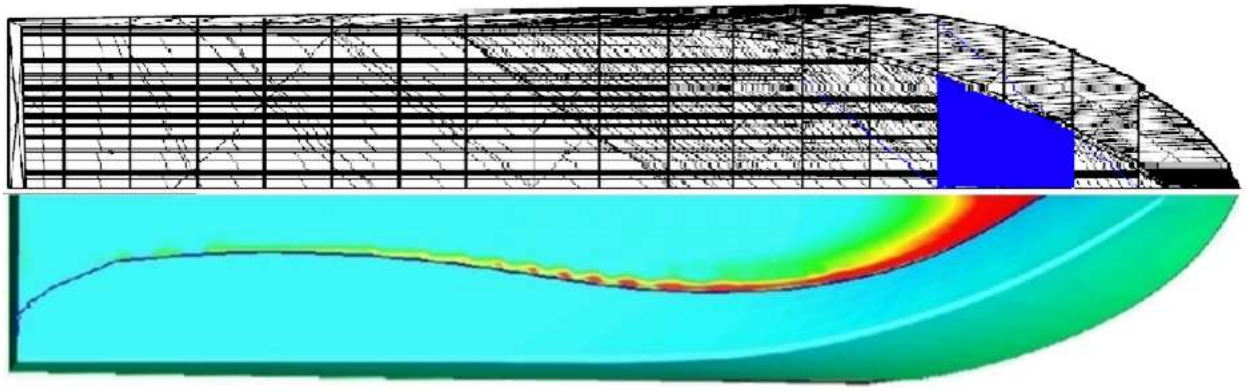

Figure 8. GPPH Grillage location

Grillage Design

Traditional Grillage

The traditional grillage was designed to model the structure in an IGES file named GPPH Structure V1.igs.[2] The grillage matched the hull curvature, since it was not possible to fit a flat grillage in this large curved region of the model. Because of the curvature requirement, the grillage and backing plate were made completely from Accura60 SLA. A coupon test was performed to determine the exact modulus of elasticity of Accura60, and the results of that test can be found in Appendix A.

The grillage and backing plate were specially designed to allow for measurements very near the keel. As can be seen in Figure 9, the backing plate (shown in light grey) and the grillage (shown in red) extend from the starboard side of the model to the port side. The grillage was held in place, fore and aft, by bolts inserted from outside the hull, while bolts were inserted from inside the hull near the chine and keel.

The backing plate was designed to provide added support to the grillage and model. Figure 10 shows a CAD rendering of the grillage and the grillage with the backing plate attached. Figure 11 shows a dimensional drawing of the traditional grillage.

[2] The IGES file was created by NSWCCD Code 653, Performance Evaluation Branch.

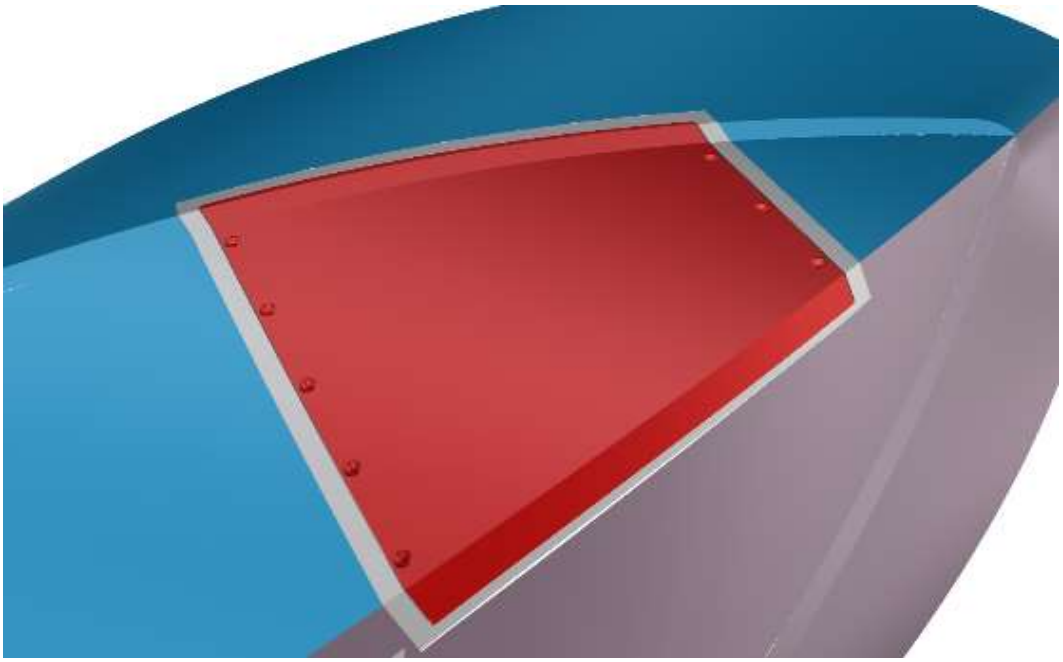

Figure 9. Bottom View of GPPH Model and Grillage

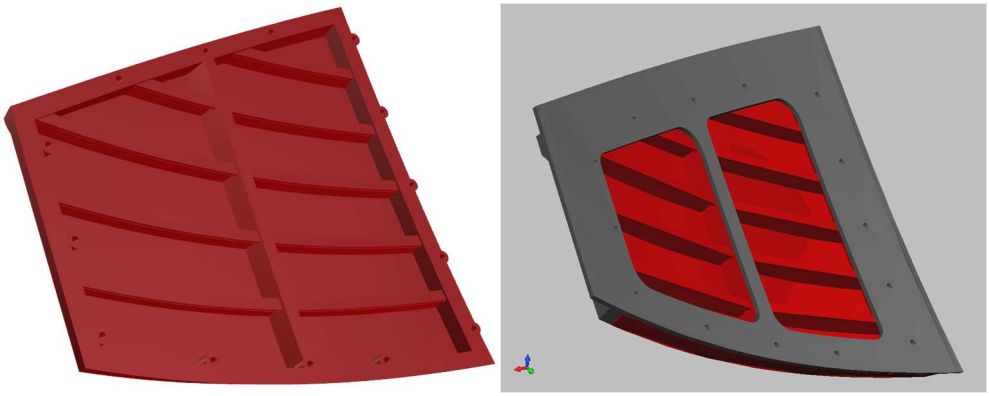

Figure 10. Rendering of Traditional Grillage and Grillage with Backing Plate

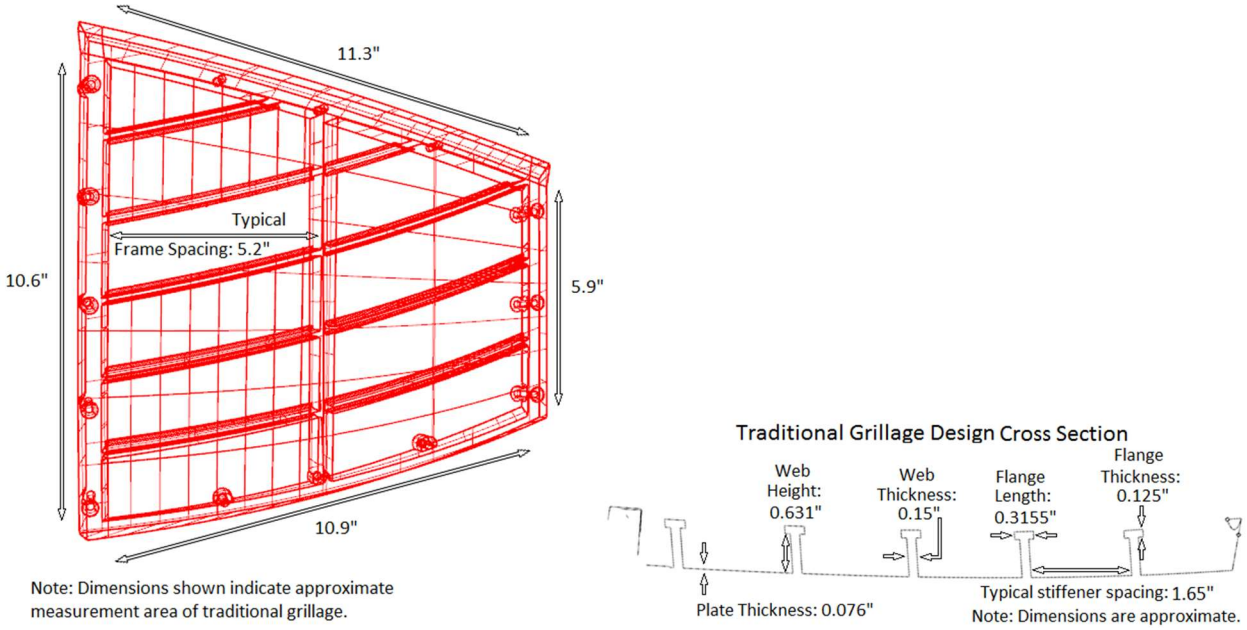

Figure 11. Traditional Grillage Drawing

The model scale dimensions of the Traditional Grillage are as follows:

- Plate thickness: 0.076 in
- Transverse bar stiffener: 0.375 in x 0.75 in
- Longitudinal T stiffeners:
  - Web: 0.15 in x 0.631 in
  - Flange: 0.125 in x 0.3155 in

Optimized Grillage

Different dimensions of plate and stiffeners were computationally analyzed to determine which combination of dimensions would yield weight savings while still maintaining the strength. Several designs were analyzed, and "Design E" was chosen as the most optimal. An illustration of Design E is shown in Figure 12 and the general stiffener dimensions are shown in Figure 13. Additional details on each of the five stiffeners can be found in Appendix B. Certain dimensions were constrained; flange thickness was constrained to 0.24 in or greater to allow for strain gages, and plate thickness was constrained to 0.020 in or greater so that the plate would not be too thin and exhibit non-linear membrane behavior.

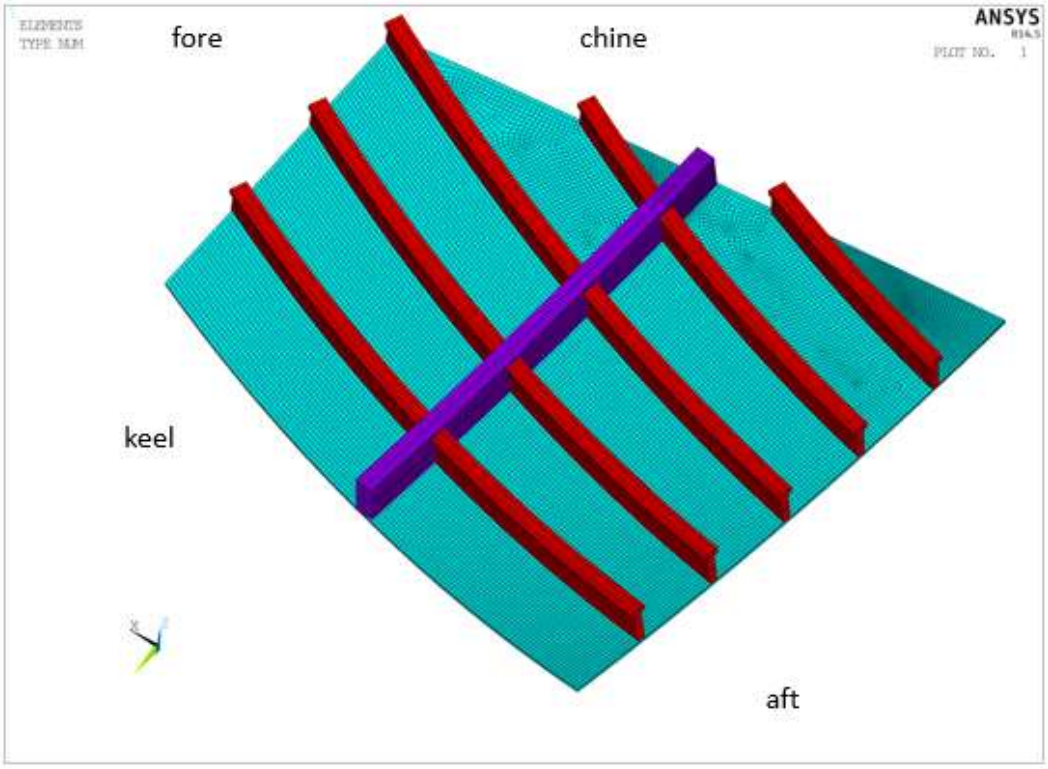

Figure 12. GPPH Optimized Grillage Design

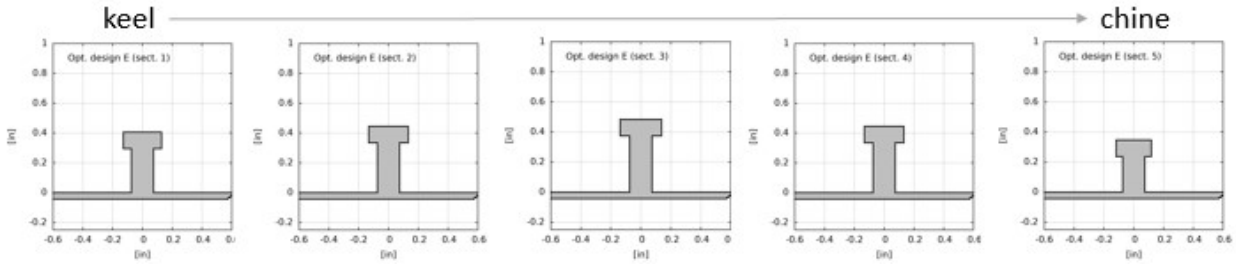

Figure 13. GPPH Optimized (Design E) Grillage Stiffener Dimensions

Grillage Fabrication

The grillages and backing plates were made completely from SLA material, Accura60. Accura60 was chosen because it is relatively transparent, as shown in Figure 14, and its modulus of elasticity is similar to that of PVC, which is typically used for pressure panel applications. The grillage and backing-plate material being transparent or clear can help troubleshoot issues with strain gages during testing. Both grillages were coated in a clear-coat to help seal the SLA material. Coating (or painting) parts constructed of Accura60 as a precaution is a standard practice for parts used in or around the water since the material is known to be susceptible to water absorption.

Figure 14. Traditional Grillage and Backing Plate Made from Accura60

Grillage Installation

Heli-Coils were installed into the six grillage bolt-holes near the chine and keel. Bolts were inserted from the inside of the model to secure it to the backing plate. Heli-Coils were installed in the fore and aft bolt holes of the backing plate, and bolts were inserted from the outside of the model to secure the grillage in place. Figure 15 shows a view of the grillage from inside the model illustrating how it was fastened to the hull.

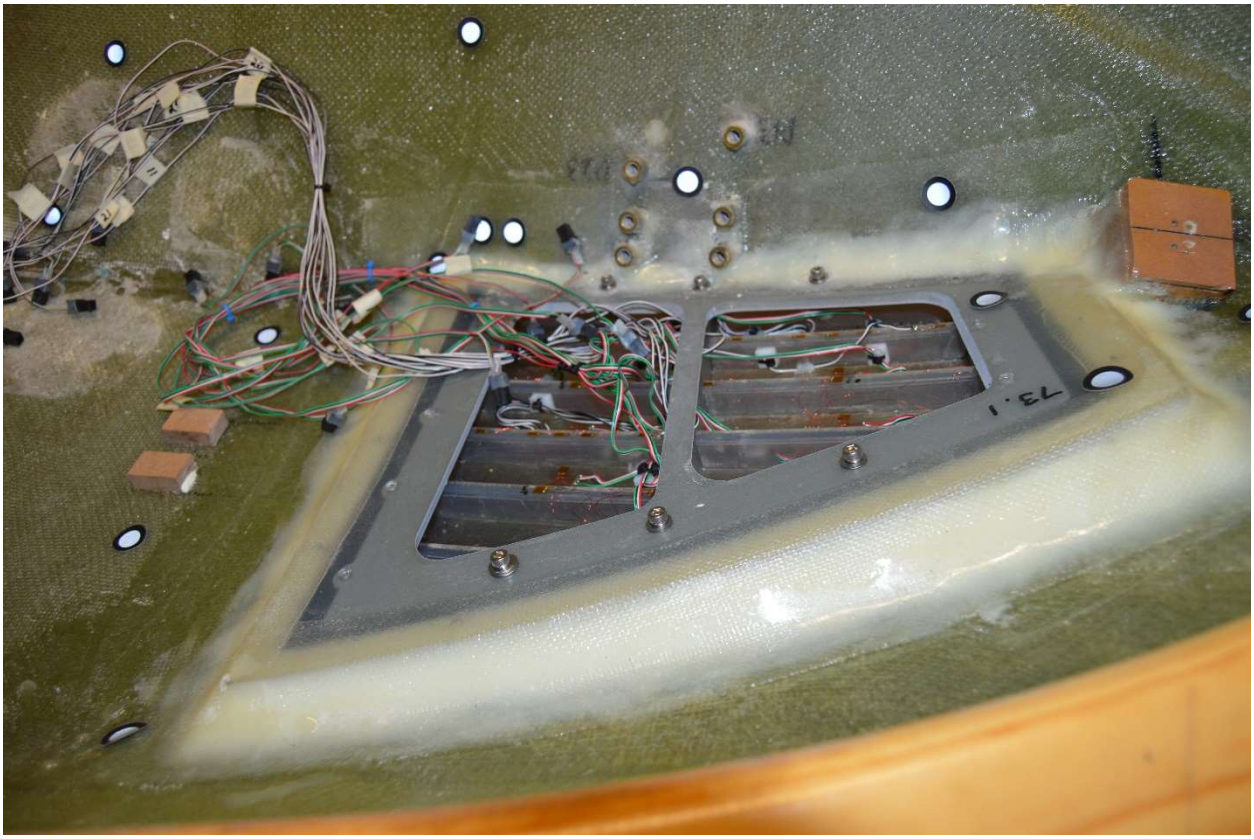

Figure 15. View of Traditional Grillage from Inside the Model

Sensor Layout

Strain Gages

Both the traditional and optimized grillages were instrumented at matching locations with Vishay double-uniaxial strain-gages (ED-DY-125PC-10C/E) and single-uniaxial strain-gages (ED-DY-125BZ-10C/E) for a total of 25 channels. Channels 1 – 7 shown in Figure 16 (circled in red) measured differential bending on plate sections. Channels 8 – 10 in Figure 16 (circled in blue) measured differential bending on stiffeners. Channels 11 – 25 in Figure 16 (circled in green) measured individual strains along the stiffeners. Since the stiffeners have a fixed support at each end, there are expected inflection points at the outer most quarter points. As such, these gages straddle the quarter points of the stiffeners, where there would theoretically be close to zero strain. During the test, and as reflected in the instrumentation list, these channels were referred to as "G1" through "G25" with the "G" indicating that the channel is associated with the grillage. The calibrations and associated instrumentation uncertainties for all grillage channels can be found in Appendix C.

Finally, it is worth noting that directly opposite of the grillage, across centerline, was an array of pressure transducers, as shown in Figure 17. The positioning of these transducers matches previous testing with exception of the two sensors nearest keel. These two sensors, now referred to *P11'* and *P12'*, were moved outboard to accommodate the grillage backing plate which would otherwise interfere. The locations of the pressure transducers are discussed in the subsection titled "Instrumentation Locations".

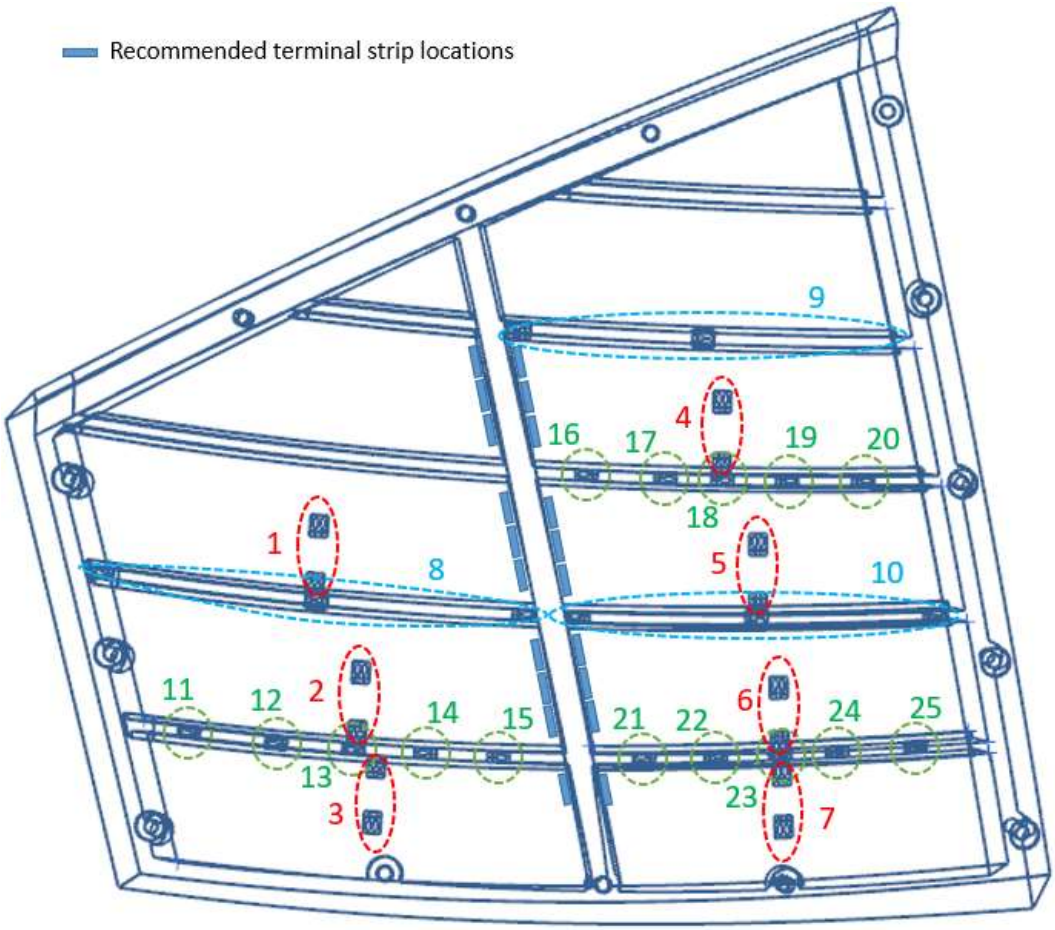

Figure 16. Grillage Strain Gage Diagram

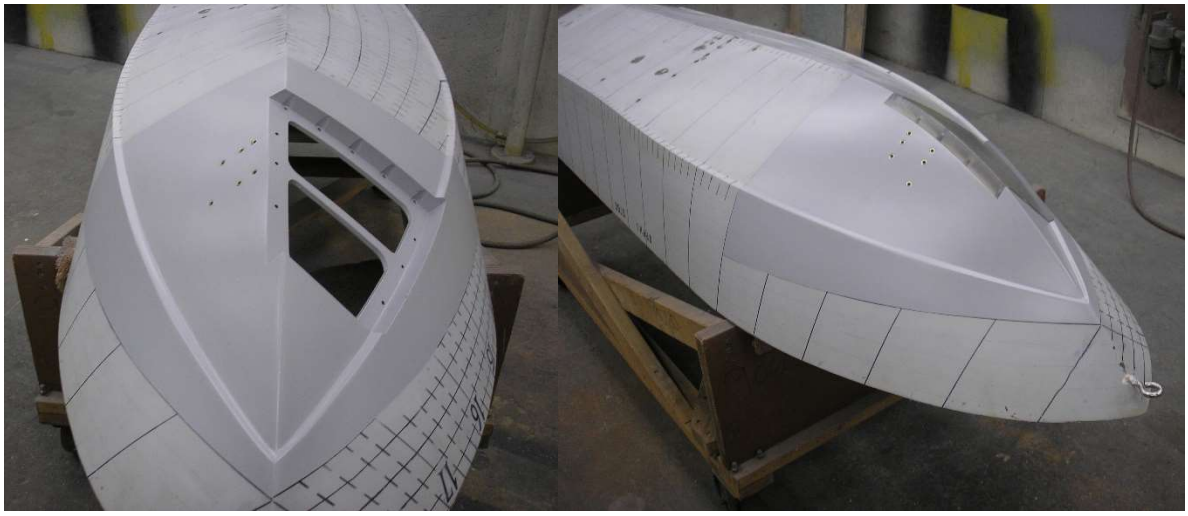

Figure 17. Grillage Panel Location Relative to Pressure Transducers

Model Ballasting

The target mass properties are provided in Table 2. The ballasting procedure followed standard practices with the use of an A-frame and the pendulum method. The process used to determine the mass properties is best described in a Journal Paper for the 30th American Towing Tank Conference [9]. The prescribed tolerances for each mass property of interest are shown in Table 3. The model was mounted to a beam (Figure 18) and the mass properties were determined for both the model and beam, as well as for the beam independently in order to arithmetically remove the influence of the beam. Static mass properties were scaled to achieve the correct trim and waterline. Correct motions and responses to external forces are achieved when the dynamic mass properties are equivalent. The values tracked throughout the ballast process were longitudinal center of gravity (LCG), vertical center of gravity (VCG), displacement, and pitch gyradius (k_{yy}). The final achieved mass properties are presented in Table 4.

The model scale for this test was 1/5.4. The desired static and dynamic properties were achieved by:

- Using the pendulum method described as described by Park, et al [9].
- Analyzing possible internal layouts of the components and ballast weights required in the model. This step was tracked using a ballasting spreadsheet to track components, positions, centers of gravity, and their effects on the model mass properties.
- Using the pendulum method with ballast weights installed.
- Confirming the waterline with photos from previous testing.

The model was suspended with the pivot directly over the longitudinal center of the tow point (Figure 19). A trim weight was required to balance the model at even keel while suspended from the A-frame (Figure 20) which allows for determination of the LCG. The trim weight was numerically removed after the swing in the ballast spreadsheet to account for the effects on the inertias and centers of gravity [10]. The total mass from the tow-post stack up, including ballast weight applied to the tow post, was accounted for mathematically and distributed as a point load at the pivot in the gimbal, with an effect on the centers of gravity but not on the inertial characteristics.

Minor adjustments were made to the ballast weights once the model was placed in the water to ensure the model was matching the waterline from the previous test [4]. The weight of the tow-post stack up was adjusted by adding weight to the top of the tow post to achieve the desired weight as well as waterline. The weight of model, including tow-post stack up, was measured as 224.09 lbs during testing and 224.12 lbs after the completion of testing.

Since the pre-test mass properties were measured before the model entered the water and therefore before any minor adjustments were made, the mass property calculations were updated after testing to reflect the adjustments. The total mass from the stack up, including weight applied to the tow post, was accounted for mathematically and distributed as a point load at the pivot in the gimbal, with an effect on the centers of gravity but not on the inertial characteristics. Table 4 presents the final achieved mass properties.

The pre-test model ballast was performed with the first grillage panel tested, the Traditional grillage. The post-test swing was performed with the second grillage panel, the

Optimized panel, which was designed by academia. The difference in weight between the two grillage panels was accounted for using large washers glued within the model (Figure 21).

The model layout and available ballast did not allow for the pitch gyradius to be achieved and acceptance of the deviation was requested from the sponsor. The achieved pitch inertia is approximately 23 % greater than the target value. As a result, the dynamic pitch response of the model can be expected to be different from past model tests from which the target was derived. This impact was understood and did not affect the objective since the measured pitch inertia could be numerically accounted for in future CFD / CSD computations.

Table 2. Target Mass Properties

Test Configuration Parameter	Target Value (As-Tested Nov. 2015)
Weight (lb)	223.8
Mass (slug)	6.9559
Longitudinal tow point, LTP (in +FTK)	33.844
LCG (in +FTK)	33.225
Vertical tow point, VTP (in +ABL)	5.75
VCG (in +ABL)	5.43
Pitch Moment of Inertia, $I_{yy,CG}$ (slug-in^2 About CG)	2,224
Pitch Gyradius, $k_{yy,CG}$ (inch About CG)	17.88

Table 3. Desired Tolerances

Nomenclature	Symbol	Tolerance (%)
Weight (lb)	Δ	± 0.2
Longitudinal Center of Gravity	LCG	± 1.0
Vertical Center of Gravity	VCG	± 2.0
Pitch Inertia	I_{yy}	± 5.0

Table 4. Mass Properties Achieved on A-Frame

Property	Desired	Achieved (Pre-Test)	Percent Difference	Achieved (Post-Test)	Percent Difference
Weight (lb)	223.8	224.09	0.13 %	224.12	0.14 %
LCG (in)	33.225	33.25	0.08 %	33.40	0.53 %
VCG (in)	5.43	5.46	0.64 %	5.45	0.42 %
Pitch Inertia (slug-in^2)	2224	2735.1	22.98 %	2725.8	22.56 %

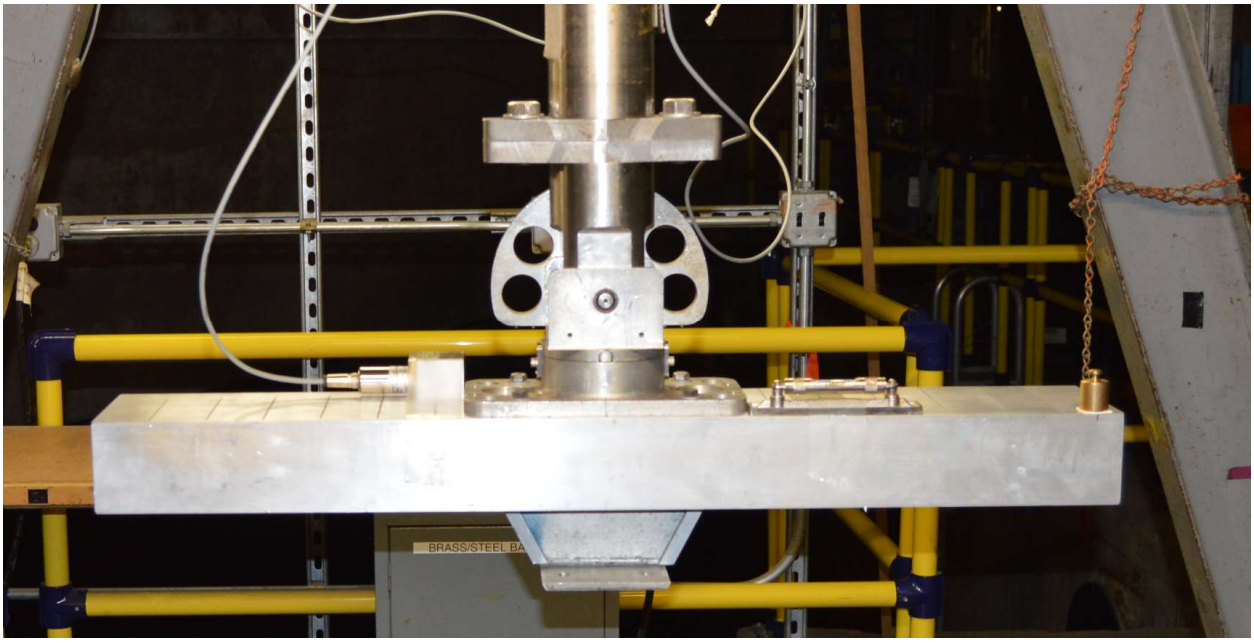

Figure 18. Beam Used for Ballasting

Figure 19. Model Suspended from A-Frame During Ballasting

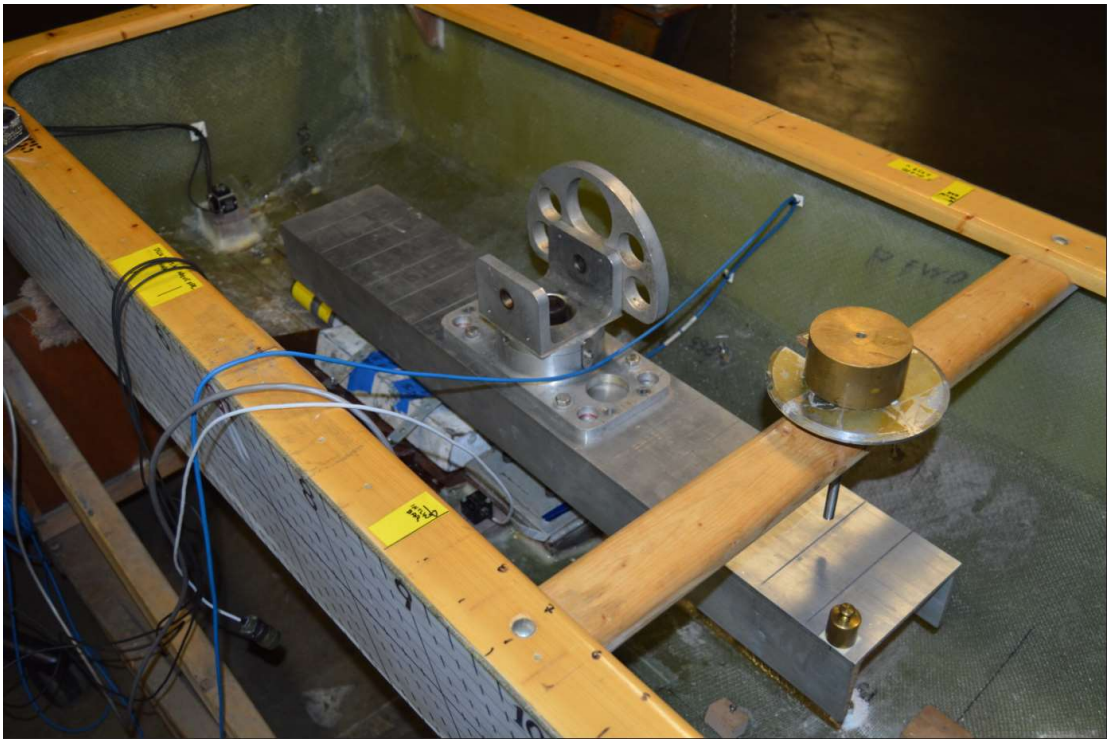

Figure 20. Inside of Model with Beam and Trim Weight Shown

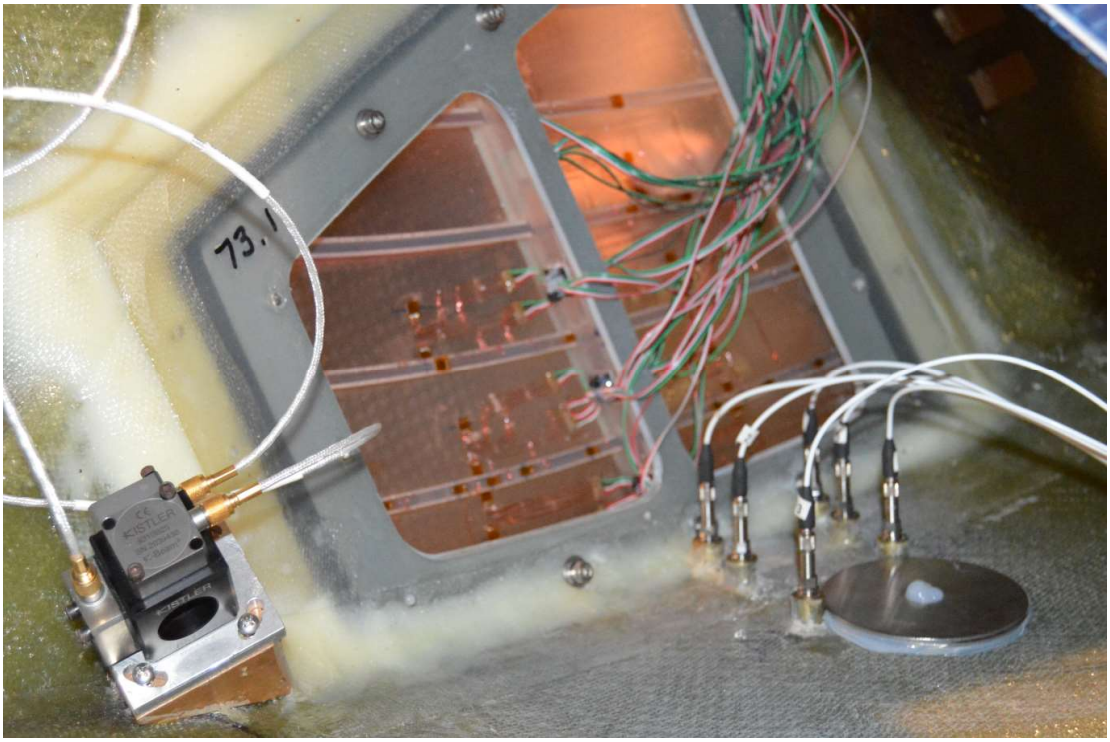

Figure 21. Optimized Grillage Panel and Washers Shown

A Note on the Target LCG

For a typical planing boat model test, it is standard practice to tow at the LCG, and as close to the theoretical thrustline as possible in the vertical direction. Most often, the test director has no choice but to tow above the thrustline due to the physical constraints involved. Full scale performance of the hull can then be estimated using thrust unloading or matrix method techniques [11].

However, for the previous model test effort [5], the same GPPH hull was towed with an LCG of 33.23 inches and a longitudinal tow point of 33.84 inches forward of the transom keel intersection, a difference of 0.61 inches. Because all comparisons generated hereafter are intended to be kept in model scale terms with no intention of estimating the full scale hull performance, and in order to ensure that the results of this test effort could be compared against the 2015 effort, the values from 2015 were carried forth for the most recent test series.

Instrumentation

The instrumentation used as part of the test effort is shown in Table 5. The table summarizes the specific instrumentation used, the sample rate and filtering used during data collection, and the bias uncertainty (U_{95}) calculated based on the pre- and post-test calibrations. Additional detail on the uncertainty calculations used can be found in Appendix D of this technical report.

The uncertainties (U_{95}) associated with the grillage panel channels (G1 through G25) are intentionally omitted from Table 5 for two reasons. First, the Traditional grillage panel was swapped with the Optimized grillage panel during testing in order to measure the response on two different grillages. Each grillage was pre-test calibrated, had its own gain values for 25 channels (G1 through G25), and its own associated instrumentation uncertainties. Second, the values were omitted due to the large differences observed in the pre- and post-test calibrations of the Traditional grillage. The panels were observed to change shape between the pre- and post-test calibrations, which therefore also would result in an expected change in grillage stiffness. This is discussed in greater detail in the Grillage and Pressure Analysis subsection. Uncertainty analysis on the two grillage panels was performed and appears in Appendix C.

It is worth mentioning that prior to testing, these grillage panels were identified as non-critical. The test team was hopeful to collect every grillage panel measurements (G1-G25 for both panels), but it was recognized that application of these SLA printed panels was experimental in nature.

Finally, it is worth noting instrumentation similarities and differences between the 2015 testing and current, 2019 test. Both tests desired to measure drag, pitch, heave, acceleration and pressures at discrete locations of the hull. Although the 2019 test used predominately Kistler accelerometers, for comparison purposes a Silicone Design tri-axis accelerometer was also placed at the LCG. This same make and model of accelerometer was used for the 2015 testing.

In terms of noted differences, pitch was measured using a Rotary Variable Inductance Transducer (RVIT) in 2019, but was calculated using two string-pot measurements in 2015. Also, drag and side force measurements were made via block gage in 2019, but these same measurements were made using a 6-degrees-of-freedom (6DOF) dynamometer in 2015.

Table 5. Table of Instrumentation

Ch No	Channel Name	Measurement Description	Transducer Description	Engineer Units	Polarity	Sample Rate (Hz)	Filter Cutoff (Hz)	Uncertainty U_{95} (Units)	Sensor ID No.
1	Time	Collection Time	NA	sec	always +	25,000	NA	NA	NA
2	Carr. Speed	Carriage 3 Speed Pickup	Encoder	knots	always +	25,000	Anti-aliasing LP at ~12.5 kHz	-	-
3	Wave Ht Bow	Carriage Mounted Sonic Wave Height Sensor (Center of Basin, East of Model)	Senix TSPC-30S1-232	in	+ up	40	-	0.12	4152026
4	Wave Ht CG	Carriage Mounted Sonic Wave Height Sensor (Side of Basin, South of Model)	Senix TSPC-30S1-232	in	+ up	40	-	0.04	4120478
5	Wave Ht Bow Corrected	Calculated Channel to Correct Dropouts	Calculated	in	+ up	NA	NA	0.12	4152026
6	Wave Ht CG Corrected	Calculated Channel to Correct Dropouts	Calculated	in	+ up	NA	NA	0.04	4120478
7	Drag	Block Gage	Stainless Steel Block Gage (500 lbs)	lbs	+ with applied drag force (pushing aft)	25,000	Anti-aliasing LP at ~12.5 kHz	0.38	039195
8	Side Force	Block Gage	Stainless Steel Block Gage (200 lbs)	lbs	+ with applied force to Port	25,000	Anti-aliasing LP at ~12.5 kHz	0.23	103
9	Pitch	RVIT at Pitch Gimbal	Schaevitz R60D RVIT	deg	+ bow down	25,000	Anti-aliasing LP at ~12.5 kHz	0.24	J2136
10	Heave	Celesco String Pot (50 inch)	PT1DC-50	in	+ up	25,000	Anti-aliasing LP at ~12.5 kHz	0.2	G1705701B
12	Long Accel at Bow	Bow Longitudinal Acceleration (25g)	Kistler 8310B25 (Single-Axis Accelerometer)	g	+ acceleration fwd	25,000	Anti-aliasing LP at ~12.5 kHz	0.042	2058329
13	Lat Accel at Bow	Bow Lateral Acceleration (25g)	Kistler 8310B25 (Single-Axis Accelerometer)	g	+ acceleration to port	25,000	Anti-aliasing LP at ~12.5 kHz	0.048	2058330
14	Vert Accel at Bow	Bow Vertical Acceleration (25g)	Kistler 8310B25 (Single-Axis Accelerometer)	g	+ accel up	25,000	Anti-aliasing LP at ~12.5 kHz	0.038	2039438
15	Long Accel at CG	CG Longitudinal Acceleration (10g)	Kistler 8395A010ATTA00 Tri-Axis Accelerometer	g	+ acceleration fwd	25,000	Anti-aliasing LP at ~12.5 kHz	0.012	2121614
16	Lat Accel at CG	CG Lateral Acceleration (10g)	Kistler 8395A010ATTA00 Tri-Axis Accelerometer	g.	+ acceleration to port	25,000	Anti-aliasing LP at ~12.5 kHz	0.003	2121614
17	Vert Accel at CG	CG Vertical Acceleration (10g)	Kistler 8395A010ATTA00 Tri-Axis Accelerometer	g	+ accel up	25,000	Anti-aliasing LP at ~12.5 kHz	0.005	2121614

(Table Continued)

Ch No	Channel Name	Measurement Description	Transducer Description	Engineer Units	Polarity	Sample Rate (Hz)	Filter Cutoff (Hz)	Uncertainty U_{95} (Units)	Sensor ID No.
18	Long Accel at CG _SD	CG Longitudinal Acceleration	Silicone Designs 2460-025 Accel (Same Accelerometer Used in Past Testing)	g	+ acceleration fwd	25,000	Anti-aliasing LP at ~12.5 kHz	0.011	1287
19	Lat Accel at CG _SD	CG Lateral Acceleration	Silicone Designs 2460-025 Accel (Same Accelerometer Used in Past Testing)	g.	+ acceleration to port	25,000	Anti-aliasing LP at ~12.5 kHz	0.010	1287
20	Vert Accel at CG _SD	CG Vertical Acceleration	Silicone Designs 2460-025 Accel (Same Accelerometer Used in Past Testing)	g	+ accel up	25,000	Anti-aliasing LP at ~12.5 kHz	0.011	1287
21	Long Accel at Stern	Stern Longitudinal Acceleration (10g)	Kistler 8315A010D0AC05 Single-Axis Accelerometer	g	+ acceleration fwd	25,000	Anti-aliasing LP at ~12.5 kHz	0.040	2117435
22	Lat Accel at Stern	Stern Lateral Acceleration (10g)	Kistler 8315A010D0AC05 Single-Axis Accelerometer	g	+ acceleration to port	25,000	Anti-aliasing LP at ~12.5 kHz	0.023	2117436
23	Vert Accel at Stern	Stern Vertical Acceleration (10g)	Kistler 8315A010D0AC05 Single-Axis Accelerometer	g	+ accel up	25,000	Anti-aliasing LP at ~12.5 kHz	0.016	2117437
24	Long Accel on Tow Post	Lonitudinal Acceleration on Tow Post (10g)	Kistler 8395A010ATTA00 Tri-Axis Accelerometer	g	+ acceleration fwd	25,000	Anti-aliasing LP at ~12.5 kHz	0.009	2121613
25	Lat Accel on Tow Post	Lateral Acceleration on Tow Post (10g)	Kistler 8395A010ATTA00 Tri-Axis Accelerometer	g	+ acceleration to port	25,000	Anti-aliasing LP at ~12.5 kHz	0.010	2121613
26	Vert Accel on Tow Post	Vertical Acceleration on Tow Post (10g)	Kistler 8395A010ATTA00 Tri-Axis Accelerometer	g	+ accel up	25,000	Anti-aliasing LP at ~12.5 kHz	0.021	2121613
27	G1	Differential Bending Channel Measuring Pressure on Shell Plating	ED-DY-125PC-10C/E	PSI	+ with postitive pressure applied	25,000	Anti-aliasing LP at ~12.5 kHz	-	-
28	G2	Differential Bending Channel Measuring Pressure on Shell Plating	ED-DY-125PC-10C/E	PSI	+ with postitive pressure applied	25,000	Anti-aliasing LP at ~12.5 kHz	-	-
29	G3	Differential Bending Channel Measuring Pressure on Shell Plating	ED-DY-125PC-10C/E	PSI	+ with postitive pressure applied	25,000	Anti-aliasing LP at ~12.5 kHz	-	-
30	G4	Differential Bending Channel Measuring Pressure on Shell Plating	ED-DY-125PC-10C/E	PSI	+ with postitive pressure applied	25,000	Anti-aliasing LP at ~12.5 kHz	-	-
31	G5	Differential Bending Channel Measuring Pressure on Shell Plating	ED-DY-125PC-10C/E	PSI	+ with postitive pressure applied	25,000	Anti-aliasing LP at ~12.5 kHz	-	-
32	G6	Differential Bending Channel Measuring Pressure on Shell Plating	ED-DY-125PC-10C/E	PSI	+ with postitive pressure applied	25,000	Anti-aliasing LP at ~12.5 kHz	-	-
33	G7	Differential Bending Channel Measuring Pressure on Shell Plating	ED-DY-125PC-10C/E	PSI	+ with postitive pressure applied	25,000	Anti-aliasing LP at ~12.5 kHz	-	-
34	G8	Differential Bending Channel Measuring Pressure Experienced by Stiffner/Shell Combination	ED-DY-125BZ-10C/E	PSI	+ with postitive pressure applied	25,000	Anti-aliasing LP at ~12.5 kHz	-	-

(Table Continued)

Ch No	Channel Name	Measurement Description	Transducer Description	Engineer Units	Polarity	Sample Rate (Hz)	Filter Cutoff (Hz)	Uncertainty U_{95} (Units)	Sensor ID No.
35	G9	Differential Bending Channel Measuring Pressure Experienced by Stiffner/Shell Combination; Grillage Panel A	ED-DY-125BZ-10C/E	PSI	+ with postitive pressure applied	25,000	Anti-aliasing LP at ~12.5 kHz	-	-
36	G10	Differential Bending Channel Measuring Pressure Experienced by Stiffner/Shell Combination; Grillage Panel A	ED-DY-125BZ-10C/E	PSI	+ with postitive pressure applied	25,000	Anti-aliasing LP at ~12.5 kHz	-	-
37	G11	Stiffener Top Surface Strain Measurements for Comparison with FEA; Grillage Panel A	ED-DY-125BZ-10C/E	µstrain	+ with postitive pressure applied	25,000	Anti-aliasing LP at ~12.5 kHz	-	-
38	G12	Stiffener Top Surface Strain Measurements for Comparison with FEA; Grillage Panel A	ED-DY-125BZ-10C/E	µstrain	+ with postitive pressure applied	25,000	Anti-aliasing LP at ~12.5 kHz	-	-
39	G13	Stiffener Top Surface Strain Measurements for Comparison with FEA; Grillage Panel A	ED-DY-125BZ-10C/E	µstrain	+ with postitive pressure applied	25,000	Anti-aliasing LP at ~12.5 kHz	-	-
40	G14	Stiffener Top Surface Strain Measurements for Comparison with FEA; Grillage Panel A	ED-DY-125BZ-10C/E	µstrain	+ with postitive pressure applied	25,000	Anti-aliasing LP at ~12.5 kHz	-	-
41	G15	Stiffener Top Surface Strain Measurements for Comparison with FEA; Grillage Panel A	ED-DY-125BZ-10C/E	µstrain	+ with postitive pressure applied	25,000	Anti-aliasing LP at ~12.5 kHz	-	-
42	G16	Stiffener Top Surface Strain Measurements for Comparison with FEA; Grillage Panel A	ED-DY-125BZ-10C/E	µstrain	+ with postitive pressure applied	25,000	Anti-aliasing LP at ~12.5 kHz	-	-
43	G17	Stiffener Top Surface Strain Measurements for Comparison with FEA; Grillage Panel A	ED-DY-125BZ-10C/E	µstrain	+ with postitive pressure applied	25,000	Anti-aliasing LP at ~12.5 kHz	-	-
44	G18	Stiffener Top Surface Strain Measurements for Comparison with FEA; Grillage Panel A	ED-DY-125BZ-10C/E	µstrain	+ with postitive pressure applied	25,000	Anti-aliasing LP at ~12.5 kHz	-	-
45	G19	Stiffener Top Surface Strain Measurements for Comparison with FEA; Grillage Panel A	ED-DY-125BZ-10C/E	µstrain	+ with postitive pressure applied	25,000	Anti-aliasing LP at ~12.5 kHz	-	-
46	G20	Stiffener Top Surface Strain Measurements for Comparison with FEA; Grillage Panel A	ED-DY-125BZ-10C/E	µstrain	+ with postitive pressure applied	25,000	Anti-aliasing LP at ~12.5 kHz	-	-
47	G21	Stiffener Top Surface Strain Measurements for Comparison with FEA; Grillage Panel A	ED-DY-125BZ-10C/E	µstrain	+ with postitive pressure applied	25,000	Anti-aliasing LP at ~12.5 kHz	-	-
48	G22	Stiffener Top Surface Strain Measurements for Comparison with FEA; Grillage Panel A	ED-DY-125BZ-10C/E	µstrain	+ with postitive pressure applied	25,000	Anti-aliasing LP at ~12.5 kHz	-	-
49	G23	Stiffener Top Surface Strain Measurements for Comparison with FEA; Grillage Panel A	ED-DY-125BZ-10C/E	µstrain	+ with postitive pressure applied	25,000	Anti-aliasing LP at ~12.5 kHz	-	-
50	G24	Stiffener Top Surface Strain Measurements for Comparison with FEA; Grillage Panel A	ED-DY-125BZ-10C/E	µstrain	+ with postitive pressure applied	25,000	Anti-aliasing LP at ~12.5 kHz	-	-
51	G25	Stiffener Top Surface Strain Measurements for Comparison with FEA; Grillage Panel A	ED-DY-125BZ-10C/E	µstrain	+ with postitive pressure applied	25,000	Anti-aliasing LP at ~12.5 kHz	-	-

(Table Continued)

Ch No	Channel Name	Measurement Description	Transducer Description	Engineer Units	Polarity	Sample Rate (Hz)	Filter Cutoff (Hz)	Uncertainty U_{95} (Units)	Sensor ID No.
52	P11'	Piezoelectric Pressure Gage (50 PSI)	PCB Model 113B28	PSI	+ with postitive pressure applied	25,000	Anti-aliasing LP at ~12.5 kHz	0.151	30702
53	P12	Piezoelectric Pressure Gage (50 PSI)	PCB Model 113B28	PSI	+ with postitive pressure applied	25,000	Anti-aliasing LP at ~12.5 kHz	0.142	30701
54	P13	Piezoelectric Pressure Gage (50 PSI)	PCB Model 113B28	PSI	+ with postitive pressure applied	25,000	Anti-aliasing LP at ~12.5 kHz	0.124	30700
55	P21'	Piezoelectric Pressure Gage (50 PSI)	PCB Model 113B28	PSI	+ with postitive pressure applied	25,000	Anti-aliasing LP at ~12.5 kHz	0.054	30699
56	P22	Piezoelectric Pressure Gage (50 PSI)	PCB Model 113B28	PSI	+ with postitive pressure applied	25,000	Anti-aliasing LP at ~12.5 kHz	0.039	30698
57	P23	Piezoelectric Pressure Gage (50 PSI)	PCB Model 113B28	PSI	+ with postitive pressure applied	25,000	Anti-aliasing LP at ~12.5 kHz	0.067	30642
58	P31	Piezoelectric Pressure Gage (50 PSI)	PCB Model 113B28	PSI	+ with postitive pressure applied	25,000	Anti-aliasing LP at ~12.5 kHz	0.059	30641
59	P41	Piezoelectric Pressure Gage (50 PSI)	PCB Model 113B28	PSI	+ with postitive pressure applied	25,000	Anti-aliasing LP at ~12.5 kHz	0.041	30640
60	P42	Piezoelectric Pressure Gage (50 PSI)	PCB Model 113B28	PSI	+ with postitive pressure applied	25,000	Anti-aliasing LP at ~12.5 kHz	0.099	30633
61	P43	Piezoelectric Pressure Gage (50 PSI)	PCB Model 113B28	PSI	+ with postitive pressure applied	25,000	Anti-aliasing LP at ~12.5 kHz	0.072	30632
62	P44	Piezoelectric Pressure Gage (50 PSI)	PCB Model 113B28	PSI	+ with postitive pressure applied	25,000	Anti-aliasing LP at ~12.5 kHz	0.099	30631
63	P45	Piezoelectric Pressure Gage (50 PSI)	PCB Model 113B28	PSI	+ with postitive pressure applied	25,000	Anti-aliasing LP at ~12.5 kHz	0.109	30630
64	P51	Piezoelectric Pressure Gage (50 PSI)	PCB Model 113B28	PSI	+ with postitive pressure applied	25,000	Anti-aliasing LP at ~12.5 kHz	0.075	30629

Instrumentation Locations

This subsection documents the placement of instrumentation within the model, and position of the wave height measurements relative to the model. Table 6 describes the placement of the 13 piezoelectric pressure transducers used to measure localized pressure on the hull. With the exception of two pressure transducers, the locations remained the same as when tested in 2015 [2]. The exceptions, P11' and P21' (note the prime), were moved outboard, and the new positions are reflected in the table below as highlighted rows.

Table 6. Pressure Transducer Locations

Transverse Row No.	Pressure Sensor No.	x (in +FTK)	y (in +PCL)	z (in +ABL)
1	P11' (lower)	75.53	0.88	3.39
	P12	75.57	1.68	3.49
	P13 (upper)	75.58	3.06	4.67
2	P21' (lower)	73.25	1.06	2.66
	P22	73.33	1.69	2.70
	P23 (upper)	73.33	2.68	3.44
3	P31	50.20	0.52	0.17
4	P41 (lower)	44.93	0.50	0.03
	P42	44.90	2.93	0.95
	P43	44.87	4.12	1.33
	P44	44.84	6.54	2.13
	P45 (upper)	44.85	10.38	3.55
5	P51 (lower)	42.88	0.49	0.17

Table 7 describes the positioning of the accelerometers. A combination of single and tri-axis accelerometers were used to measure acceleration at various locations on the hull. In total, there were 9 accelerometers.

It's worth noting that the measurement at the CG was made by two tri-axis accelerometers fabricated by two different manufacturers, allowing for a redundant measurement. One was fabricated by Silicone Design and the other by Kistler. With the exception of the Silicone Design accelerometer, all of the accelerometers used were Kistler accelerometers of similar type. The Silicone design accelerometer was used to provide an acceleration measurement with same instrumentation and location used during 2015 testing [4]. And the redundant measurement was used as a control to rule out any differences in measurement due to instrumentation differences.

It's also worth noting that a tri-axis accelerometer was placed on the flange at the bottom of the tow post, and not technically on the model. The intention was to measure the response of tow post when the post was rapidly loaded and unloaded as model encountered waves at high speed.

Table 7. Accelerometer Locations

Accelerometer Name	Serial Number	x (in +FTK)	y (in +PCL)	z (in +ABL)
Long Accel at Bow	2058329	85.96	0.00	9.77
Lat Accel at Bow	2058330	84.81	-0.21	9.77
Vert Accel at Bow	2039438	84.81	0.00	10.60
Long Accel at CG	2121614	33.84 (Center of Tow Point)	4.57	3.26
Lat Accel at CG				
Vert Accel at CG				
Long Accel at CG _SD	1287	33.84 (Center of Tow Point)	-4.57	3.04
Lat Accel at CG _SD				
Vert Accel at CG _SD				
Long Accel at Stern	2117435	2.52	0.00	3.48
Lat Accel at Stern	2117436	1.78	-0.74	3.48
Vert Accel at Stern	2117437	1.78	0.00	4.22
Long Accel on Tow Post	2121613	N/A Physically fastened to flange of tow post; Not inside of the model		
Lat Accel on Tow Post				
Vert Accel on Tow Post				

Finally, the wave measurement locations relative to the tow point of the model are shown in Figure 22. Conceptually, the "bow" wave height was positioned forward of the model and not far from the centerline of the tow tank. This position is generally the preferred location to consider when characterizing the waves observed, and is referred to in the instrumentation list as "Wave Ht Bow". A second measurement location was referred to as "Wave Ht CG" and was positioned close to the tow point location in the longitudinal direction. In the transverse direction, the location was biased toward, but offset from, the basin wall.

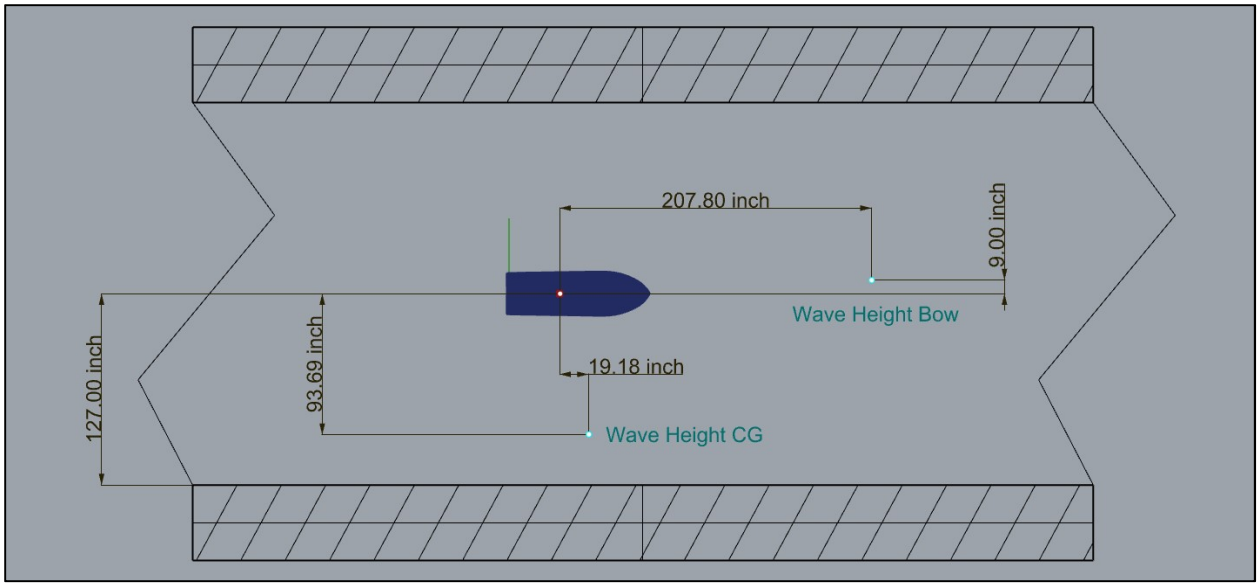

Figure 22. Wave Measurement Locations

Polarity Convention

The polarity convention used for this test series was a right-handed coordinate system with the origin at the keel transom intersection. The polarity convention is shown in Figure 23. This convention is used throughout the report unless noted otherwise.

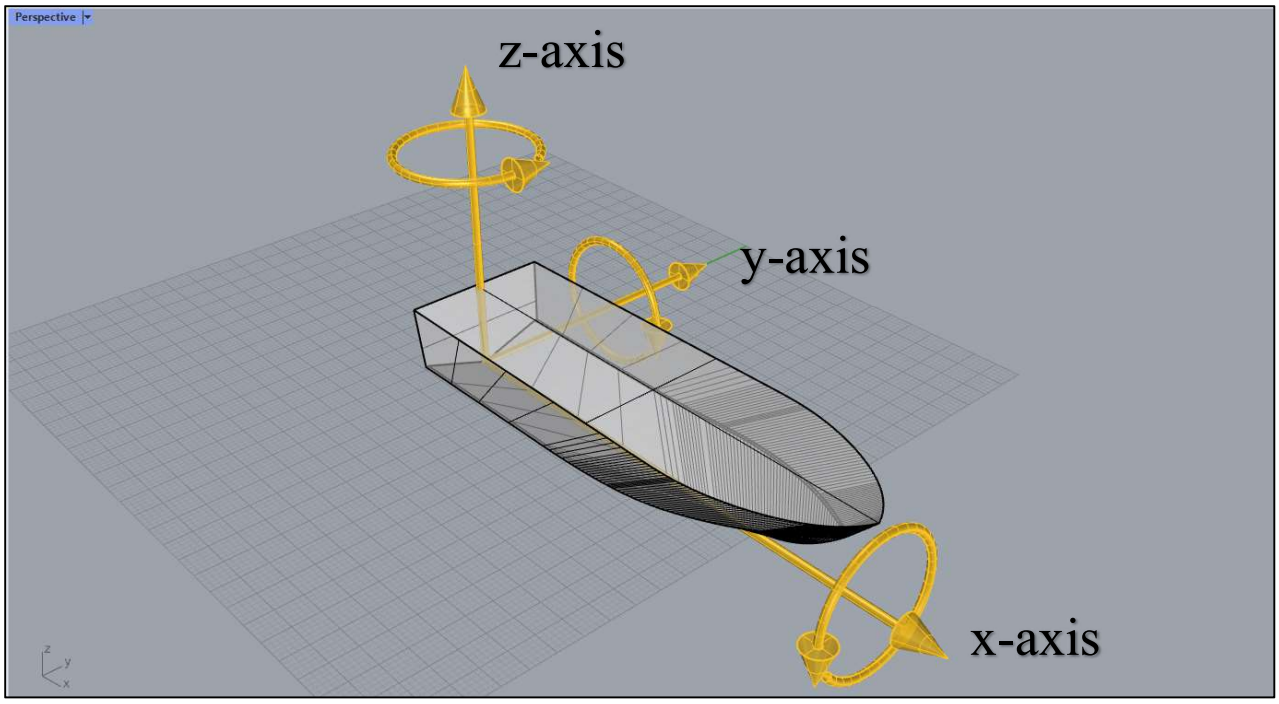

Figure 23. GPPH Polarities (+ in Direction of Arrows)

Data Acquisition

The data acquisition system consisted of three National Instruments (NI) 9188 cDAQ chassis containing a variety of modules of data collection. All channels for this test, with exception of the Senix channels, were analog channels. The model speed encoder signal was fed through a frequency-to-voltage converter (F/V) to convert it to an analog channel. The Senix sensors (measuring wave height) were collected serially. One accelerometer, the Silicone Designs accelerometer, and the pressure gages had separate electronics that convert the sensor signals to a high level analog signal. Strain gage channels were collected using NI 9237 modules, and all analog channels were collected with NI 9239 modules. The chassis was hardware synchronized using NI 9469 modules.

Sigma DAQ 1.0 was the data acquisition software used to collect the data. This acquisition program was developed at NSWCCD using LabVIEW 2018. The data acquisition software collected two sets of data. A raw data set of measurements was collected during the entire run which was referred to as a "pass". And an engineering data set (with calibration gains and offsets applied) was collected during sections, or "spots", contained within the pass. The software provided the statistics in engineering units for each spot.

Test Details

Approach

The model test approach was to test in conditions that could be simulated using the numerical software packages STAR-CCM+ and CFDShip-Iowa, and that was generally consistent with past testing of the GPPH hull form [4]. It's worth noting that the intention of this test program was to produce data for comparison with existing numerical tools at model scale. That is, there was no desire to scale model-scale measurements into full-scale predictions for the hull form. Therefore, thrust unloading or matrix method techniques were not required nor desired for this test effort [11]. The test approach was beneficial to the overall test effort because the savings in basin time by limiting testing to a single ballast condition was reallocated to collect more test data in the conditions of greatest interest.

Test Setup

The model was towed using a single heave post attached near, but not at, the model LCG, allowing the motions of the model to be free in pitch and heave, but fixed in surge, roll, yaw, and sway. Figure 24 shows the towing apparatus used for testing. The entire apparatus could be traversed vertically to raise or lower the model from the water. To facilitate lifting the model, four lines made of steel cabling were connected to four swivel-hoist rings in the corners of the model. The forward two lines were connected to an actuator capable of shortening the lines to forcibly alter the pitch angle to avoid a plow-in or swamping event. This capability was not needed during this particular test effort.

Tow Gear

The tow gear stack-up, shown in Figure 25, consisted of a heave staff, two block gages (one to measure drag and one for side force), and a pitch gimbal. The heave post, referred to as the "extended tow post", was specifically designed in support of this test effort. More information on the design and fabrication of the extended tow post can be found in the subsection titled Extended Tow Post of this technical report.

Figure 24. Towing Apparatus

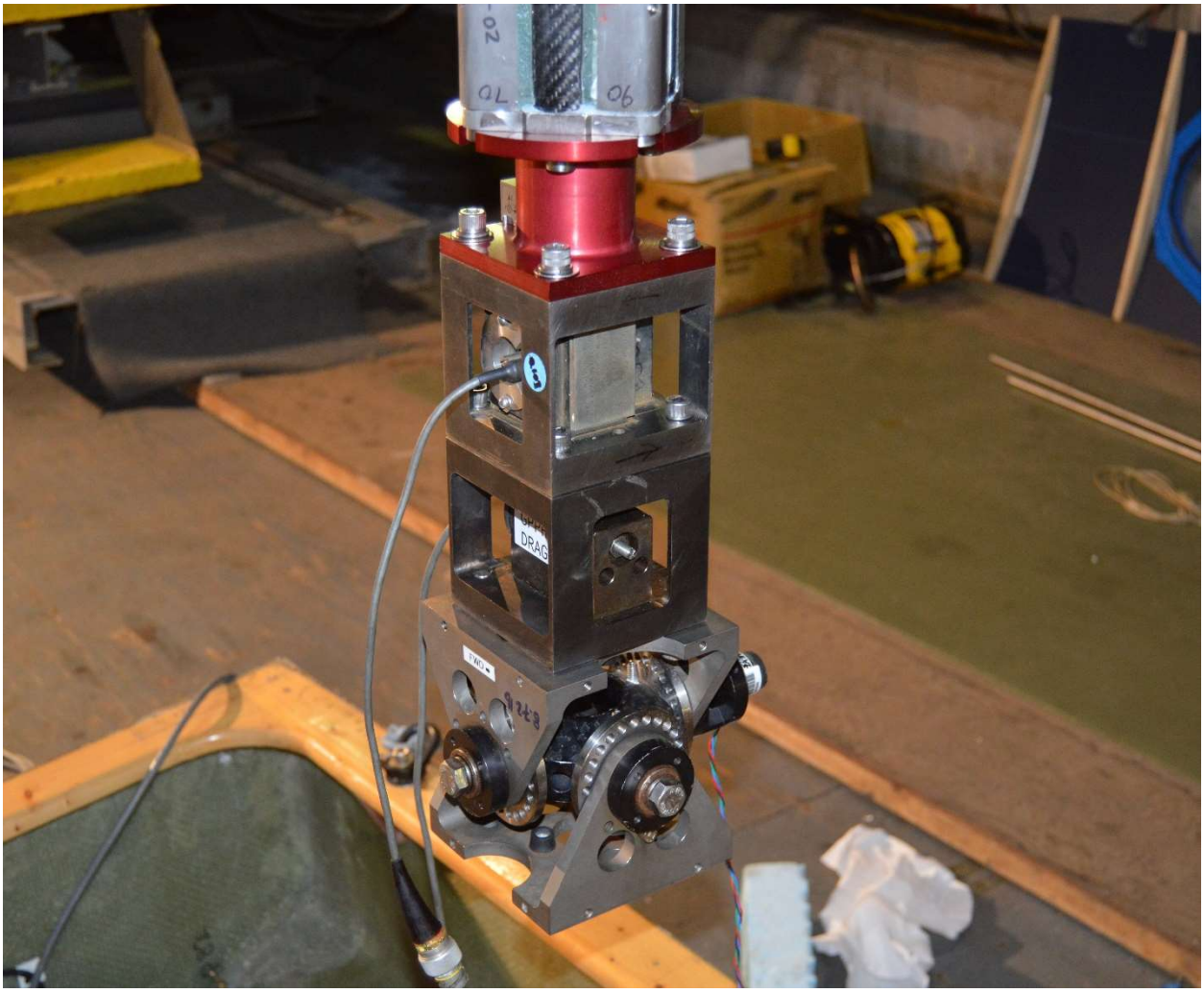

Figure 25. Tow Gear Stack-Up

Test Procedure

The test procedure used for calm-water, regular-wave, and irregular-wave testing is described as follows. For calm water testing, prior to each carriage pass, a "zero" collect was taken at zero forward speed. After the zero, the model was accelerated to the speed of interest, a short pause at constant speed was observed to allow motions due to the acceleration up to speed to settle out, and a collect, or "spot", was taken. The durations of the zero collect were 10 seconds and 30 seconds for calm-water and wave testing respectively.

Multiple spots at increasing target speeds were collected in a single pass across the high speed basin. This allowed for efficient use of the available basin time. Since the depth of the basin changes from shallow to deep as Carriage 3 traverses in the forward (or East) direction, discrete calm water runs were taken over each depth so the effects could later be explored.

When testing in waves, the basin water level was dropped 30 in to facilitate wave making. Due to the reduction in depth associated with the water level drop, only the deep portion of the high speed basin was used for testing in waves.

During regular wave testing, a group of regular waves was sent across the basin. The waves travel from East to West. In the opinion of the authors, the best location to collect regular wave data is East of the photo pit and at a safe distance before the trips (where the carriage must slow down as it reaches the end of the basin). The basin wall is not flat and uniform at the photo pit which has some small effect that can be noted through visual observation. The challenge was timing the test such that the target speed was achieved and the model passed through the wave grouping simultaneously, all at the most favorable location in the test basin. In each test the desire was to collect 7 - 10 regular wave cycles. Prior to each regular wave run, a "zero" collect was taken.

During irregular wave testing the procedure was slightly different. At each opportunity when the basin was calm, a "zero" collect was taken. This usually occurred at the start of each day, and after the lunch break. After the zero collect was taken, the irregular wave condition was sent to the wavemaker. A waiting period was observed until all wavelengths reached the region of interest in the basin. At this time, the model was accelerated to the desired speed and a single, long collect or "spot" was taken at constant speed across the basin. In order to obtain the desired number of wave encounters, multiple runs of the same condition were collected. Before each run, a "rough water zero" was collected at zero speed for a duration of at least 30 seconds.

Test Matrix

The test matrix for the GPPH test series is summarized in Table 8. The entire test matrix was completed during the test effort.

Table 8. Prioritized Test Matrix

Priority	Matrix ID	Sea Condition	Grillage Panel Type	Speed (Model Scale; knots)	Fr	Rationale	# Passes Required
A	*1*	Calm Water	Traditional	10.8	1.14	To measure potential depth effects	1.0
A	*2*	Calm Water	Traditional	17.5	1.85	To measure potential depth effects	1.0
A	*3*	Calm Water	Traditional	23.8	2.52	To measure potential depth effects	1.0
A	*4*	Calm Water	Traditional	10.8	1.14	To establish repeatability with past testing (see CY19 SOW)	0.5
A	*5*	Calm Water	Traditional	13.0	1.37	To establish repeatability with past testing (see CY19 SOW)	0.5
A	*6*	Calm Water	Traditional	14.8	1.56	To establish repeatability with past testing (see CY19 SOW)	0.5
A	*7*	Calm Water	Traditional	17.5	1.85	To establish repeatability with past testing (see CY19 SOW)	0.5
A	*8*	Calm Water	Traditional	19.5	2.06	To establish repeatability with past testing (see CY19 SOW)	0.5
A	*9*	Calm Water	Traditional	21.6	2.28	To establish repeatability with past testing (see CY19 SOW)	0.5
A	*10*	Calm Water	Traditional	23.8	2.52	To establish repeatability with past testing (see CY19 SOW)	1.0
B	*11*	Calm Water	Traditional	17.5	1.85	A series of 10 repeat runs to help quantify variability in data	10.0
		Water Level Change					
A	*12*	Regular Wave / DA = 5.23 in; T = 2.1 sec	Traditional	14.8	1.6	As tested in November 2015 [D6] (to investigate repeatability)	3.0
A	*13*	Regular Wave / DA = 5.23 in; T = 2.1 sec	Traditional	17.5	1.9	As tested in November 2015 [D6] (to investigate repeatability)	3.0
A	*14*	Irregular Wave / Hs = 7.4 in; Tm = 2.4 sec	Traditional	17.5	1.9	Desired wave condition and speed from the March 2015 Test Plan (300 Encounters)	12.6
B	*15*	Irregular Wave / Hs = 7.4 in; Tm = 2.4 sec	Traditional	17.5	1.9	Desired wave condition and speed from the March 2015 Test Plan (200 Encounters)	8.4
B	*16*	Irregular Wave / Hs = 7.4 in; Tm = 2.4 sec	Traditional	14.8	1.6	Desired wave condition and speed from the March 2015 Test Plan (300 Encounters)	8.8
C	*17*	Irregular Wave / Hs = 7.4 in; Tm = 2.4 sec	Traditional	14.8	1.6	Desired wave condition and speed from the March 2015 Test Plan (200 Encounters)	5.9
C	*18*	Reg wave - regular span	Traditional	14.8	1.6	study tow post stiffness by changing tow post span	1.0
C	*19*	Reg wave - reduced span (by changing to post position)	Traditional	14.8	1.6	study tow post stiffness by changing tow post span	1.0
		Grillage Panel Change					
A	*20*	Regular Wave / DA = 5.23 in; T = 2.1 sec	Optimized	14.8	1.6	As tested in November 2015 [D6]	3.0
A	*21*	Regular Wave / DA = 5.23 in; T = 2.1 sec	Optimized	17.5	1.9	As tested in November 2015 [D6]	3.0
A	*22*	Irregular Wave / Hs = 7.4 in; Tm = 2.4 sec	Optimized	17.5	1.9	Desired wave condition and speed from the March 2015 Test Plan (300 Encounters)	12.6
B	*23*	Irregular Wave / Hs = 7.4 in; Tm = 2.4 sec	Optimized	17.5	1.9	Desired wave condition and speed from the March 2015 Test Plan (200 Encounters)	8.4
B	*24*	Irregular Wave / Hs = 7.4 in; Tm = 2.4 sec	Optimized	14.8	1.6	Desired wave condition and speed from the March 2015 Test Plan (300 Encounters)	8.8
C	*25*	Irregular Wave / Hs = 7.4 in; Tm = 2.4 sec	Optimized	14.8	1.6	Desired wave condition and speed from the March 2015 Test Plan (200 Encounters)	5.9

Test Facility

Testing was conducted in the High Speed Basin using Carriage 3 at the Naval Surface Warfare Center (NSWCCD) in Bethesda, Maryland. Note that the facilities details described herein have been made publicly available by the International Towing Tank Conference (ITTC) [12].

The high speed basin is 2,968 ft in length with a beach at the 0 ft mark and a pneumatic wavemaker at the 2,968 ft mark. The basin has both a shallow and deep water section. The entire length was used for calm water measurements and only the deep section for rough water measurements. The shallow water section extends from the 0 ft mark to the 1,200 ft mark and has a nominal depth of 10 ft. The rest of the tank has a nominal depth of 16 ft. Although the Basin is 904 m (2,968 ft) in length, only 1,000 ft of the shallow end and 1,500 ft of the deep end can be used for testing due to the location of the Carriage safety trips. When using the wavemaker, the water depth was reduced from its nominal depth by 30 in to 7.5 ft in the shallow end and 13.5 ft in the deep end. The basin has a width of 21 ft and the carriage has a maximum speed of 32 knots.

Carriage 3

Carriage 3 was built in 1941 and modified in 1973. A schematic of the carriage is shown in Figure 26, and photographs of the carriage are shown in Figure 27. The carriage is triangular in shape, in effect a monorail structure with two outrigger idle wheels supporting the light side of the carriage frame, four drive wheels and four opposed pairs of horizontal guide wheels operate in tandem on the main rail. A "U"-shaped observation/camera platform attaches to the front of the carriage and spans the basin ahead of the model to allow viewing and photography from many angles while tests are in progress.

Carriage 3 has an electro-hydraulic drive and regenerative braking system with four drive wheels each direct coupled to an in-line axial piston type hydraulic motor receiving oil from hydraulic pumps driven by a constant speed AC synchronous motor. This single electric motor is rated 149 kW (200 hp) and gives the carriage a maximum speed of 32 knots uniform to within 0.01 knots total variation (16.5 m/s, 54.0 ft/s). The maximum average acceleration rate is about 0.07 g in either direction.

Data collection is supported from within an air-conditioned instrument room (7 m (23 ft) long by 3 m (10 ft) wide by 2.1 m (7 ft) high) that houses the computerized data acquisition equipment. Motorized work platforms are also mounted under the carriage that can be extended out in front of the carriage 3.3 m (11 ft) to facilitate model changes with the carriage located anywhere along the basin.

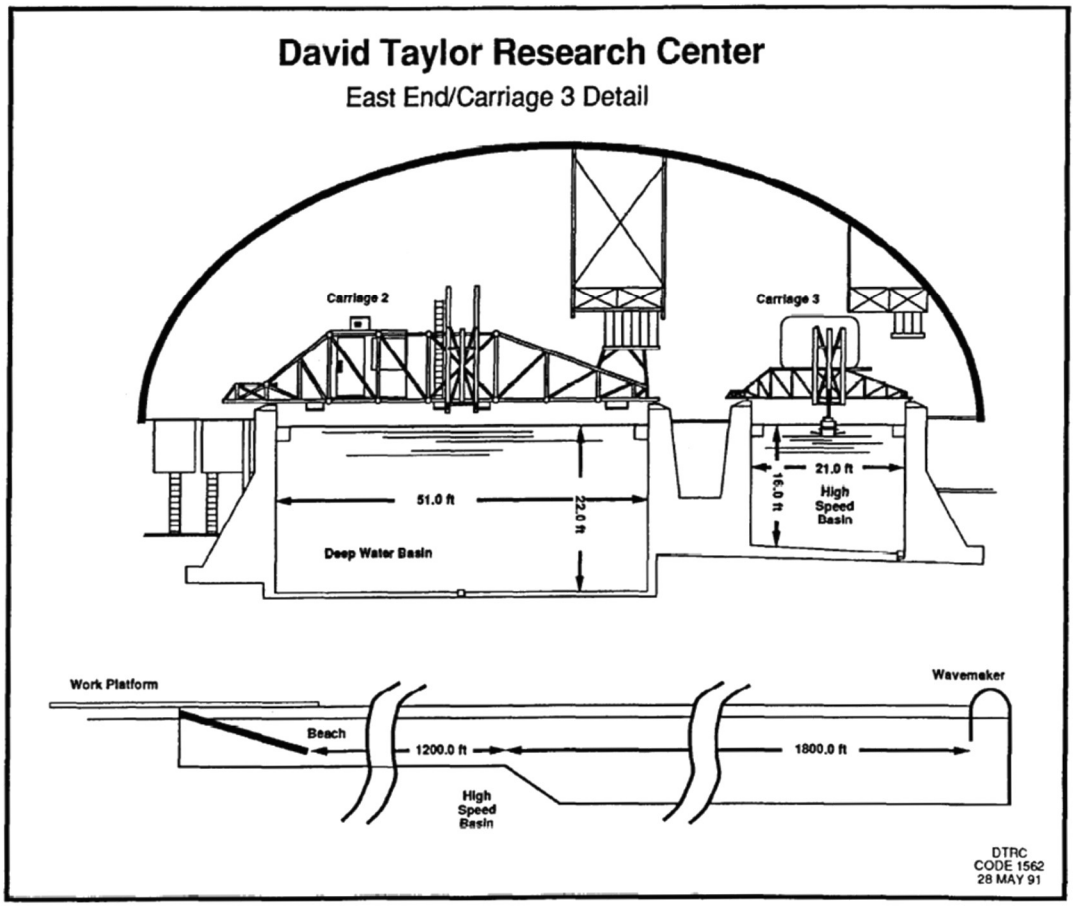

Figure 26. Linear Towing Basin; Section View at East End.

Figure 27. Towing Carriage 3

Wavemaker Description

The pneumatic wavemaker is located at the east end of the basin and a wave absorbing beach is located at the west end. A schematic of the wavemaker is shown in Figure 28. The 6.4

m (21 ft) wide wavemaker dome is connected to a centrifugal type blower driven by a direct coupled variable speed DC electric motor rated at 75 kW (100 hp), 1,150 rpm.

The beach or wave absorber spans the full width of the basin at the shallow end opposite the wavemaker dome. The absorbers are a discontinuous 20° slope-type made up of seven permeable layers of rectangular precast concrete bar panels resting on an impermeable concrete slab supported by a structural steel framework. Extending along the walls on each side of the basin are "U"-shaped steel wave absorber skimming troughs with their upper edges set about 6 mm (0.25 in) below the normal water level surface.

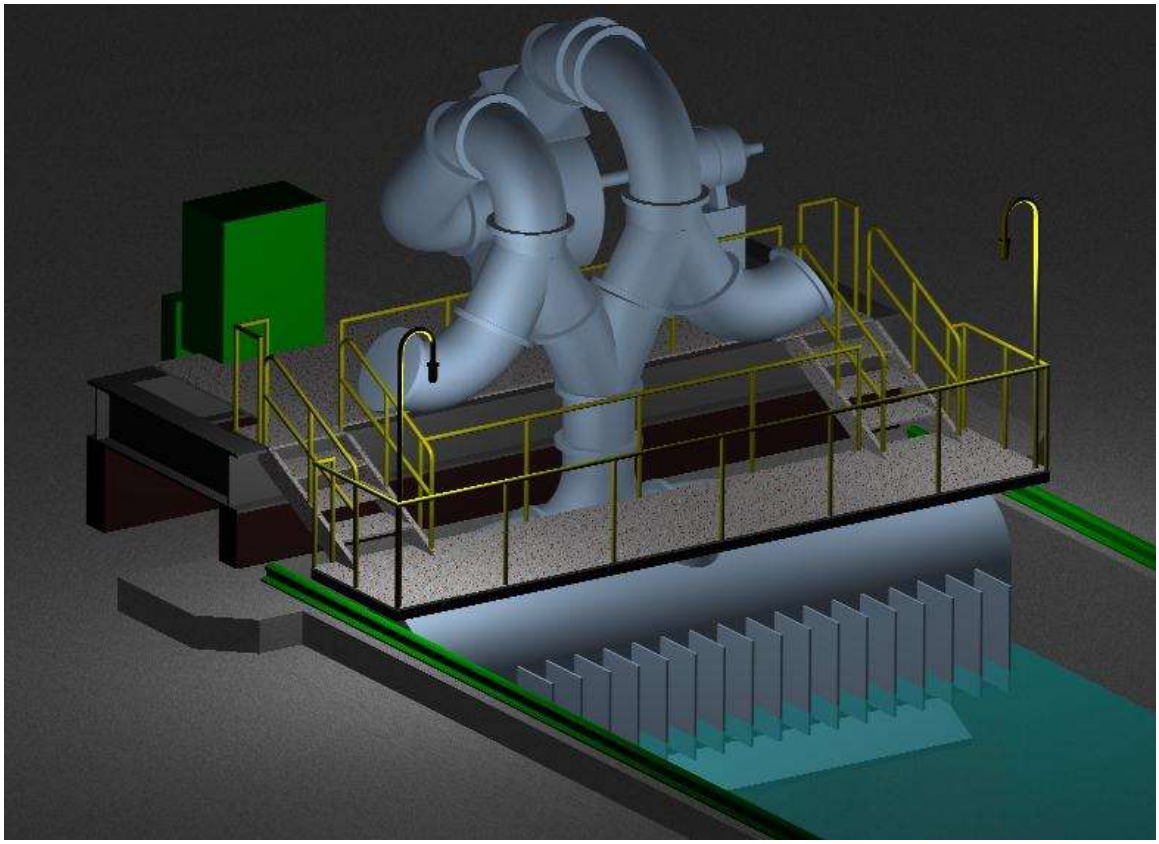

Figure 28. NSWCCD High Speed Basin Pneumatic Wavemaker

Waves Achieved

Most of the test matrix focused on collecting data in an irregular wave condition that would be representative of sea state 3 when characterized by significant wave height [13]. The target condition was a Bretschneider spectrum with a significant wave height of 7.44 in and a modal period of 2.4 seconds.

Wave Iterations

A process referred to as “wave iterations” was performed in the high speed basin on May 9th, 2019, prior to testing. The advantage of performing wave iterations in advance of testing is

to provide the test team with an indication of how closely the wavemaker is able to match the target wave condition.

Figure 29 shows a comparison of the spectrum measured during wave iterations versus the desired Bretschneider spectrum. Iteration 2, shown as a blue curve, was used for all testing in irregular waves. The measured spectrum was 0.7 % high in terms of significant wave height.

The reader should recognize that the waves generated at the East end of the basin, nearest the wavemaker, are larger than those towards the West end. Therefore, it is standard practice to slowly traverse the carriage across, or "scan", the basin to determine the wave condition that is representative of the desired condition for the region of interest. The region of interest in this case was the deep portion of the basin (approximately between light markers 1290 and 2310). By traveling at 0.65 knots, approximately 15 minutes of data was collected. The wave data collected was converted from encountered to stationary and compared against the desired wave spectrum as shown in the plot below.

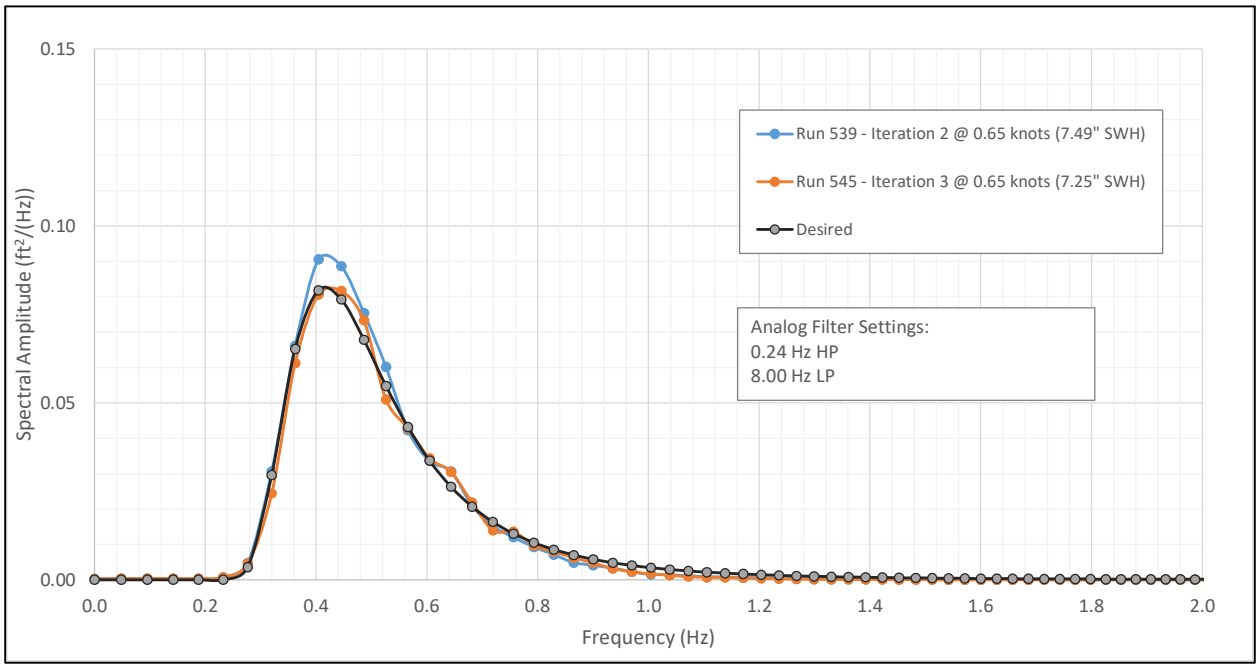

Figure 29. Measured versus Desired during Wave Iterations

Wave Measurements during Testing

Since each test condition involved collecting a minimum of 500 wave encounters, many spots were collected for each condition producing ensembles of data. Because of the large number of wave encounters, the data generated was sufficient to examine the waves achieved during testing for a given condition. The wave data was converted from encountered to stationary by accounting for the forward speed of the carriage, and the results are compared against the desired wave spectrum in Figure 30. This comparison shows the measured spectrum versus the desired for the test condition involving all passes at 14.8 knots. The measured spectrum for this grouping of data is approximately 4 % low relative to the desired spectrum. The measured values appear at the top of the figure.

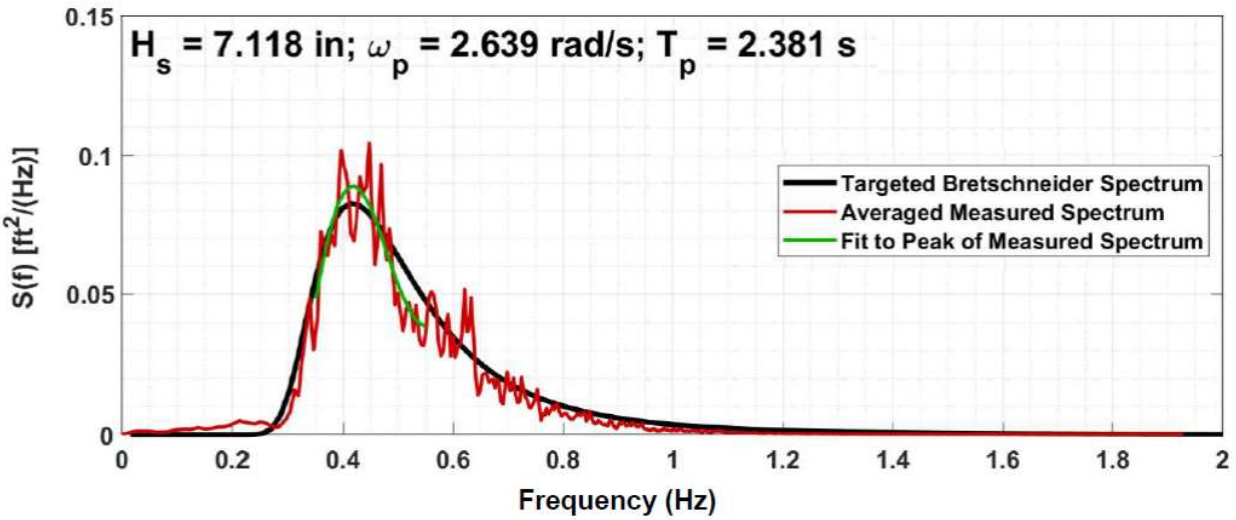

Figure 30. Measured Versus Desired during Testing

Extended Tow Post

In past planing boat tests, one of the most common constraints has been the limited amount of heave travel present in tow gear. This planing boat test was the first to use a newly designed extended tow post which, in combination with a modification to the lifting mechanism, allowed for greater heave travel. The standard post (the "SES" tow post) is limited to under 23 in of travel, and the newly fabricated extended tow post has approximately 36.6 in of travel from bump-stop to bump-stop.

The extended tow post was designed to be lightweight for use on future scaled models of planing craft. The overall weight is approximately the same as the current post (54 in "SES" tow post), making it lighter per linear foot. The extended tow post is also stiffer than the current tow post. From a structures perspective it was designed to withstand the relatively large expected loads produced by towing a planing craft model, like GPPH, when traveling through the desired, large irregular wave condition at high speed.

As fabricated, the extended tow post is comprised of a roughly 4 in diameter carbon-fiber tube, and rails formed of titanium angle to create a surface sufficiently hard for the existing rollers to bear against. All of the remaining parts on the two post were fabricated from titanium to avoid potential corrosion. The parts were joined together by a two part epoxy called ScotchWeld DP 460, with mechanical connections also present. Figure 31 shows a schematic of the extended tow post, and a photographs are shown in Figure 32 and Figure 33.

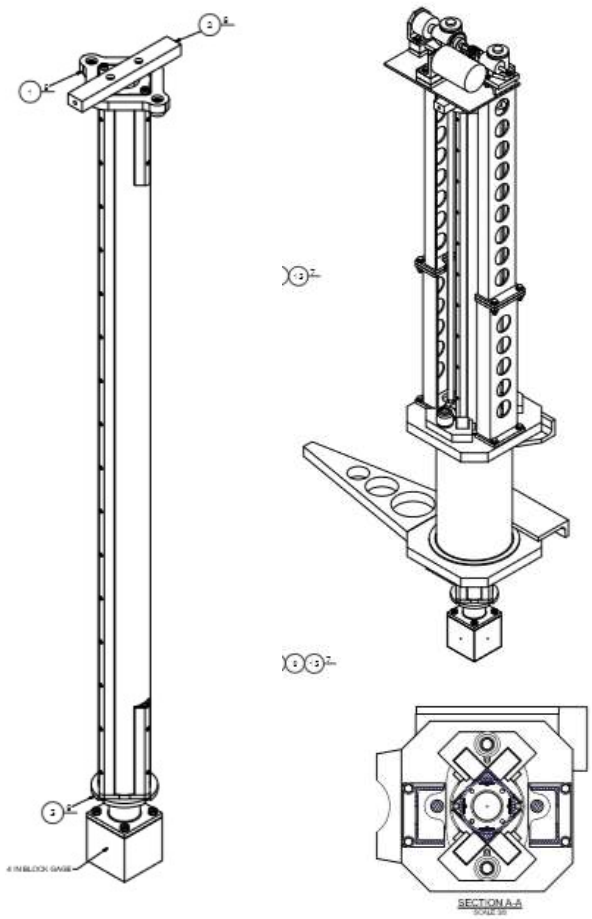

Figure 31. Schematic of Extended Tow Post[3]

[3] The corresponding drawings are numbers E80-4501-1 through E80-4501-9.

Figure 32. Photograph of the Extended Tow Post

Figure 33. Close-up of Extended Tow Post

The tow post was designed using data from past planing boat tests and engineering judgement. A set of maximum loads was used as design criteria to arrive at the current design. The values in Table 9 serve as limitations on loads. The tow post was designed to handle the force in surge, force in sway and yaw moment *simultaneously*. However, these loads are also *instantaneous* load limits. That is, these are not average load limits. This is an important distinction to make since there are large expected differences between instantaneous maxima and average values when testing, especially when testing in waves. In general the test engineer must be mindful of the limitation of the extended tow post and the expected loads of the model while accounting for an adequate margin for the uncertainty in the load predictions for the test. Consideration should also be made to the possibility and susceptibility of a model to an extreme yaw event. In no instance should the values in Table 9 ever be exceeded.

Table 9. Limitations on Load

Maximum Loads		
Working Load for Surge Force at Full Length/Span	1300	lbs
Working Load for Sway Force at Full Length/Span	500	lbs
Yaw Moment	440	ft*lbs
Vertical Impact Force (Due to Top Out)	4500	lbs

The extended tow post should be inspected prior to and periodically during testing. While this is generally good practice, it is of especially high importance with this tow post. The tow post relies heavily on the bond between the carbon fiber tube and the titanium parts. In fact, without the contributions of the epoxy, and considering a hypothetical scenario such that the post is held together only by its mechanical fasteners, the post would fail when subjected to the loads in Table 9. Therefore, the post should be inspected for any signs that epoxy bond is compromised.

It is also worth noting that while in the current test configuration the travel is 36.6 in which was more than sufficient for this model test, the extended tow post travel can be increased to approximately 39 in through repositioning and replacement of the existing bump-stops. Prior to making this modification for a future test, the engineer responsible should take into consideration potential impact loading for their particular test setup.

The extended tow post represents a new capability for NSWCCD. On a relative basis, the post has a large amount of heave travel, is lightweight, is stiff, and withstands large loads. It lends itself to future towed model tests involving planing craft and other high speed vehicles. Table 10 illustrates some typical planing boat parameters for which the extended tow post is a very likely option.

For more information on the extended tow post, please reach out to Code 85 Surface Ship Hydromechanics Division, Code 89 Facilities Engineering and Operations Division, or any of the authors of this technical report.

Table 10. Typical Model Parameters

Typical Planing Boat Model Sizes for Use with Extended Tow Post		
Model Weight	≤ 275	lbs
Model Length	≤ 120	in
Model Beam	≤ 34	in
Model Speed	≤ 65	fps
Wave Slope	≥ 1/50	-
Significant Wave Height	≤ 14	in
Model Acceleration	≤ 16	g

METHODOLOGY

Prior to the discussion on the analysis of test data, the methodology will be called out and documented in this section. As is often the case in any data analysis effort, there are often multiple methods that can be considered.

Physical Variables

It is useful to first state the primary variables that were considered in the statistical analyses. These variables consist of the time series values of the following: wave elevation (ς, positive up), x-force (F_x, positive forward), heave (z, positive up), pitch (θ, positive bow down), vertical acceleration at the bow (a_{bow}, positive up), vertical acceleration at the CG (a_{CG}, positive up), point pressure ($P11' - P51$, positive values only), grillage plating differential pressure ($G1$-$G10$, positive values only), and grillage stiffener strain measurements ($G11$-$G25$, positive in tension).

From each of these primary variables, at least one secondary variable was calculated via peak identification. The secondary variables were calculated using the Zero Crossing (ZC) method, the Standard "g" (STDG) method, and/or a pressure and grillage (P/G) peak identification method for irregular wave data.

Zero Crossing Method for Peak Identification

The Zero Crossing method to determine secondary variables finds the height or amplitude (maximum or minimum) value associated with the mean zero crossing period; this value is referred to as the secondary variable. The ZC method was used in Diez et al. [14] to statistically compare experimental data to CFDShip-Iowa calculations of a towed Delft Catamaran in rough water. First, each time series is segmented by the zero crossings. Then, the maximum or minimum value, and the corresponding time step for this value, is determined for each time series segment; the maximum is evaluated if the time series segment has positive data, and the minimum is evaluated if the time series segment has negative data. If the secondary variable of interest is an amplitude value, the ZC method is complete. If the secondary variable of interest is height, the sequential maximum and minimum values are differenced.

For both regular wave (RW) and irregular wave (IW) runs, height was determined for time series of ς, F_x, z, and θ, and the maximum amplitude was determined for a_{bow} and a_{CG}. The

time between sequential maxima of the ς time series was also used to calculate wave period from the ZC method.

Standard G Method for Peak Identification

The Standard G method, based on Riley et al. [15] and Riley and Coats [16], presents a standardized method to compute the 1/nth highest accelerations from acceleration data recorded from small craft full-scale trials. This peak identification method uses standardized minimum vertical and horizontal thresholds to prevent identification of low amplitude, high frequency peaks that are found in test data. The standard deviation of the time series was used as the vertical threshold. The mean value of the time series was removed prior to the calculation of this standard deviation for variables ς, a_{bow}, a_{CG}, z, and θ but not F_x. The horizontal threshold was set to 0.22 s, which is the scaled encounter period cutoff from Riley et al. [15]. These thresholds were implemented using the built-in "islocalmax" and "islocalmin" functions in MATLAB to identify positive and negative peaks.

A comparison of the Zero Crossing and Standard G peak identification methods is shown in Figure 34. Positive peaks, or crests, are identified in blue; and negative peaks, or trough, are identified in red. The solid circles indicate the ZC method, while the open circles indicate STDG method. In this way, the apparent differences in method can be observed by the reader. The STDG method identified fewer low amplitude peaks, and therefore the identified wave height values will not be the same between the two methods.

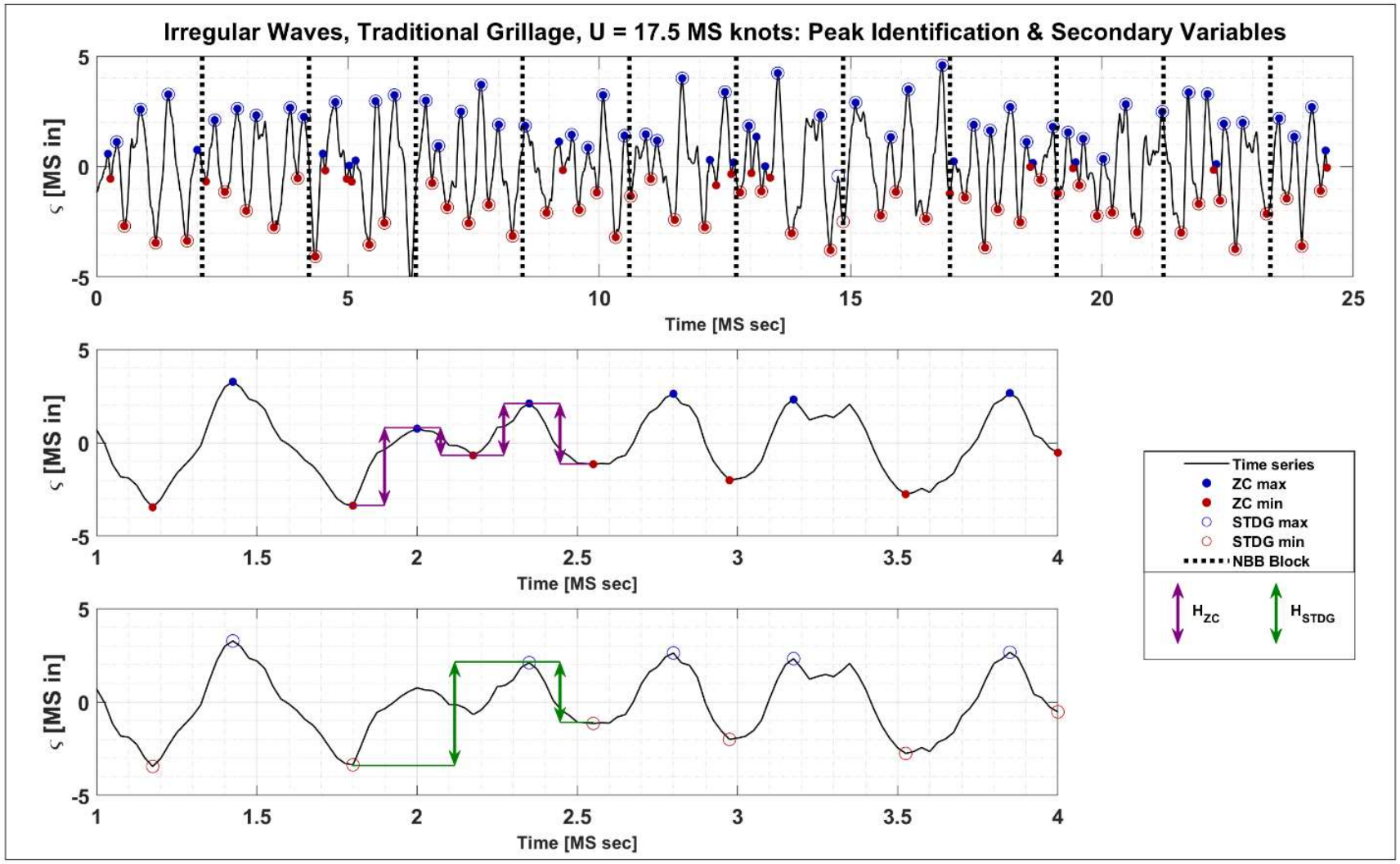

Figure 34. Example of Peak Identification Methods

Pressure and Grillage Peak Identification Method for Irregular Waves

For both grillages and the pressure transducer channels, each channel was mode-zeroed before the peaks were located. Figure 35 provides an example of the mode-zero procedure. The magnitude of the peaks (blue circles) was corrected by finding the mode (given by the red circle for positive peaks, green circle for negative peaks) of the 10,000 points before the peak (this range is given by the two red x's for positive peaks, two green x's for negative peaks) and subtracting that baseline from the magnitude of the peak. This corrected for any drifting that occurred throughout the run. For channels with sporadic noise spikes, any erroneously identified noise peaks were corrected during a manual inspection, if possible. Peaks have been collected and tabulated for each set of channels; positive peaks were recorded for differential bending channels (G1-G10) and pressure transducer channels (P11-P23). Positive and negative peaks were recorded for single strain channels (G11-G25). Note positive values of strain correspond to the gage in tension, and negative values of strain correspond to the gage in compression. To identify peaks, a vertical threshold of 15 % of the time series maximum was used, and a horizontal threshold of 3,500 samples (0.14 s) was used.

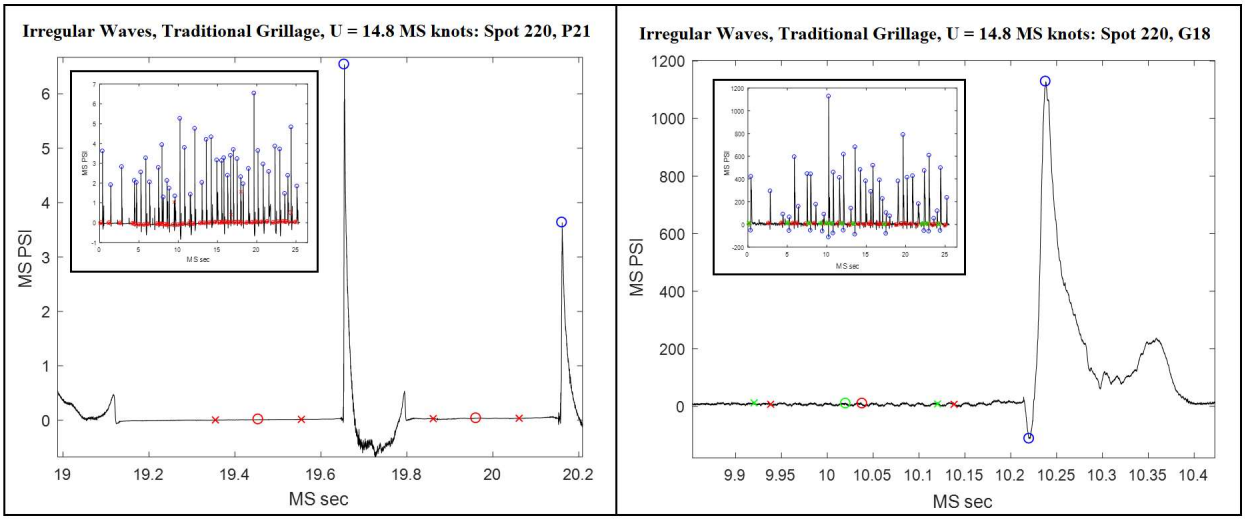

Figure 35. Example of the Pressure and Grillage Peak Identification

Statistical Variables

Future comparisons of model test data to numerical predictions (CFD/CSD) will be made on statistical variables of interest. These include the mean value or expected value, EV, the standard deviation, SD, the average of the one-nth largest peaks, $EV_{1/n}$, for n of 3, 10, and 100 (i.e. $EV_{1/3}$, $EV_{1/10}$, and $EV_{1/100}$). These statistical variables of interest have been calculated for the model test dataset and are presented within this technical report.

The statistical variables of interest are defined as follows. For a primary variable time series $x_i = x(t_i)$ for $i = 1, \ldots, N$ samples. For a secondary variable, where N values of height/amplitude have been identified, the corresponding series of x_i defined by Equations 1, 2, and 3 are the standard definitions of EV, SD, and $EV_{1/n}$, respectively.

$$EV = \frac{1}{N}\sum_i^N x_i \qquad \text{for } i = 1, \dots, N \tag{1}$$

$$SD = \left(\frac{1}{N-1}\sum_i^N (x_i - EV)^2\right)^{1/2} \quad \text{for } i = 1, \dots, N \tag{2}$$

$$EV_{1/n} = \frac{1}{\frac{1}{n}N}\sum_i^{\frac{1}{n}N} x_i \qquad \text{for } x_i \text{ sorted largest to smallest} \tag{3}$$

The test matrix, shown in Table 8, indicates the number of wave encounters required for each irregular wave test condition. For regular wave configurations, three to five repeat spots were completed for each configuration. For irregular wave configurations, 15 to 43 repeat spots were completed for each configuration in order to collect the desired number of wave encounters. Consequently, the equations for the statistical variables need to be adapted to account for the multiple-spot data acquisition per Belenky et al. [17] and ITTC 7.5-02-01-08 [18].

The mean value for a single spot, EV_j, is then computed with Equation 4. A set of $j = 1, \dots, N_r$ expected values is generated for N_r spots/runs. Next, the ensemble or configuration mean value, EV_a, is computed from all EV_j with Equation 5, where W_j are the run weights (Equation 6). The ensemble or configuration number samples, N_a, is computed with Equation 7.

$$EV_j = \frac{1}{N_j}\sum_i^{N_j} x_i \qquad \text{for } i = 1, \dots, N_j \tag{4}$$

$$EV_a = \sum_j^{N_r} W_j EV_j \qquad \text{for } j = 1, \dots, N_r \tag{5}$$

$$W_j = \frac{N_j}{N_a} \tag{6}$$

$$N_a = \sum_j^{N_r} N_j \qquad \text{for } j = 1, \dots, N_r \tag{7}$$

The standard deviation for a single spot, SD_j, is a function of the ensemble mean and is computed with Equation 8. Lastly, the ensemble or configuration standard deviation, SD_a, is computed from all SD_j with Equation 9. Note Equations 8 and 9 are formulated in the form of the variance but written using the SD_j and SD_a variables, respectively, since the variance is equal to the square of the standard deviation.

$$(SD_j)^2 = \frac{1}{N_j - 1}\sum_i^{N_j} (x_i - EV_a)^2 \text{ for } \; i = 1, \dots, N_j \tag{8}$$

$$(SD_a)^2 = \sum_j^{N_r} W_j (SD_j)^2 \qquad \text{for } j = 1, \dots, N_r \tag{9}$$

The average of the one-nth largest peaks, $EV_{1/n}$, statistical variable by definition is associated with secondary variables only. Equation 3 specifies that the x_i values must be sorted largest to smallest. Consequently, the spot averaged of the one-nth largest peaks, $EV_{\frac{1}{n},j}$, and the ensemble averaged of the one-nth largest peaks, $EV_{\frac{1}{n},a}$, were calculated with Equations 10 and 11, respectively.

$$EV_{\frac{1}{n},j} = \frac{1}{\frac{1}{n}N_j}\sum_i^{\frac{1}{n}N_j} x_i \qquad \text{for } x_i \text{ sorted largest to smallest} \tag{10}$$

$$EV_{\frac{1}{n},a} = \frac{1}{\frac{1}{n}N_a}\sum_{i}^{\frac{1}{n}N_a} x_i \qquad \text{for } x_i \text{ sorted largest to smallest} \tag{11}$$

Statistical Estimators and Confidence Intervals

The autocovariance (AC) method for primary variables, non-overlapping bootstrap (NBB) method for primary variables, and bootstrap method for secondary variables were used to calculate validation values and confidence interval values for EV and SD. The bootstrap method for secondary variables was also used to calculate validation values and confidence interval values for $EV_{1/3}$, $EV_{1/10}$, and $EV_{1/100}$. These methods and confidence interval based uncertainty calculations are further described in Appendix E.

Validation Metrics

Total uncertainty at the 95% confidence level for any of the aforementioned methods (AC, NBB, or bootstrapping) is computed with Equation 12, where U_V is total uncertainty for statistical estimator and variable V, B is the bias or calibration uncertainty at the 95% uncertainty level, and P_V is the precision uncertainty for statistical estimator and variable for method specified (described above). For example, the total uncertainty for the ensemble mean value will be represented as U_{EV_a} and can be reported for the AC, NBB, or bootstrapping methods.

Tabulated uncertainties will be reported as both dimensional values and as percentages computed in the form of Equations 13, 14, and 15; the percentage values were calculated to easily assess the primary source of uncertainty, bias or precision.

$$U_V = \sqrt{B^2 + (P_V)^2} \tag{12}$$

$$\mathrm{B}\%V = 100\frac{B}{V} \tag{13}$$

$$P_V\%V = 100\frac{P_V}{V} \tag{14}$$

$$U_V\%V = 100\frac{U_V}{V} \tag{15}$$

ANALYSIS

This section documents the data analysis effort. The effort began with trimming any spot files for which the speed was not constant. Next, occasional observed dropouts were removed from the wave elevation channels. Appropriate channels were zeroed by removing an offset (including drag force, side force and heave).

The grillage and pressure data was then processed through filtering and peak identification, as were the acceleration measurements. The grillage and pressure data was analyzed and considered from a variety of perspectives. These perspectives include consideration of the single largest magnitude pressure and strain measurement; the largest observed strain at the center of stiffener and associated strains of adjacent locations on the same stiffener at the same instant in time; and the largest observed strain events for a stiffener with consideration that adjacent stiffener responses reach their maximum values at slightly different times for the same wave impact (separated by a few thousandths of a second). Additionally, the rate of severe pressure and strain events was analyzed, and the measured pressure and grillage responses were fit to

Weibull probability distributions to make extreme value estimations. For cases in which the Weibull distribution did not fit the data, a multiplier method approach was used.

Acceleration Analysis

All acceleration data channels were filtered using Kaiser low pass filter with a 250 Hz cutoff frequency to eliminate high frequency noise in these data channels. The filter was selected after analyzing the effect of both cutoff frequency and filter window (Kaiser and Butterworth) in both the time and frequency domains. Vertical acceleration was also corrected for gravitational effects.

Grillage and Pressure Analysis

To document the analysis methods used, the case of a single test condition will be used to serve as an example. The test condition will be the 17.5 knots speed in the irregular wave condition (Hs = 7.4 in, Tp = 2.4 s) using the traditional grillage, which corresponds to Matrix IDs 14 and 15 in the test matrix. Statistics produced for the remaining test conditions using the same analysis methodology can be found in Appendix F.

Channel Quality

Both grillages were manufactured from Accura 60 SLA material, and experienced some distortion over a short amount of time as they were exposed to light and moisture. The optimized grillage seemed to be more dimensionally unstable due to the thinner SLA material as compared to the traditional grillage. Differential bending, single strain, and pressure transducer channels opposite the grillage were analyzed. However, point pressure channels P31 – P51 were not analyzed due to unexplainable characteristic in the time histories. These pressure transducers were lower priority, as they were located further aft on the model.

Table 11 - Table 13 provide a summary of data quality for the traditional grillage, Matrix IDs 14 and 15. The data corresponding to Table 12 and Table 13 that are not marked with channel quality symbol from Table 11 do not have a disqualifier or caveat and can be considered trustworthy. Channel G9 was excluded from the analysis, as the time histories of this channel contained significant noise. For the majority of spot runs, data from channel G13 was excluded as data was distorted by large bands of noise. Investigation of time history data in channels G11, G12, G14, G15, and G16 revealed occurrences of spikes or noise, either near or at the peak event. For these channels, a normalized triangular window filter was applied to localized noisy regions to remove the unwanted noise without attenuating the magnitudes of the peak events. This is explained in the analysis process section.

Table 11. Channel Quality Legend

Legend	Description
**	Bad channel due to noise. Data for this channel not analyzed.
^**	Data is filtered; data is still bad and channel is not analyzed.
$	Channel is not to be trusted. Magnitudes are unreasonably high, likely due to the dimensionally unstable characteristics of the SLA material.
$$	Magnitudes questionable based on quantitative comparison to traditional grillage.
!	Few large noise spikes; generally good data.
^	Peaks distorted by noise; filtered further after smoothing.
^*	Some good events after filtering; other events still distorted by noise.
	Channel ignored.

Table 12. Summary of Data Quality for Matrix ID 14 of the Traditional Grillage

			Differential Bending Channels										Single Strain Channels														Pressure Transducer Channels											
Grillage	Matrix ID	Spot #	G1	G2	G3	G4	G5	G6	G7	G8	G9	G10	G11	G12	G13	G14	G15	G16	G17	G18	G19	G20	G21	G22	G23	G24	G25	P11	P12	P13	P21	P22	P23	P31	P41	P42	P43	P44	P45	P51
Traditional	14	184									**		^**	^**	!										!															
Traditional	14	187									**		^**	^**	!										!															
Traditional	14	190									**		^**	^**	!										!															
Traditional	14	193									**		^**	^**	!										!															
Traditional	14	196									**		^**	^**	!																									
Traditional	14	199									**		^*	^*	**	^	^	^							!															
Traditional	14	202									**		^*	^*	**	^	^	^																						
Traditional	14	205									**		^*	^*	**	^	^	^																						
Traditional	14	208									**		^*	^*	**	^	^	^																						
Traditional	14	237									**		^**	^**	**	^	^	^																						
Traditional	14	240									**		^*	^*	**	^	^	^																						
Traditional	14	243									**		^**	^**	**	^	^	^																						
Traditional	14	246									**		^*	^*	**	^	^	^																						

Table 13. Summary of Data Quality for Matrix ID 15 of the Traditional Grillage

			Differential Bending Channels										Single Strain Channels														Pressure Transducer Channels											
Grillage	Matrix ID	Spot #	G1	G2	G3	G4	G5	G6	G7	G8	G9	G10	G11	G12	G13	G14	G15	G16	G17	G18	G19	G20	G21	G22	G23	G24	G25	P11	P12	P13	P21	P22	P23	P31	P41	P42	P43	P44	P45	P51
Traditional	15	249									**		^*	^*	**	^	^	^																						
Traditional	15	257									**		^*	^*	**	^	^	^																						
Traditional	15	260									**		^*	^*	**	^	^	^																						
Traditional	15	263									**		^*	^*	**	^	^	^																						
Traditional	15	266									**		^*	^*	**	^	^	^																						
Traditional	15	269									**		^*	^*	**	^	^	^																						
Traditional	15	273									**		^*	^*	**	^	^	^																						
Traditional	15	276									**		^*	^*	**	^	^	^																						

Before analyzing the data, each channel's time history was visually inspected to ensure there was no noise interference or other indications that the quality of the channel was compromised. Inspections of physical instrumentation and measured response revealed some channels' polarities were switched during physical installation and wiring of sensors. Affected channels included G1, G2, G4, G5, G8, G10, G15, G16, G20, G21, and G25 for the traditional grillage data, and channels G1, G4, G5, and G16 for the optimized grillage data. This was corrected for the affected channels by way of a -1 multiplier applied to the measured data prior to analysis. This correction is not reflected in the calibration factors in the appendix.

For the traditional grillage, regions of data in channels G11, G12, G14, G15, and G16 exhibited frequencies that were too high to be natural and were believed to be electrical in nature. These dropouts needed to be removed to identify peak magnitudes. These spikes often occurred either at or near the peak event, which distorted the reading of the peak event. This is depicted in Figure 36. The reader should note that Spot 290 is associated with Matrix ID 16, not 14 or 15, and is presented as a good example.

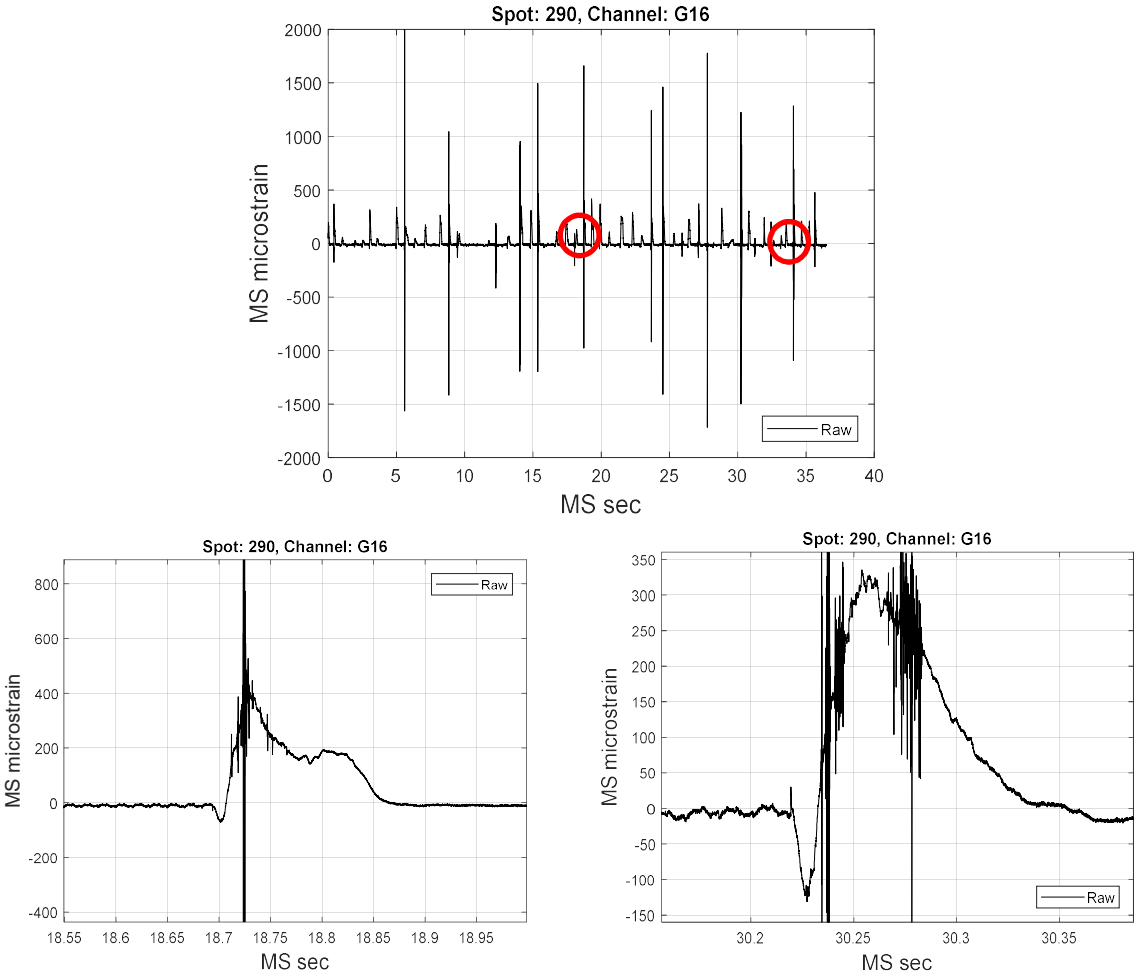

Figure 36. Traditional Grillage Strain Time History of Channel G16 at Spot 290, Displaying Peak Distortions

To address this issue, a normalized triangular window was applied to portions of the data (where noise was significant) to filter and attenuate these spikes using the filtfilt function in MATLAB. An iterative approach was employed to refine the filter and determine the optimal window size (Nw) that would significantly reduce the non-physical spurious points while minimizing the reduction of peak magnitudes. Figure 37 and Figure 38 illustrate this approach on the peaks from Spot 290. It was observed that Nw > 15 attenuates the noise spikes to a point where they no longer interfere with peak detection. A normalized triangular window of Nw = 20 was conservatively selected for filtering to optimize signal peak detection, and was applied to channels G11, G12, G14, G15, and G16 before the peaks were found.

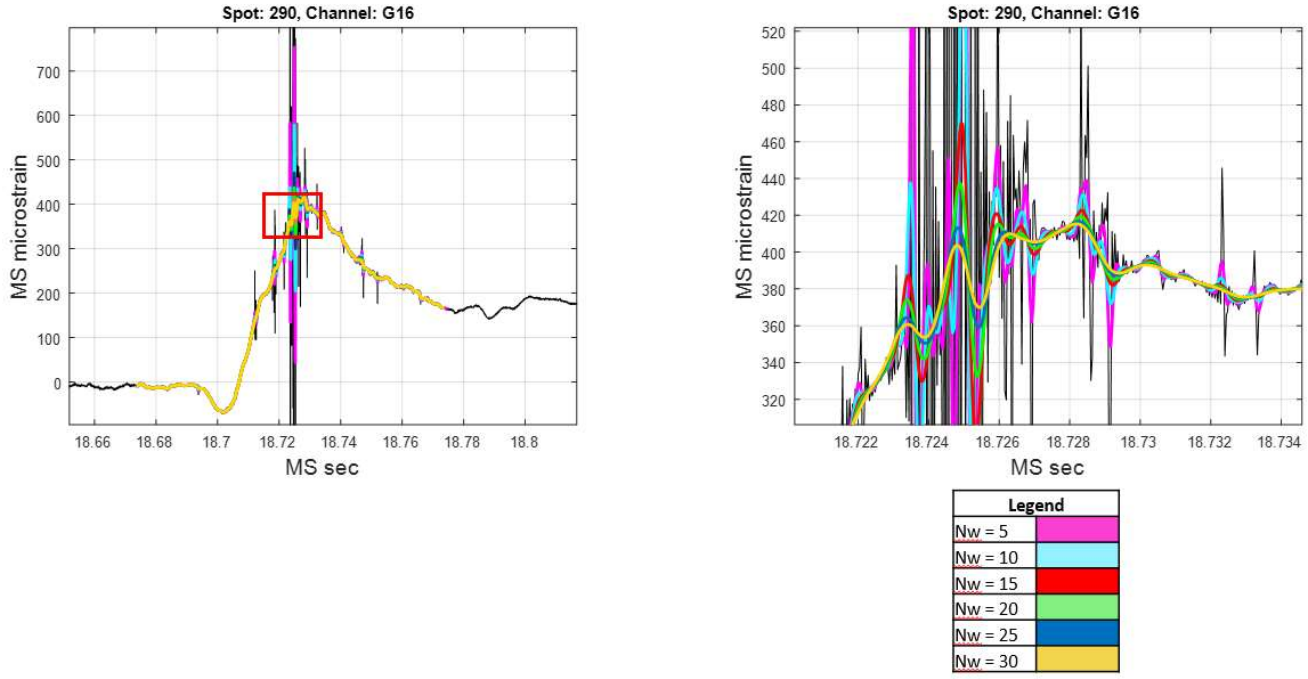

Figure 37. Traditional Grillage Filter Refinement for Peak 1 of Channel G16, Spot 290

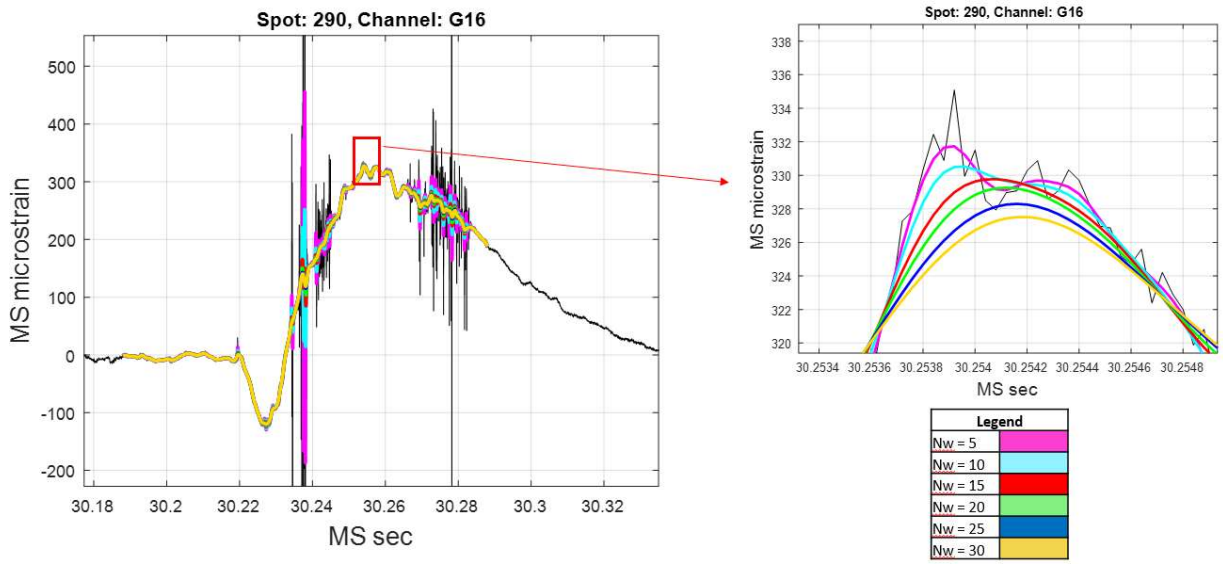

Figure 38. Traditional Grillage Filter Refinement for Peak 2 of Channel G16, Spot 290

Maximum Events by Channel

As part of the analysis procedure maximum events were examined and tabulated. Table 14 - Table 17 provide summaries of the extrema for each pressure and grillage channel during measurements of the traditional grillage. The magnitudes are expressed in terms of model-scale pounds per square inch (MS PSI) in Table 14 and Table 17; and in terms of microstrain in Table 15 and Table 16. The largest event for each type of channel is shown in Figure 39 - Figure 41 for the traditional grillage measurements.

Table 14. Summary Table of Extrema on Differential Bending Channels (Traditional Grillage)

		Extrema									
		Differential Bending Channels (MS PSI)									
Matrix ID	Test Time (MS s)	G1 (+)	G2 (+)	G3 (+)	G4 (+)	G5 (+)	G6 (+)	G7 (+)	G8 (+)	G9 (+)	G10 (+)
14 & 15	761	5	2	11	5	5	6	17	4	--	6
16 & 17	535	4	2	9	4	4	5	14	4	--	6

Table 15. Summary Table of Positive Extrema on Single Strain Channels (Traditional Grillage)

		Extrema														
		Single Strain Channels (microstrain)														
Matrix ID	**Test Time (MS s)**	**G11 (+)**	**G12 (+)**	**G13 (+)**	**G14 (+)**	**G15 (+)**	**G16 (+)**	**G17 (+)**	**G18 (+)**	**G19 (+)**	**G20* (+)**	**G21 (+)**	**G22 (+)**	**G23 (+)**	**G24 (+)**	**G25* (+)**
14 & 15	761	471	1052	1279	1214	506	140	1266	1327	1153	115	168	1164	1241	1173	95
16 & 17	535	448	865	1221	1008	446	117	1021	1093	987	101	209	1004	1084	1044	91

*Results are presented for full disclosure, but the response of this channel was unreliable and it is recommended that these results are not used for comparison with CFD.

Table 16. Summary Table of Negative Extrema on Single Strain Channels (Traditional Grillage)

		Extrema														
		Single Strain Channels (microstrain)														
Matrix ID	**Test Time (MS s)**	**G11 (-)**	**G12 (-)**	**G13 (-)**	**G14 (-)**	**G15 (-)**	**G16 (-)**	**G17 (-)**	**G18 (-)**	**G19 (-)**	**G20* (-)**	**G21 (-)**	**G22 (-)**	**G23 (-)**	**G24 (-)**	**G25* (-)**
14 & 15	761	-188	-335	-320	-464	-437	-910	-191	-198	-186	-603	-254	-137	-158	-173	-352
16 & 17	535	-111	-347	-254	-388	-343	-683	-159	-164	-155	-510	-272	-100	-109	-116	-325

*Results are presented for full disclosure, but the response of this channel was unreliable and it is recommended that these results are not used for comparison with CFD.

Table 17. Summary Table of Extrema on Pressure Transducer Channels (Traditional Grillage)

		Extrema					
		Pressure Transducers (MS PSI)					
Matrix ID	Test Time (MS s)	P11 (+)	P12 (+)	P13 (+)	P21 (+)	P22 (+)	P23 (+)
14 & 15	761	12	11	7	10	7	11
16 & 17	535	9	6	4	9	6	4

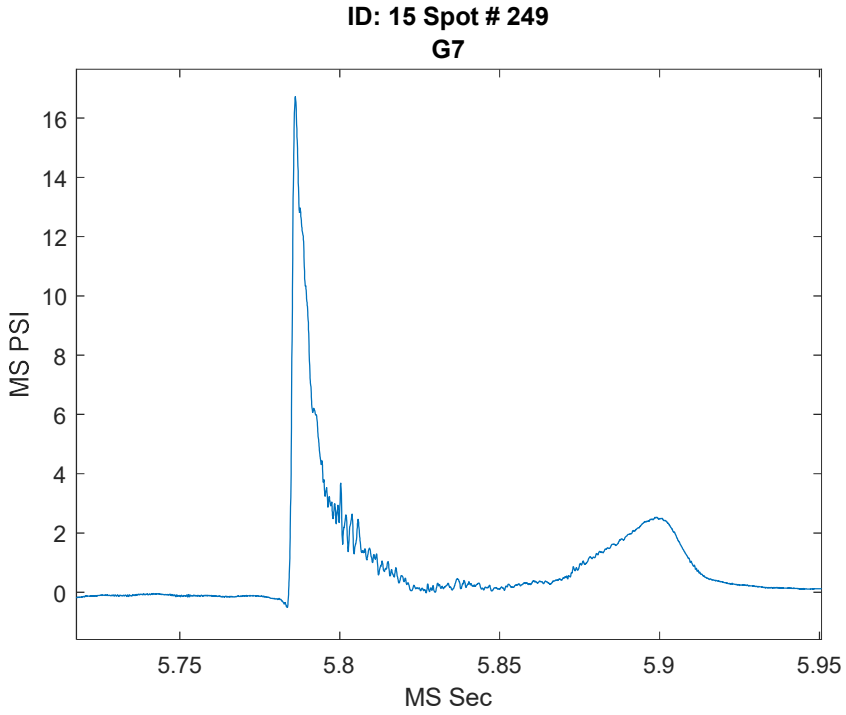

Figure 39. Maximum Event on Channel G7 (Traditional Grillage)

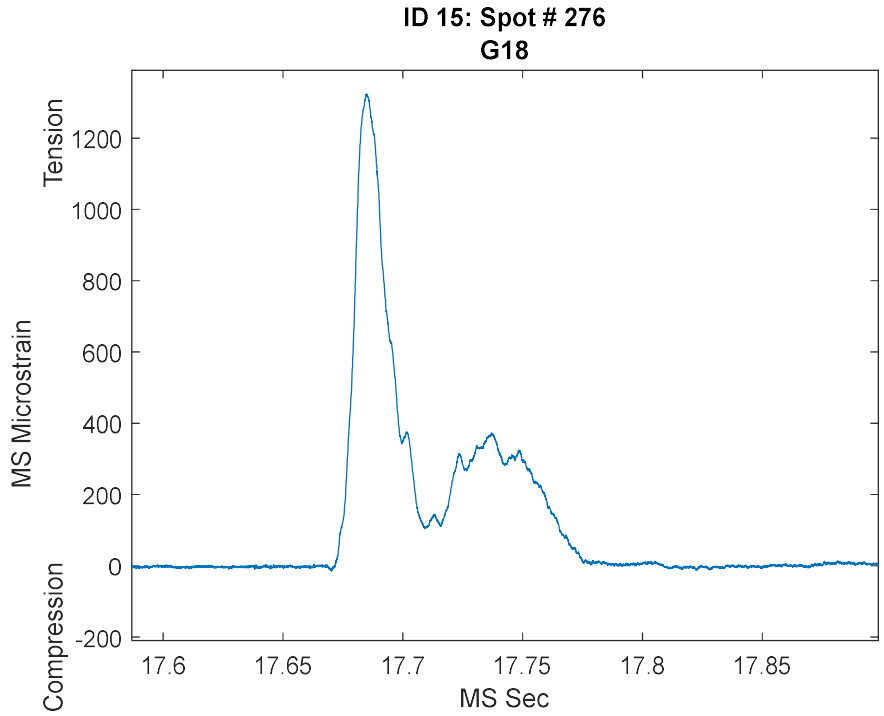

Figure 40. Maximum Event on Channel G18 (Traditional Grillage)

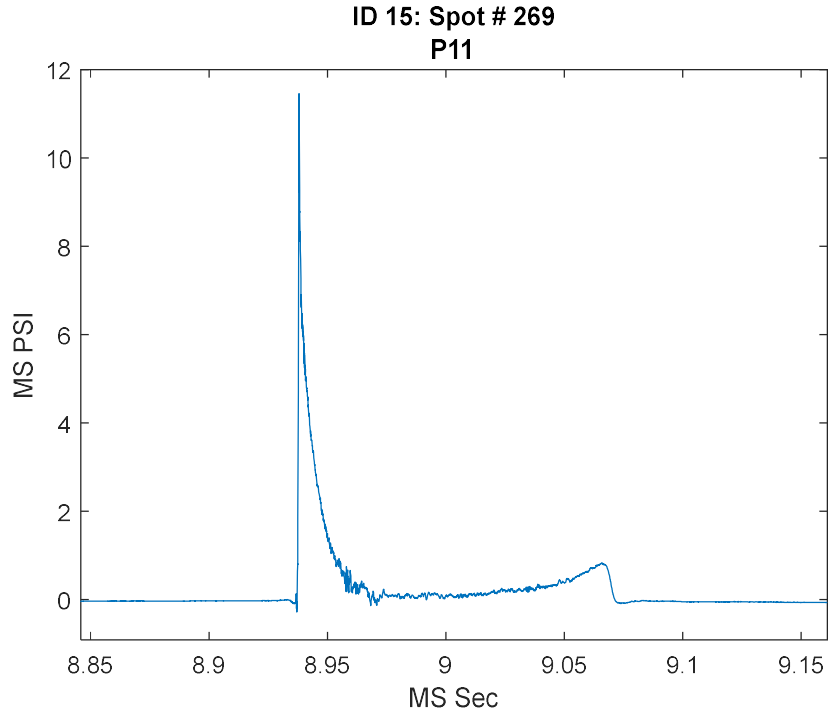

Figure 41. Maximum Event on Channel P11 (Traditional Grillage)

Maximum Events on Center Stiffener Channels by Condition

For the single strain channels, the traditional grillage experienced the largest strains at the center of the stiffeners (at channels G18, and G23). Table 18 and Table 19 list the maximum strains on the center stiffener gages as well as the strains on the other four stiffener gages of the traditional grillage at the time the center gage reached its maximum for each condition. Figure 42 - Figure 46 show the time histories of the five largest events on the center stiffener gages. Maximum strains on gages G11 - G15 were not compiled, as the majority of data in channel G13 was distorted by noise and not considered for this analysis. The strains in matrix condition 14 and 15 (17.5 knots forward speed) are seen to have higher strains than matrix condition 16 and 17 (14.8 knots). This is expected given the higher speed in matrix condition 14 and 15. A more detailed list of the maximum strains on the center gages for each run can be found in Appendix G.

Table 18. Maximum Strain on Channel 18 and Corresponding Stiffener Gage Strains (Traditional Grillage)

		Stiffener Channels G16-G20					
Matrix ID	Run #	Time of Max Strain on Center Stiffener (seconds)	Magnitude of Strain on G16 (microstrain)	Magnitude of Strain on G17 (microstrain)	Magnitude of Strain on G18 (microstrain)	Magnitude of Strain on G19 (microstrain)	Magnitude of Strain on G20 (microstrain)
15	276	17.6848	-815	1253	**1324**	1142	-467

Table 19. Maximum Strain on Channel 23 and Corresponding Stiffener Gage Strains (Traditional Grillage)

		Stiffener Channels G21-G25					
Matrix ID	Run #	Time of Max Strain on Center Stiffener (seconds)	Magnitude of Strain on G21 (microstrain)	Magnitude of Strain on G22 (microstrain)	Magnitude of Strain on G23 (microstrain)	Magnitude of Strain on G24 (microstrain)	Magnitude of Strain on G25 (microstrain)
15	249	5.7888	-150	1145	**1239**	1170	-220

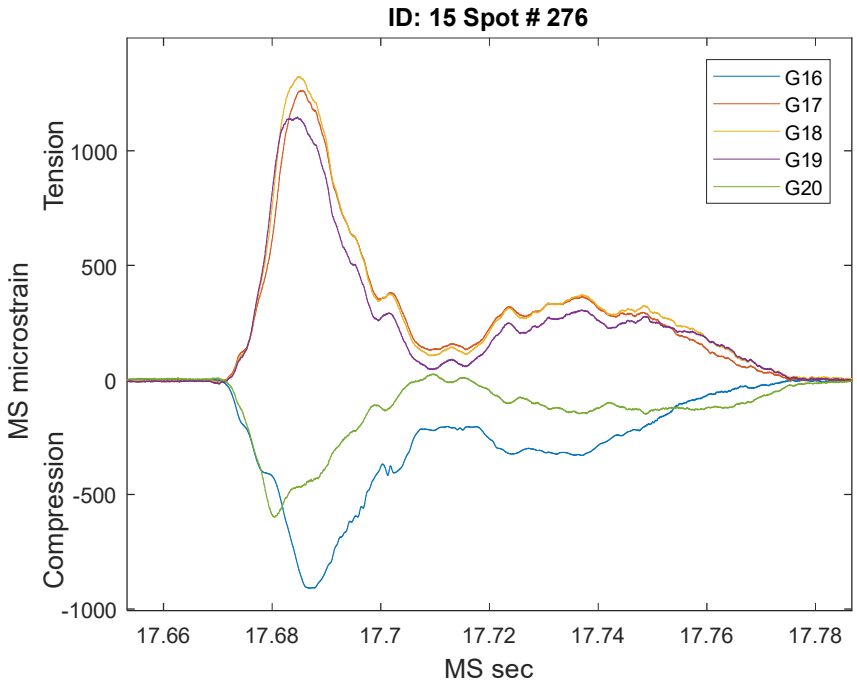

Figure 42. Largest Event on a Stiffener, Condition ID: 15 (Traditional Grillage)

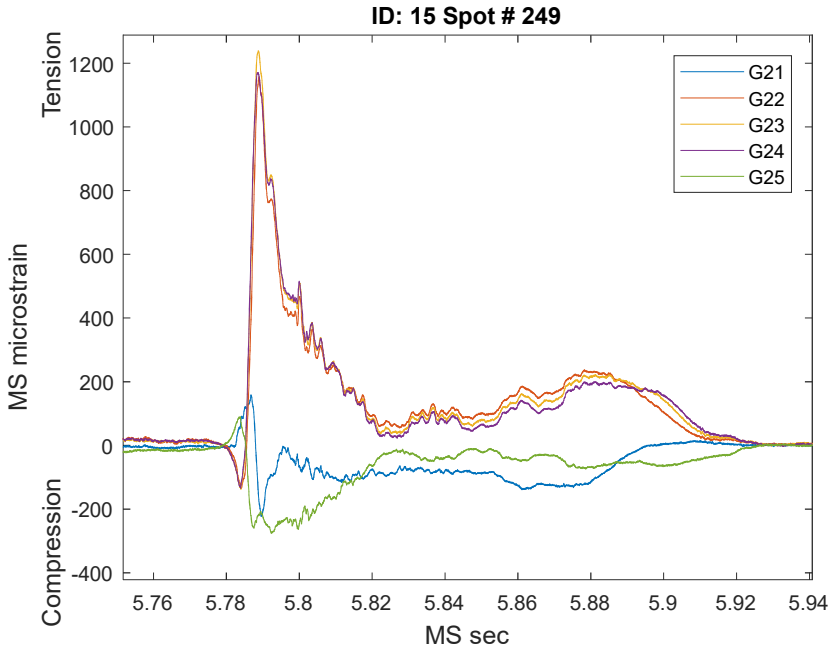

Figure 43. Second Largest Event on a Stiffener, Condition ID: 15 (Traditional Grillage)

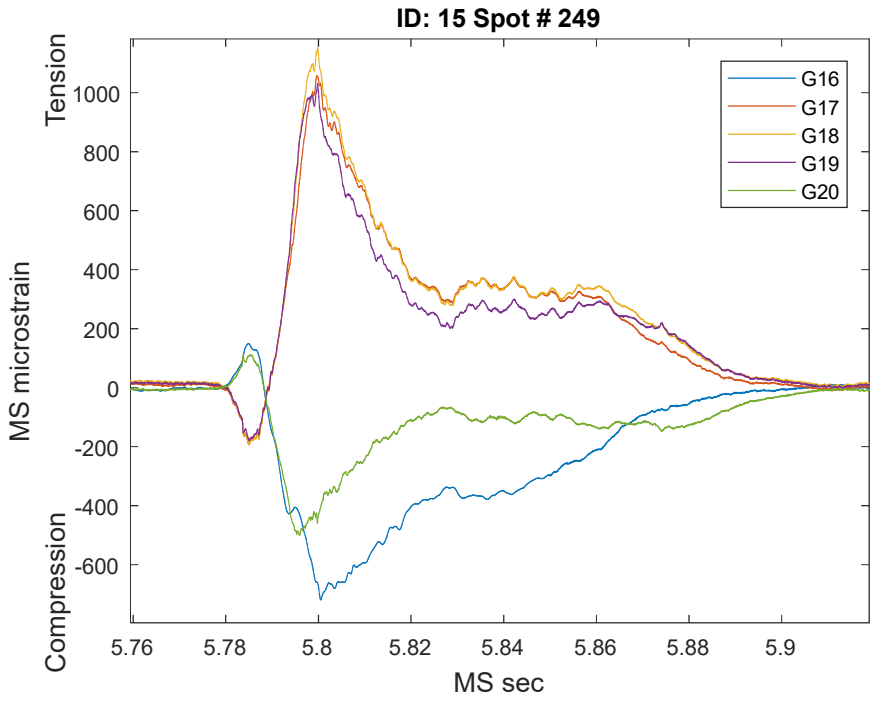

Figure 44. Third Largest Event on a Stiffener, Condition ID: 15 (Traditional Grillage)

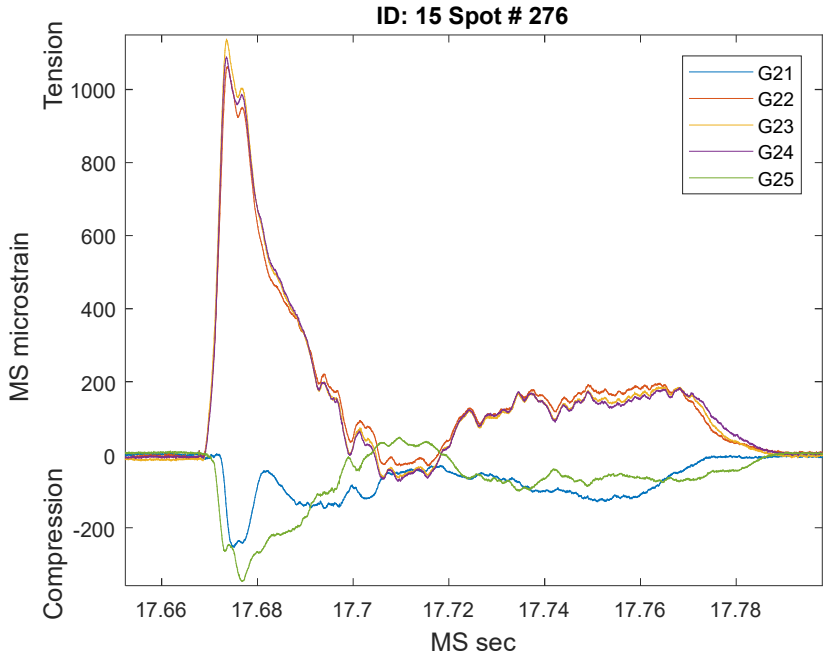

Figure 45. Fourth Largest Event on a Stiffener, Condition ID: 15 (Traditional Grillage)

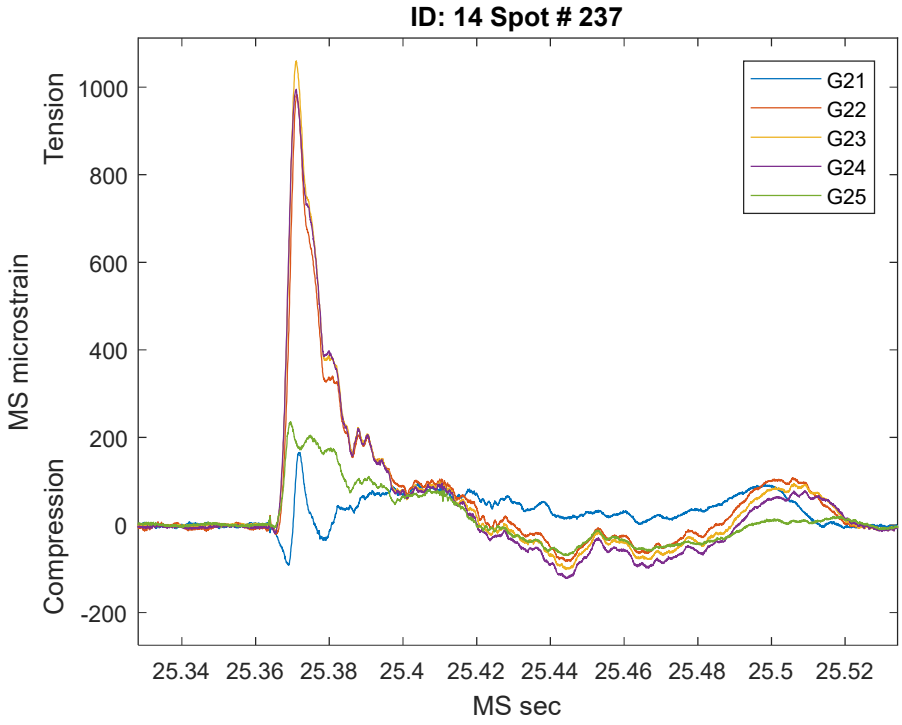

Figure 46. Fifth Largest Event on a Stiffener, Condition ID: 14 (Traditional Grillage)

Maximum Events and Responses on Each Stiffener Channel

Below are the maximum strains at each stiffener channel, as well as the strain values on the other four stiffener channels at the exact time their peak value is reached. These maximum values are tabulated in Table 20 and the events are plotted in Figure 47 and Figure 48. For the spot runs shown, the maximum strain on each stiffener channel is shown to approximately occur at the same point in time. The exception is the 3rd highest extrema (spot run 249) which is shown in Appendix F. The table associated plots are shown for the single largest event observed on the traditional grillage. Tables and plots for the largest five events observed on both the traditional and optimized grillages can be found in Appendix F.

Table 20. Maximum Strains on Each Channel for Largest Event (Traditional Grillage)

Extrema	Matrix ID	Run #	Max Channel	Time of Max Strain (sec)	Magnitude of Strain on G16 (microstrain)	Magnitude of Strain on G17 (microstrain)	Magnitude of Strain on G18 (microstrain)	Magnitude of Strain on G19 (microstrain)	Magnitude of Strain on G20 (microstrain)
1st	15	276	G16	17.6869	-909	1211	1251	1062	-441
			G17	17.6855	-873	1263	1315	1128	-461
			G18	17.6848	-815	1253	1324	1142	-467
			G19	17.6847	-807	1249	1322	1147	-468
			G20	17.6804	-436	695	856	907	-599

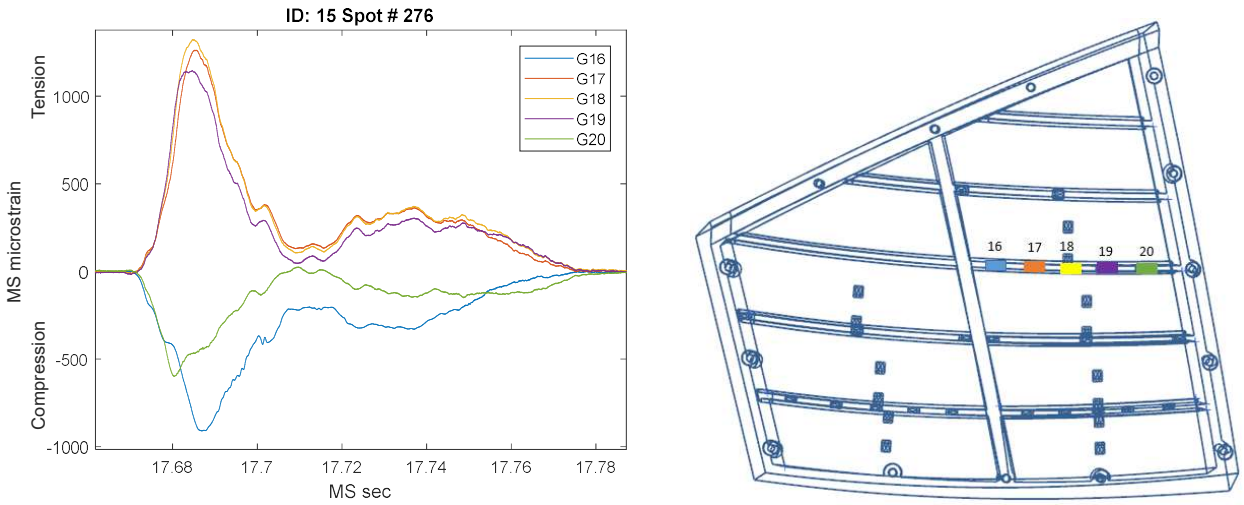

Figure 47. Time History of Largest Event of Traditional Grillage (Left) and Layout of Channels 16-20 on Grillage (Right)

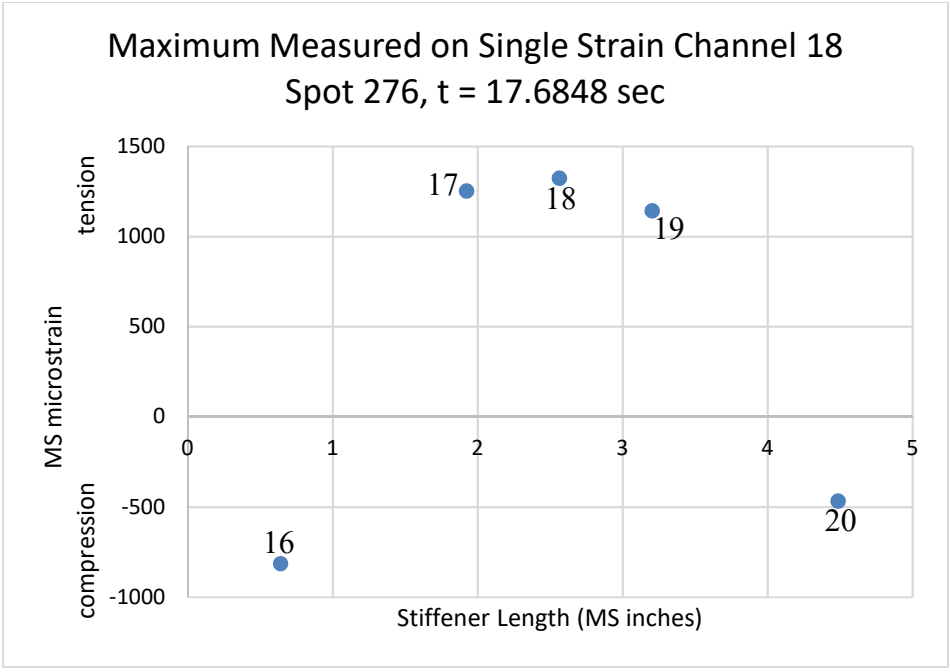

Figure 48. Spatial Distribution of Strains During Peak of Channel 18's Largest Measured Event, Traditional Grillage, Spot 276, t =17.6848 seconds

Severity

As defined in Judge et al. [5], a severe event is one that has a Z greater than 1.5, given by Equation (16) where P is the event magnitude, μ_p is the population mean, and σ is the standard deviation.

$$Z = \frac{P-\mu_p}{\sigma} \tag{16}$$

Severity has been calculated for all measured events for both grillages as a metric for comparison with past tests as well as for future comparison with CFD results.

The number of severe events and rate of severe events for both the traditional and optimized grillages are tabulated and appear in Appendix F. Note that in the tables below, the (+) notation indicates tension on the sensor, while (-) indicates compression.

The rate of severe events was calculated by dividing the number of severe events by the total time in condition. Table 21 - Table 23 summarize the rate of severe events for G1-G25; and Table 24 summarizes the rate of severe events for P11 – P23.

The significance of defining and reporting the number and rate of severe events is that these are statistical measures obtained from testing which allow for future comparisons with CFD/CSD results. Also, this methodology is consistent with analysis conducted following past testing of the GPPH hull form [6].

Table 21. Rate of Severe Events on Differential Bending Channels (Traditional Grillage)

		Rate of Severe Events (Number of Severe Events / Model Scale Seconds)									
		Differential Bending Channels									
Matrix ID	Test Time (MS s)	G1 (+)	G2 (+)	G3 (+)	G4 (+)	G5 (+)	G6 (+)	G7 (+)	G8 (+)	G9 (+)	G10 (+)
14 & 15	761	0.05	0.05	0.05	0.07	0.09	0.09	0.11	0.04	--	0.09

Table 22. Rate of Severe Events on Single Strain Channels G11 - G18 (Traditional Grillage)

		Rate of Severe Events (Number of Severe Events / Model Scale Seconds)														
		Single Strain Channels														
Matrix ID	Test Time (MS s)	G11 (+)	G11 (-)	G12 (+)	G12 (-)	G13 (+)	G13 (-)	G14 (+)	G14 (-)	G15 (+)	G15 (-)	G16 (+)	G16 (-)	G17 (+)	G17 (-)	G18 (+)
14 & 15	761	0.04	0.02	0.03	0.01	0.01	0.01	0.06	0.00	0.10	0.05	0.02	0.00	0.06	0.00	0.06

Table 23. Rate of Severe Events on Single Strain Channels G18 - G25 (Traditional Grillage)

		Rate of Severe Events (Number of Severe Events / Model Scale Seconds)														
		Single Strain Channels														
Matrix ID	Test Time (MS s)	G18 (-)	G19 (+)	G19 (-)	G20* (+)	G20* (-)	G21 (+)	G21 (-)	G22 (+)	G22 (-)	G23 (+)	G23 (-)	G24 (+)	G24 (-)	G25* (+)	G25* (-)
14 & 15	761	0.00	0.07	0.00	0.01	0.07	0.06	0.06	0.10	0.00	0.10	0.01	0.11	0.00	0.01	0.02

*Results are presented for full disclosure, but the response of this channel was unreliable and it is recommended that these results are not used for comparison with CFD.

Table 24. Rate of Severe Events on Pressure Transducer Channels (Traditional Grillage)

		Rate of Severe Events (Number of Severe Events / Model Scale Seconds)					
		Pressure Transducers					
Matrix ID	Test Time (MS s)	P11 (+)	P12 (+)	P13 (+)	P21 (+)	P22 (+)	P23 (+)
14 & 15	761	0.07	0.06	0.03	0.09	0.08	0.04

Weibull Analysis

Weibull Analysis was performed on measured events for both grillages as a metric for comparison with future CFD studies. The goal for Weibull analysis is to estimate maximum loads and pressures that the grillage will experience throughout its operation. This is accomplished by creating a cumulative distribution of the measured peak events and fitting a straight line to the distribution in the Weibull space (modified-log-log space). The Weibull fit can then be used to estimate the probability of event occurrences and/or estimate extrapolated load magnitudes.

The Weibull cumulative density function (CDF) is the governing equation for Weibull analysis and is defined as Equation (17). Rearranging Equation (17) to solve for x results in Equation (18).

$$\boldsymbol{P(x) = \left[1 - e^{-\left(\frac{x-x_0}{\eta-x_0}\right)^{\beta}}\right]} \quad \textbf{(17)}$$

$$\boldsymbol{x_n = (\eta - x_0)\left(ln\left(\frac{1}{1-P(x_n)}\right)^{\frac{1}{\beta}}\right) + x_0} \quad \textbf{(18)}$$

The Weibull fit parameters are as follows:

- ***Magnitude of the nth event, x_n***
- ***Shape parameter, β***: Slope of the Weibull fit. The shape parameter identifies the distribution of the data sample.
- ***Threshold value, x_0***: Analogous to the y-intercept of the fit, and is the value for which no event magnitudes fall below.
- ***Characteristic value, η***: corresponds to a cumulative probability of 0.632. For multiple-point methods, the characteristic value is determined by computing a local fit between 0.5 and 0.764, to estimate the characteristic value corresponding to a 0.632 cumulative probability.
- ***Cumulative probability, P(x)***: When x is equal to the extreme value, the probability of non-exceedance (PNE) of the extreme value is ***P(x)***. This is used to characterize the probability that an event of a certain magnitude is not exceeded.

Two methods were used to fit a linear trend to the distribution in Weibull space: three-parameter linear regression (LR3) and three-parameter moment method (MM3). The Weibull analysis was performed on events from Matrix IDs corresponding to the same conditions. These were matrix IDs 14 and 15 (17.5 knots, Hs = 7.4 in, Tp = 2.4 s) and matrix IDs 16 and 17 (14.8 knots, Hs = 7.4 in, Tp = 2.4 s) for the traditional grillage and matrix IDs 22 and 23 (17.5 knots, Hs = 7.4 in, Tp = 2.4 s) and matrix IDs 24 and 25 (14.8 knots, Hs = 7.4 in, Tp = 2.4 s) for the optimized grillage. The Weibull fit parameters and PNE calculations for the two methods (LR3 and MM3) are presented in the Results section of this technical report for the condition represented by matrix IDs 14 and 15 combined (17.5 knots, traditional grillage). The results for the other conditions are presented in Appendix H.

For cases where the Weibull distribution did not fit the data, a multiplier was applied to the largest values to approximate the 36.8% PNE estimates. The multipliers were derived from cases in which the Weibull distribution fit the data well.

RESULTS AND DISCUSSION

The subsections below will present results of the calm water, regular waves, and irregular wave testing. Extreme value results of the irregular wave data based on the best fits of a probability distribution (Weibull) will also be presented.

Since the purpose of the calm water testing was to ensure consistency relative to previous testing of the GPPH model, the focus of this section of the technical report will be on presenting the measured comparison to illustrate the observed agreement. The purpose of the regular and irregular results, however, is for future comparison with existing CFD/CSD numerical tools as part of a follow-on effort. Therefore, the results are generally presented in tabular form and using the validation variables discussed the methodology section of this technical report.

For common test conditions the measured secondary loads on two grillage panels are contrasted against one another. These results, expressed as a percentage difference, illustrate the extent to which the loads measured on the two grillages differed.

Finally, the results section focuses on a Weibull analysis of the secondary loads measured on the Traditional grillage panel. The results are calculated using two different methods of fitting the probability distribution, and the result with the better fit is presented. Results are shown for various exposure times, and for different PNEs. These Weibull results will serve as additional data for comparison with future CFD/CSD numerical tools.

A set of tabulated results has been created and stored on the Compact Disk (CD) that accompanies this technical report. Please see Appendix H for additional information on the tabulated results.

Calm Water Comparisons with Past Testing

The calm water test results were compared against data collected from previous GPPH test series. The comparisons indicate general agreement as shown in Figure 49 - Figure 51. The variables U, F_X, Θ and z represent model speed, longitudinal force, pitch angle and heave displacement respectively. The apparent offset in running trim between the 2015 test (conducted

at NSWC) and the USNA test was previously documented [6]. The measured running trim of the latest test series remains closer to the 2015 test and within the pitch gage calibration uncertainty of 0.240 deg.

Please note that "GPPH Nov 2015" refers to the testing during November of 2015 also using same high speed basin and carriage, but using a different tow post and different instrumentation [4]. "USNA" refers to testing conducted at the United States Naval Academy [6] [7].

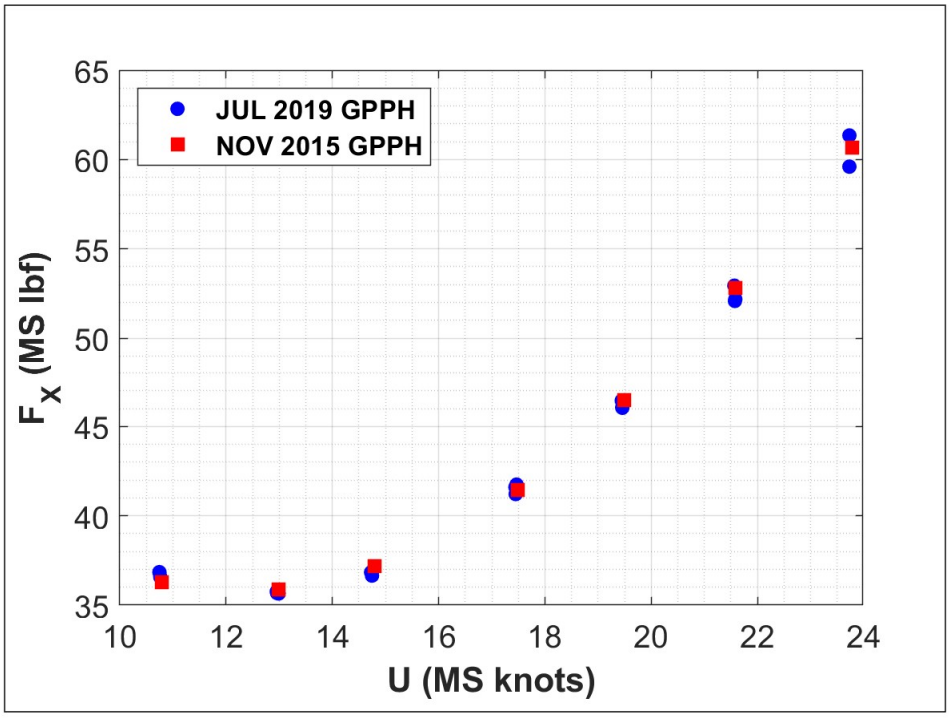

Figure 49. Resistance in Calm Water

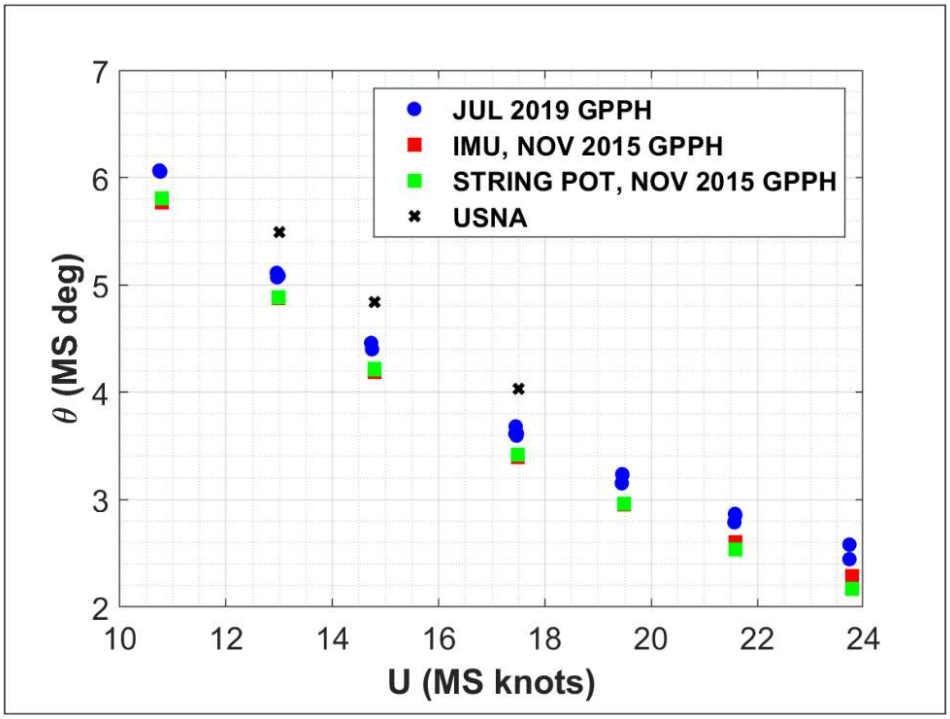

Figure 50. Running Trim in Calm Water

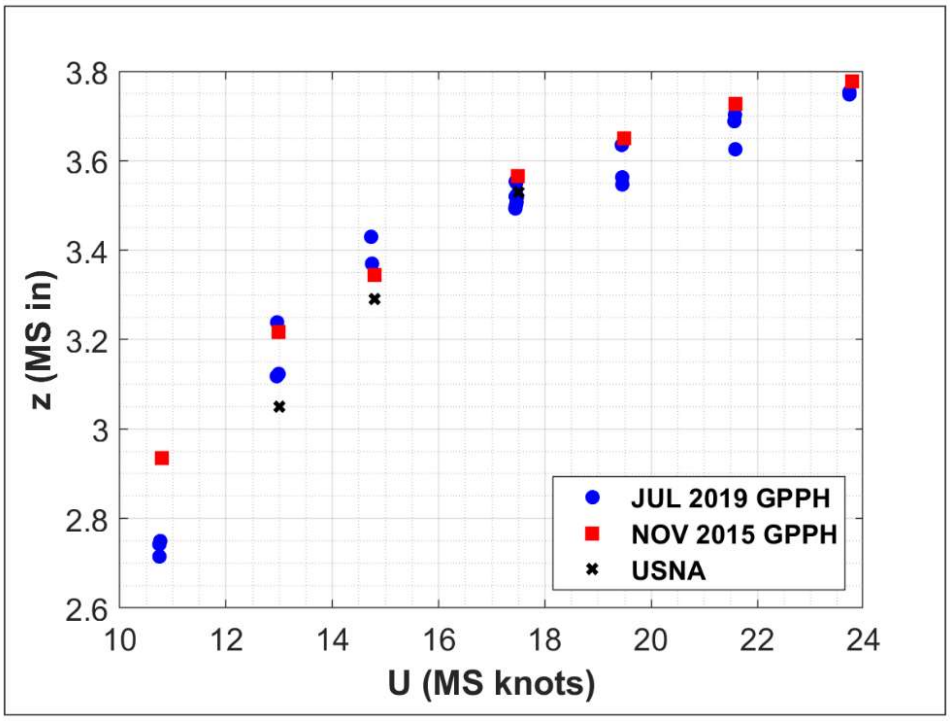

Figure 51. Heave in Calm Water

Regular Waves

The regular wave data included 15 spots; seven spots for the model with the Traditional grillage installed and eight spots for the Optimized grillage. Recall that the desired regular wave consisted of a 5.23 in double-amplitude height, and 2.1 s period. The measured double amplitude wave height, the spot values of EV_j for H, varied from 4.912 ± 0.157 in to 5.515 ± 0.278 in, with all $U_{EV_j}\%EV_j$ <5.4 % for N_j of 6-17 RW cycles. The configuration/ensemble values of EV_a for H vary from 5.037 ± 0.147 MS in to 5.217 ± 0.182 in, with all $U_{EV_a}\%EV_a$ ≤3.5 % for N_a of 43-70 RW cycles. It is worth noting that the configuration/ensemble values are closer to the desired double amplitude height than the spot value and have a maximum percentage of uncertainty, $U_{EV_a}\%EV_a$, that is approximately 35 % smaller. These statistical values for double amplitude height, and the others presented in this subsection, were calculated using the bootstrapping method.

The regular wave results for the measured wave, model drag, and motions appear in Table 25. Since this is the first of a series of similar tables, it's worth mentioning how the table is presented. The first column titled "Variable" is the measurement being presented. The next column, "Grillage", refers to the configuration of the model. That is, whether the model was tested with the Traditional or Optimized grillage installed. Next, "U", refers to the carriage speed. "N_a" refers to the sample size.

The remaining columns refer to the validation variables calculated using the bootstrapping method. It is anticipated that these results will be used for future comparisons with numerical tools. Those columns are as follows: $EV_a, B, P_V, U_V, B\%V, P_V\%V, and\ U_{EV_a}\%EV_a$, representing the ensemble mean (expressed in engineering units), the bias uncertainty (expressed in engineering units), the precision uncertainty (expressed in engineering units), the percentage bias uncertainty, the percentage precision uncertainty, and the percentage total uncertainty. Therefore, this style of table serves as a convenient presentation of the test results.

Table 25. Regular Wave Ensemble Results for H, T_p, a_{bow}, a_{CG}, F_x, θ, and z

Variable	Grillage	U knots	N_a #	V: EV_a	B	P_V	U_V	B%V	P_V%V	U_V%V
H [in]	Traditional	14.8	47	5.037	0.12	0.084	0.147	2.38	1.67	2.91
	Optimized	14.8	70	5.164	0.12	0.118	0.169	2.32	2.29	3.26
	Traditional	17.5	46	5.095	0.12	0.118	0.168	2.36	2.31	3.30
	Optimized	17.5	43	5.217	0.12	0.137	0.182	2.30	2.63	3.50
T_p [sec]	Traditional	14.8	47	2.106	0.007217	0.008	0.011	0.34	0.37	0.51
	Optimized	14.8	70	2.104	0.007217	0.007	0.010	0.34	0.33	0.48
	Traditional	17.5	46	2.103	0.007217	0.008	0.011	0.34	0.39	0.52
	Optimized	17.5	43	2.106	0.007217	0.010	0.012	0.34	0.48	0.59
a_{bow} [g]	Traditional	14.8	47	6.345	0.026	0.279	0.280	0.41	4.40	4.42
	Optimized	14.8	70	6.551	0.026	0.288	0.289	0.40	4.39	4.41
	Traditional	17.5	46	7.915	0.026	0.291	0.292	0.33	3.68	3.69
	Optimized	17.5	43	8.224	0.026	0.244	0.245	0.32	2.97	2.98
a_{cg} [g]	Traditional	14.8	47	1.917	0.0023	0.081	0.082	0.12	4.25	4.25
	Optimized	14.8	70	2.094	0.0023	0.118	0.118	0.11	5.61	5.61
	Traditional	17.5	46	3.233	0.0023	0.214	0.214	0.07	6.62	6.62
	Optimized	17.5	43	3.530	0.0023	0.321	0.321	0.07	9.09	9.09
F_X [lbf]	Traditional	14.8	47	165.120	0.38	7.242	7.252	0.23	4.39	4.39
	Optimized	14.8	70	170.990	0.38	7.281	7.291	0.22	4.26	4.26
	Traditional	17.5	46	210.530	0.38	6.054	6.066	0.18	2.88	2.88
	Optimized	17.5	43	213.350	0.38	4.189	4.206	0.18	1.96	1.97
θ [deg]	Traditional	14.8	47	9.352	0.24	0.075	0.252	2.57	0.81	2.69
	Optimized	14.8	70	9.347	0.24	0.090	0.256	2.57	0.96	2.74
	Traditional	17.5	46	7.598	0.24	0.107	0.263	3.16	1.40	3.46
	Optimized	17.5	43	7.511	0.24	0.133	0.274	3.20	1.77	3.65
z [in]	Traditional	14.8	47	7.018	0.2	0.095	0.222	2.85	1.36	3.16
	Optimized	14.8	70	7.058	0.2	0.129	0.238	2.83	1.83	3.38
	Traditional	17.5	46	6.741	0.2	0.141	0.245	2.97	2.10	3.63
	Optimized	17.5	43	6.774	0.2	0.180	0.269	2.95	2.65	3.97

Table 26. Regular Wave Ensemble Results for $P11$-$P23$

Variable	Grillage	U knots	N_a #	V: EV_a	B	P_V	U_V	B%V	P_V%V	U_V%V
P11 [PSI]	Traditional	14.8	47	2.554	0.034	0.076	0.083	1.33	2.97	3.25
	Optimized	14.8	70	2.579	0.034	0.071	0.079	1.32	2.77	3.07
	Traditional	17.5	46	2.881	0.034	0.065	0.074	1.18	2.27	2.56
	Optimized	17.5	43	2.933	0.034	0.039	0.051	1.16	1.31	1.75
P12 [PSI]	Traditional	14.8	47	2.497	0.032	0.049	0.059	1.28	1.97	2.35
	Optimized	14.8	70	2.530	0.032	0.054	0.063	1.26	2.14	2.49
	Traditional	17.5	46	3.039	0.032	0.044	0.055	1.05	1.45	1.79
	Optimized	17.5	43	3.021	0.032	0.036	0.048	1.06	1.19	1.59
P13 [PSI]	Traditional	14.8	47	1.620	0.013	0.050	0.052	0.80	3.10	3.21
	Optimized	14.8	70	1.635	0.013	0.053	0.054	0.80	3.22	3.31
	Traditional	17.5	46	1.812	0.013	0.031	0.034	0.72	1.71	1.85
	Optimized	17.5	43	1.839	0.013	0.049	0.051	0.71	2.67	2.77
P21 [PSI]	Traditional	14.8	47	3.589	0.038	0.099	0.106	1.06	2.76	2.96
	Optimized	14.8	70	3.380	0.038	0.092	0.100	1.12	2.73	2.95
	Traditional	17.5	46	4.368	0.038	0.082	0.091	0.87	1.89	2.08
	Optimized	17.5	43	4.237	0.038	0.060	0.071	0.90	1.43	1.68
P22 [PSI]	Traditional	14.8	47	2.043	0.039	0.057	0.069	1.91	2.81	3.39
	Optimized	14.8	70	2.212	0.039	0.072	0.082	1.76	3.28	3.72
	Traditional	17.5	46	2.394	0.039	0.062	0.073	1.63	2.58	3.05
	Optimized	17.5	43	2.445	0.039	0.039	0.055	1.60	1.60	2.26
P23 [PSI]	Traditional	14.8	47	1.805	0.067	0.038	0.077	3.71	2.10	4.27
	Optimized	14.8	70	1.815	0.067	0.041	0.078	3.69	2.25	4.32
	Traditional	17.5	46	2.282	0.067	0.039	0.078	2.94	1.72	3.40
	Optimized	17.5	43	2.237	0.067	0.025	0.072	2.99	1.13	3.20

Next, the point pressure results, P11-P23, are presented in Table 26. All $U_{EV_a}\%EV_a$ for $P11$-$P23$ variables were ≤4.32 %. And similar to the motion results, $P11$-$P23$ variables are statistically independent of the grillage type.

The secondary load results, expressed as G1-G25, are presented in Table 27 through Table 30. In Table 27 the results are expressed in pounds per square inch (PSI); in Table 28 to Table 31 the results are expressed in microstrain (denoted μs in these tables). Please note that instances where no data exists are highlighted in blue and instances where the percentage uncertainty exceeds 25 % are highlighted in red. It's also worth noting that the regular wave impacts produced both a positive and a negative spike in the strain measurements located on the grillage stiffeners, channels G11-G25. For this reason the positive spikes were denoted with a "P" and processed separated from the negative spikes, denoted with an "N".

The Traditional grillage and the Optimized grillage results for $G1$, $G3$, $G4$, $G8$, and $G10$ were statistically different. The Optimized grillage differential bending pressures were larger than the Traditional grillage for channels $G1$ and $G4$ and smaller than the Traditional grillage for $G3$, $G8$, and $G10$. Note the results were not statistically different for channel $G5$, and there is insufficient data to complete a comparison for $G2$, $G6$, $G7$, and $G9$.

The optimized grillage channels did not have any positive peaks identified on $G11$, $G20$, and $G25$. The primary peak direction on an outer channel of a stiffener (i.e. $G11$, $G15$, $G16$, $G20$, $G21$, and $G25$) is expected to be negative, and the primary peak direction on an inner channel of a stiffener (i.e. $G12$, $G13$, $G14$, $G17$, $G18$, $G19$, $G22$, $G23$, and $G24$) is expected to be positive. Table 31 presents the percent difference between Optimized grillage and Traditional grillage ensemble mean values, where the results have been separated by primary and secondary directions of strain gauge response; differences that were not statistically significant are highlighted in light orange. The Optimized grillage shows significantly larger strains than the Traditional grillage in the primary response direction on two of the three stiffeners, $G11$-$G15$ and $G21$-$G25$, where these two stiffeners are aligned and closest to keel. The stiffener with channels $G16$-$G20$, which is further away from the keel, shows a varying response along the stiffener: the forward edge channel, $G16$, has a significantly lower strain for the Optimized grillage compared to the Traditional grillage; the two grillages have a statistically equivalent response for the center three channels of the stiffener, $G17$, $G18$, and $G19$; the aft edge channel, $G20$, has a significantly higher strain for the Optimized grillage compared to the Traditional grillage. In general, the measurements between the two grillages (Traditional versus Optimized) are significantly different and the extent to which they differ is quantified in Table 31.

Table 27. Regular Wave Ensemble Results for $G1$-$G10$

Variable	Grillage	U knots	N_a #	V: EV_a	B	P_V	U_V	B%V	P_V%V	U_V%V
G1 [PSI]	Traditional	14.8	47	1.631	0.142	0.041	0.148	8.73	2.51	9.08
	Optimized	14.8	70	2.796	0.173	0.070	0.187	6.18	2.51	6.68
	Traditional	17.5	46	1.850	0.142	0.034	0.147	7.70	1.86	7.92
	Optimized	17.5	43	3.012	0.173	0.075	0.188	5.74	2.49	6.26
G2 [PSI]	Traditional	14.8	47	0.806	0.152	0.015	0.153	18.89	1.85	18.98
	Optimized	14.8	0	NaN	0.500	NaN	NaN	NaN	NaN	NaN
	Traditional	17.5	46	1.132	0.152	0.011	0.153	13.45	0.95	13.48
	Optimized	17.5	0	NaN	0.500	NaN	NaN	NaN	NaN	NaN
G3 [PSI]	Traditional	14.8	47	3.772	0.051	0.060	0.079	1.35	1.60	2.10
	Optimized	14.8	70	2.611	0.377	0.050	0.381	14.45	1.91	14.58
	Traditional	17.5	46	4.654	0.051	0.040	0.065	1.10	0.85	1.39
	Optimized	17.5	43	3.285	0.377	0.035	0.379	11.49	1.07	11.54
G4 [PSI]	Traditional	14.8	47	2.160	0.126	0.044	0.134	5.85	2.02	6.19
	Optimized	14.8	70	2.832	0.138	0.071	0.155	4.87	2.52	5.48
	Traditional	17.5	46	2.706	0.126	0.038	0.132	4.67	1.40	4.87
	Optimized	17.5	43	3.324	0.138	0.039	0.143	4.15	1.16	4.31
G5 [PSI]	Traditional	14.8	47	1.480	0.155	0.030	0.158	10.48	2.01	10.67
	Optimized	14.8	70	1.800	0.199	0.038	0.203	11.06	2.13	11.26
	Traditional	17.5	46	1.996	0.155	0.018	0.156	7.77	0.90	7.82
	Optimized	17.5	43	2.240	0.199	0.024	0.201	8.89	1.08	8.95
G6 [PSI]	Traditional	14.8	47	2.176	0.130	0.044	0.137	5.97	2.04	6.31
	Optimized	14.8	0	NaN	0.603	NaN	NaN	NaN	NaN	NaN
	Traditional	17.5	46	2.701	0.130	0.042	0.136	4.81	1.54	5.05
	Optimized	17.5	0	NaN	0.603	NaN	NaN	NaN	NaN	NaN
G7 [PSI]	Traditional	14.8	47	5.730	0.122	0.132	0.179	2.12	2.30	3.13
	Optimized	14.8	0	NaN	0.294	NaN	NaN	NaN	NaN	NaN
	Traditional	17.5	46	7.550	0.122	0.153	0.196	1.61	2.03	2.59
	Optimized	17.5	0	NaN	0.294	NaN	NaN	NaN	NaN	NaN
G8 [PSI]	Traditional	14.8	47	1.497	0.067	0.060	0.090	4.46	4.03	6.01
	Optimized	14.8	70	1.200	0.065	0.051	0.083	5.42	4.25	6.89
	Traditional	17.5	46	1.142	0.067	0.070	0.097	5.84	6.13	8.47
	Optimized	17.5	43	0.912	0.065	0.064	0.092	7.14	7.05	10.04
G9 [PSI]	Traditional	14.8	0	NaN	0.158	NaN	NaN	NaN	NaN	NaN
	Optimized	14.8	70	0.652	0.409	0.026	0.410	62.69	3.92	62.82
	Traditional	17.5	0	NaN	0.158	NaN	NaN	NaN	NaN	NaN
	Optimized	17.5	43	0.653	0.409	0.026	0.410	62.65	4.05	62.79
G10 [PSI]	Traditional	14.8	47	2.157	0.067	0.045	0.081	3.11	2.10	3.75
	Optimized	14.8	70	1.777	0.064	0.044	0.077	3.57	2.50	4.36
	Traditional	17.5	46	2.590	0.067	0.035	0.076	2.59	1.37	2.93
	Optimized	17.5	43	2.088	0.064	0.027	0.069	3.04	1.27	3.30

NaN: No available data or results | **Uncertainty values where U_V%V > 25%**

Table 28. Regular Wave Ensemble Results for $G11\ P$-$G15\ P$ and $G11\ N$-$G15\ N$

Variable	Grillage	U knots	N_a #	V: EV_a	B	P_V	U_V	B%|V|	P_V%|V|	U_V%|V|
G11 P [με]	Traditional	14.8	0	NaN	37.849	NaN	NaN	NaN	NaN	NaN
	Optimized	14.8	0	NaN	31.012	NaN	NaN	NaN	NaN	NaN
	Traditional	17.5	0	NaN	37.849	NaN	NaN	NaN	NaN	NaN
	Optimized	17.5	0	NaN	31.012	NaN	NaN	NaN	NaN	NaN
G11 N [με]	Traditional	14.8	0	NaN	37.849	NaN	NaN	NaN	NaN	NaN
	Optimized	14.8	70	-898.940	31.012	20.940	37.420	3.45	2.33	4.16
	Traditional	17.5	0	NaN	37.849	NaN	NaN	NaN	NaN	NaN
	Optimized	17.5	43	-1017.100	31.012	14.247	34.128	3.05	1.40	3.36
G12 P [με]	Traditional	14.8	0	NaN	36.420	NaN	NaN	NaN	NaN	NaN
	Optimized	14.8	70	733.780	42.706	20.507	47.374	5.82	2.79	6.46
	Traditional	17.5	0	NaN	36.420	NaN	NaN	NaN	NaN	NaN
	Optimized	17.5	43	840.320	42.706	17.396	46.113	5.08	2.07	5.49
G12 N [με]	Traditional	14.8	0	NaN	36.420	NaN	NaN	NaN	NaN	NaN
	Optimized	14.8	70	-195.790	42.706	7.463	43.353	21.81	3.81	22.14
	Traditional	17.5	0	NaN	36.420	NaN	NaN	NaN	NaN	NaN
	Optimized	17.5	43	-236.850	42.706	5.863	43.106	18.03	2.48	18.20
G13 P [με]	Traditional	14.8	47	458.340	38.746	11.347	40.374	8.45	2.48	8.81
	Optimized	14.8	70	952.420	56.820	21.064	60.599	5.97	2.21	6.36
	Traditional	17.5	46	595.330	38.746	29.339	48.601	6.51	4.93	8.16
	Optimized	17.5	43	1110.700	56.820	14.743	58.702	5.12	1.33	5.29
G13 N [με]	Traditional	14.8	47	-172.890	38.746	4.915	39.057	22.41	2.84	22.59
	Optimized	14.8	70	-243.440	56.820	8.971	57.524	23.34	3.69	23.63
	Traditional	17.5	46	-212.770	38.746	5.827	39.182	18.21	2.74	18.42
	Optimized	17.5	43	-294.150	56.820	7.060	57.257	19.32	2.40	19.47
G14 P [με]	Traditional	14.8	47	479.160	37.531	10.722	39.032	7.83	2.24	8.15
	Optimized	14.8	70	823.550	40.376	15.181	43.136	4.90	1.84	5.24
	Traditional	17.5	46	571.400	37.531	7.120	38.200	6.57	1.25	6.69
	Optimized	17.5	43	984.220	40.376	10.437	41.703	4.10	1.06	4.24
G14 N [με]	Traditional	14.8	47	-152.050	37.531	4.446	37.793	24.68	2.92	24.86
	Optimized	14.8	70	-267.430	40.376	9.418	41.460	15.10	3.52	15.50
	Traditional	17.5	46	-185.950	37.531	4.408	37.789	20.18	2.37	20.32
	Optimized	17.5	43	-323.220	40.376	7.005	40.979	12.49	2.17	12.68
G15 P [με]	Traditional	14.8	47	181.930	24.783	4.492	25.187	13.62	2.47	13.84
	Optimized	14.8	70	56.009	31.902	0.689	31.909	56.96	1.23	56.97
	Traditional	17.5	46	221.660	24.783	4.731	25.230	11.18	2.13	11.38
	Optimized	17.5	43	85.777	31.902	0.912	31.915	37.19	1.06	37.21
G15 N [με]	Traditional	14.8	47	-162.910	24.783	4.459	25.181	15.21	2.74	15.46
	Optimized	14.8	70	-276.810	31.902	8.989	33.144	11.53	3.25	11.97
	Traditional	17.5	46	-188.030	24.783	2.854	24.947	13.18	1.52	13.27
	Optimized	17.5	43	-334.550	31.902	6.190	32.497	9.54	1.85	9.71

NaN: No available data or results | **Uncertainty values where U_V%|V| > 25%**

Table 29. Regular Wave Ensemble Results for $G16\ P$-$G20\ P$ and $G16\ N$-$G20\ N$

Variable	Grillage	U	N_a	V: EV_a	B	P_V	U_V	B%|V|	P_V%|V|	U_V%|V|
		knots	#							
G16 P [με]	Traditional	14.8	47	53.570	55.360	1.818	55.389	103.34	3.39	103.40
	Optimized	14.8	70	64.896	20.673	2.455	20.818	31.86	3.78	32.08
	Traditional	17.5	46	58.701	55.360	1.749	55.387	94.31	2.98	94.36
	Optimized	17.5	43	74.290	20.673	2.584	20.834	27.83	3.48	28.04
G16 N [με]	Traditional	14.8	47	-305.250	55.360	7.690	55.891	18.14	2.52	18.31
	Optimized	14.8	70	-203.470	20.673	6.735	21.743	10.16	3.31	10.69
	Traditional	17.5	46	-363.470	55.360	5.484	55.631	15.23	1.51	15.31
	Optimized	17.5	43	-242.900	20.673	3.190	20.918	8.51	1.31	8.61
G17 P [με]	Traditional	14.8	47	393.410	67.572	8.582	68.115	17.18	2.18	17.31
	Optimized	14.8	70	464.960	59.488	10.417	60.393	12.79	2.24	12.99
	Traditional	17.5	46	470.990	67.572	5.533	67.798	14.35	1.17	14.40
	Optimized	17.5	43	553.920	59.488	6.045	59.794	10.74	1.09	10.80
G17 N [με]	Traditional	14.8	47	-67.282	67.572	2.063	67.604	100.43	3.07	100.48
	Optimized	14.8	70	-127.980	59.488	4.259	59.640	46.48	3.33	46.60
	Traditional	17.5	46	-74.979	67.572	2.159	67.607	90.12	2.88	90.17
	Optimized	17.5	43	-149.420	59.488	4.976	59.696	39.81	3.33	39.95
G18 P [με]	Traditional	14.8	47	416.730	83.573	8.530	84.007	20.05	2.05	20.16
	Optimized	14.8	70	433.380	46.515	9.260	47.428	10.73	2.14	10.94
	Traditional	17.5	46	502.020	83.573	5.656	83.764	16.65	1.13	16.69
	Optimized	17.5	43	520.360	46.515	5.374	46.825	8.94	1.03	9.00
G18 N [με]	Traditional	14.8	47	-71.134	83.573	2.261	83.604	117.49	3.18	117.53
	Optimized	14.8	70	-136.010	46.515	4.396	46.723	34.20	3.23	34.35
	Traditional	17.5	46	-79.715	83.573	2.381	83.607	104.84	2.99	104.88
	Optimized	17.5	43	-160.090	46.515	5.291	46.815	29.06	3.31	29.24
G19 P [με]	Traditional	14.8	47	368.870	88.384	6.922	88.654	23.96	1.88	24.03
	Optimized	14.8	70	293.210	64.510	5.838	64.774	22.00	1.99	22.09
	Traditional	17.5	46	445.860	88.384	5.143	88.533	19.82	1.15	19.86
	Optimized	17.5	43	356.900	64.510	4.218	64.648	18.08	1.18	18.11
G19 N [με]	Traditional	14.8	47	-64.039	88.384	1.959	88.405	138.02	3.06	138.05
	Optimized	14.8	70	-127.170	64.510	4.009	64.635	50.73	3.15	50.83
	Traditional	17.5	46	-71.625	88.384	2.225	88.412	123.40	3.11	123.44
	Optimized	17.5	43	-150.530	64.510	4.697	64.681	42.86	3.12	42.97
G20 P [με]	Traditional	14.8	47	39.497	130.540	1.139	130.550	330.51	2.88	330.52
	Optimized	14.8	0	NaN	36.690	NaN	NaN	NaN	NaN	NaN
	Traditional	17.5	46	43.474	130.540	1.137	130.550	300.28	2.62	300.29
	Optimized	17.5	0	NaN	36.690	NaN	NaN	NaN	NaN	NaN
G20 N [με]	Traditional	14.8	47	-200.180	130.540	3.791	130.600	65.21	1.89	65.24
	Optimized	14.8	70	-401.150	36.690	10.213	38.085	9.15	2.55	9.49
	Traditional	17.5	46	-247.260	130.540	3.101	130.580	52.80	1.25	52.81
	Optimized	17.5	43	-437.770	36.690	8.148	37.584	8.38	1.86	8.59

Table 30. Regular Wave Ensemble Results for $G21\ P$-$G25\ P$ and $G21\ N$-$G25\ N$

Variable	Grillage	U knots	N_a #	V: EV_a	B	P_V	U_V	B%|V|	P_V%|V|	U_V%|V|
G21 P [με]	Traditional	14.8	47	75.664	25.204	1.967	25.281	33.31	2.60	33.41
	Optimized	14.8	70	54.556	19.330	1.236	19.369	35.43	2.26	35.50
	Traditional	17.5	46	88.560	25.204	1.699	25.261	28.46	1.92	28.52
	Optimized	17.5	43	80.375	19.330	0.859	19.349	24.05	1.07	24.07
G21 N [με]	Traditional	14.8	47	-108.230	25.204	2.409	25.319	23.29	2.23	23.39
	Optimized	14.8	70	-371.080	19.330	10.387	21.944	5.21	2.80	5.91
	Traditional	17.5	46	-143.790	25.204	2.083	25.290	17.53	1.45	17.59
	Optimized	17.5	43	-448.340	19.330	7.651	20.789	4.31	1.71	4.64
G22 P [με]	Traditional	14.8	47	432.930	38.897	10.284	40.234	8.98	2.38	9.29
	Optimized	14.8	70	809.510	16.099	21.383	26.765	1.99	2.64	3.31
	Traditional	17.5	46	531.380	38.897	8.426	39.799	7.32	1.59	7.49
	Optimized	17.5	43	971.110	16.099	11.914	20.028	1.66	1.23	2.06
G22 N [με]	Traditional	14.8	47	-47.803	38.897	0.926	38.908	81.37	1.94	81.39
	Optimized	14.8	70	-105.310	16.099	2.931	16.363	15.29	2.78	15.54
	Traditional	17.5	46	-50.253	38.897	0.980	38.909	77.40	1.95	77.43
	Optimized	17.5	43	-123.260	16.099	4.043	16.599	13.06	3.28	13.47
G23 P [με]	Traditional	14.8	16	471.220	41.110	18.331	45.011	8.72	3.89	9.55
	Optimized	14.8	70	857.620	30.279	22.495	37.721	3.53	2.62	4.40
	Traditional	17.5	33	566.870	41.110	12.114	42.857	7.25	2.14	7.56
	Optimized	17.5	43	1029.500	30.279	13.331	33.084	2.94	1.29	3.21
G23 N [με]	Traditional	14.8	16	-51.353	41.110	1.131	41.125	80.05	2.20	80.08
	Optimized	14.8	70	-109.360	30.279	2.479	30.380	27.69	2.27	27.78
	Traditional	17.5	33	-51.163	41.110	1.464	41.136	80.35	2.86	80.40
	Optimized	17.5	43	-126.380	30.279	4.094	30.554	23.96	3.24	24.18
G24 P [με]	Traditional	14.8	47	435.840	45.227	10.746	46.486	10.38	2.47	10.67
	Optimized	14.8	52	629.580	28.448	17.034	33.157	4.52	2.71	5.27
	Traditional	17.5	46	532.290	45.227	9.107	46.135	8.50	1.71	8.67
	Optimized	17.5	43	811.250	28.448	22.789	36.450	3.51	2.81	4.49
G24 N [με]	Traditional	14.8	47	-53.914	45.227	0.962	45.237	83.89	1.79	83.91
	Optimized	14.8	52	-102.240	28.448	3.938	28.719	27.83	3.85	28.09
	Traditional	17.5	46	-53.236	45.227	1.064	45.239	84.96	2.00	84.98
	Optimized	17.5	43	-121.540	28.448	6.646	29.214	23.41	5.47	24.04
G25 P [με]	Traditional	14.8	47	44.519	65.669	0.788	65.674	147.51	1.77	147.52
	Optimized	14.8	0	NaN	15.599	NaN	NaN	NaN	NaN	NaN
	Traditional	17.5	46	41.507	65.669	0.808	65.674	158.21	1.95	158.22
	Optimized	17.5	0	NaN	15.599	NaN	NaN	NaN	NaN	NaN
G25 N [με]	Traditional	14.8	47	-123.260	65.669	2.892	65.733	53.28	2.35	53.33
	Optimized	14.8	70	-535.670	15.599	15.270	21.829	2.91	2.85	4.08
	Traditional	17.5	46	-144.990	65.669	2.486	65.716	45.29	1.71	45.32
	Optimized	17.5	43	-651.750	15.599	10.867	19.011	2.39	1.67	2.92
NaN: No available data or results						Uncertainty values where U_V%|V| > 25%				

Table 31. Contrast of Traditional to Optimized Grillage in Regular Waves

Primary Direction of Response for the Strain Gauge								
Variable	U knots	V: EV_a $(V_O - V_T)/(V_T)$	Variable	U knots	V: EV_a $(V_O - V_T)/(V_T)$	Variable	U knots	V: EV_a $(V_O - V_T)/(V_T)$
G11 N [με]	14.8	NaN	G16 N [με]	14.8	-33.3%	G21 N [με]	14.8	242.9%
	17.5	NaN		17.5	-33.2%		17.5	211.8%
G12 P [με]	14.8	NaN	G17 P [με]	14.8	18.2%	G22 P [με]	14.8	87.0%
	17.5	NaN		17.5	17.6%		17.5	82.8%
G13 P [με]	14.8	107.8%	G18 P [με]	14.8	4.0%	G23 P [με]	14.8	82.0%
	17.5	86.6%		17.5	3.7%		17.5	81.6%
G14 P [με]	14.8	71.9%	G19 P [με]	14.8	-20.5%	G24 P [με]	14.8	44.5%
	17.5	72.2%		17.5	-20.0%		17.5	52.4%
G15 N [με]	14.8	69.9%	G20 N [με]	14.8	100.4%	G25 N [με]	14.8	334.6%
	17.5	77.9%		17.5	77.0%		17.5	349.5%
Secondary Direction of Response for the Strain Gauge								
G11 P [με]	14.8	NaN	G16 P [με]	14.8	21.1%	G21 P [με]	14.8	-27.9%
	17.5	NaN		17.5	26.6%		17.5	-9.2%
G12 N [με]	14.8	NaN	G17 N [με]	14.8	90.2%	G22 N [με]	14.8	120.3%
	17.5	NaN		17.5	99.3%		17.5	145.3%
G13 N [με]	14.8	40.8%	G18 N [με]	14.8	91.2%	G23 N [με]	14.8	113.0%
	17.5	38.2%		17.5	100.8%		17.5	147.0%
G14 N [με]	14.8	75.9%	G19 N [με]	14.8	98.6%	G24 N [με]	14.8	89.6%
	17.5	73.8%		17.5	110.2%		17.5	128.3%
G15 P [με]	14.8	-69.2%	G20 P [με]	14.8	NaN	G25 P [με]	14.8	NaN
	17.5	-61.3%		17.5	NaN		17.5	NaN
NaN: No available data or results								
Result is not statistically significant based on U_V values								

V_O: Optimized Grillage

V_T: Traditional Grillage

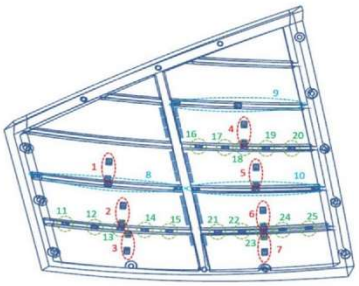

Irregular Waves

The irregular wave dataset included 94 spots, where 36 spots had the Traditional grillage installed and 58 spots had the Optimized grillage installed. The target irregular wave condition was a Bretschneider spectrum with a significant wave height, H_s, of 7.4 in and modal period, T_p, of 2.4 s. The spots were grouped in terms of carriage speed for the two speeds of interest: 30 spots at 14.8 knots and 64 spots at 17.5 knots. Once grouped the measured wave spectrum was calculated for each group. The measured significant wave heights were 7.118 ± 0.154 in and 7.144 ± 0.144 in for the 14.8 knots and 17.5 knots test speeds, respectively. The measured waves were 3.8 % and 3.4 % lower than the desired wave condition. The peak wave frequency was evaluated by fitting a 5th order polynomial function to the peak of the stationary frequency spectrum and was determined to be 2.381 s for both test speeds; this achieved peak wave frequency is 0.8 % less than the targeted value. The aforementioned, relatively small measured differences in significant wave height and modal period between the measured wave condition and the desired indicate that testing was conducted in waves representative of the target condition.

The irregular wave results for the measured wave, model drag, and motions appear in Table 32. Table 32 was calculated using the NBB method for primary variables. Since testing involved an irregular condition it is more meaningful to express the results in terms of standard deviation, SD, rather than mean value. For convenience four times the standard deviation is also

expressed in the table. This quantity can be interpreted as the significant double amplitude provided the data represent a Rayleigh distribution.

Table 32. Irregular Wave Ensemble Results for ς, a_{bow}, a_{CG}, F_x, θ, and z

Variable	Grillage	U	N_a	N_B	4 SD_a	V: SD_a	B	P_V	U_V	B%V	P_V%V	U_V%V
		knots	#	#								
ς [in]	Traditional	14.8	20928	96	7.060	1.765	0.120	0.049	0.130	6.80	2.77	7.34
	Optimized	14.8	20640	96	7.129	1.782	0.120	0.046	0.129	6.73	2.59	7.21
	Traditional	17.5	21165	85	7.184	1.796	0.120	0.048	0.129	6.68	2.66	7.19
	Optimized	17.5	46750	85	7.126	1.782	0.120	0.030	0.124	6.74	1.68	6.94
a_{bow} [g]	Traditional	14.8	13100000	60000	5.145	1.286	0.026	0.034	0.042	2.02	2.61	3.30
	Optimized	14.8	12900000	60000	5.022	1.256	0.026	0.030	0.040	2.07	2.42	3.19
	Traditional	17.5	13200000	53125	5.903	1.476	0.026	0.035	0.043	1.76	2.36	2.95
	Optimized	17.5	29200000	53125	5.893	1.473	0.026	0.022	0.034	1.76	1.52	2.33
a_{cg} [g]	Traditional	14.8	13100000	60000	2.445	0.611	0.002	0.020	0.020	0.38	3.26	3.28
	Optimized	14.8	12900000	60000	2.408	0.602	0.002	0.018	0.018	0.38	2.93	2.96
	Traditional	17.5	13200000	53125	3.009	0.752	0.002	0.020	0.020	0.31	2.62	2.64
	Optimized	17.5	29200000	53125	2.976	0.744	0.002	0.013	0.014	0.31	1.80	1.83
F_X [lbf]	Traditional	14.8	13100000	60000	136.990	34.248	0.380	1.095	1.159	1.11	3.20	3.38
	Optimized	14.8	12900000	60000	136.940	34.236	0.380	1.077	1.142	1.11	3.15	3.34
	Traditional	17.5	13200000	53125	177.370	44.342	0.380	1.146	1.208	0.86	2.59	2.72
	Optimized	17.5	29200000	53125	177.310	44.327	0.380	0.757	0.847	0.86	1.71	1.91
θ [deg]	Traditional	14.8	13100000	60000	10.584	2.646	0.240	0.078	0.252	9.07	2.95	9.54
	Optimized	14.8	12900000	60000	10.546	2.637	0.240	0.076	0.252	9.10	2.89	9.55
	Traditional	17.5	13200000	53125	10.106	2.526	0.240	0.065	0.249	9.50	2.56	9.84
	Optimized	17.5	29200000	53125	10.238	2.560	0.240	0.042	0.244	9.38	1.65	9.52
z [in]	Traditional	14.8	13100000	60000	9.929	2.482	0.200	0.103	0.225	8.06	4.15	9.06
	Optimized	14.8	12900000	60000	9.808	2.452	0.200	0.095	0.221	8.16	3.86	9.02
	Traditional	17.5	13200000	53125	10.567	2.642	0.200	0.103	0.225	7.57	3.90	8.52
	Optimized	17.5	29200000	53125	10.544	2.636	0.200	0.061	0.209	7.59	2.32	7.93

The irregular wave results of peak values of the measured wave, model drag, and motions were determined using the STDG and bootstrapping methods previously described in the Methodology section. These results are expressed as the average of the 1/3rd largest ensemble values, $EV_{\frac{1}{3},a}$, and appear in Table 33.

In similar fashion, the average of the 1/3rd largest ensemble values associated with pressure gages, P11-P23, are shown in Table 34, and those associated with the loads on the grillage, G1-G25, are shown in Table 35 through Table 38. These results are recommended points of comparison for future studies using CFD/CSD numerical tools.

For example, a future comparison may want to examine the 17.5 knots speed for the Traditional grillage (in the irregular condition). In this example, a point of comparison could be the average of the largest 1/3rd peaks of vertical acceleration at the center of gravity, a_{CG}. For the model test the value would be 1.105 g (using Table 33). The value could then be compared against a value derived using an existing numerical tool, and compared, to quantify the similitude. The pressures and secondary loads on the grillage are also recommended points of comparison. The reader should note the relatively high uncertainties associated with the grillage measurements, and read through the Grillage Panel section of this report prior to making comparisons.

Finally, it is worth noting the calculated percentage difference observed between the two grillages on the basis of the largest 1/3rd ensemble value, $EV_{\frac{1}{3},a}$. The comparison is summarized in Table 39. The Optimized grillage shows significantly larger strains than the Traditional grillage in the primary response direction on two of three stiffeners, $G11$-$G15$ and $G21$-$G25$, where these two stiffeners are aligned and closest to keel. Stiffener $G16$-$G20$, which is further away from the keel, shows a varying response along the stiffener: the forward edge gauge, $G16$, has a significantly lower strain for the Optimized grillage compared to the Traditional grillage; the two grillages have a statistically equivalent response for the center three gauges of the stiffener, $G17$, $G18$, and $G19$; the aft edge gauge, $G20$, has a significantly higher strain for the Optimized grillage compared to the Traditional grillage. The trends observed in the primary response direction are generally consistent between the regular wave and irregular wave data (shown in Table 31 and Table 39).

Table 33. Average of Largest 1/3rd Ensemble Values, $EV_{\frac{1}{3},a}$, for H, a_{bow}, a_{CG}, F_x, θ, and z

Variable	Grillage	U	⅓ N_a	V: $EV_{⅓, a}$	B	P_V	U_V	B%V	P_V%V	U_V%V
		knots	#							
H [in]	Traditional	14.8	373	6.483	0.120	0.197	0.230	1.85	3.03	3.55
	Optimized	14.8	367	6.664	0.120	0.204	0.237	1.80	3.07	3.56
	Traditional	17.5	419	6.734	0.120	0.183	0.219	1.78	2.71	3.25
	Optimized	17.5	959	6.552	0.120	0.127	0.175	1.83	1.94	2.66
a_{bow} [g]	Traditional	14.8	885	4.097	0.026	0.212	0.214	0.63	5.17	5.21
	Optimized	14.8	969	3.807	0.026	0.216	0.217	0.68	5.67	5.71
	Traditional	17.5	992	4.965	0.026	0.233	0.235	0.52	4.70	4.73
	Optimized	17.5	2296	4.775	0.026	0.165	0.167	0.54	3.46	3.50
a_{cg} [g]	Traditional	14.8	3154	0.762	0.002	0.035	0.035	0.30	4.58	4.59
	Optimized	14.8	3030	0.776	0.002	0.037	0.037	0.30	4.79	4.80
	Traditional	17.5	3387	1.105	0.002	0.047	0.047	0.21	4.24	4.25
	Optimized	17.5	7299	1.090	0.002	0.030	0.030	0.21	2.79	2.80
F_X [lbf]	Traditional	14.8	781	122.730	0.380	3.776	3.795	0.31	3.08	3.09
	Optimized	14.8	794	123.210	0.380	3.835	3.853	0.31	3.11	3.13
	Traditional	17.5	836	164.480	0.380	4.305	4.321	0.23	2.62	2.63
	Optimized	17.5	1885	161.220	0.380	2.873	2.898	0.24	1.78	1.80
θ [deg]	Traditional	14.8	298	9.681	0.240	0.254	0.349	2.48	2.62	3.61
	Optimized	14.8	302	9.563	0.240	0.250	0.346	2.51	2.61	3.62
	Traditional	17.5	332	8.875	0.240	0.195	0.309	2.70	2.19	3.48
	Optimized	17.5	712	9.116	0.240	0.152	0.284	2.63	1.67	3.12
z [in]	Traditional	14.8	245	8.933	0.200	0.322	0.379	2.24	3.61	4.25
	Optimized	14.8	240	8.849	0.200	0.279	0.343	2.26	3.15	3.88
	Traditional	17.5	270	9.192	0.200	0.293	0.354	2.18	3.18	3.86
	Optimized	17.5	597	9.260	0.200	0.191	0.276	2.16	2.06	2.99

Table 34. Average of Largest 1/3rd Ensemble Values, $EV_{\frac{1}{3},a}$, for $P11$-$P23$

Variable	Grillage	U knots	⅓ N_a #	V: $EV_{⅓,\,a}$	B	P_V	U_V	B%V	P_V%V	U_V%V
P11 [PSI]	Traditional	14.8	216	3.171	0.034	0.184	0.188	1.07	5.81	5.91
	Optimized	14.8	197	3.179	0.034	0.171	0.175	1.07	5.39	5.50
	Traditional	17.5	240	3.729	0.034	0.179	0.182	0.91	4.79	4.88
	Optimized	17.5	549	3.824	0.034	0.124	0.129	0.89	3.25	3.37
P12 [PSI]	Traditional	14.8	195	3.120	0.032	0.141	0.145	1.03	4.52	4.64
	Optimized	14.8	179	3.223	0.032	0.133	0.137	0.99	4.12	4.24
	Traditional	17.5	212	3.904	0.032	0.150	0.153	0.82	3.84	3.93
	Optimized	17.5	489	3.958	0.032	0.097	0.103	0.81	2.46	2.59
P13 [PSI]	Traditional	14.8	133	2.274	0.013	0.107	0.108	0.57	4.72	4.75
	Optimized	14.8	124	2.261	0.013	0.100	0.101	0.58	4.44	4.48
	Traditional	17.5	138	2.921	0.013	0.139	0.139	0.45	4.75	4.77
	Optimized	17.5	332	2.896	0.013	0.081	0.082	0.45	2.79	2.83
P21 [PSI]	Traditional	14.8	273	3.794	0.038	0.149	0.154	1.00	3.93	4.05
	Optimized	14.8	262	3.615	0.038	0.152	0.156	1.05	4.19	4.32
	Traditional	17.5	314	4.610	0.038	0.162	0.166	0.82	3.51	3.61
	Optimized	17.5	711	4.548	0.038	0.102	0.109	0.84	2.24	2.39
P22 [PSI]	Traditional	14.8	232	2.451	0.039	0.120	0.127	1.59	4.91	5.16
	Optimized	14.8	215	2.626	0.039	0.140	0.145	1.49	5.33	5.53
	Traditional	17.5	262	2.899	0.039	0.129	0.135	1.35	4.44	4.64
	Optimized	17.5	605	2.934	0.039	0.080	0.089	1.33	2.74	3.05
P23 [PSI]	Traditional	14.8	221	2.139	0.067	0.085	0.108	3.13	3.97	5.06
	Optimized	14.8	200	2.194	0.067	0.083	0.107	3.05	3.80	4.88
	Traditional	17.5	235	2.708	0.067	0.113	0.131	2.47	4.16	4.84
	Optimized	17.5	548	2.761	0.067	0.060	0.090	2.43	2.18	3.26

Table 35. Average of Largest 1/3rd Ensemble Values, $EV_{\frac{1}{3},a}$, for $G1$-$G10$

Variable	Grillage	U	⅓ N_a	V: $EV_{⅓, a}$	B	P_V	U_V	B%V	P_V%V	U_V%V
		knots	#							
G1 [PSI]	Traditional	14.8	165	2.131	0.142	0.090	0.168	6.68	4.22	7.90
	Optimized	14.8	136	3.810	0.173	0.172	0.244	4.54	4.51	6.40
	Traditional	17.5	257	2.773	0.142	0.083	0.165	5.14	3.00	5.95
	Optimized	17.5	380	4.882	0.173	0.137	0.221	3.54	2.81	4.52
G2 [PSI]	Traditional	14.8	219	1.053	0.152	0.046	0.159	14.46	4.41	15.11
	Optimized	14.8	0	NaN	0.500	NaN	NaN	NaN	NaN	NaN
	Traditional	17.5	341	1.326	0.152	0.034	0.156	11.48	2.54	11.76
	Optimized	17.5	0	NaN	0.500	NaN	NaN	NaN	NaN	NaN
G3 [PSI]	Traditional	14.8	155	4.760	0.051	0.237	0.242	1.07	4.97	5.08
	Optimized	14.8	136	3.307	0.377	0.144	0.404	11.41	4.36	12.22
	Traditional	17.5	230	6.170	0.051	0.188	0.194	0.83	3.04	3.15
	Optimized	17.5	398	3.984	0.377	0.129	0.399	9.47	3.24	10.01
G4 [PSI]	Traditional	14.8	242	2.420	0.126	0.084	0.151	5.22	3.45	6.26
	Optimized	14.8	215	3.124	0.138	0.113	0.178	4.41	3.60	5.70
	Traditional	17.5	377	3.097	0.126	0.076	0.147	4.08	2.46	4.76
	Optimized	17.5	598	3.996	0.138	0.077	0.158	3.45	1.94	3.96
G5 [PSI]	Traditional	14.8	280	1.799	0.155	0.071	0.170	8.62	3.93	9.48
	Optimized	14.8	266	1.824	0.199	0.059	0.208	10.92	3.24	11.39
	Traditional	17.5	439	2.257	0.155	0.057	0.165	6.87	2.51	7.32
	Optimized	17.5	709	2.390	0.199	0.042	0.203	8.33	1.76	8.51
G6 [PSI]	Traditional	14.8	274	2.404	0.130	0.098	0.163	5.41	4.08	6.77
	Optimized	14.8	0	NaN	0.603	NaN	NaN	NaN	NaN	NaN
	Traditional	17.5	454	2.931	0.130	0.080	0.153	4.44	2.73	5.21
	Optimized	17.5	0	NaN	0.603	NaN	NaN	NaN	NaN	NaN
G7 [PSI]	Traditional	14.8	293	6.574	0.122	0.270	0.296	1.85	4.11	4.50
	Optimized	14.8	0	NaN	0.603	NaN	NaN	NaN	NaN	NaN
	Traditional	17.5	464	8.028	0.122	0.206	0.239	1.51	2.56	2.98
	Optimized	17.5	0	NaN	0.603	NaN	NaN	NaN	NaN	NaN
G8 [PSI]	Traditional	14.8	95	2.241	0.067	0.111	0.129	2.98	4.95	5.77
	Optimized	14.8	96	1.840	0.065	0.102	0.121	3.54	5.54	6.57
	Traditional	17.5	158	2.840	0.067	0.098	0.119	2.35	3.46	4.18
	Optimized	17.5	258	2.399	0.065	0.090	0.111	2.71	3.75	4.63
G9 [PSI]	Traditional	14.8	0	NaN	0.158	NaN	NaN	NaN	NaN	NaN
	Optimized	14.8	109	0.923	0.409	0.052	0.412	44.29	5.61	44.64
	Traditional	17.5	0	NaN	0.158	NaN	NaN	NaN	NaN	NaN
	Optimized	17.5	285	1.193	0.409	0.053	0.412	34.27	4.43	34.56
G10 [PSI]	Traditional	14.8	246	2.543	0.067	0.116	0.134	2.63	4.55	5.25
	Optimized	14.8	220	2.114	0.064	0.103	0.121	3.00	4.85	5.71
	Traditional	17.5	406	3.027	0.067	0.086	0.109	2.21	2.86	3.61
	Optimized	17.5	613	2.628	0.064	0.071	0.095	2.42	2.71	3.63

NaN: No available data or results | **Uncertainty values where U_V%V > 25%**

Table 36. Average of Largest 1/3rd Ensemble Values, $EV_{\frac{1}{3},a}$, for $G11\ P$-$G15\ P$

Variable	Grillage	U knots	⅓ N_a #	V: $EV_{⅓,\,a}$	B	P_V	U_V	B%|V|	P_V%|V|	U_V%|V|
G11 P [με]	Traditional	14.8	178	205.270	37.849	10.784	39.356	18.44	5.25	19.17
	Optimized	14.8	5	83.410	31.012	23.509	38.916	37.18	28.19	46.66
	Traditional	17.5	138	269.050	37.849	13.769	40.276	14.07	5.12	14.97
	Optimized	17.5	32	73.658	31.012	10.403	32.711	42.10	14.12	44.41
G11 N [με]	Traditional	14.8	43	-91.498	37.849	3.042	37.971	41.37	3.32	41.50
	Optimized	14.8	187	-1120.100	31.012	48.631	57.678	2.77	4.34	5.15
	Traditional	17.5	62	-133.700	37.849	6.310	38.372	28.31	4.72	28.70
	Optimized	17.5	558	-1383.300	31.012	32.546	44.956	2.24	2.35	3.25
G12 P [με]	Traditional	14.8	141	515.180	36.420	21.673	42.381	7.07	4.21	8.23
	Optimized	14.8	134	948.840	42.706	40.100	58.582	4.50	4.23	6.17
	Traditional	17.5	127	646.920	36.420	29.768	47.037	5.63	4.60	7.27
	Optimized	17.5	389	1238.700	42.706	30.526	52.494	3.45	2.46	4.24
G12 N [με]	Traditional	14.8	203	-150.920	36.420	7.044	37.095	24.13	4.67	24.58
	Optimized	14.8	240	-232.140	42.706	10.978	44.094	18.40	4.73	18.99
	Traditional	17.5	169	-205.050	36.420	21.976	42.536	17.76	10.72	20.74
	Optimized	17.5	696	-262.760	42.706	6.604	43.213	16.25	2.51	16.45
G13 P [με]	Traditional	14.8	18	657.610	38.746	115.550	121.880	5.89	17.57	18.53
	Optimized	14.8	158	1199.300	56.820	48.164	74.487	4.74	4.02	6.21
	Traditional	17.5	38	779.030	38.746	65.986	76.521	4.97	8.47	9.82
	Optimized	17.5	454	1543.900	56.820	37.492	68.075	3.68	2.43	4.41
G13 N [με]	Traditional	14.8	23	-182.990	38.746	21.056	44.098	21.17	11.51	24.10
	Optimized	14.8	237	-269.380	56.820	11.863	58.045	21.09	4.40	21.55
	Traditional	17.5	45	-214.960	38.746	16.373	42.064	18.03	7.62	19.57
	Optimized	17.5	679	-302.830	56.820	7.050	57.256	18.76	2.33	18.91
G14 P [με]	Traditional	14.8	176	585.650	37.531	23.359	44.207	6.41	3.99	7.55
	Optimized	14.8	173	1007.800	40.376	38.852	56.033	4.01	3.86	5.56
	Traditional	17.5	196	750.900	37.531	25.175	45.192	5.00	3.35	6.02
	Optimized	17.5	487	1287.800	40.376	29.751	50.153	3.14	2.31	3.89
G14 N [με]	Traditional	14.8	235	-170.600	37.531	6.971	38.173	22.00	4.09	22.38
	Optimized	14.8	257	-287.500	40.376	12.718	42.332	14.04	4.42	14.72
	Traditional	17.5	298	-183.690	37.531	6.259	38.049	20.43	3.41	20.71
	Optimized	17.5	696	-326.230	40.376	7.314	41.033	12.38	2.24	12.58
G15 P [με]	Traditional	14.8	276	194.090	24.783	7.279	25.830	12.77	3.75	13.31
	Optimized	14.8	165	114.340	31.902	6.620	32.581	27.90	5.79	28.50
	Traditional	17.5	325	218.050	24.783	6.659	25.662	11.37	3.05	11.77
	Optimized	17.5	515	134.650	31.902	4.138	32.169	23.69	3.07	23.89
G15 N [με]	Traditional	14.8	197	-207.170	24.783	7.812	25.985	11.96	3.77	12.54
	Optimized	14.8	282	-345.210	31.902	17.653	36.460	9.24	5.11	10.56
	Traditional	17.5	223	-263.840	24.783	8.707	26.268	9.39	3.30	9.96
	Optimized	17.5	826	-409.690	31.902	12.704	34.338	7.79	3.10	8.38
						Uncertainty values where U_V%|V| > 25%				

Table 37. Average of Largest 1/3rd Ensemble Values, $EV_{\frac{1}{3},a}$, for $G16\ P$-$G20\ P$ and $G16\ N$-$G20\ N$

Variable	Grillage	U knots	⅓ N_a #	V: $EV_{⅓,\,a}$	B	P_V	U_V	B%|V|	P_V%|V|	U_V%|V|
G16 P [με]	Traditional	14.8	35	75.109	55.360	6.057	55.690	73.71	8.06	74.15
	Optimized	14.8	64	99.873	20.673	6.584	21.696	20.70	6.59	21.72
	Traditional	17.5	62	78.859	55.360	4.483	55.541	70.20	5.68	70.43
	Optimized	17.5	243	101.130	20.673	3.693	21.000	20.44	3.65	20.77
G16 N [με]	Traditional	14.8	209	-366.760	55.360	15.303	57.436	15.09	4.17	15.66
	Optimized	14.8	215	-257.900	20.673	10.431	23.156	8.02	4.04	8.98
	Traditional	17.5	242	-459.970	55.360	16.561	57.784	12.04	3.60	12.56
	Optimized	17.5	618	-328.930	20.673	8.181	22.233	6.29	2.49	6.76
G17 P [με]	Traditional	14.8	224	476.780	67.572	19.466	70.320	14.17	4.08	14.75
	Optimized	14.8	211	587.220	59.488	23.020	63.787	10.13	3.92	10.86
	Traditional	17.5	255	594.950	67.572	21.416	70.885	11.36	3.60	11.91
	Optimized	17.5	599	705.200	59.488	16.722	61.793	8.44	2.37	8.76
G17 N [με]	Traditional	14.8	61	-85.985	67.572	5.314	67.781	78.59	6.18	78.83
	Optimized	14.8	190	-135.130	59.488	5.930	59.783	44.02	4.39	44.24
	Traditional	17.5	100	-91.397	67.572	4.439	67.718	73.93	4.86	74.09
	Optimized	17.5	593	-151.050	59.488	4.462	59.655	39.38	2.95	39.49
G18 P [με]	Traditional	14.8	231	502.420	83.573	20.828	86.129	16.63	4.15	17.14
	Optimized	14.8	214	538.950	46.515	22.463	51.655	8.63	4.17	9.58
	Traditional	17.5	264	621.730	83.573	21.241	86.230	13.44	3.42	13.87
	Optimized	17.5	597	647.000	46.515	15.101	48.905	7.19	2.33	7.56
G18 N [με]	Traditional	14.8	80	-86.405	83.573	4.745	83.708	96.72	5.49	96.88
	Optimized	14.8	205	-141.090	46.515	6.136	46.918	32.97	4.35	33.26
	Traditional	17.5	108	-95.608	83.573	4.810	83.711	87.41	5.03	87.56
	Optimized	17.5	636	-161.360	46.515	4.687	46.751	28.83	2.90	28.97
G19 P [με]	Traditional	14.8	242	444.900	88.384	18.642	90.328	19.87	4.19	20.30
	Optimized	14.8	224	354.370	64.510	13.898	65.991	18.20	3.92	18.62
	Traditional	17.5	270	547.000	88.384	18.972	90.397	16.16	3.47	16.53
	Optimized	17.5	615	423.300	64.510	10.097	65.296	15.24	2.39	15.43
G19 N [με]	Traditional	14.8	60	-83.623	88.384	5.302	88.542	105.69	6.34	105.88
	Optimized	14.8	197	-143.100	64.510	5.720	64.764	45.08	4.00	45.26
	Traditional	17.5	83	-91.995	88.384	4.961	88.523	96.07	5.39	96.23
	Optimized	17.5	630	-167.630	64.510	4.660	64.679	38.48	2.78	38.58
G20 P [με]	Traditional	14.8	10	75.693	130.540	9.141	130.860	172.46	12.08	172.88
	Optimized	14.8	17	93.044	36.690	13.427	39.070	39.43	14.43	41.99
	Traditional	17.5	22	80.289	130.540	6.986	130.730	162.59	8.70	162.82
	Optimized	17.5	95	82.042	36.690	3.821	36.888	44.72	4.66	44.96
G20 N [με]	Traditional	14.8	252	-237.150	130.540	9.185	130.860	55.05	3.87	55.18
	Optimized	14.8	205	-528.750	36.690	22.984	43.295	6.94	4.35	8.19
	Traditional	17.5	292	-279.000	130.540	8.820	130.840	46.79	3.16	46.90
	Optimized	17.5	631	-639.790	36.690	17.790	40.776	5.73	2.78	6.37
						Uncertainty values where U_V%|V| > 25%				

Table 38. Average of Largest 1/3rd Ensemble Values, $EV_{\frac{1}{3},a}$, for $G21\ P$-$G25\ P$ and $G21\ N$-$G25\ N$

Variable	Grillage	U knots	⅓ N_a #	V: $EV_{⅓,\,a}$	B	P_V	U_V	B%|V|	P_V%|V|	U_V%|V|
G21 P [με]	Traditional	14.8	128	93.510	25.204	4.353	25.577	26.95	4.65	27.35
	Optimized	14.8	170	76.219	19.330	2.579	19.501	25.36	3.38	25.59
	Traditional	17.5	193	101.310	25.204	3.361	25.427	24.88	3.32	25.10
	Optimized	17.5	563	111.590	19.330	2.130	19.447	17.32	1.91	17.43
G21 N [με]	Traditional	14.8	266	-126.090	25.204	3.644	25.466	19.99	2.89	20.20
	Optimized	14.8	305	-407.760	19.330	16.010	25.099	4.74	3.93	6.16
	Traditional	17.5	292	-160.370	25.204	3.875	25.500	15.72	2.42	15.90
	Optimized	17.5	894	-461.630	19.330	10.420	21.959	4.19	2.26	4.76
G22 P [με]	Traditional	14.8	315	482.900	38.897	17.875	42.808	8.05	3.70	8.86
	Optimized	14.8	335	860.700	16.099	33.832	37.467	1.87	3.93	4.35
	Traditional	17.5	344	577.050	38.897	17.199	42.530	6.74	2.98	7.37
	Optimized	17.5	876	1087.700	16.099	24.863	29.620	1.48	2.29	2.72
G22 N [με]	Traditional	14.8	15	-79.291	38.897	8.864	39.894	49.06	11.18	50.31
	Optimized	14.8	192	-142.710	16.099	7.233	17.649	11.28	5.07	12.37
	Traditional	17.5	37	-89.561	38.897	6.680	39.466	43.43	7.46	44.07
	Optimized	17.5	595	-195.370	16.099	6.851	17.496	8.24	3.51	8.96
G23 P [με]	Traditional	14.8	328	508.780	41.110	19.282	45.407	8.08	3.79	8.92
	Optimized	14.8	348	925.420	30.279	39.279	49.595	3.27	4.24	5.36
	Traditional	17.5	345	607.680	41.110	19.380	45.449	6.77	3.19	7.48
	Optimized	17.5	913	1151.900	30.279	27.078	40.620	2.63	2.35	3.53
G23 N [με]	Traditional	14.8	21	-81.033	41.110	8.251	41.929	50.73	10.18	51.74
	Optimized	14.8	203	-163.300	30.279	7.758	31.257	18.54	4.75	19.14
	Traditional	17.5	60	-86.675	41.110	6.341	41.596	47.43	7.32	47.99
	Optimized	17.5	624	-227.510	30.279	7.108	31.102	13.31	3.12	13.67
G24 P [με]	Traditional	14.8	337	479.690	45.227	19.455	49.234	9.43	4.06	10.26
	Optimized	14.8	292	806.100	28.448	36.802	46.515	3.53	4.57	5.77
	Traditional	17.5	360	573.060	45.227	17.434	48.471	7.89	3.04	8.46
	Optimized	17.5	817	892.980	28.448	24.622	37.623	3.19	2.76	4.21
G24 N [με]	Traditional	14.8	31	-82.271	45.227	6.731	45.725	54.97	8.18	55.58
	Optimized	14.8	173	-168.510	28.448	6.797	29.248	16.88	4.03	17.36
	Traditional	17.5	60	-96.033	45.227	7.080	45.778	47.10	7.37	47.67
	Optimized	17.5	556	-230.710	28.448	6.064	29.087	12.33	2.63	12.61
G25 P [με]	Traditional	14.8	8	71.965	65.669	8.702	66.243	91.25	12.09	92.05
	Optimized	14.8	3	99.127	15.599	33.273	36.748	15.74	33.57	37.07
	Traditional	17.5	27	76.253	65.669	4.588	65.829	86.12	6.02	86.33
	Optimized	17.5	28	85.499	15.599	13.255	20.470	18.25	15.50	23.94
G25 N [με]	Traditional	14.8	288	-143.160	65.669	5.345	65.886	45.87	3.73	46.02
	Optimized	14.8	271	-604.740	15.599	28.155	32.188	2.58	4.66	5.32
	Traditional	17.5	332	-167.650	65.669	5.129	65.869	39.17	3.06	39.29
	Optimized	17.5	753	-742.770	15.599	19.439	24.924	2.10	2.62	3.36
						Uncertainty values where U_V%|V| > 25%				

Table 39. Percent Difference $EV_{\frac{1}{3},a}$ between the Optimized and Traditional Grillage

Primary Direction of Response for the Strain Gauge								
Variable	U knots	V: $EV_{⅓,a}$ $(V_O - V_T)/(V_T)$	Variable	U knots	V: $EV_{⅓,a}$ $(V_O - V_T)/(V_T)$	Variable	U knots	V: $EV_{⅓,a}$ $(V_O - V_T)/(V_T)$
G11 N [με]	14.8	1124.2%	G16 N [με]	14.8	-29.7%	G21 N [με]	14.8	223.4%
	17.5	934.6%		17.5	-28.5%		17.5	187.9%
G12 P [με]	14.8	84.2%	G17 P [με]	14.8	23.2%	G22 P [με]	14.8	78.2%
	17.5	91.5%		17.5	18.5%		17.5	88.5%
G13 P [με]	14.8	82.4%	G18 P [με]	14.8	7.3%	G23 P [με]	14.8	81.9%
	17.5	98.2%		17.5	4.1%		17.5	89.6%
G14 P [με]	14.8	72.1%	G19 P [με]	14.8	-20.3%	G24 P [με]	14.8	68.0%
	17.5	71.5%		17.5	-22.6%		17.5	55.8%
G15 N [με]	14.8	66.6%	G20 N [με]	14.8	123.0%	G25 N [με]	14.8	322.4%
	17.5	55.3%		17.5	129.3%		17.5	343.0%
Secondary Direction of Response for the Strain Gauge								
G11 P [με]	14.8	-59.4%	G16 P [με]	14.8	33.0%	G21 P [με]	14.8	-18.5%
	17.5	-72.6%		17.5	28.2%		17.5	10.1%
G12 N [με]	14.8	53.8%	G17 N [με]	14.8	57.2%	G22 N [με]	14.8	80.0%
	17.5	28.1%		17.5	65.3%		17.5	118.1%
G13 N [με]	14.8	47.2%	G18 N [με]	14.8	63.3%	G23 N [με]	14.8	101.5%
	17.5	40.9%		17.5	68.8%		17.5	162.5%
G14 N [με]	14.8	68.5%	G19 N [με]	14.8	71.1%	G24 N [με]	14.8	104.8%
	17.5	77.6%		17.5	82.2%		17.5	140.2%
G15 P [με]	14.8	-41.1%	G20 P [με]	14.8	22.9%	G25 P [με]	14.8	37.7%
	17.5	-38.2%		17.5	2.2%		17.5	12.1%
NaN: No available data or results								
Result is not statistically significant based on U_V values								

V_O: Optimized Grillage

V_T: Traditional Grillage

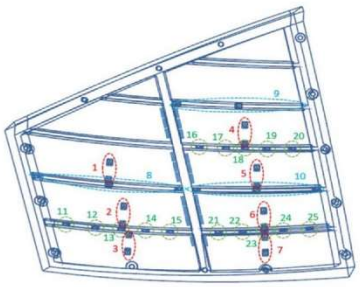

Extreme Value Analysis

Grillage and Pressure Measurements

The Weibull distribution was used to estimate extreme values for the grillage measurements and localized pressures given various exposure times. Two methods of Weibull fit were used: LR3 and MM3. The results from the method which fit the data best are presented. Exposure times of 100 (model scale) hours, 500 hours, and 1,000 hours were considered when calculating the PNE.

For cases where the Weibull distribution did not fit the data well, a multiplier was applied to the largest measured values to approximate the 36.8 % PNE. The multipliers are shown in Table 40, and were calculated as the averages of multipliers derived from 36.8 % PNE predictions for data that fit the distribution well.

Table 40. Multipliers to Estimate 36.8 % PNE Predictions

Multipliers for Traditional and Optimized Grillages to Estimate 36.8 % PNE Predictions	
100 hr	1.28
500 hr	1.36
1000 hr	1.40

The results presented in this subsection are for a single condition: 17.5 knots using the traditional grillage panel (Matrix IDs 14 and 15 combined). The results are presented in the following order: A table of the Weibull parameters, a table of PNE results for various exposure times based on the best fit method (LR3 or MM3), and plot showing the fit of both methods to the dataset for a select channel. The results are presented for the grillage channels (G1-G25), and the pressure sensors of interest (P11 - P23). These results are presented in Table 41 - Table 50 and in Figure 52 - Figure 56. The PNE values for the other conditions tested can be found in Appendix I.

This set of tabulated results is intended to be used for future comparison with data generated by existing numerical CFD tools. Comparisons between CFD tools and the experiment are planned as part of a follow-on effort and may include comparisons of predicted extreme values of localized pressures and grillage loads.

Table 41. Weibull Shape Parameters for Differential Bending Channels in Matrix ID 14 and 15

Channel	Number of Events	Best Fit Method	σ (PSI)	Best Fit Parameters			
				β	η (PSI)	x_0 (PSI)	R^2
G1 (+)	535	MM3	0.8	2.3	2.1	0.0	--
G2 (+)	739	MM3	0.4	2.7	1.1	0.0	--
G3 (+)	485	MM3	1.5	2.4	5.0	1.2	--
G4 (+)	813	MM3	0.9	2.5	2.4	0.1	--
G5 (+)	958	MM3	0.6	2.5	1.8	0.2	--
G6 (+)	960	Multiplier	0.8	--	--	--	--
G7 (+)	970	Multiplier	2.2	--	--	--	--
G8 (+)	324	MM3	0.9	2.1	2.1	0.0	--
G10 (+)	846	LR3	0.9	2.6	2.4	0.0	0.9178

Table 42. Lifetime Extreme Estimates for Differential Bending Channels in Matrix ID 14 and 15

Channel	Number of Events	Best Fit Method	PNE @ 100 hr (PSI)			PNE @ 500 hr (PSI)			PNE @ 1000 hr (PSI)		
			36.8 %	90.0 %	99.0 %	36.8 %	90.0 %	99.0 %	36.8 %	90.0 %	99.0 %
G1 (+)	535	MM3	6	7	7	6	7	7	7	7	7
G2 (+)	739	MM3	3	3	3	3	3	3	3	3	3
G3 (+)	485	MM3	12	13	14	13	13	14	13	14	14
G4 (+)	813	MM3	6	7	7	7	7	7	7	7	8
G5 (+)	958	MM3	5	5	5	5	5	6	5	5	6
G6 (+)	960	Multiplier	9	--	--	10	--	--	10	--	--
G7 (+)	970	Multiplier	22	--	--	23	--	--	24	--	--
G8 (+)	324	MM3	7	7	8	7	8	8	7	8	8
G10 (+)	846	LR3	6	7	7	7	7	8	7	7	8

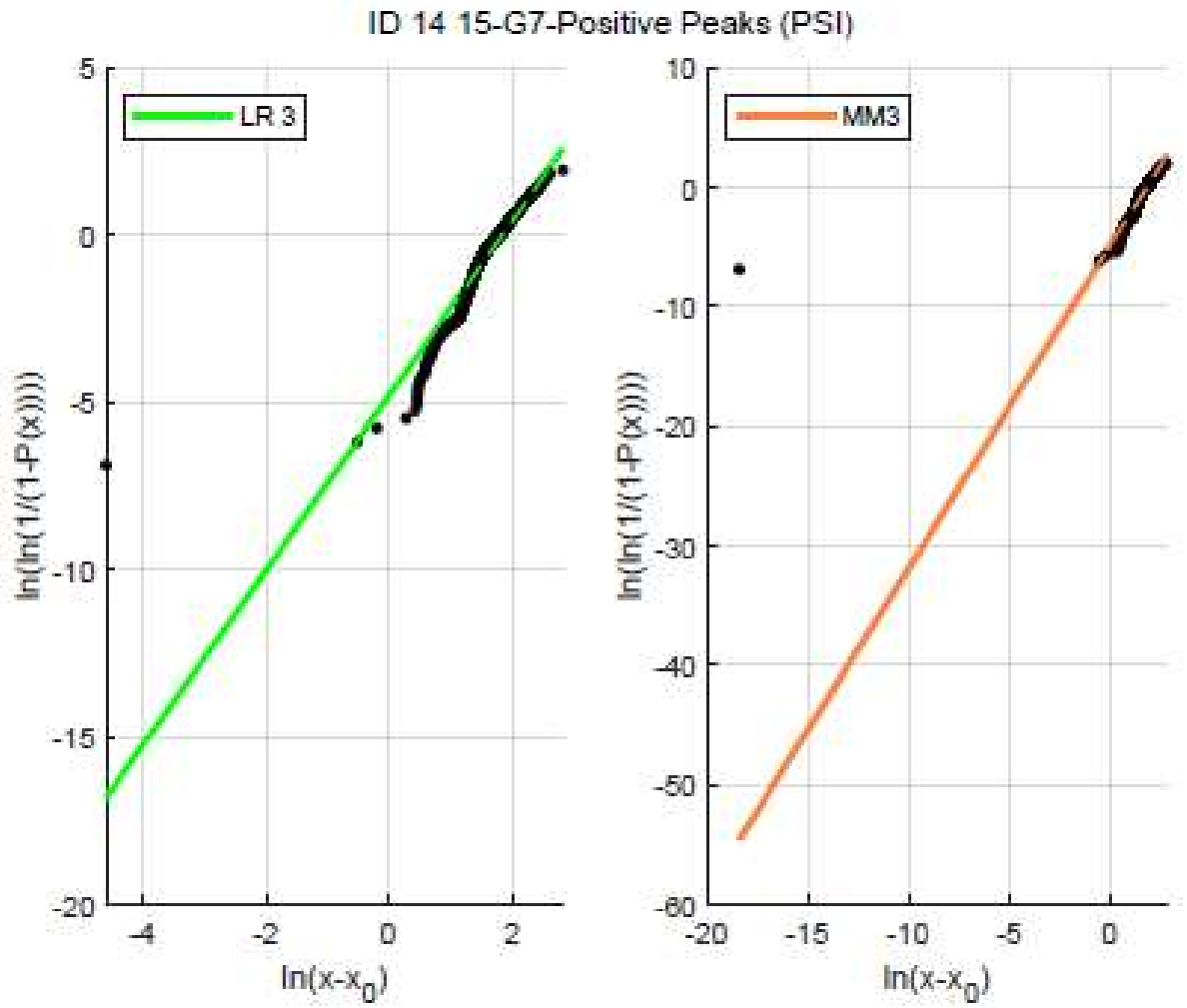

Figure 52. LR3 and MM3 Weibull Plots of Channel G7 for Matrix ID 14 and 15

Table 43. Weibull Shape Parameters for Single Strain Channels G11 - G15 in Matrix ID 14 and 15

Channel	Number of Events	Best Fit Method	σ (microstrain)	Best Fit Parameters			
				β	η (microstrain)	x_0 (microstrain)	R^2
G11 (+)	416	MM3	82	1.7	192	42	--
G11 (-)	187	MM3	36	2.9	107	0	--
G12 (+)	383	Multiplier	238	--	--	--	--
G12 (-)	508	MM3	58	2.0	144	17	--
G13 (+)	115	MM3	249	2.2	583	0	--
G13 (-)	136	MM3	57	2.2	164	31	--
G14 (+)	590	MM3	254	2.0	541	0	--
G14 (-)	895	Multiplier	52	--	--	--	--
G15 (+)	975	Multiplier	62	--	--	--	--
G15 (-)	669	MM3	75	2.5	201	5	--

Table 44. Lifetime Extreme Estimates for Single Strain Channels G11 - G15 in Matrix ID 14 and 15

Channel	Number of Events	Best Fit Method	PNE @ 100 hr (microstrain)			PNE @ 500 hr (microstrain)			PNE @ 1000 hr (microstrain)		
			36.8 %	90.0 %	99.0 %	36.8 %	90.0 %	99.0 %	36.8 %	90.0 %	99.0 %
G11 (+)	416	MM3	723	793	861	773	840	906	794	860	925
G11 (-)	187	MM3	-253	-268	-283	-264	-279	-292	-269	-283	-296
G12 (+)	383	Multiplier	1347	--	--	1431	--	--	1473	--	--
G12 (-)	508	MM3	-465	-502	-538	-492	-527	-561	-503	-537	-571
G13 (+)	115	MM3	1866	2010	2149	1970	2106	2238	2013	2146	2275
G13 (-)	136	MM3	-464	-498	-530	-488	-520	-551	-498	-529	-559
G14 (+)	590	MM3	1951	2121	2286	2074	2235	2392	2125	2283	2437
G14 (-)	895	Multiplier	-594	--	--	-631	--	--	-650	--	--
G15 (+)	975	Multiplier	648	--	--	689	--	--	709	--	--
G15 (-)	669	MM3	-549	-586	-621	-575	-610	-643	-586	-620	-652

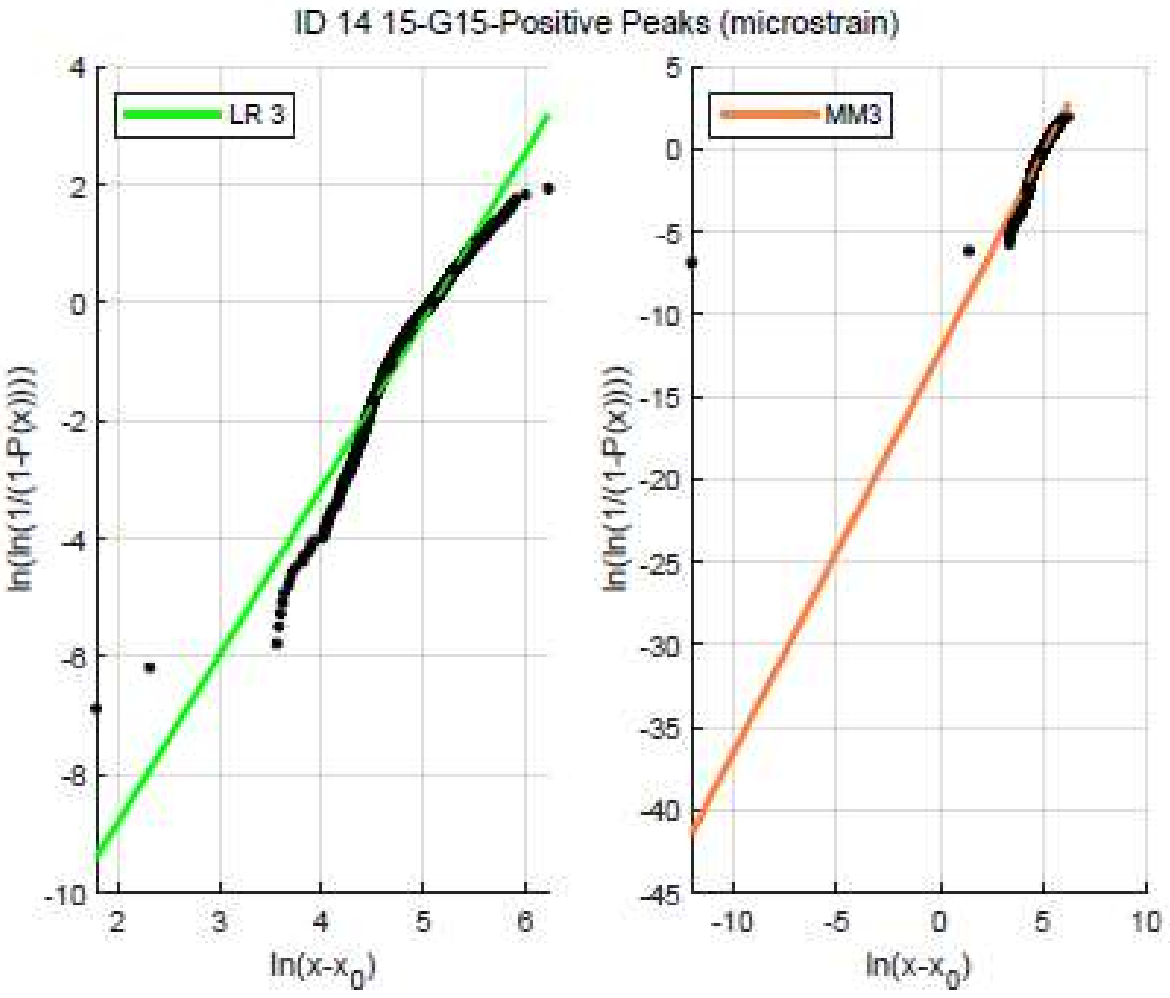

Figure 53. LR3 and MM3 Weibull Plots of Channel G15 for Matrix ID 14 and 15

Table 45. Weibull Shape Parameters for Single Strain Channels G16 - G20 in Matrix ID 14 and 15

Channel	Number of Events	Best Fit Method	σ (microstrain)	Best Fit Parameters			
				β	η (microstrain)	x_0 (microstrain)	R^2
G16 (+)	186	MM3	16	1.6	64	37	--
G16 (-)	720	MM3	163	1.7	305	0	--
G17 (+)	766	MM3	210	1.8	404	0	--
G17 (-)	300	MM3	20	1.3	71	44	--
G18 (+)	793	MM3	217	1.8	429	0	--
G18 (-)	326	MM3	21	1.6	75	40	--
G19 (+)	812	MM3	185	1.9	386	0	--
G19 (-)	250	MM3	20	1.5	73	42	--
G20 (+)*	66	MM3	15	1.3	66	45	--
G20 (-)*	876	Multiplier	80	--	--	--	--

*Results are presented for full disclosure, but the response of this channel was unreliable and it is recommended that these results are not used for comparison with CFD.

Table 46. Lifetime Extreme Estimates for Single Strain Channels G16 - G20 in Matrix ID 14 and 15

Channel	Number of Events	Best Fit Method	PNE @ 100 hr (microstrain)			PNE @ 500 hr (microstrain)			PNE @ 1000 hr (microstrain)		
			36.8 %	90.0 %	99.0 %	36.8 %	90.0 %	99.0 %	36.8 %	90.0 %	99.0 %
G16 (+)	186	MM3	161	176	191	172	186	200	177	190	204
G16 (-)	720	MM3	-1342	-1476	-1606	-1439	-1566	-1692	-1479	-1604	-1727
G17 (+)	766	MM3	1710	1874	2034	1828	1985	2139	1877	2031	2182
G17 (-)	300	MM3	-218	-243	-267	-236	-260	-284	-243	-267	-290
G18 (+)	793	MM3	1749	1912	2070	1866	2021	2173	1915	2067	2217
G18 (-)	326	MM3	-207	-226	-245	-221	-239	-257	-227	-245	-262
G19 (+)	812	MM3	1449	1575	1697	1540	1660	1777	1578	1695	1810
G19 (-)	250	MM3	-197	-216	-234	-210	-228	-246	-216	-234	-251
G20 (+)*	66	MM3	170	191	211	185	205	224	191	210	230
G20 (-)*	876	Multiplier	-771	--	--	-820	--	--	-844	--	--

*Results are presented for full disclosure, but the response of this channel was unreliable and it is recommended that these results are not used for comparison with CFD.

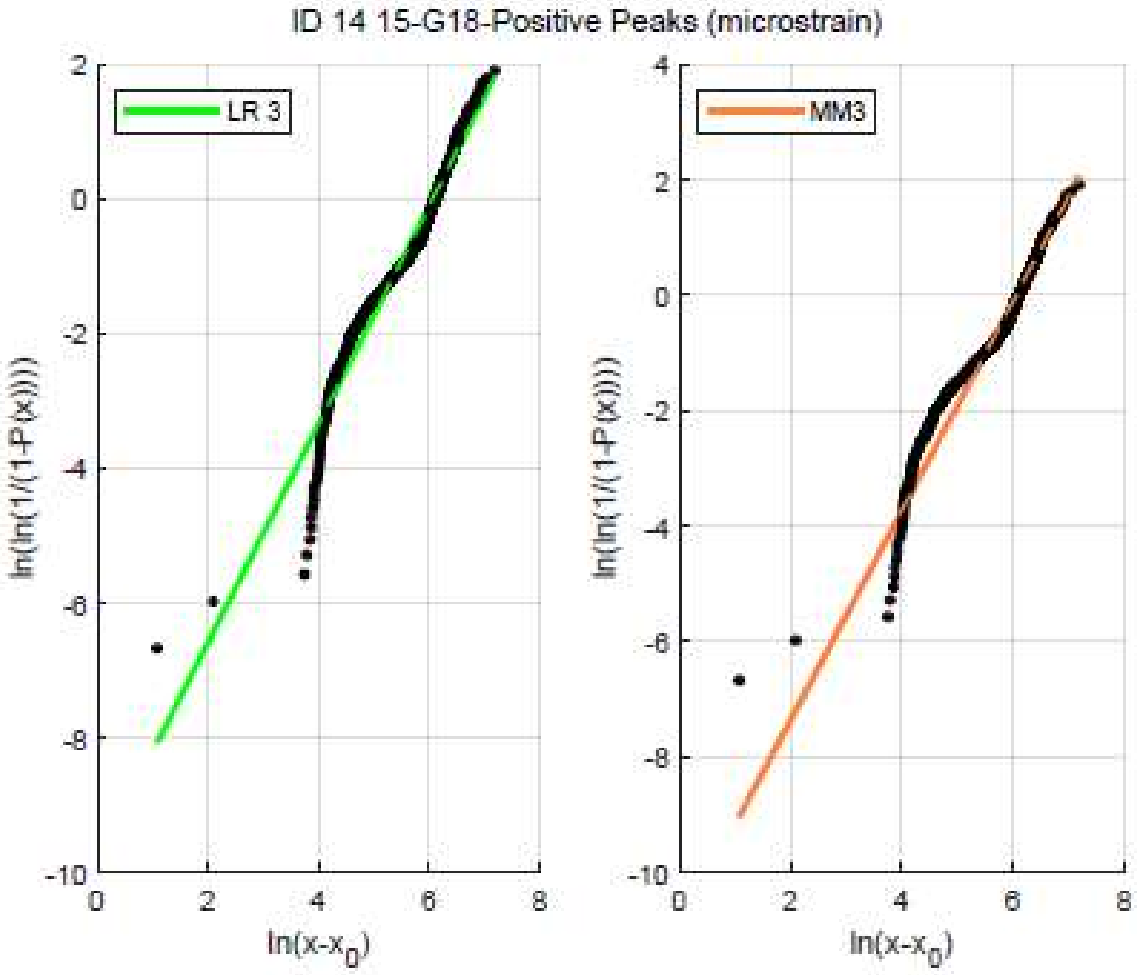

Figure 54. LR3 and MM3 Weibull Plots of Channel G18 for Matrix ID 14 and 15

Table 47. Weibull Shape Parameters for Single Strain Channels G21 - G25 in Matrix ID 14 and 15

Channel	Number of Events	Best Fit Method	σ (microstrain)	Best Fit Parameters			
				β	η (microstrain)	x_0 (microstrain)	R^2
G21 (+)	579	MM3	22	1.8	80	37	--
G21 (-)	878	LR3	33	3.8	138	0	0.8936
G22 (+)	1033	MM3	177	2.3	432	7	--
G22 (-)	112	MM3	19	1.4	72	42	--
G23 (+)	1037	MM3	190	2.2	448	8	--
G23 (-)	181	MM3	23	2.6	70	7	--
G24 (+)	1081	MM3	181	2.1	421	7	--
G24 (-)	182	MM3	23	1.7	76	34	--
G25 (+)*	82	MM3	11	1.6	65	45	--
G25 (-)*	998	Multiplier	44	--	--	--	--

*Results are presented for full disclosure, but the response of this channel was unreliable and it is recommended that these results are not used for comparison with CFD.

Table 48. Lifetime Extreme Estimates for Single Strain Channels G21 - G25 in Matrix ID 14 and 15

Channel	Number of Events	Best Fit Method	PNE @ 100 hr (microstrain)			PNE @ 500 hr (microstrain)			PNE @ 1000 hr (microstrain)		
			36.8 %	90.0 %	99.0 %	36.8 %	90.0 %	99.0 %	36.8 %	90.0 %	99.0 %
G21 (+)	579	MM3	215	233	250	228	244	261	233	249	265
G21 (-)	878	LR3	-269	-280	-291	-277	-288	-298	-280	-291	-300
G22 (+)	1033	MM3	1333	1430	1522	1403	1494	1582	1432	1520	1607
G22 (-)	112	MM3	-195	-216	-237	-210	-231	-251	-217	-237	-257
G23 (+)	1037	MM3	1459	1570	1677	1539	1644	1745	1573	1675	1774
G23 (-)	181	MM3	-166	-177	-188	-174	-185	-195	-177	-188	-197
G24 (+)	1081	MM3	1386	1492	1594	1463	1563	1660	1494	1592	1687
G24 (-)	182	MM3	-211	-231	-251	-226	-245	-263	-232	-250	-269
G25 (+)*	82	MM3	134	145	157	142	153	164	146	157	167
G25 (-)*	998	Multiplier	-451	--	--	-479	--	--	-493	--	--

*Results are presented for full disclosure, but the response of this channel was unreliable and it is recommended that these results are not used for comparison with CFD.

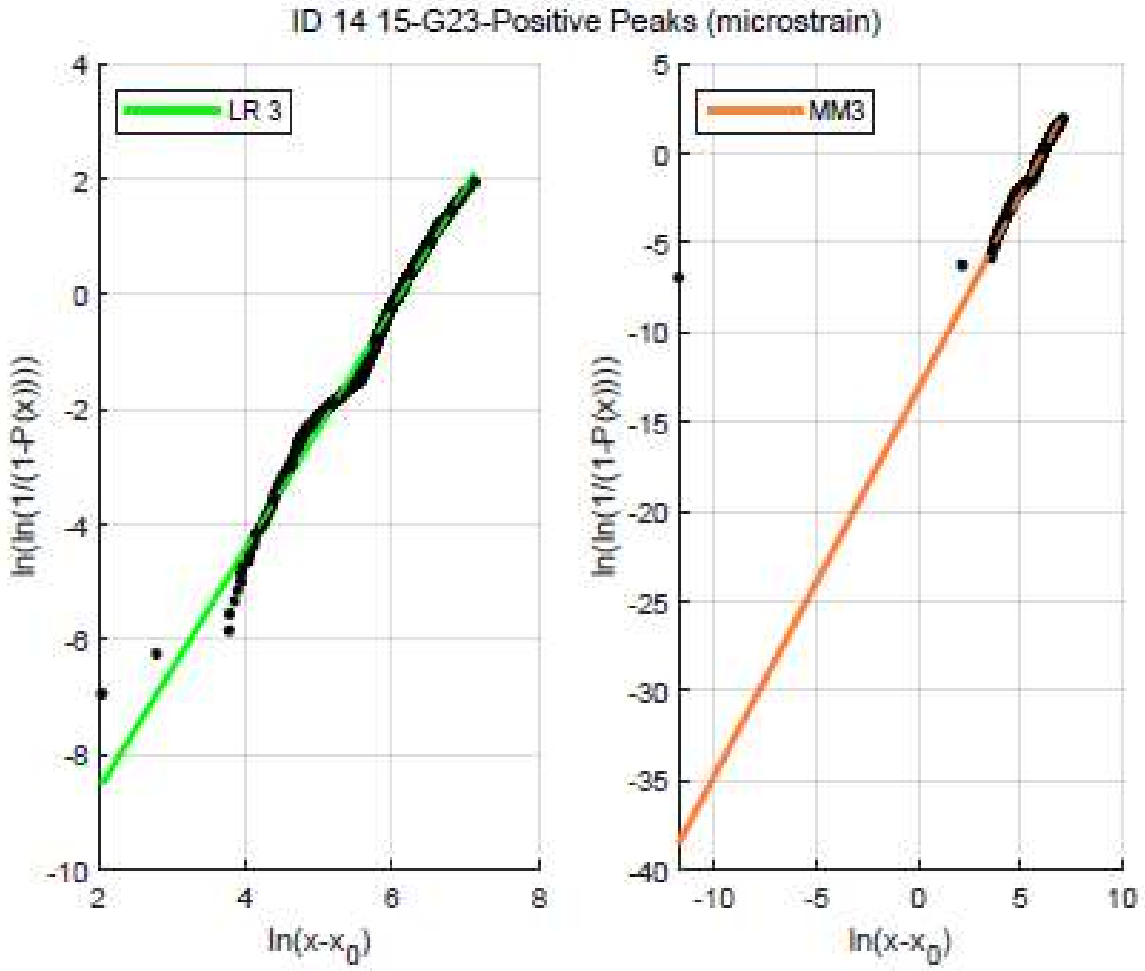

Figure 55. LR3 and MM3 Weibull Plots of Channel G23 for Matrix ID 14 and 15

Table 49. Weibull Shape Parameters for Pressure Transducer Channels in Matrix ID 14 and 15

Channel	Number of Events	Best Fit Method	σ (PSI)	Best Fit Parameters			
				β	η (PSI)	x_0 (PSI)	R^2
P11 (+)	722	Multiplier	1.0	--	--	--	--
P12 (+)	636	Multiplier	1.0	--	--	--	--
P13 (+)	414	Multiplier	0.8	--	--	--	--
P21 (+)	942	Multiplier	1.3	--	--	--	--
P22 (+)	787	MM3	0.9	1.7	2.1	0.4	--
P23 (+)	706	Multiplier	0.8	--	--	--	--

Table 50. Lifetime Extreme Estimates for Pressure Transducer Channels in Matrix ID 14 and 15

Channel	Number of Events	Best Fit Method	PNE @ 100 hr (PSI)			PNE @ 500 hr (PSI)			PNE @ 1000 hr (PSI)		
			36.8 %	90.0 %	99.0 %	36.8 %	90.0 %	99.0 %	36.8 %	90.0 %	99.0 %
P11 (+)	722	Multiplier	15	--	--	16	--	--	16	--	--
P12 (+)	636	Multiplier	14	--	--	15	--	--	15	--	--
P13 (+)	414	Multiplier	9	--	--	9	--	--	10	--	--
P21 (+)	942	Multiplier	13	--	--	13	--	--	14	--	--
P22 (+)	787	MM3	8	9	9	9	9	10	9	9	10
P23 (+)	706	Multiplier	14	--	--	14	--	--	15	--	--

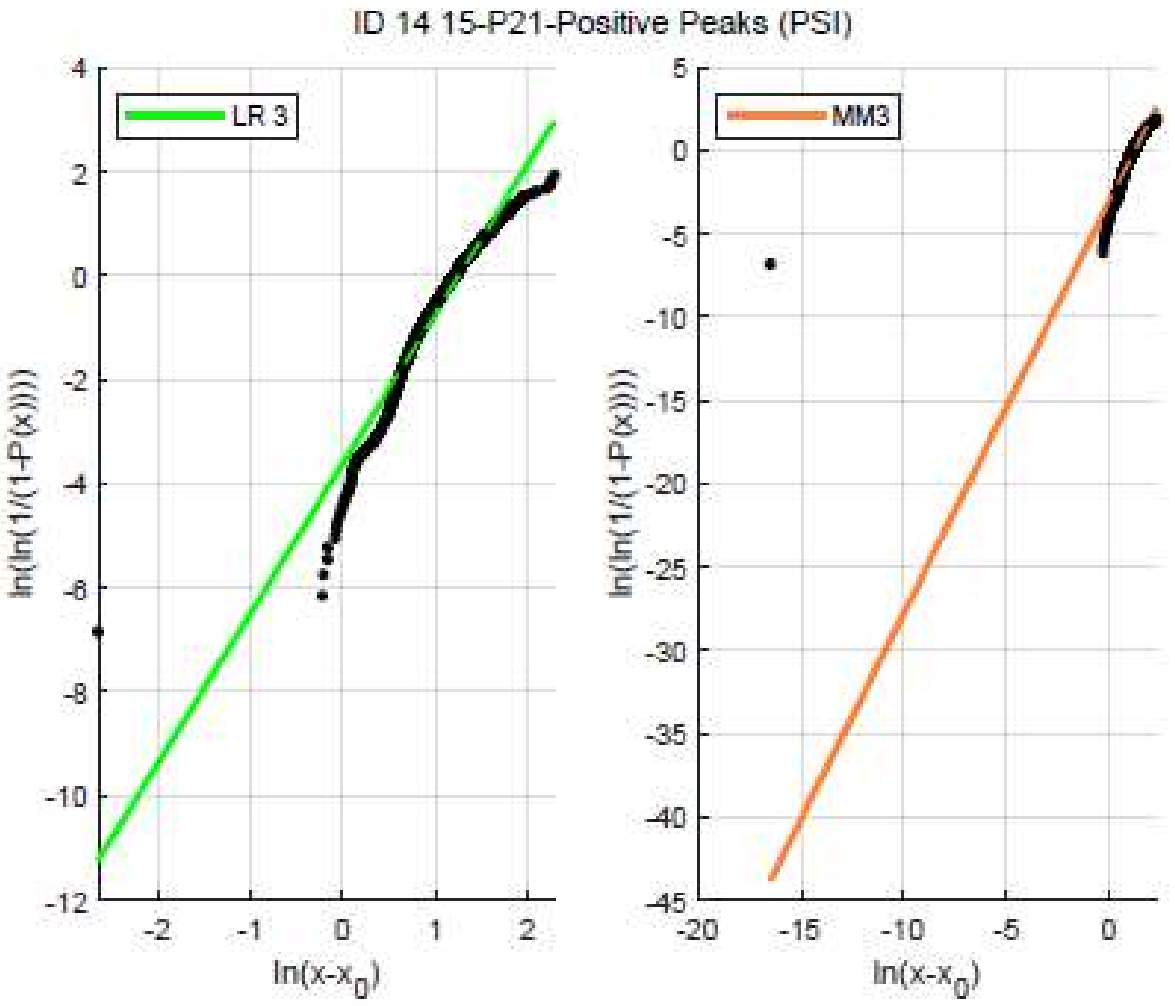

Figure 56. LR3 and MM3 Weibull Plots of Channel P21 for Matrix ID 14 and 15

CONCLUSIONS AND RECOMMENDATIONS

This technical report documents the GPPH secondary loads testing conducted in calm water, and in regular, and irregular wave conditions. The calm water data collected as part of this test effort and was plotted and compared with previous GPPH testing at NSWCCD and the USNA. The regular wave data was successfully collected, analyzed, and tabulated for future comparison with CFD/CSD numerical tools. Since multiple regular wave runs were collected, ensemble analysis was used to reduce statistical uncertainty. The uncertainties for an ensemble were approximately 35 % smaller than the uncertainties for a mean value for a given spot. The ensemble mean values of the primary variables calculated using both statistical methods (AC and NBB) are equivalent so results from either method would be acceptable for the future validation of numerical tools. It is also recommended that the ensemble mean values of the secondary variables be used for any future validation effort.

The irregular wave condition was also successfully collected, analyzed and tabulated for future use. This was a bright spot for the test effort since this was the first time that the irregular wave condition of interest could be tested at NSWCCD due to limitations of the carriage hardware. Prior to testing, a new tow post was designed and fabricated which enabled the GPPH model to be tested in a relatively large irregular wave condition which was not feasible during testing of the same hull years earlier.

The precision uncertainty was driven down by collecting over 500 wave encounters with each grillage panel and two speeds of interest. Again, the precision uncertainty was reduced through ensemble analysis and results were tabulated using statistical methods (AC and NBB).

The Traditional grillage and the Optimized grillage produced statistically different results that were consistent for both regular and irregular waves. Due to observed change in shape of the Optimized grillage with time, including prior to testing, it is recommended that comparisons using the Optimized grillage only be used with caution exercised. It is also recommended that the validation used for future numerical tools focus upon the ensemble mean values for regular wave comparisons and average one-nth values for irregular wave comparisons.

The test matrix was completed and yielded a large amount of motion and structural data that will be used for future comparisons with CFD/CSD numerical tools. The model test data was analyzed and presented within this technical report and can be referenced for future use. Two journal papers have been developed using the data contained in this report in combination with CFD/CSD numerical predictions. CFD/CSD comparisons to study FSI remain an ongoing effort.

Recommendations

A very large data set involving the GPPH hull form in the irregular wave condition at two discrete speeds of interest was collected. Due to the large number of wave encounters collected over many carriage passes, the statistical uncertainty of the measurement was minimized. It is therefore recommended that future CFD/CSD studies make use of and focus upon the measurements collected in the irregular wave conditions.

REFERENCES

1. Experimental and Computational Fluid-Structure Interaction Studies of a Semi-Planing Hull. Weil, Charles R, et al. Hamburg, Germany : Office of Naval Research, 2018. 32nd Symposium on Naval Hydrodynamics.
2. Fullerton, Anne, et al. R/V Athena Model (5365) Response in Waves. Bethesda, MD : Naval Surface Warfare Center Carderock Division, 2019c. NSWCCD-80-TR-2019/037.
3. Assessment of Experiments and CFD for the Semi-Planing R/V Athena Model in Waves. Lee, Evan J, et al. 2020b, Journal of Ocean Engineering.
4. Lee, Evan, Weil, Charles and Fullerton, Anne. Experimental Results for the Calm Water Resistance of the Generic Prismatic Planing Hull (GPPH). West Bethesda : Naval Surface Warfare Center Carderock Division, May 2017. NSWCCD-80-TR-2017/015.
5. Benchmark Testing of Generic Prismatic Planing Hull (GPPH) for Validation of CFD Tools. Lee, E.J., et al. Bethesda, Maryland : Society of Naval Architects and Marine Engineers, 2017. 30th American Towing Tank Conference (ATTC).
6. Experiments and CFD of high-speed deep-V planing hull--Part I: Calm water. Judge, Carolyn, et al. s.l. : Applied Ocean Research, Jan 2020.
7. Experiments and CFD of high-speed deep-V planing hull - part II: Slamming in waves. Judge, Carolyn, et al. Applied Ocean Research 97 (2020) 102059, s.l. : Applied Ocean Research, 2019.
8. Diez, M., Lee, E. J., Harrison, E. L., Powers, A. M., Snyder, L. A., Jiang, M. J., . . . Frederick, S. (September 2022). Experimental and Computational Fluid-Structure Interaction Analysis and Optimization of Deep-V Planing - Hull Grillage Panels Subject to Slamming Loads - Part I: Regular Waves. 85.
9. New Methodology in Analysis of Physical Properties and Roll Decay with Uncertainty Estimates for Surface-Ship Model Experiments. Park, Joel T, Turner, Charles R and Melendez, Mark P. West Bethesda, MD : American Towing Tank Conference, 2017, Vol. 30th.
10. Stahl, Ralph G. Ship Model Size Selection, Facilities, and Notes on Experimental Techniques. West Bethesda : Naval Surface Warfare Center Carderock Division, May 1995. CRDKNSWC/HD-1448-01.
11. Hoyt III, John G and Dipper, Martin. A Matrix Data Base Approach to Planing Craft Resistance Model Experiments. New Foundland, Aug 1998 : Proceedings of the 22nd American Towing Tank, Aug. 1998. pp. 92-102.
12. David Taylor Model Basin, Carderock Division, NSWC. ITTC Catalogue of Facilities; Towing Carriage No. 3. Iternational Towing Tank Conference. [Online] https://ittc.info/memebers/member-organizations/naval-surface-warfare-center-carderock-division/.

13. Standardized Wave and Wind Environments and Shipboard Reporting of Sea Conditions. STANAG 4194, s.l. : North Atlantic Treaty Organization (NATO), 1983.

14. Statistical Assessment and Validation of Experimental and Computational Ship Response in Irregular Waves. Diez, Matteo, et al. 021004, s.l. : Journal of Verification, Validation and Uncertainty Qualification , Jne 2018, Vol. Vol. 3.

15. Riley, Michael R., Haupt, K.D., and Jacobson, D.R. A Generalized Approach and Interim Criteria for Computing A1/n Accelerations Using Full-Scale High-Speed Craft Trials Data. West Bethesda : Naval Surface Warfare Center Carderock Division, April 2010. NSWCCD-23-TM-2010/13.

16. A Simplified Approach for Analyzing Accelerations Induced by Wave-Impacts in High-Speed Planing Craft. Riley, Michael R. and Coats, Timothy W. Annapolis, MD : Chesapeake Power Boat Symposium, June 2012, Vol. Third.

17. Statistical Uncertainty of Ship Motion Data. Belenky, V., V., Pipiras and Weems, K. Glasgow, UK : International Conference on the Stability of Ships and Ocean Vehicles, 2015, Vol. 12.

18. Single Significant Amplitude and Confidence Intervals for Stochastic Processes. pp. 1-16, s.l. : International Towing Tank Conference (ITTC), 2017. ITTC 7.5-02-01-08.

APPENDIX A: ACCURA60 COUPON TEST

In this appendix the nominal material properties of Accura60 are compared against a coupon test performed by Code 653, Performance Evaluation Branch, in the "Electronics Lab", room B17 of building 19 at Naval Surface Warfare Center, Carderock Division (NSWCCD).

From the Manufacturer

Table A - 1 shows the nominal material properties of Accura60. Note the average flexural modulus was used for design calculations (E = 413.5 KSI) for the traditional grillage.

Table A - 1. Accura60 Material Properties Provided from Manufacturer

MEASUREMENT	CONDITION	METRIC	U.S.
Tensile Strength (MPa/PSI)	ASTM D 638	58-68	8410-9860
Tensile Modulus (MPa/KSI)	ASTM D 638	2690-3100	390-450
Elongation at Break (%)	ASTM D 638	5-13 %	5-13 %
Flexural Strength (MPa/PSI)	ASTM D 790	87-101	12620-14650
Flexural Modulus (MPa/KSI)	ASTM D 790	2700-3000	392-435
Impact Strength (J/m /Ft-lbs/in)	ASTM D 256	15-25	0.3-0.5
Heat Deflection Temperature	ASTM D 648 @ 66 PSI @ 264 PSI	 53-55 °C 48-50 °C	 127-131 °F 118-122 °F
Coefficient of Thermal Expansion (CTE)	ASTM E 831-93 TMA (T<Tg, 0-40 °C) TMA (T<Tg, 75-140 °C)	 71-131 153	
Glass Transition (Tg)	DMA, E"	58 °C	136 °F
Hardness, Shore D		86	86

From Code 653 Lab Test

The manufacturer provides two values of modulus (E) for Accura60: one based on flexure and the other based on tension. For each of these, the manufacturer provided ranges for the product:

- Flexural Modulus: 392 - 435 ksi
- Tensile Modulus: 390 - 450 ksi

From a lab coupon test, performed by Naval Surface Warfare Center Carderock (NSWCCD), Code 653, the recommended values to use are:

- Flexural Modulus: 434 ksi
- Tensile Modulus: 483 ksi

The tensile modulus is outside of the manufacturer range, however, this test was conducted with multiple coupons and each was repeated twice to confirm the results.

The grillage was instrumented to measure both differential bending strain and unidirectional point strain. The differential bending strains only give a result based on bending. The unidirectional point strain yield results based on combined bending and axial tension or compression that may also exist. If the finite element model (FEM) only allows one modulus value, it is recommended to use the flexural (bending) modulus, as this was expected to be the dominant mode of response.

APPENDIX B: STIFFENER DETAILS FOR THE OPTIMUM GRILLAGE

In this appendix the details on each stiffener associated with the optimum grillage (design E) are further specified. Each stiffener is unique relative its neighbor. The details of interest can be found in Figure B - 1 though Figure B - 6.

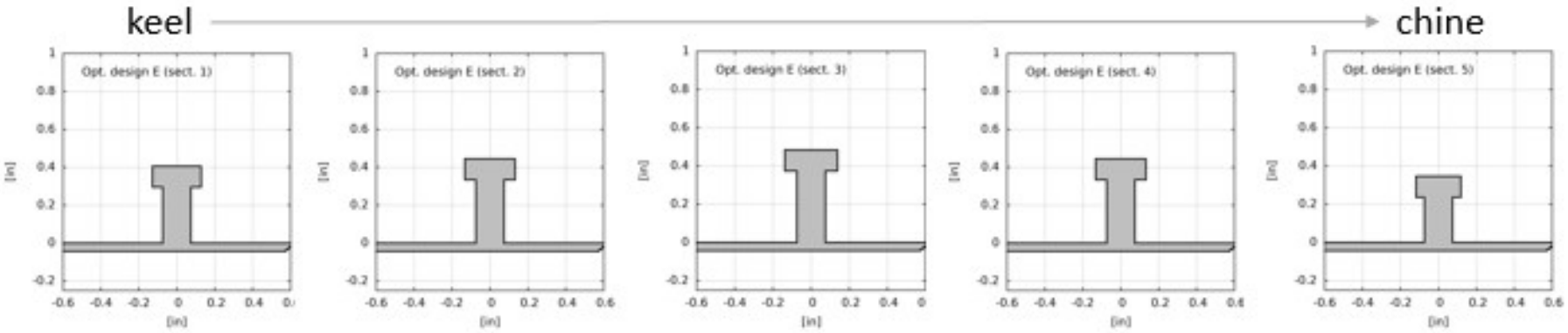

Figure B - 1. GPPH Optimized Grillage Stiffener Dimensions

Opt. design E (sect. 1)

Sections are numbered from keel to chine, where the section close to the keel is 1 and the section close to the chine is 5

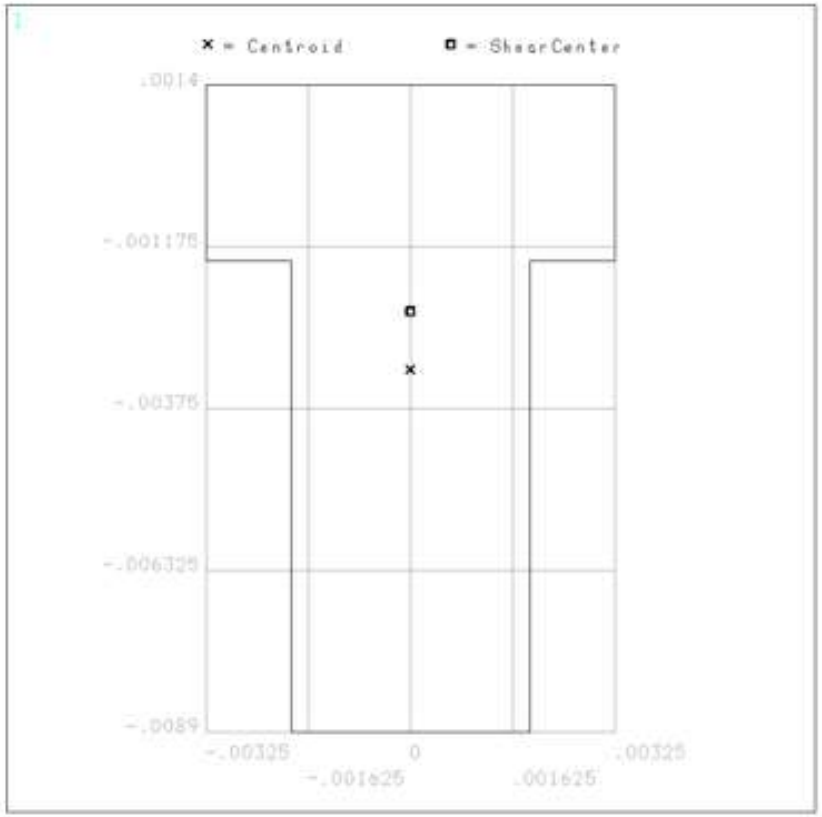


```
SECTION ID 31
DATA SUMMARY

Section Name
  =
Area
  = .467E-04
Iyy
  = .440E-09
Iyz
  = 0
Izz
  = .984E-10
Warping Constant
  = .477E-15
Torsion Constant
  = .188E-09
Centroid Y
  = .248E-18
Centroid Z
  = -.003143
Shear Center Y
  = .122E-18
Shear Center Z
  = -.0022
Shear Corr. YY
  = .744633
Shear Corr. YZ
  = .704E-15
Shear Corr. ZZ
  = .7264
```

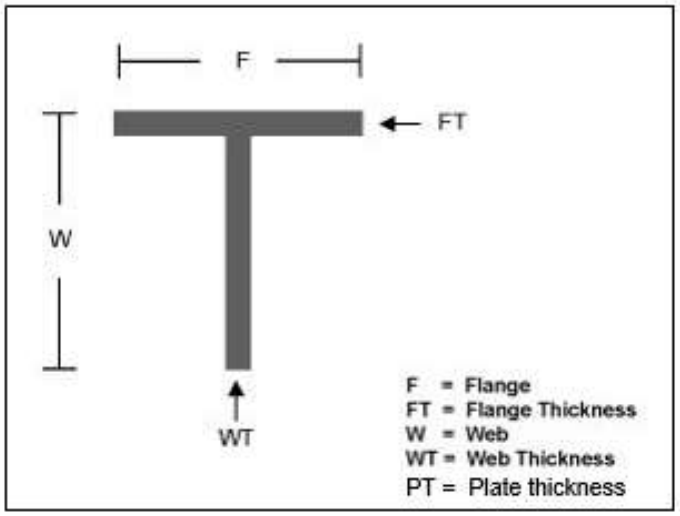

FT = 0.1102”
WT = 0.1496”
F = 0.2559”
W = 0.4055”
PT = 0.0433”

Figure B - 2. Dimensions of Stiffener Closest to Keel

Opt. design E (sect. 2)

Sections are numbered from keel to chine, where the section close to the keel is 1 and the section close to the chine is 5

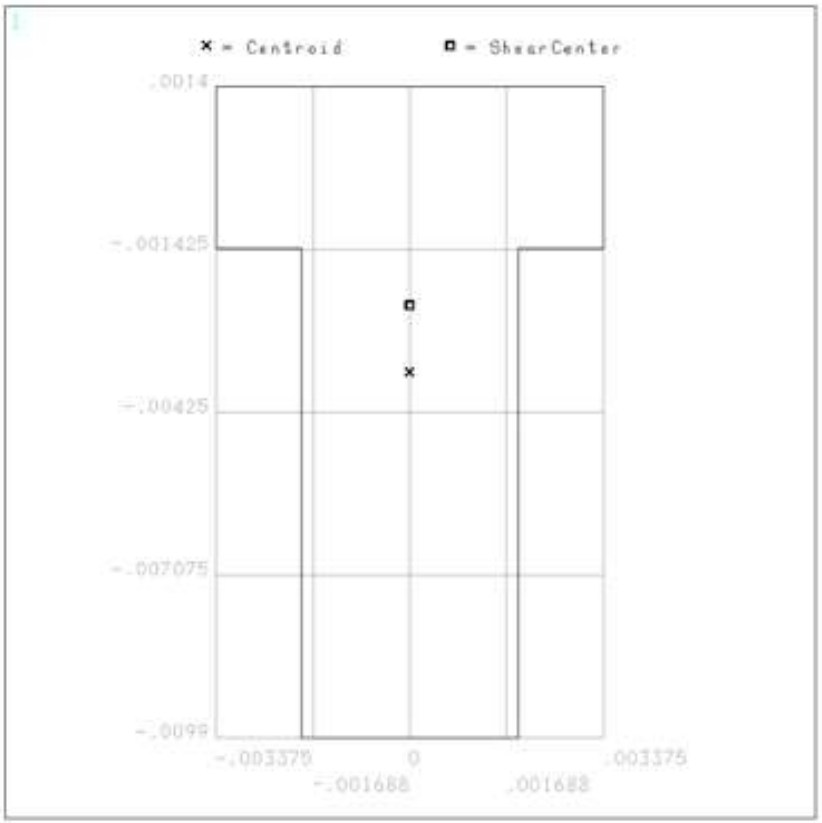


```
SECTION ID 32
DATA SUMMARY

Section Name
  =
Area
  = .512E-04
Iyy
  = .587E-09
Iyz
  = 0
Izz
  = .111E-09
Warping Constant
  = .709E-15
Torsion Constant
  = .210E-09
Centroid Y
  = .178E-18
Centroid Z
  = -.003564
Shear Center Y
  = .151E-17
Shear Center Z
  = -.002391
Shear Corr. YY
  = .720931
Shear Corr. YZ
  = .173E-14
Shear Corr. ZZ
  = .723016
```

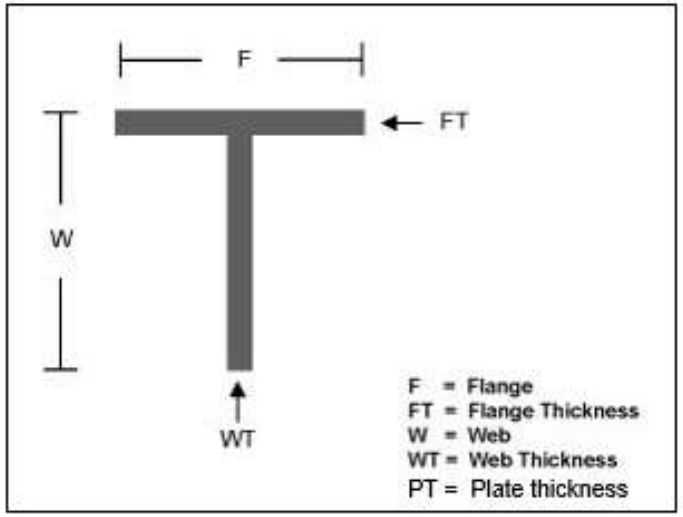

FT = 0.1102”
WT = 0.1496”
F = 0.2657”
W = 0.4449”
PT = 0.0433”

Figure B - 3. Dimensions of Second Stiffener from Keel

Opt. design E (sect. 3)

Sections are numbered from keel to chine, where the section close to the keel is 1 and the section close to the chine is 5

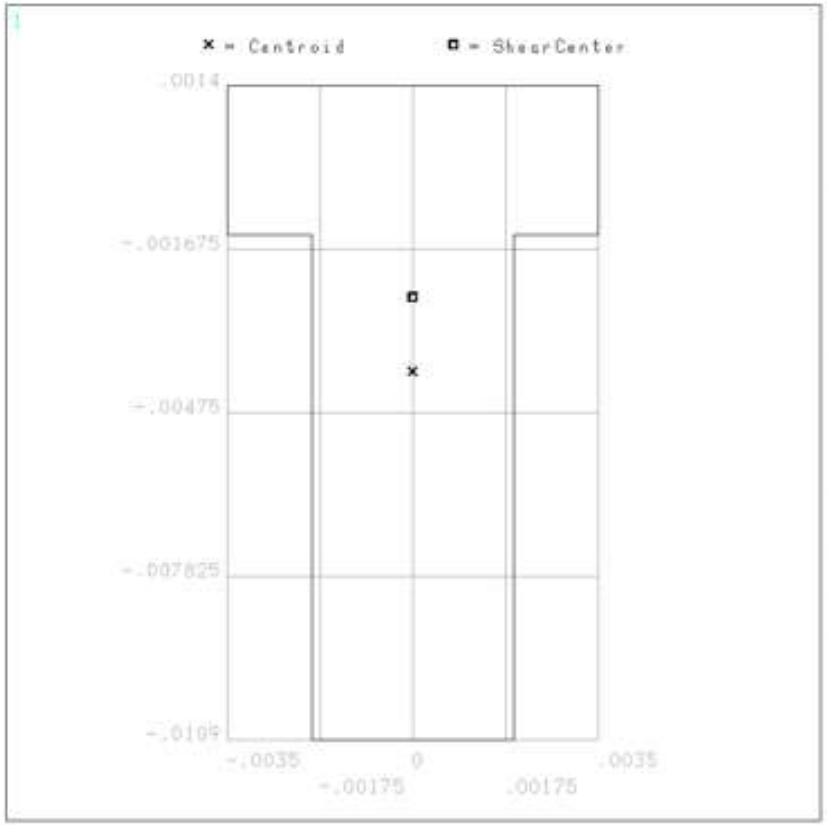


```
SECTION ID 33
DATA SUMMARY

Section Name
  =
Area
  = .557E-04
Iyy
  = .765E-09
Iyz
  = 0
Izz
  = .123E-09
Warping Constant
  = .100E-14
Torsion Constant
  = .231E-09
Centroid Y
  = .594E-19
Centroid Z
  = -.003986
Shear Center Y
  = -.142E-17
Shear Center Z
  = -.002572
Shear Corr. YY
  = .697935
Shear Corr. YZ
  = -.207E-14
Shear Corr. ZZ
  = .720882
```

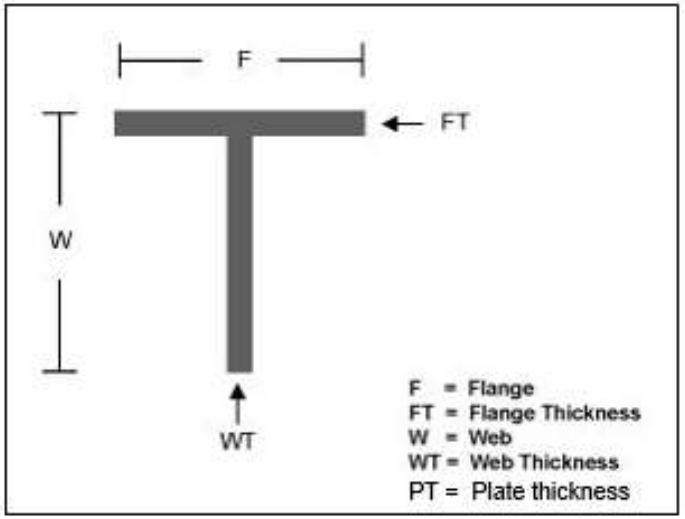

FT = 0.1102”
WT = 0.1496”
F = 0.2756”
W = 0.4843”
PT = 0.0433”

Figure B - 4. Dimensions of Third Stiffener from Keel

Opt. design E (sect. 4)

Sections are numbered from keel to chine, where the section close to the keel is 1 and the section close to the chine is 5

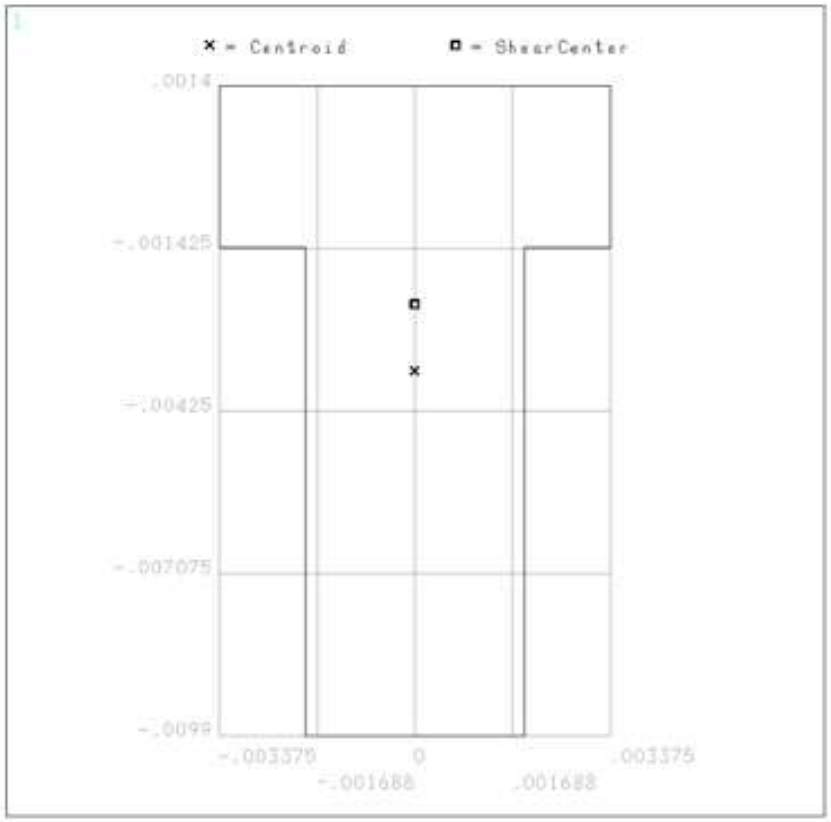


```
SECTION ID 34
DATA SUMMARY

Section Name
  =
Area
  = .512E-04
Iyy
  = .587E-09
Iyz
  = 0
Izz
  = .111E-09
Warping Constant
  = .709E-15
Torsion Constant
  = .210E-09
Centroid Y
  = .178E-18
Centroid Z
  = -.003564
Shear Center Y
  = .151E-17
Shear Center Z
  = -.002391
Shear Corr. YY
  = .720931
Shear Corr. YZ
  = .173E-14
Shear Corr. ZZ
  = .723016
```

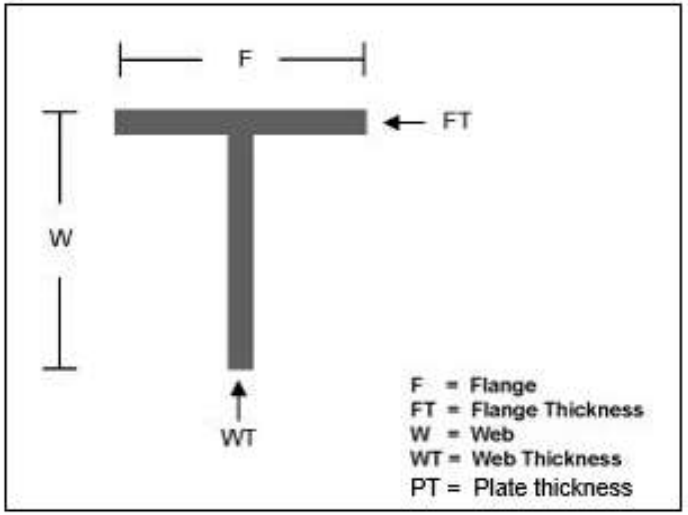

FT = 0.1102”
WT = 0.1496”
F = 0.2657”
W = 0.4449”
PT = 0.0433”

Figure B - 5. Dimensions of Fourth Stiffener from Keel

Opt. design E (sect. 5)

Sections are numbered from keel to chine, where the section close to the keel is 1 and the section close to the chine is 5

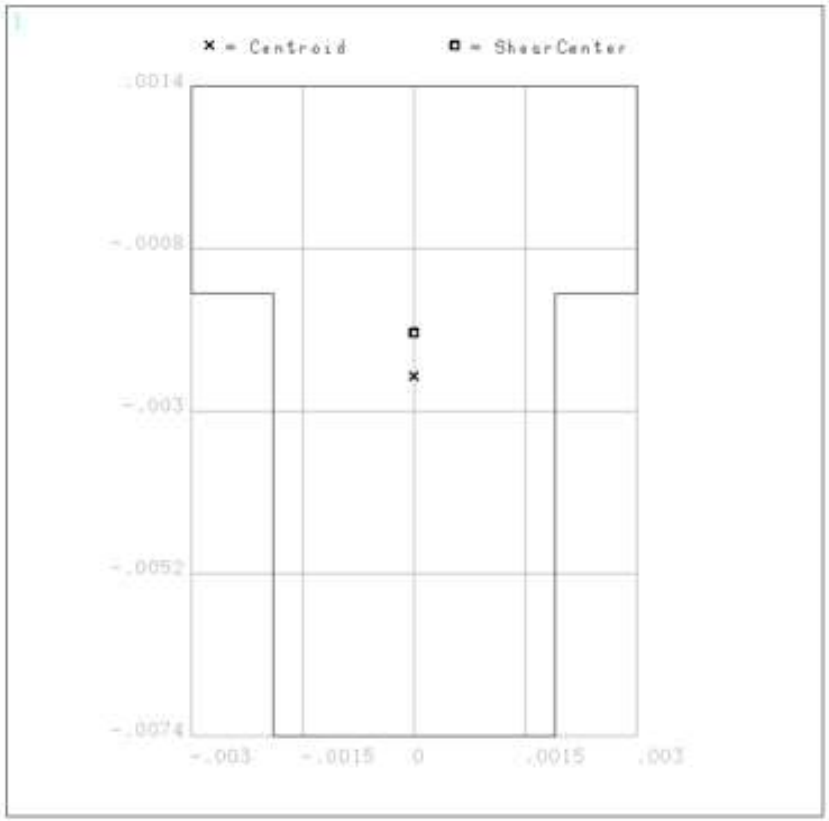


```
SECTION ID 35
DATA SUMMARY

Section Name
  =
Area
  = .396E-04
Iyy
  = .267E-09
Iyz
  = 0
Izz
  = .778E-10
Warping Constant
  = .227E-15
Torsion Constant
  = .155E-09
Centroid Y
  = .104E-19
Centroid Z
  = -.002533
Shear Center Y
  = .829E-18
Shear Center Z
  = -.001937
Shear Corr. YY
  = .790926
Shear Corr. YZ
  = -.446E-16
Shear Corr. ZZ
  = .741593
```

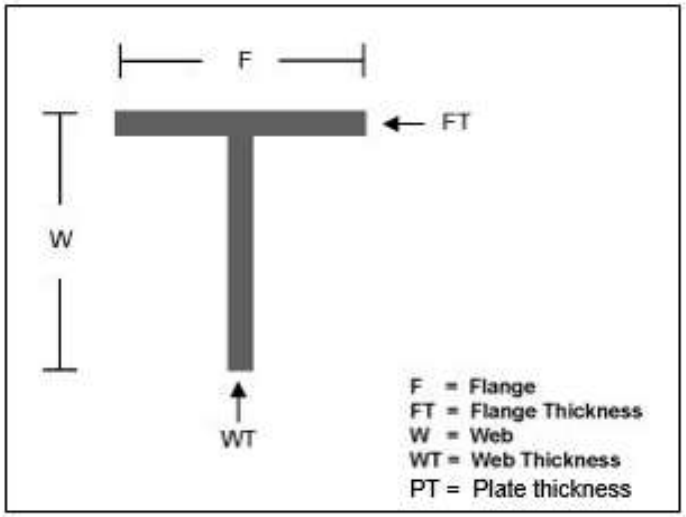

FT = 0.1102”
WT = 0.1496”
F = 0.2362”
W = 0.3465”
PT = 0.0433”

Figure B - 6. Dimensions of Fifth Stiffener from Keel, Closest to Chine

APPENDIX C: CALIBRATION OF GRILLAGES

In this appendix, the calibration process, data and associated instrumentation uncertainty for the two grillages is presented.

GRILLAGE CALIBRATION PROCESS

A unique calibration fixture was designed to mate to the measurement area of each grillage. The fixture had a single open chamber sealed with black neoprene rubber. The fixture was mounted to each grillage during the calibration process such that the fixture's open chamber aligned with the grillage's measurement area. When assembled in this way, the black neoprene rubber functioned as a gasket, such that no air could escape as pressure was applied to the chamber. A manufacture-calibrated pressure transducer recorded the pressure within the chamber during calibrations as pressures were gradually increased from 0 PSI – 4 PSI. This setup allowed for pressure to be applied uniformly over the entire measurement area of the grillage.

GRILLAGE CALIBRATION DATA

Traditional Grillage

The values shown in Table C - 1 are the calibration factors which were applied to the traditional grillage during testing. Channels 20 and 25 should be disregarded because the data collected indicates that the stiffener is too stiff for the strain gages to have meaningful output. The bolded values are the calibration factors that were applied to the raw data, and the red values correspond to channels that produced erroneous results during calibration.

Table C - 1. GPPH Traditional Grillage Pre-Test Calibration Factors

Channel		Traditional Grillage		
		(PSI / Volt)	(PSI / με)	(με / Volt)
Differential Bending Channels	1	**1406**	0.00235	598737
	2	**1373**	0.00229	599862
	3	**2333**	0.00389	599399
	4	**3088**	0.00259	1191335
	5	**3268**	0.00272	1200159
	6	**1666**	0.00278	599843
	7	**2604**	0.00434	599343
	8	**1844**	0.00307	599907
	9	**7760**	0.01294	599816
	10	**2569**	0.00430	597330
Single Strain Channels	11	7075	0.00588	**1203436**
	12	8189	0.00678	**1207995**
	13	4544	0.00377	**1205305**
	14	5421	0.00449	**1207081**
	15	6622	0.00550	**1204438**
	16	4258	0.00354	**1204526**
	17	3936	0.00326	**1205513**
	18	4267	0.00354	**1204687**
	19	5502	0.00457	**1204730**
	20	26306	0.02082	**1263497**
	21	8066	0.00670	**1204240**
	22	5446	0.00452	**1205401**
	23	6036	0.00502	**1203589**
	24	7303	0.00606	**1205712**
	25	65054	0.05454	**1192754**

Optimized Grillage

The optimized grillage deformed during testing, and cracked upon removal from the model, so no post-test calibrations were performed. Pre-test calibration factors were used for all data analysis. The PSI/Volt calibration factors were applied to the differential bending channels (CH 1 – 10), and the microstrain per Volt (με/Volt) calibration factors were applied to the single strain channels (CH 11 – 25). The values that were applied during testing are bolded in Table C - 2, and were later revised, as explained below, to the values presented in Table C-3 for final data analysis.

The original pre-test calibration factors for the optimized grillage are listed in Table C-2. Following testing, these values were later modified during post-processing to account for mechanical properties which may have affected how the grillage responded to very low pressures. The correction was performed for channels on the optimized grillage which did not have points at zero pressure that coincided with the best-fit line for the calibration data. The revised calibration factors were calculated by omitting the points at zero pressure to achieve a new best fit line. This applied to channels 2, 3, 6, 7, 15, and 20.

This correction was not needed for the traditional grillage because there was no apparent difference in response between high and low pressures. The adjusted calibration factors for the optimized grillage that were used for all analyses are shown in Table C - 3.

Table C - 2. GPPH Optimized Grillage Pre-Test Calibration Factors

	Optimized Grillage			
	Channel	PSI/Volt	PSI/με	με/Volt
Differential Bending Channels	CH 1	**1593**	0.00262	607698
	CH 2	**6235**	0.01022	610199
	CH 3	**799**	0.00130	612795
	CH 4	**3010**	0.00491	613105
	CH 5	**2152**	0.00350	615742
	CH 6	**4327**	0.00703	615520
	CH 7	**888**	0.00146	609331
	CH 8	**538**	0.00088	612265
	CH 9	**898**	0.00147	611657
	CH 10	**738**	0.00118	624018
Single Strain Channels	CH 11	2945	0.00245	**1200830**
	CH 12	2810	0.00234	**1199331**
	CH 13	2196	0.00184	**1195521**
	CH 14	2479	0.00207	**1197886**
	CH 15	12285	0.01024	**1200029**
	CH 16	6615	0.00551	**1201300**
	CH 17	2318	0.00194	**1196073**
	CH 18	2335	0.00194	**1204856**
	CH 19	2727	0.00227	**1201350**
	CH 20	31604	0.02625	**1203950**
	CH 21	7943	0.00662	**1199592**
	CH 22	3650	0.00305	**1197772**
	CH 23	3075	0.00256	**1203034**
	CH 24	3750	0.00313	**1199819**
	CH 25	12814	0.01068	**1200106**

Table C - 3. GPPH Optimized Grillage Revised Calibration Factors

	Optimized Grillage			
	Channel	PSI / Volt	(PSI / με)	με / Volt
Differential Bending Channels	CH 1	1593	0.00262	607698
	CH 2	7617	0.01248	610199
	CH 3	674	0.00110	612795
	CH 4	3010	0.00491	613105
	CH 5	2152	0.00350	615742
	CH 6	3602	0.00585	615520
	CH 7	776	0.00127	609331
	CH 8	538	0.00088	612265
	CH 9	898	0.00147	611657
	CH 10	738	0.00118	624018
Single Strain Channels	CH 11	2945	0.00245	1200830
	CH 12	2810	0.00234	1199331
	CH 13	2196	0.00184	1195521
	CH 14	2479	0.00207	1197886
	CH 15	13039	0.01087	1200029
	CH 16	6615	0.00551	1201300
	CH 17	2318	0.00194	1196073
	CH 18	2335	0.00194	1204856
	CH 19	2727	0.00227	1201350
	CH 20	25268	0.02099	1203950
	CH 21	7943	0.00662	1199592
	CH 22	3650	0.00305	1197772
	CH 23	3075	0.00256	1203034
	CH 24	3750	0.00313	1199819
	CH 25	12814	0.01068	1200106

GRILLAGE UNCERTAINTY

The calibration uncertainties were calculated for both the traditional and optimized grillages and are shown in Table C - 4. For the case of the optimized grillage, the revised calibration factors, shown in Table C - 3, were used. As is the case in the earlier tables, channels deemed erroneous are highlighted in red. The methodology used to determine the calibration uncertainties can be found in Appendix D, Instrument Calibration with Uncertainty Estimates.

Table C - 4. Grillage Uncertainties

	Average U_{95} Uncertainty (PSI/Volt)	
	Traditional	*Optimized*
Channel 1	0.129	0.157
Channel 2	0.138	0.428
Channel 3	0.047	0.330
Channel 4	0.115	0.124
Channel 5	0.140	0.178
Channel 6	0.118	0.499
Channel 7	0.110	0.261
Channel 8	0.061	0.060
Channel 9	0.143	0.249
Channel 10	0.061	0.058
Channel 11	0.200	0.069
Channel 12	0.221	0.091
Channel 13	0.132	0.095
Channel 14	0.152	0.078
Channel 15	0.124	0.299
Channel 16	0.176	0.105
Channel 17	0.198	0.104
Channel 18	0.263	0.084
Channel 19	0.355	0.132
Channel 20	2.074	0.623
Channel 21	0.152	0.118
Channel 22	0.159	0.045
Channel 23	0.185	0.071
Channel 24	0.244	0.082
Channel 25	2.664	0.149

THIS PAGE INTENTIONALLY LEFT BLANK

APPENDIX D: INSTRUMENT CALIBRATION WITH UNCERTAINTY ESTIMATES

CONTENTS

Figures……D-1
Tables……D-2
Symbols……..D-3
Theory……D-4
Uncertainty Analysis……..D-4
Acceleration ……...D-6
Tilt Table……D-6
Uncertainty in Acceleration ……...D-7
Results……D-9
Accelerometers ……..D-9
CG Acclerometers……..D-9
Local Acceleration of Gravity……..D-10
Drag and Side Force……D-16
Conclusions……..D-36
Recommendations……D-36
References……D-38

FIGURES

Figure D - 1. Expanded Uncertainty in Acceleration at 95 % Confidence Limit D-8
Figure D - 2. CG1 Accelerometer 1 g Calibration for DTMB Model 5765 ..... D-11
Figure D - 3. CG1 Accelerometer 10 g Calibration for DTMB Model 5765 ..... D-11
Figure D - 4. CG2 Accelerometer Calibration 1 g for DTMB Model 5765 ..... D-12
Figure D - 5. CG2 Accelerometer Calibration 25 g for DTMB Model 5765 ..... D-12
Figure D - 6. Tow-Post Accelerometer Calibration 1 g for DTMB Model 5765 ..... D-13
Figure D - 7. Tow-Post Accelerometer Calibration 10 g for DTMB Model 5765 ..... D-13
Figure D - 8. Bow Accelerometer 1 g Calibration for DTMB Model 5765 ..... D-14
Figure D - 9. Bow Accelerometer 25 g Calibration for DTMB Model 5765 ..... D-14
Figure D - 10. Stern Accelerometer 1 g Calibration for DTMB Model 5765..... D-15
Figure D - 11. Stern Accelerometer 10 g Calibration for DTMB Model 5765..... D-15
Figure D - 12. Block Gage Drag Calibration for DTMB Model 5765..... D-17
Figure D - 13. Block Gage Side - Force Calibration for DTMB Model 5765 ..... D-18

Figure D - 14. Celesco Heave Calibration for DTMB Model 5765 ..... D-19
Figure D - 15. Schaevitz Pitch Angle Calibration for DTMB Model 5765 ..... D-19
Figure D - 16. PCB Pressure Transducer Locations for DTMB Model 5765 ..... D-20
Figure D - 17. PCB Pressure Calibration for DTMB Model 5765 at Location P51 ..... D-21
Figure D - 18. PCB 113B28 Pre - and Post - Test Uncertainty Comparison D-21
Figure D - 19. Maximum Difference between Pre - & Post - Test PCB Calibration D-22
Figure D - 20. Strain Gage Locations on Grillage Panel for DTMB Model 5765 ..... D-23
Figure D - 21. CG Wave Height Probe Calibration D-34
Figure D - 22. Bow Wave Height Probe Calibration D-35

TABLES

Table D - 1. Calibration Summary of DTMB Model 5765 Accelerometers D-25
Table D - 2. Calibration Summary of DTMB Model 5765 Other Instruments D-27
Table D - 3. PCB Pressure Calibration Summary D-28
Table D - 4. Comparison of Computed Slope Calibration to PCB Value D-32

SYMBOLS

F ..... Force N

g ..... Local acceleration of gravity m/s^2

g_c ..... Conventional acceleration of gravity, $g_c = 9.80665$m/s^2

k ..... Coverage factor, usually $k = 2$

m ..... Mass kg

n ..... Number of samples or parameters

SEE ..... Standard error of estimate

s ..... Standard deviation

t ..... Time s

U ..... Expanded uncertainty, $U = ku$

u ..... Standard uncertainty

u ..... Axial velocity in x direction m/s

v ..... Transverse velocity in y direction m/s

w ..... Vertical velocity in z direction m/s

x ..... Axial Cartesian coordinate, positive toward bow m

y ..... Transverse Cartesian coordinate, positive toward port (left) m

z ..... Vertical Cartesian coordinate, positive up m

θ ..... Pitch angle, positive bow down (rad)

ρ_a ..... Density of air (kg/m$^{3)}$

ρ_w ..... Density of weight (kg/m^3)

φ ..... Roll angle, positive port (left side) side up (rad)

ψ ..... Yaw angle, positive bow to port (left) (rad)

THEORY

Uncertainty Analysis

An uncertainty analysis applied to this report is based upon the Joint Committee for Guides in Metrology JCGM Guide to the Uncertainty in Measurement (GUM) [D-1] and the uncertainty analysis procedure from the International Towing Tank Conference (ITTC) [D-2]. The analysis consists of two methods of evaluation: Type A and Type B. For this report, all uncertainties are defined at the 95 % confidence limit (U95). The Type A standard uncertainty is computed from the time series data acquired during the test or from repeat observations and is defined in Equation (D - 1) for the mean value:

$$u = s_x/\sqrt{n} \tag{D - 1}$$

Where u is the standard uncertainty, and the standard deviation of x, s_x, is

$$s_x^2 = [1/(n-1)] \sum_{i=1}^{n} (x_i - \bar{x})^2 \tag{D - 2}$$

And the mean of x is

$$\bar{x} = (1/n) \sum_{i=1}^{n} x_i \tag{D - 3}$$

Where n is the number of samples or observations.

The standard uncertainty in Equation (D - 1) is also the standard deviation of the mean. The expanded uncertainty is defined as follows:

$$U = ku \tag{D - 4}$$

Where k is the coverage factor. At the 95 % confidence level, k equals 2. For small sample sizes, the coverage factor may be replaced by the inverse Student-t at the 95 % confidence level, $t_{95} = t_{0.025,\, n-1}$.

The Type B method [D-1] for standard uncertainty is evaluation by means other than statistical as defined by Equation (D - 1). Per the JCGM GUM [D-1], these include the following:

- Previous measurement data
- Experience or general knowledge
- Manufacturer's specifications
- Calibration data or other certificates
- Uncertainties assigned to the reference data from handbooks

For this report, the Type B uncertainty is determined primarily from calibration of the instruments with traceability to the National Institute for Standards and Technology (NIST),

which is the National Metrology Institute (NMI) for the USA. For most electronic instruments, the uncertainty in the reference standards is small in comparison to the uncertainty in the electronic transducers. For conversion of the voltages from the analog to digital converter or data acquisition card (DAQ) in the data acquisition system to engineering units or physical units, the slopes and intercepts from regression analysis of the calibration data are applied to the data analysis. The uncertainty in calibration is described in an International Towing Tank Conference (ITTC) procedure [D-3], and the details described by calibration theory from Scheffe [D-4] and Carroll, et al.[D-5].

Scheffe [D-4] has developed a statistical theory of calibration. A simplified method with detailed examples has been provided by Carroll, et al. [D-5]. The prediction limit in this case is given by

$$f(x) - SEE(c_1 + c_2 s_{xx}) \le y \le f(x) + SEE(c_1 + c_2 s_{xx}) \quad \text{(D - 5)}$$

Where

$$c_1 = t_{0.025,n-2},\ c_2 = \sqrt{2F_{2,n-2}}$$

And

$$s_{xx} = \sum_{i=1}^{n} (x_i - \bar{x})^2 \quad \text{(D - 6)}$$

t is the inverse Student-t probability density function (pdf) and F is the inverse Fisher PDF.

The uncertainty in x for a linear equation in physical units is then from Scheffe [D-4]

$$x_h = \bar{x} + \left[bD - (-1)^h (SEE \times c_2)(C/n + D^2/s_{xx})^{1/2}\right]/C \quad \text{(D - 7)}$$

$$C = b^2 - (SEE \times c_2)^2/s_{xx}$$

$$D = b(x - \bar{x}) - (-1)^h SEE \times c_1$$

Where h = 1 and 2 are the upper and lower bounds, respectively.

The inverse Student - t and Fisher PDFs may be found in tables in standard statistical references and mathematical handbooks such as Ross [D-6]. These functions are also available in Microsoft Excel. Other statistical functions such as the slope (a), intercept (b), average ($\bar{x}$) and standard error of estimate (*SEE*), effectively the standard deviation of the curve fit, are available in Excel.

For those quantities not measured directly such as acceleration of gravity, Froude number, and non-dimensional wavelength and height, the uncertainties are propagated to obtain the combined expanded uncertainty from the following equation from the GUM JCGM [D-1] and ITTC [D-2].

$$U_c^2 = \sum_{i=1}^{N} [(\partial f/\partial x_i) U(x_i)]^2 \quad \text{(D - 8)}$$

Where the derivative is known as the sensitivity coefficient. This equation is applicable to uncorrelated or statistically independent measurement quantities.

For this test series, the model instruments were calibrated twice: May and June 2019 (pre-test calibration), and August and September 2019 (post-test calibration). Since multi - calibrations were performed, data will be shown which compares the more recent calibration with the older one with the older calibration values of slope and intercept as the reference.

Acceleration

Tilt Table

Accelerations were measured at four model locations: the bow, stern, tow post, and center of gravity (CG). Acceleration is referenced to local acceleration of gravity, g, by a tilt table with a resolution of 10 min of arc. The table was calibrated with the Wyler Clino 2000 multi - purpose inclination - measuring instrument, which has a resolution of 5 arc seconds and an uncertainty of ±30 arc seconds (±0.0083°), and the angles checked with an Applied Geomechanics Pro 3600 with a measurement uncertainty of ±0.20°.

Acceleration Calibration by Inclination

Longitudinal Acceleration

For longitudinal acceleration, an accelerometer is calibrated by tilting it about the y-axis in pitch, θ. The acceleration is then

$$du/dt = \dot{u} = -g \sin\theta \qquad \text{(D - 9)}$$

$$(du/dt)/g = \dot{u}/g = -\sin\theta$$

The longitudinal acceleration is positive for pitch bow up or a negative pitch angle. From Equation (D - 8), a negative pitch angle produces a negative value of the sine function; consequently the acceleration is positive. Pitch down or positive pitch angle produces a negative acceleration.

Vertical Acceleration

Vertical acceleration may be calibrated in either pitch (θ) or roll (φ). Acceleration is always negative for either positive or negative roll angles. The vertical acceleration is given by

$$dw/dt = \dot{w} = g(\cos\varphi - 1) \qquad \text{(D - 10)}$$

$$(dw/dt)/g = \dot{w}/g = \cos\varphi - 1$$

The vertical acceleration is referenced to local gravity so that under static conditions the vertical acceleration is zero. Calibration results for vertical acceleration in this document are reported for tilt in roll.

The sensor arrangement for the vertical component is also sensitive to pitch; consequently, the vertical component should also be calibrated in pitch so that the vertical acceleration can be corrected for deviations of the sensor in pitch and roll. The equations for the pitch calibration are then

$$dw/dt = \dot{w} = g(\cos\theta - 1) \qquad \text{(D - 11)}$$

$$(dw/dt)/g = \dot{w}/g = \cos\theta - 1$$

Transverse Acceleration

For transverse acceleration, an accelerometer is calibrated by tilting it about the *x*-axis in roll. The acceleration is then

$$dv/dt = \dot{v} = g \sin\theta \qquad \text{(D - 12)}$$

$$(dv/dt)/g = \dot{v}/g = \sin\theta$$

The transverse acceleration is negative for roll to port (left) or a negative roll angle. Roll to starboard (right) produces a positive acceleration. The acceleration is opposite that in a static calibration as previously discussed.

Uncertainty in Acceleration

Since the accelerometers are calibrated by inclination, the uncertainty in acceleration must be computed from the law of propagation of uncertainty from Equation (D - 8). The uncertainty in acceleration from the uncertainty in angle of inclination is then as follows.

From Equation (D - 9), the expanded uncertainty in longitudinal acceleration is

$$U_{\dot{u}}/g = (\cos\theta)U_\theta \qquad \text{(D - 13)}$$

For transverse acceleration from Equation (D - 12)

$$U_{\dot{v}}/g = (\cos\varphi)U_\varphi \qquad \text{(D - 14)}$$

For vertical acceleration in roll from Equation (D - 11)

$$U_{\dot{w}}/g = |\sin\varphi|U_\varphi \qquad \text{(D - 15)}$$

The expanded uncertainty at the 95 % confidence limit in local *g* from the uncertainty in tilt angle is shown in Figure D - 1 for transverse and vertical accelerations. As indicated in Equations (D - 13) and (D - 14), the result is the same for transverse and longitudinal accelerations. From this figure, the uncertainty in g from calibration with the digital protractor can be large in comparison to the manufacturer's specification of 0.1 % or 1 mg (0.001 g) for a 1 g range transducer. However, calibration with the calibrated settings of the tilt table with a measured uncertainty of ±0.05° yields an uncertainty that is much smaller. The uncertainty in reference angle for the accelerometers should be better than ±0.05°. The Applied Geomechanics Pro 3600 Digital Protractor is inadequate for this calibration; consequently, the tilt-table angles were applied for the calibration data in this test.

Force

For the calibration of the block gages for drag and side force for this test, the calibration on a calibration stand was in British Imperial units. The unit of mass for the weight set, usually NIST Class F [D-7], is pounds mass, lbm, while the unit of force is pounds force, lbf. Force is computed as follows from ASTM E74 - 18 [D-8]:

$$F = m(g/g_c)(1 - \rho_a/\rho_w) \qquad \text{(D - 16)}$$

Where m is the total mass, g is local gravity, g_c is standard gravity, ρ_a is standard air density, ρ_w is the weight density. The last term is a buoyancy correction term from Archimedes principle. The following are the numerical values:

- g = 9.80101 ±0.00004 m/s^2 at Naval Surface Warfare Center Carderock (NSWCCD)

- g_c = 9.80665 m/s^2
- ρ_a = 1.2 kg/m^3
- ρ_w = 8,000 kg/m^3 (conventional mass)

Since a weight set is calibrated on the same equipment and by the same standard, the weights are correlated. The NIST Class F tolerance of ±0.010 % [D-7] should be applied to the total load as the uncertainty estimate.

The load on the calibration fixture is changed by adding or removing weights. The applied load is then

$$m = \sum_{i=1}^{n} m_i \qquad \text{(D - 17)}$$

The expanded uncertainty in mass, m, is

$$U_m = \sum_{i=1}^{n} U_{mi} \qquad \text{(D - 18)}$$

Since the dominant term in the uncertainty in the calibration force is mass, the relative uncertainty in force is

$$U_F/F = U_m/m \qquad \text{(D - 19)}$$

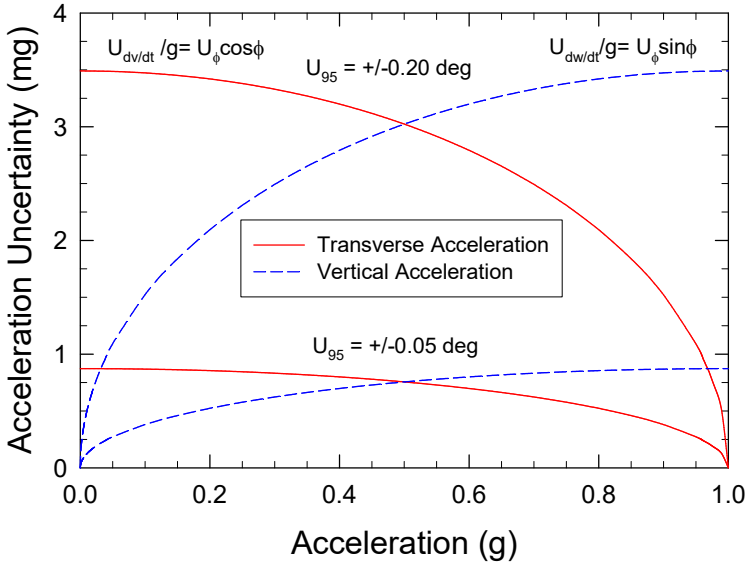

Figure D - 1. Expanded Uncertainty in Acceleration at 95 % Confidence Limit

RESULTS

Accelerometers

CG Acclerometers

Acceleration at the CG was measured by Kistler 8395A010 and Silicon Designs Inc. (SDI) 2460 - 025 triaxial accelerometers. The Kistler had a range of 10 g, while the SDI range was 25 g. They were calibrated over a ±1 g range on the tilt table previously described. Example plots of the residuals in calibration of acceleration for the Kistler are shown in Figure D - 2 and Figure D - 3, where the residuals are the differences between the data and the straight line fit from linear regression analysis. The results for the SDI are in Figure D - 4 and Figure D - 5. The dashed lines are the calibration uncertainties at the 95 % prediction limit from statistical calibration theory while the error bars are the uncertainty in the measurement during calibration. This convention is applied to the plots in this section. In this calibration, the error bars are from a combination of the Type A uncertainty calculated during acquisition of the data and the Type B from the calibration uncertainty of the reference angle, ±0.050°. In a residual plot, the error bars are readily apparent but would be smaller than the symbols in a conventional linear plot.

For the Kistler CG accelerometer in Figure D - 2, the slopes for the vertical and longitudinal components pass a hypothesis test in a comparison or pre- and post-test results. Passing a hypothesis test means that the two results in the comparison are identical statistically, and the results are very reproducible. Although the transverse component does not pass, the data are quite similar as indicated in the figure. Additional details of the hypothesis test for slope and intercept are described in more detail in a subsequent section. However, the uncertainty increases significantly for the longitudinal and vertical components in the post-test calibration, while the results for pre- and post-test are similar for the transverse component.

Figure D - 3 shows the uncertainty for the full - scale output (FSO) of the Kistler CG accelerometer. The uncertainty increases linearly outside the calibration range of ±1 g. The estimated uncertainty from this curve should be applied to measurements outside the ±1 g calibration range.

For the SDI CG accelerometer in Figure D - 4, the calibration results are similar to those of the Kistler. All components pass a hypothesis test for slope comparison for pre - test to post - test results. The uncertainty results in the transverse component are similar for the pre- and post-test calibrations. The post - test calibration uncertainty for the longitudinal component is higher than the pre-test and is similar to the pre-test uncertainty of the vertical component. The post-test uncertainty for the vertical is lower than the pre-test and is similar to the longitudinal pre-test uncertainty. The FSO is shown in Figure D - 5.

For the vertical acceleration, the calibration is offset by 1 g as indicated by Equation (D - 10). Normally, zeroes are recorded under calm water conditions. Consequently, all channels are referenced to zero such as pitch, roll, and all acceleration components. For the calibrations described in this appendix, the slope is the most significant as the intercept is corrected with the calm - water zeroes.

Tow-Post Accelerometer

The acceleration at the tow post is measured by a Kistler 8395A010 triaxial accelerometer with a range of 10 g. It is the same model as the CG1 accelerometer described in the previous section and Figure D - 2 and Figure D - 3. The calibration results are plotted in Figure D - 6 for the 1 g range and Figure D - 7 for the 10 g range. The uncertainty estimates for pre- and post-test calibrations are about the same as indicated in the figures. For the vertical component, the uncertainty is higher for the pre-test calibration, while the uncertainty is higher for the post-test calibration of the transverse component.

Bow and Stern Accelerometers

For the bow and stern acceleration, the measurements are from single component Kistler accelerometers mounted on a cube similar to the arrangement for the triaxial accelerometers for the CG and tow post in the previous sections. The accelerometers were calibrated in the same manner as the vertical component for the triaxial accelerometers. Consequently, the calibration results are from 0 to 1 g by Equation (D - 10) without the 1 g offset for the transverse and longitudinal components. The bow accelerometers were Kistler 8310B025 with a 25 g range, while the stern was a Kistler 8315A010 with a range of 10 g. The calibration results are in Figure D - 8 and Figure D - 9, while the stern are in Figure D - 10 and Figure D - 11. As the figures indicate, data are missing for - 1 to 0 g for the longitudinal and transverse components by this method of calibration.

Local Acceleration of Gravity

Local gravity in absolute units from Moose [D-9] is 9.80100 ±0.00004 m/s^2 at the Maneuvering and Seakeeping Basin (MASK). This value was computed from the National Oceanic and Atmospheric Administration (NOAA) National Geodetic Survey (NGS) of the U.S. Department of Commerce, with a latitude of 38° 58’ 25” North and longitude of 77° 11’ 20” East. Actual local g should be applied in all calculations involving *g*, such as Froude number and the conversion of pounds mass (lbm) to pounds force (lbf) in dynamometer calibration with weights; however, the difference will likely be small in comparison to other uncertainties in the measurements.

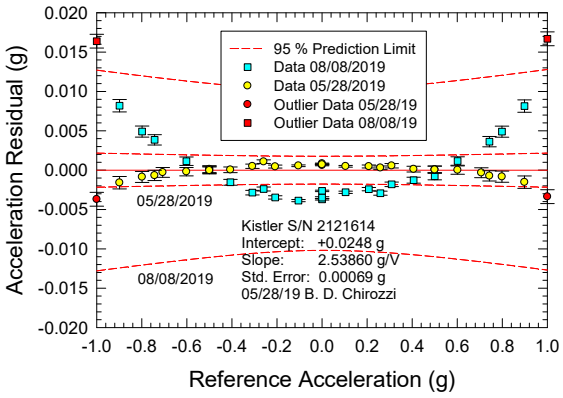

a. Longitudinal Acceleration

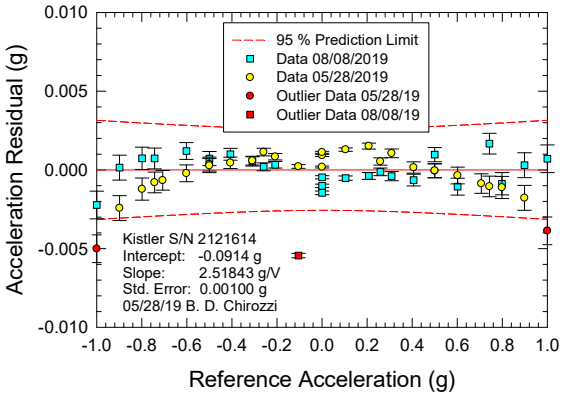

b. Transverse Acceleration

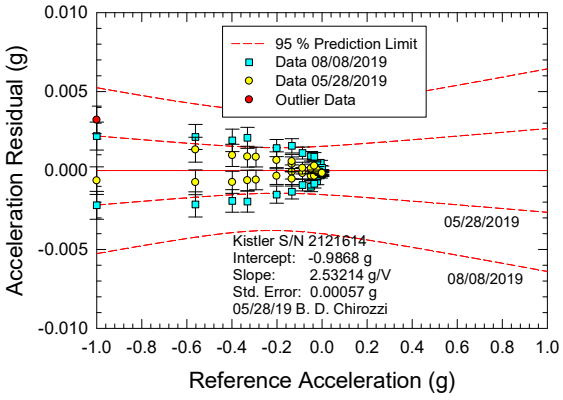

c. Vertical Acceleration

Figure D - 2. CG1 Accelerometer 1 g Calibration for DTMB Model 5765

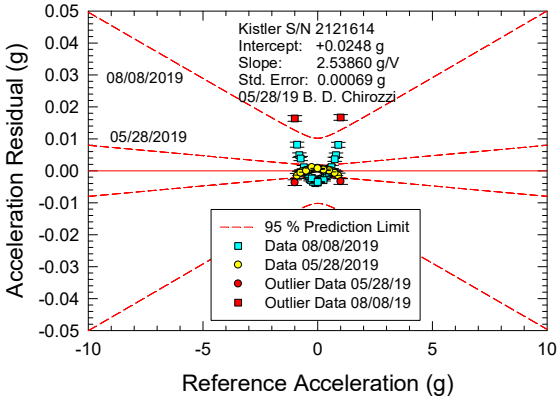

a. Longitudinal Acceleration

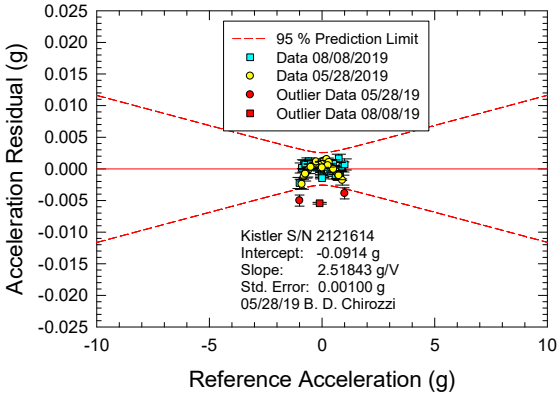

b. Transverse Acceleration

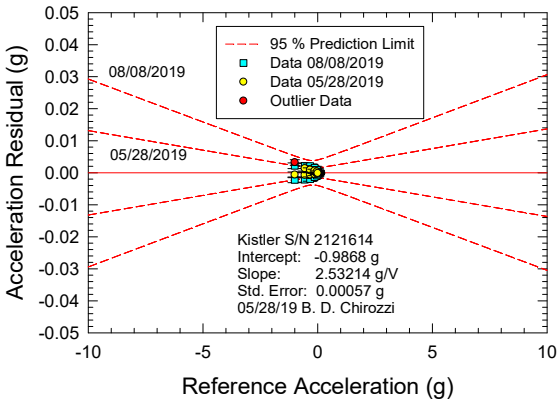

c. Vertical Acceleration

Figure D - 3. CG1 Accelerometer 10 g Calibration for DTMB Model 5765

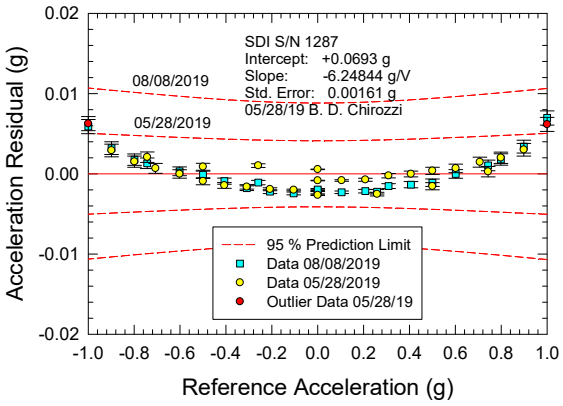

a. Longitudinal Acceleration

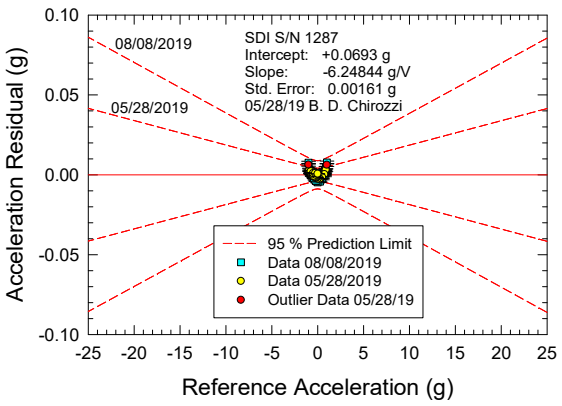

a. Longitudinal Acceleration

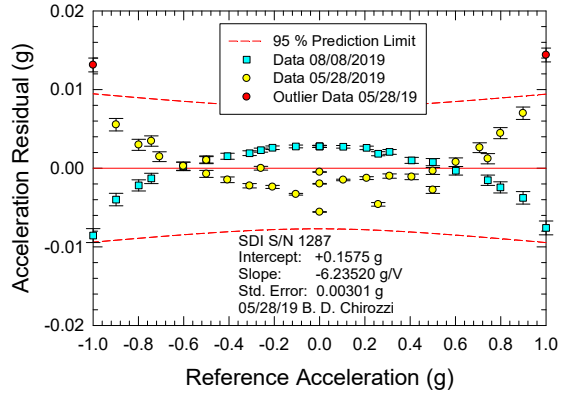

b. Transverse Acceleration

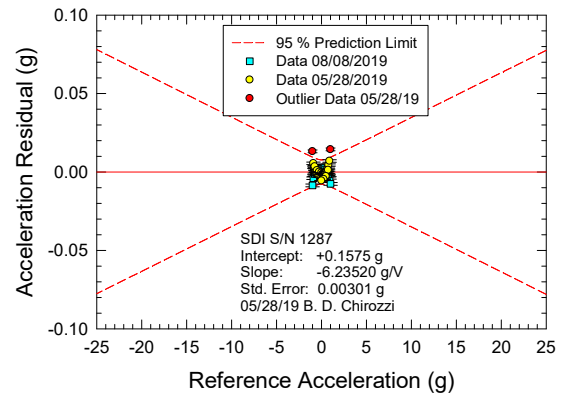

b. Transverse Acceleration

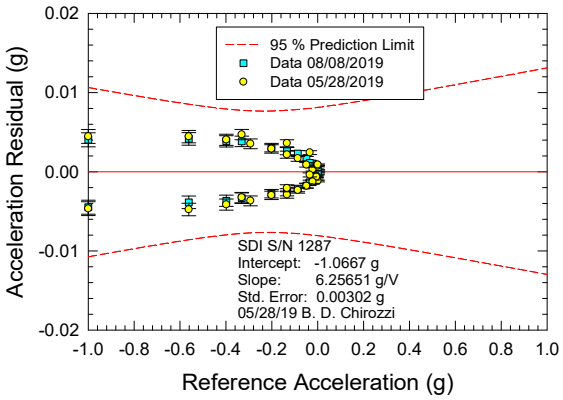

c. Vertical Acceleration

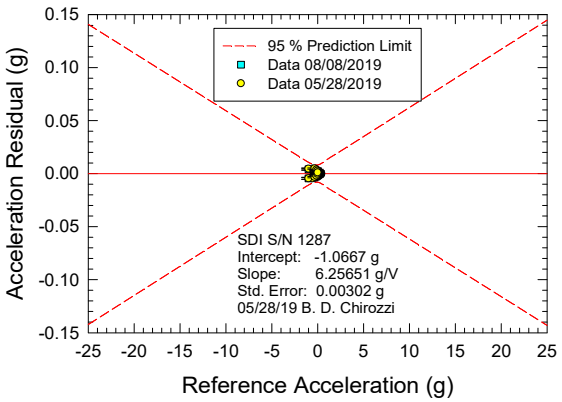

c. Vertical Acceleration

Figure D - 4. CG2 Accelerometer Calibration 1 g for DTMB Model 5765

Figure D - 5. CG2 Accelerometer Calibration 25 g for DTMB Model 5765

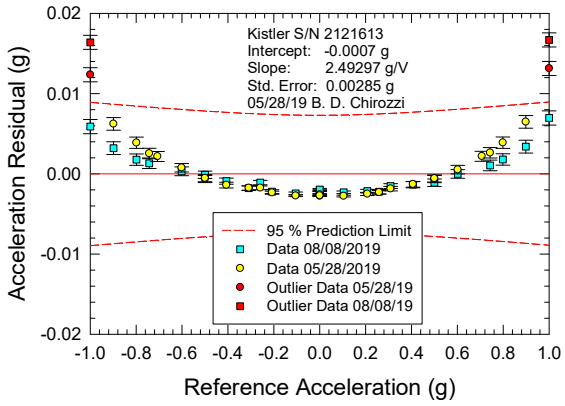

a. Longitudinal Acceleration

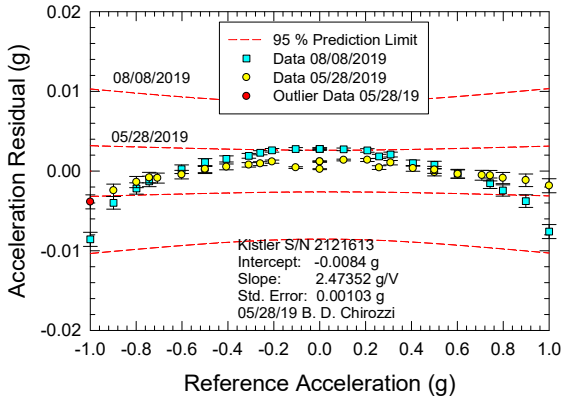

b. Transverse Acceleration

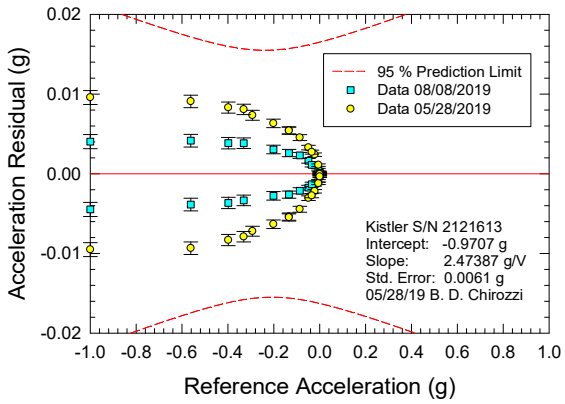

c. Vertical Acceleration

Figure D - 6. Tow-Post Accelerometer Calibration 1 g for DTMB Model 5765

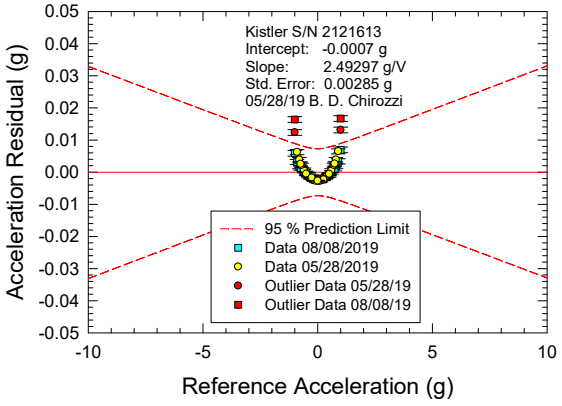

a. Longitudinal Acceleration

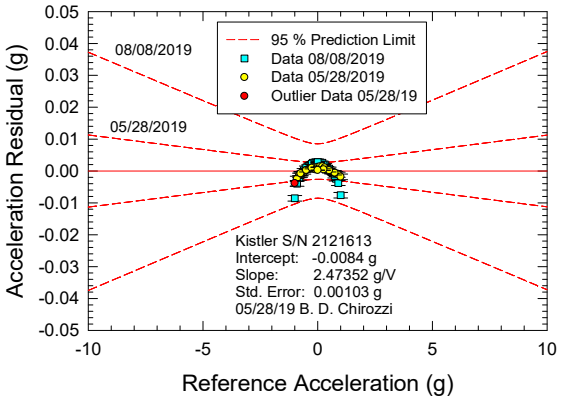

b. Transverse Acceleration

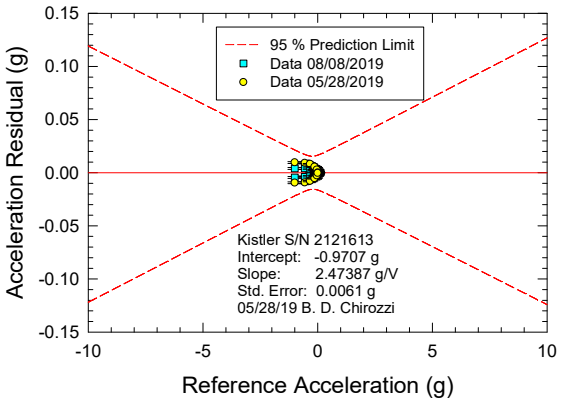

c. Vertical Acceleration

Figure D - 7. Tow-Post Accelerometer Calibration 10 g for DTMB Model 5765

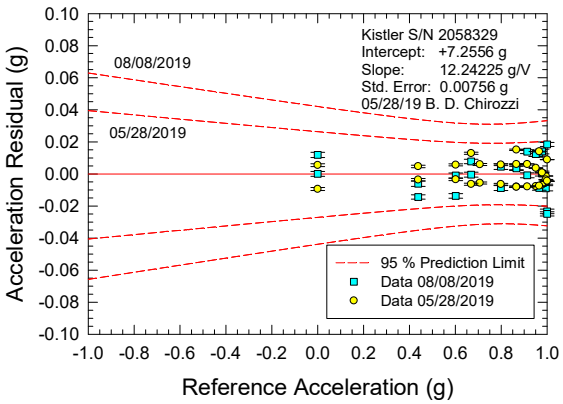

a. Longitudinal Acceleration

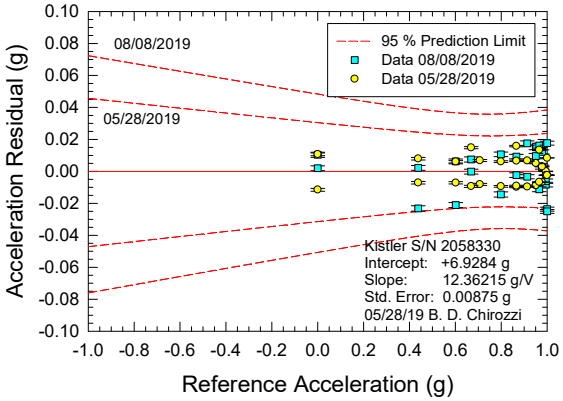

b. Transverse Acceleration

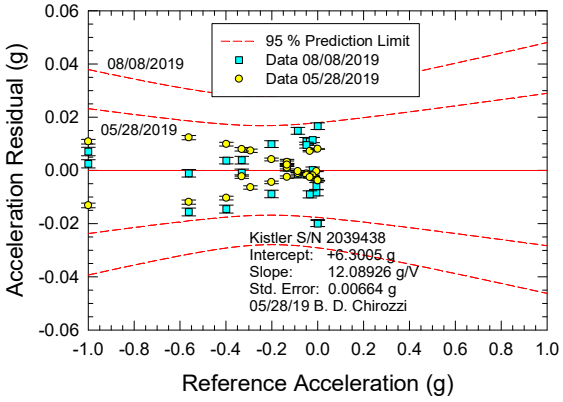

c. Vertical Acceleration

Figure D - 8. Bow Accelerometer 1 g Calibration for DTMB Model 5765

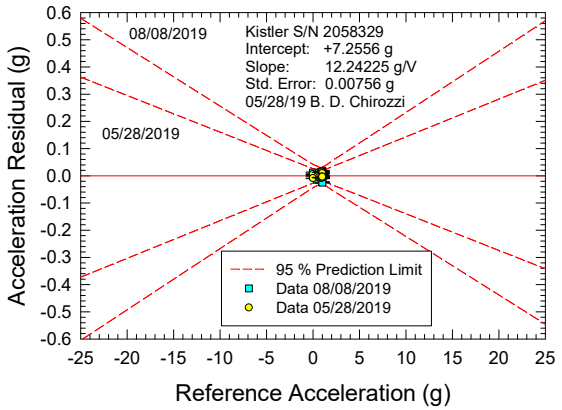

a. Longitudinal Acceleration

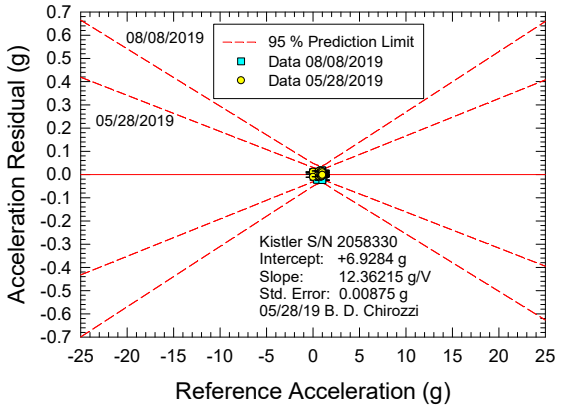

b. Transverse Acceleration

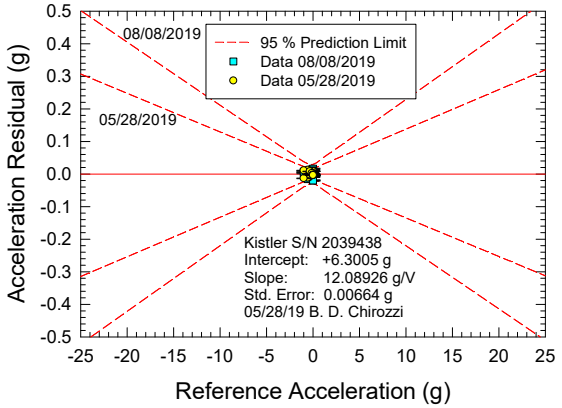

c. Vertical Acceleration

Figure D - 9. Bow Accelerometer 25 g Calibration for DTMB Model 5765

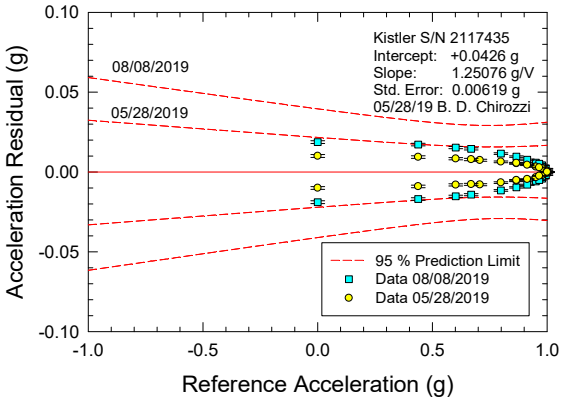

a. Longitudinal Acceleration

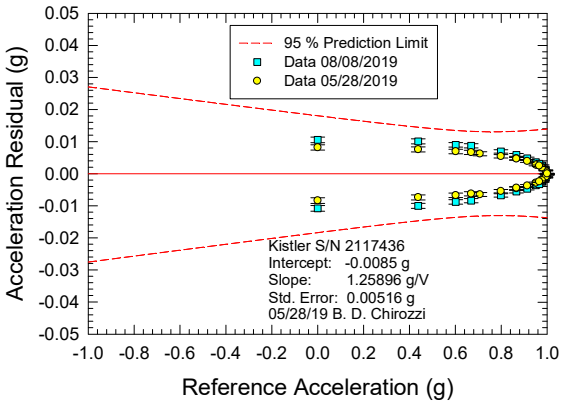

b. Transverse Acceleration

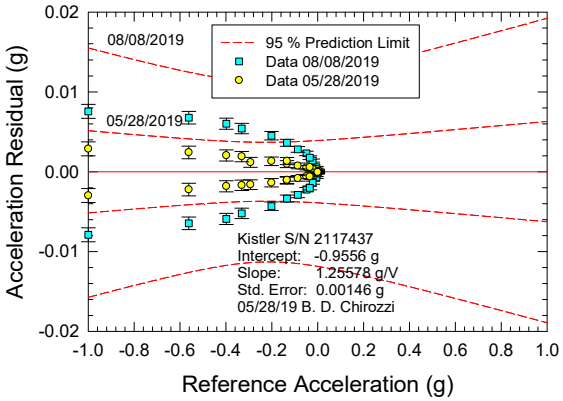

c. Vertical Acceleration

Figure D - 10. Stern Accelerometer 1 g Calibration for DTMB Model 5765

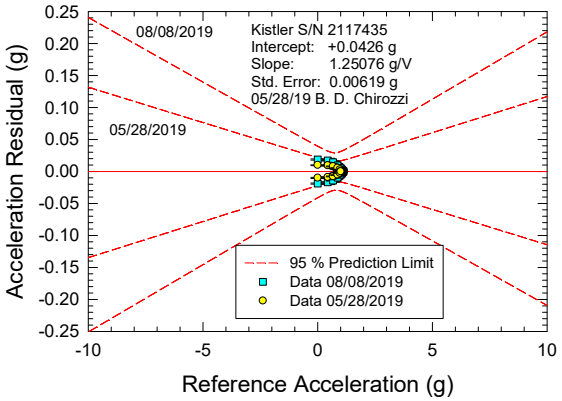

a. Longitudinal Acceleration

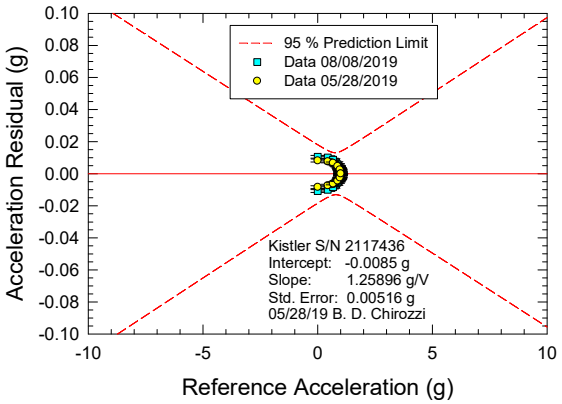

b. Transverse Acceleration

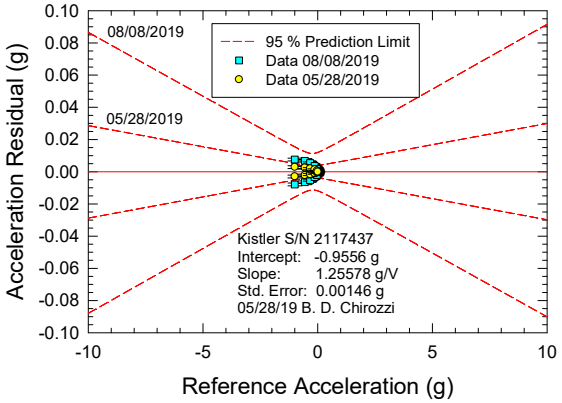

c. Vertical Acceleration

Figure D - 11. Stern Accelerometer 10 g Calibration for DTMB Model 5765

Drag and Side Force

Model drag and side forces were measured with stainless steel block gages manufactured at NSWCCD. In a typical calibration, the calibration load is increased with the addition of weights and then reduced by removal of the weights. The resulting calibration curves are presented in Figure D - 12 and Figure D - 13 for drag and side force, respectively. A slight hysteresis loop is evident in the drag calibration of Figure D - 12. The data at +200 lbf was removed as an outlier in the analysis of the drag gage calibration. For the side force, the calibration deviates significantly from linearity below - 20 lbf. The linear region is shown in Figure D - 13a, while the whole calibration range is shown in Figure D - 13b. The maximum uncertainty for drag is ±0.38 lbf (±0.19 % FSO at - 200 lbf) in comparison to ±0.23 lbf (±0.46 % FSO at +50 lbf) for the side-force gage.

Heave

Heave is measured by a string potentiometer mounted at the model CG for quantification of sinkage during the test. The calibration results are shown in Figure D - 14 for a Celesco PT1DC - 50, which has a range of 50 inches. The maximum uncertainty over the range of calibration is ±0.20 inches in comparison to the manufacturer's specification of ±0.075 inches.

Pitch Angle

For this test series, the pitch angle was measured with a Schaevitz R60D SN J2136 for the trim measurements during the test. Pitch angle was calibrated with the same equipment as the accelerometers. Results for pitch are shown as a residual plot in Figure D - 15. The maximum uncertainty is ±0.24° over the calibration range of ±26°.

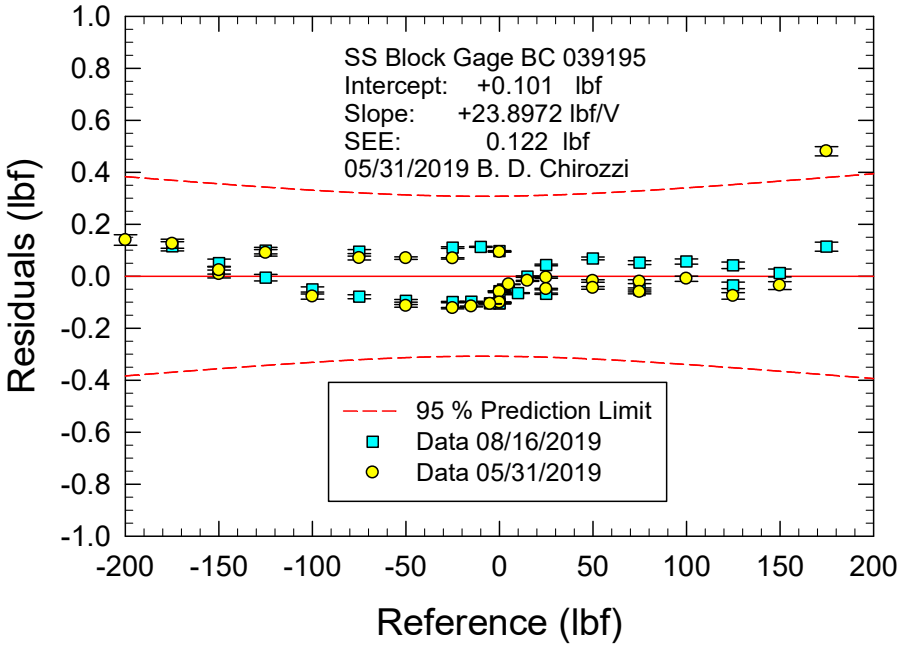

Figure D - 12. Block Gage Drag Calibration for DTMB Model 5765

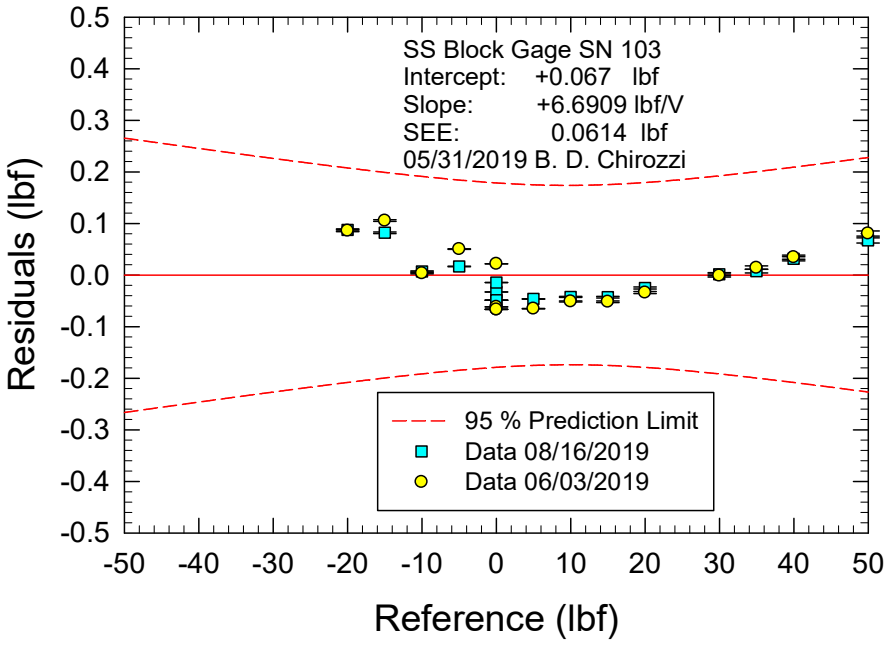

a. Linear Range

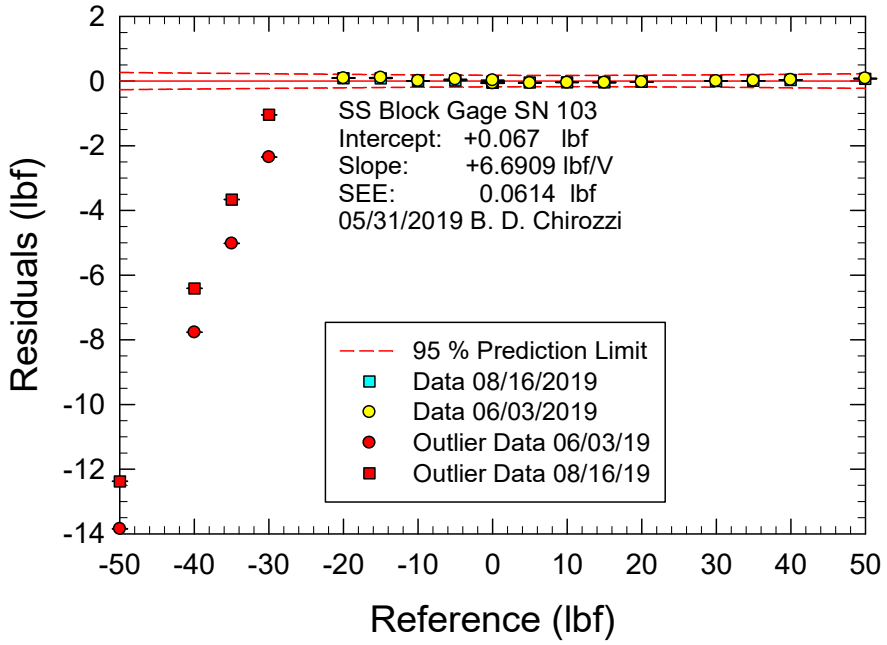

b. All Data

Figure D - 13. Block Gage Side - Force Calibration for DTMB Model 5765

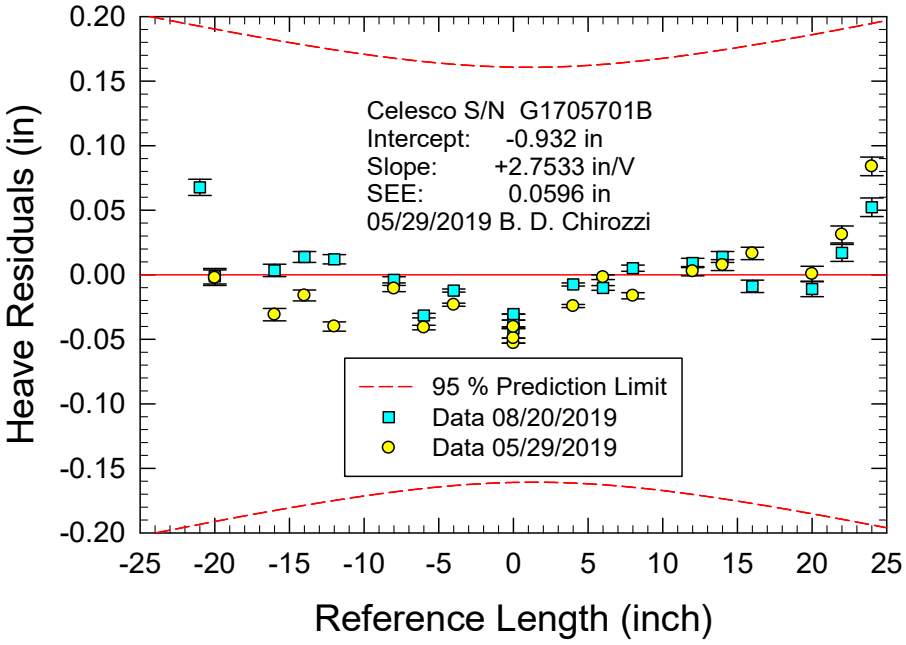

Figure D - 14. Celesco Heave Calibration for DTMB Model 5765

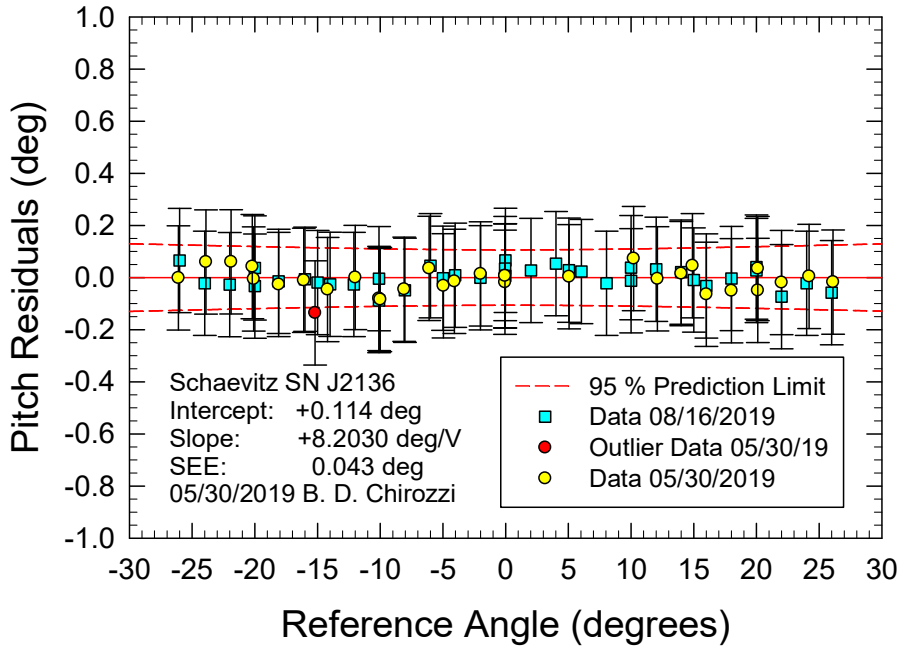

Figure D - 15. Schaevitz Pitch Angle Calibration for DTMB Model 5765

Hull - Bottom Pressure

Thirteen PCB 113B28 pressure transducers were located on the bottom of the hull during testing. The locations of seven transducers (P11 through P31) on the port side as viewed from the bottom are shown in Figure D - 16. An example calibration curve is in Figure D - 17. Slopes of 10 of the 13 were in agreement by a hypothesis test in a comparison of the pre- and post-test calibration results. For the three that failed the hypothesis test, the maximum difference between pre- and post-test results was within the uncertainty estimate. The manufacturer's specification was ±0.050 psi (±1.0 % of FSO at 5 psi). The uncertainty range from calibration was ±0.032 to ±0.15 psi (±0.65 to ±3.0 % FSO).

In the pre - test calibrations, 9 of 13 transducers or 69 % were within manufacturer's specification of ±0.050 psi (±1.0 % FSO). In the post - test calibration, 9 of 13 calibrations had uncertainties exceeding the pre-test values. The results are summarized in Figure D - 18 in a comparison of pre- and post-test uncertainties.

The maximum difference of the post - test data was evaluated with calibration constants from the pre-test calibration. With one exception, the maximum difference was less than the pre-test calibration uncertainty. The maximum difference in comparison to the post - test uncertainty is summarized in Figure D - 19. The one exception was P31, where the *SEE* from the curve fit was exactly zero and all of the uncertainty was from the reference standard of ±0.0013 psi.

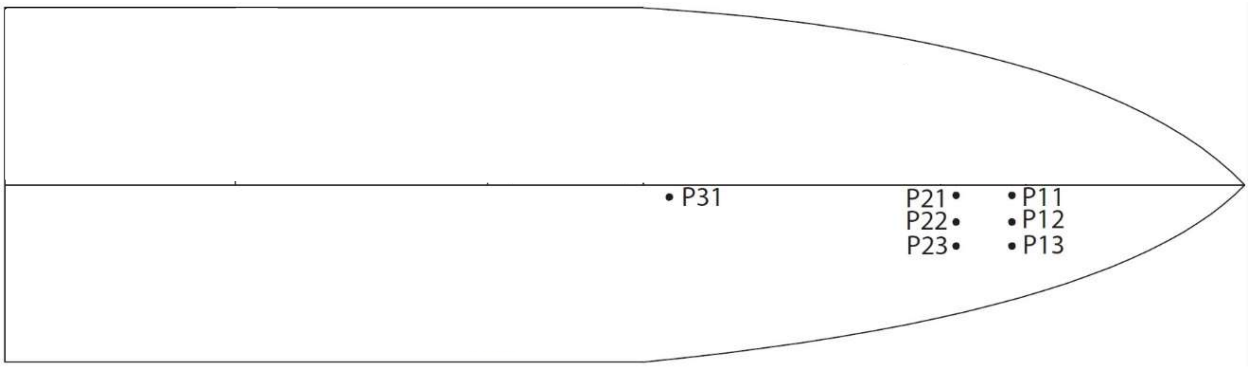

Figure D - 16. PCB Pressure Transducer Locations for DTMB Model 5765

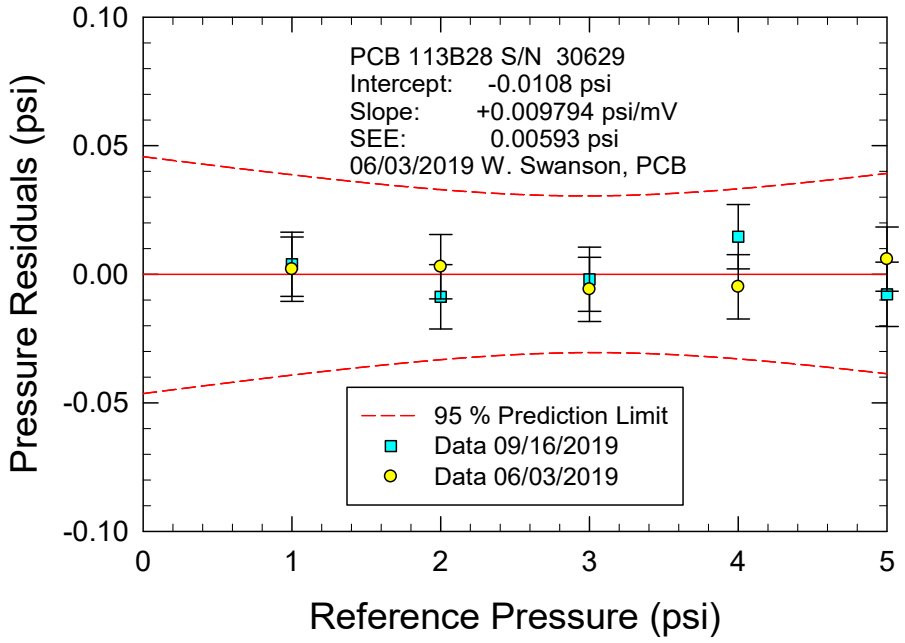

Figure D - 17. PCB Pressure Calibration for DTMB Model 5765 at Location P51

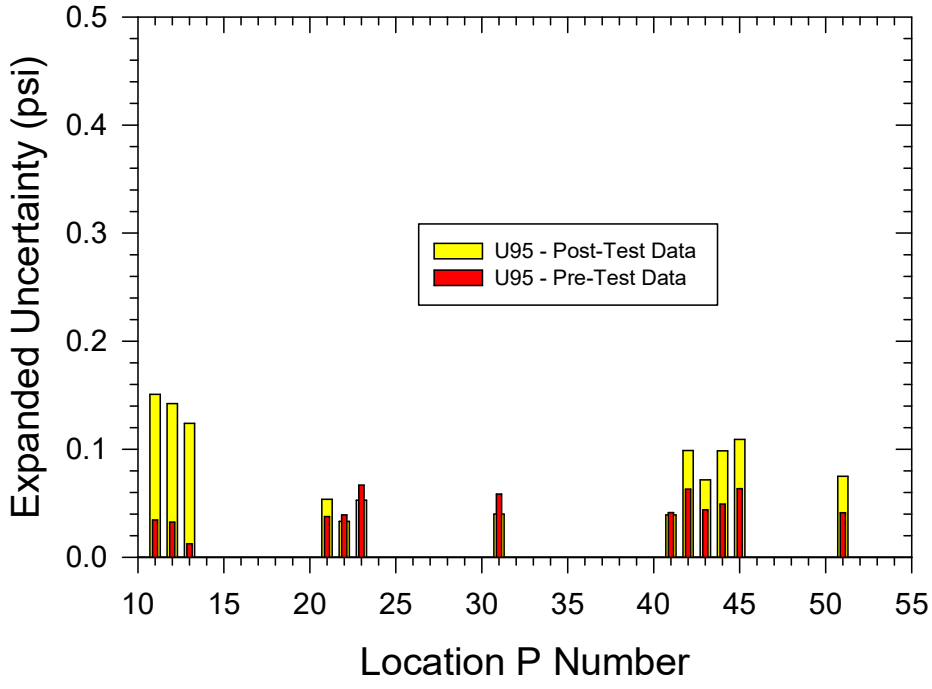

Figure D - 18. PCB 113B28 Pre - and Post - Test Uncertainty Comparison

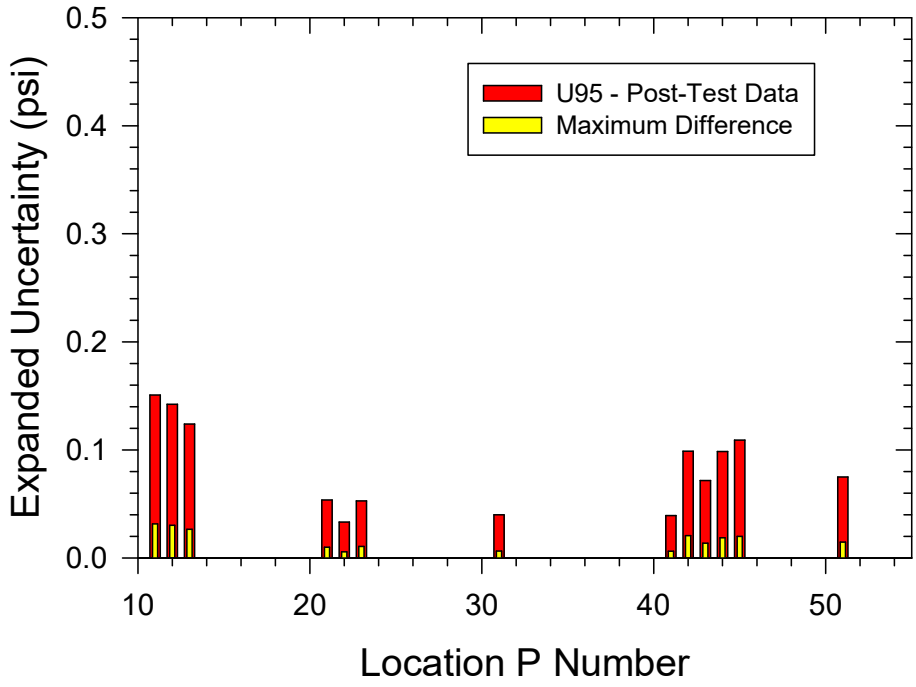

Figure D - 19. Maximum Difference between Pre - & Post - Test PCB Calibration

Grillage Panel

A grillage panel with 25 strain gages was located on the bottom of DTMB model 5765 on the starboard side opposite the PCB pressure transducers, P11 to P23, in Figure D - 16. The strain-gage locations on the panel are shown in Figure D - 20. The purpose was to measure the slamming loads on the hull near the bow during testing.

Two panels of different structural designs were manufactured for the test. The first labelled "Traditional" was a conventional structural design with uniform beams. The second defined as "Optimized" was designed on the basis of the computed structural loads. The arrangement of the strain gages was the same in both designs as depicted in Figure D - 20.

A special panel was designed for coverage of the panel so that all 25 strain gages were pressurized simultaneously for pressure calibration. The reference pressure was a calibrated Honeywell TJE pressure transducer with a range of 15 psig. The grillage panels were calibrated in a range of 0 to 3 and 4 psi, though some of the peak pressures during test were 6 psi.

Both (traditional and optimized) grillages represent custom-fabricated instrumentation. The traditional grillage was calibrated prior to and after the completion of testing. The optimized panel was calibrated prior to testing, however due to a crack that formed upon removal from the model, a post test calibration was not possible. The calibration values, and associated uncertainties are presented in their own in appendix. The reader is referred to Appendix C for additional details on the calibration and associated uncertainty of the grillage panels.

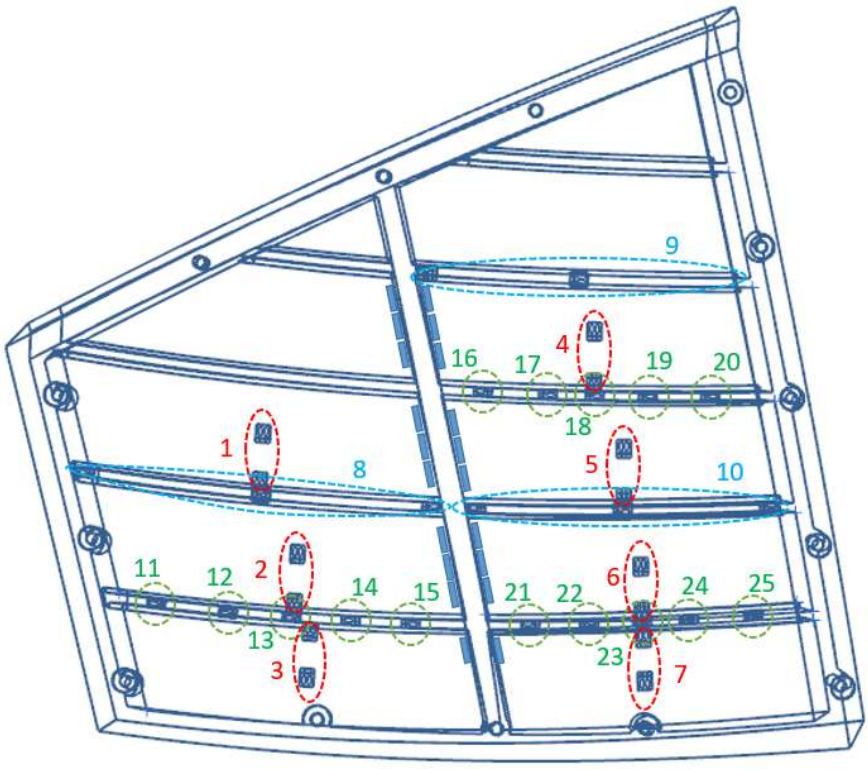

Double uniaxial gages:
ED-DY-125PC-10C/E
Single uniaxial gages:
ED-DY-125BZ-10C/E

- Channels 1 – 7 are differential bending on plate (circled in red)
- Channels 8 – 10 are differential bending on stiffeners (circled in blue)
- Channels 11 – 25 are individual strain measurements (circled in green)

Note: these gages straddle the quarter points of the stiffeners.

Total 25 Channels on the Traditional Grillage

Figure D - 20. Strain Gage Locations on Grillage Panel for DTMB Model 5765

Model Instrumentation Summary

The calibration constants, statistics, and uncertainty estimates for the model instrumentation are summarized in the following tables:

- Accelerometers in Table D - 1
- Other instruments, block gages, heave gage, pitch transducer, and wave height sensors, in Table D - 2
- PCB pressure transducers in Table D - 3 and Table D - 4
- Traditional and optimized grillages in Appendix C

In these tables, the recommended calibration constants from the pre - test calibrations are indicated in bold red font.

Post - test calibration data are a measure of the reproducibility of the data as defined in the JCGM GUM [D-1]. Reproducibility may increase the uncertainty estimate. A comparison of the slope and intercept data of the post - test to the pre - test calibration is then a measure of the reproducibility of the data. A statistical hypothesis test is applied to both the slope and the intercept. In a *t* - test, a Pass indicates that the more recent value is statistically the same as the previous one at the 95 % confidence level. A Fail means that this statistical test did not pass, and the slopes are different. For the slope, the *t* - test from [D-10]

$$T = |b_1 - b_2| / S_{b1-b2} \qquad \text{(D - 20)}$$

Where b_1 and b_2 are the slopes of the two calibrations and $S_{b1\,-\,b2}$ is the standard deviation of the slope difference.

Accept H_0 if $T \le t_{0.025,n_1+n_2-4}$

Reject H_0 if $T > t_{0.025,n_1+n_2-4}$

The variance of the slope difference is

$$S_{b1-b2}^2 = S_{\mathrm{p}}^2[1/S_{xx1} + 1/S_{xx2}] \qquad \text{(D - 21)}$$

Where the pooled estimate is

$$S_{\mathrm{p}}^2 = [(n_1 - 2)SEE_1^2 + (n_2 - 2)SEE_2^2]/[n_1 + n_2 - 4] \qquad \text{(D - 22)}$$

And n is the number of points in each calibration, *SEE* is the standard error of estimate, and

$$S_{xx} = \sum_{i=1}^{n} (x_i - \bar{x})^2 \qquad \text{(D - 23)}$$

Where $\bar{x}$ is the average of x from Equation (D - 3). The number of degrees of freedom for the Student-t comparison in Equation (D - 20) is $\nu = n_1 + n_2 - 4$.

Table D - 1. Calibration Summary of DTMB Model 5765 Accelerometers

Manu	Model #	Serial #	Function	Cal Date	Units	CH	Slope	*t* - test	Intercept	*t* - test	Correl.	Std Error	Max Diff	U95	Spec.
Kistler	8395A010	2121614	CG Vert	8-Aug-19	g	15	2.52969	Pass	-0.9871	Fail	0.9999878	0.00147	-0.0022	0.0053	0.01
Kistler	8395A010	2121614	CG Vert	28-May-19	g		2.53214		-0.9868		0.9999971	0.00057		0.0024	0.01
Kistler	8395A010	2121614	CG Trans	8-Aug-19	g	14	2.53226	Fail	-0.0954	Fail	0.9999987	0.00095	-0.0022	0.0031	0.01
Kistler	8395A010	2121614	CG Trans	28-May-19	g		2.51843		-0.0914		0.9999983	0.001		0.0032	0.01
Kistler	8395A010	2121614	CG Long	8-Aug-19	g	13	2.53925	Pass	0.0053	Fail	0.9999736	0.00388	-0.0039	0.012	0.01
Kistler	8395A010	2121614	CG Long	28-May-19	g		2.5386		0.0248		0.9999992	0.00069		0.0023	0.01
SDI	2460 - 025	1287	CG Vert	8-Aug-19	g	18	6.24287	Pass	-1.0623	Fail	0.9999884	0.00143	0.0029	0.0052	0.5
SDI	2460 - 025	1287	CG Vert	28-May-19	g		6.25651		-1.0667		0.99994	0.00302		0.011	0.5
SDI	2460 - 025	1287	CG Trans	8-Aug-19	g	17	-6.23143	Pass	0.1731	Fail	-0.999986	0.00314	0.008	0.0099	0.5
SDI	2460 - 025	1287	CG Trans	28-May-19	g		-6.2352		0.1575		-0.999985	0.00301		0.0092	0.5
SDI	2460 - 025	1287	CG Long	8-Aug-19	g	16	-6.23628	Pass	0.0612	Fail	-0.999983	0.0034	0.0077	0.011	0.5
SDI	2460 - 025	1287	CG Long	28-May-19	g		-6.24844		0.0693		-0.999996	0.00161		0.005	0.5
Kistler	8310B25	2039438	Bow Vert	8-Aug-19	g	12	12.38595	Fail	6.549	Pass	0.9993446	0.01076	-0.02	0.038	0.025
Kistler	8310B25	2039438	Bow Vert	28-May-19	g		12.08926		6.3005		0.9997108	0.00664		0.023	0.025
Kistler	8310B25	2058330	Bow Trans	8-Aug-19	g	11	12.66722	Fail	7.1785	Fail	0.9989225	0.01379	-0.025	0.048	0.025
Kistler	8310B25	2058330	Bow Trans	28-May-19	g		12.36215		6.9284		0.9994972	0.00875		0.03	0.025
Kistler	8310B25	2058329	Bow Long	8-Aug-19	g	10	12.5916	Fail	7.5059	Fail	0.9991884	0.01197	-0.0249	0.042	0.025

(Table Continued)

Manu	Model #	Serial #	Function	Cal Date	Units	CH	Slope	*t* - test	Intercept	*t* - test	Correl.	Std Error	Max Diff	U95	Spec.
Kistler	8310B25	2058329	Bow Long	28-May-19	g		12.24225		7.2556		0.9996251	0.00756		0.026	0.025
Kistler	8315A010	2117437	Stern Vert	16-Aug-19	g	21	1.25462	Pass	-0.9505	Fail	0.9998925	0.00436	-0.0079	0.016	0.01
Kistler	8315A010	2117437	Stern Vert	28-May-19	g		1.25578		-0.9556		0.9999861	0.00146		0.0052	0.01
Kistler	8315A010	2117436	Strn Trans	16-Aug-19	g	20	1.25869	Pass	0.0048	Fail	0.9997536	0.0066	-0.0108	0.023	0.01
Kistler	8315A010	2117436	Strn Trans	28-May-19	g		1.25895		-0.0085		0.9998255	0.00516		0.018	0.01
Kistler	8315A010	2117435	Stern Long	16-Aug-19	g	19	1.25064	Pass	0.0429	Pass	0.9992853	0.01124	-0.0189	0.04	0.01
Kistler	8315A010	2117435	Stern Long	28-May-19	g		1.25076		0.0426		0.9997489	0.00619		0.022	0.01
Kistler	8395A010	2121613	Tow Post Ver	8-Aug-19	g	24	2.47285	Pass	-0.9734	Fail	0.9999568	0.00276	-0.0045	0.0099	0.01
Kistler	8395A010	2121613	Tow Post Ver	28-May-19	g		2.47387		-0.9707		0.9997546	0.00612		0.021	0.01
Kistler	8395A010	2121613	Tow Post Tr	8-Aug-19	g	23	2.47455	Pass	-0.0061	Fail	0.9999844	0.00329	-0.0086	0.01	0.01
Kistler	8395A010	2121613	Tow Post Tr	28-May-19	g		2.47352		-0.0084		0.9999984	0.00103		0.0032	0.01
Kistler	8395A010	2121613	Tow Post Ln	8-Aug-19	g	22	2.49186	Pass	0.0051	Fail	0.9999897	0.00267	0.007	0.0084	0.01
Kistler	8395A010	2121613	Tow Post Ln	28-May-19	g		2.49297		-0.0007		0.9999864	0.00285		0.0087	0.01

Table D - 2. Calibration Summary of DTMB Model 5765 Other Instruments

Manufac.	Model #	Serial #	Function	Cal Date	Units	CH	Slope	*t* - test	Intercept	*t* - test	Correl.	Std Error	Max Diff	U95	Spec.
NSWCCD	Block Gage	39195	Drag	16-Aug-19	lbf	6	23.9396	Fail	0.104	Pass	1	0.0812	0.114	0.25	
NSWCCD	Block Gage	39195	Drag	31-May-19	lbf		23.8972		0.101		0.999999	0.1215		0.38	
NSWCCD	Block Gage	103	Side Force	16-Aug-19	lbf	7	6.6764	Fail	0.049	Pass	0.999997	0.0484	0.088	0.18	
NSWCCD	Block Gage	103	Side Force	3-Jun-19	lbf		6.6909		0.067		0.999996	0.06145		0.23	
Celesco	PT1DC - 50	G1705701B	Heave	20-Aug-19	in	9	-2.814	Fail	1.153	Fail	0.999998	0.0276	0.068	0.09	0.075
Celesco	PT1DC - 50	G1705701B	Heave	29-May-19	in		-2.7533		0.932		0.999991	0.0596		0.2	0.075
Schaevitz	R60D	J2136	Pitch	16-Aug-19	°	8	8.1896	Fail	-0.05	Fail	0.999997	0.037	-0.088	0.23	0.3
Schaevitz	R60D	J2136	Pitch	30-May-19	°		8.203		0.114		0.999996	0.043		0.24	0.3
Senix	TSPC	4152026	CG Wave Ht	23-Aug-19	in	3	-1.0079	Fail	-0.0323	Fail	1	0.0116		0.04	0.3
Senix	TSPC	4120478	Bow Wave Ht	23-Aug-19	In	2	-1.0122	Fail	-0.0448	Pass	0.999995	0.04		0.12	0.3

Bold red indicates recommended calibration constants for the test.

Table D - 3. PCB Pressure Calibration Summary

Manu.	Model #	Serial #	Function	Cal Date	Units	CH	Slope	*t* - test	Intercept	*t* - test	Correl.	Std Error	Max Diff	U95	Spec.
PCB	113B28	30629	P51	16-Sep-19	psi		0.009737	Pass	0.013	Pass	0.999982	0.0111	0.015	0.075	0.05
PCB	113B28	30629	P51	3-Jun-19	psi		0.009794		-0.011		0.999995	0.0059		0.041	0.05
PCB	113B28	30630	P45	16-Sep-19	psi		0.00984	Pass	0.015	Pass	0.999961	0.0162	0.02	0.109	0.05
PCB	113B28	30630	P45	3-Jun-19	psi		0.009891		-0.005		0.999987	0.0094		0.064	0.05
PCB	113B28	30631	P44	16-Sep-19	psi		0.009794	Pass	0.015	Pass	0.999968	0.0146	0.019	0.099	0.05
PCB	113B28	30631	P44	3-Jun-19	psi		0.009843		-0.006		0.999992	0.0072		0.049	0.05
PCB	113B28	30632	P43	16-Sep-19	psi		0.010053	Pass	0.022	Fail	0.999983	0.0106	0.014	0.072	0.05
PCB	113B28	30632	P43	3-Jun-19	psi		0.01006		-0.006		0.999994	0.0064		0.044	0.05
PCB	113B28	30633	P42	16-Sep-19	psi		0.009814	Pass	0.015	Pass	0.999968	0.0147	0.021	0.099	0.05
PCB	113B28	30633	P42	3-Jun-19	psi		0.009814		-0.001		0.999987	0.0093		0.063	0.05
PCB	113B28	30640	P41	16-Sep-19	psi		0.009906	Fail	0.018	Fail	0.999995	0.0056	-0.006	0.039	0.05
PCB	113B28	30640	P41	3-Jun-19	psi		0.009833		0.001		0.999995	0.006		0.041	0.05
PCB	113B28	30641	P31	16-Sep-19	psi		0.009867	Pass	0.018	Fail	0.999995	0.0057	-0.006	0.04	0.05
PCB	113B28	30641	P31	3-Jun-19	psi		0.009852		-0.003		0.999989	0.0086		0.059	0.05
PCB	113B28	30642	P23	16-Sep-19	psi		0.009737	Pass	0.009	Fail	0.999991	0.0077	-0.011	0.053	0.05
PCB	113B28	30642	P23	3-Jun-19	psi		0.009718		0.001		0.999985	0.0099		0.067	0.05

(Table Continued)

Manu.	Model #	Serial #	Function	Cal Date	Units	CH	Slope	*t* - test	Intercept	*t* - test	Correl.	Std Error	Max Diff	U95	Spec.
PCB	113B28	30698	P22	16-Sep-19	psi		0.01	Pass	0.024	Fail	0.999997	0.0047	-0.006	0.033	0.05
PCB	113B28	30698	P22	3-Jun-19	psi		0.009991		0.005		0.999995	0.0056		0.039	0.05
PCB	113B28	30699	P21	16-Sep-19	psi		0.010081	Pass	0.011	Fail	0.999991	0.0079	0.01	0.054	0.05
PCB	113B28	30699	P21	3-Jun-19	psi		0.010008		0.004		0.999996	0.0054		0.038	0.05
PCB	113B28	30700	P13	16-Sep-19	psi		0.010257	Fail	0	Fail	0.999949	0.0184	0.027	0.124	0.05
PCB	113B28	30700	P13	3-Jun-19	psi		0.01		-0.02		1	0		0.013	0.05
PCB	113B28	30701	P12	16-Sep-19	psi		0.010601	Fail	0.003	Fail	0.999934	0.0211	0.03	0.142	0.05
PCB	113B28	30701	P12	3-Jun-19	psi		0.010125		-0.015		0.999997	0.0045		0.032	0.05
PCB	113B28	30702	P11	16-Sep-19	psi		0.010163	Pass	0.001	Pass	0.999925	0.0223	0.032	0.151	0.05
PCB	113B28	30702	P11	3-Jun-19	psi		0.010241		-0.015		0.999997	0.0049		0.034	0.05
Bold red indicates recommended calibration constants for the test.										Max	1	0.022	0.032	0.151	
Range	0 - 5	psi								Min	0.99993	0	-0.011	0.013	

For the *t* - test of the intercept, the slopes are assumed to be the same. The *t* - test in this case is as follows [D-11]:

$$T = |d|/S_d \tag{D - 24}$$

Accept H_0 if $T \le t_{0.025,n_1+n_2-3}$

Reject H_0 if $T > t_{0.025,n_1+n_2-3}$

The difference, *d*, in intercepts given by

$$d = \overline{y_1} - \overline{y_2} - b(\overline{x_1} - \overline{x_2}) \tag{D - 25}$$

And the pooled slope, *b*, for the two calibrations is

$$b = (b_1 S_{xx1} + b_2 S_{xx2})/(S_{xx1} + S_{xx2}) \tag{D - 26}$$

The variance of *d* is given by

$$S_d^2 = S_c^2[1/n_1 + 1/n_2 + (\overline{x_1} - \overline{x_2})^2/(S_{xx1} + S_{xx2})] \tag{D - 27}$$

And the residual mean square about the lines is

$$S_c^2 = [S_{yy1} + S_{yy2} + (b_1 S_{xx1} + b_2 S_{xx2})^2/(S_{xx1} + S_{xx2})]/[n_1 + n_2 - 3] \tag{D - 28}$$

The number of degrees of freedom for the Student-*t* comparison in this case is $\nu = n_1 + n_2 - 3$.

For some calibrations, comparison with a known slope and intercept may be useful. Some instruments are calibrated directly in physical units. In that case, a linear fit over the range of the instrument should produce a slope and intercept of one and zero, respectively. From Ross [D-6] and Devore [D-12], the *t* - test for the intercept is

$$T = |a - \alpha| \sqrt{n(n-2)S_{xx} \Big/ \sum_{i=1}^{n} x_i^2 SS_R} \tag{D - 29}$$

And for the slope

$$T = |b - \beta| \sqrt{(n-2)S_{xx} \Big/ \sum_{i=1}^{n} x_i^2 SS_R} \tag{D - 30}$$

Where α and β are the theoretically known intercept and slope, respectively.

Accept H_0 if $T \le t_{0.025,n-2}$

Reject H_0 if $T > t_{0.025,n-2}$

For the case where the instrument output is in physical units, the intercept is $\alpha = 0$, and the slope $\beta = 1$. The number of degrees of freedom is $\nu = n - 2$.

In addition to the hypothesis test, the data from the newer calibration are computed with the slope and intercept from the previous calibration, and the residuals are calculated. The maximum difference in this calculation appears in the tables as Max Diff. If the calibration fails the hypothesis test, then Max Diff should be compared to the estimated uncertainty in the U95 column. The U95 column is the expanded and combined uncertainty of the calibration including the Type A from the individual calibration points, Type B from the calibration uncertainty of the reference, and the uncertainty from the curve fit. The uncertainty varies slightly as shown in the plots previously presented over the calibration range but is nearly constant. The maximum uncertainty in the calibration range was included in the expanded combined uncertainty estimate. If the magnitude of Max Diff is larger than U95, consideration should be given to assigning the magnitude of Max Diff as a better estimate of the uncertainty. Additionally, large differences may be the basis for removal of an instrument from future service.

Additional statistics in the tables include the correlation coefficient and the standard error of estimate (*SEE*). The correlation coefficient is a measure of the linearity. For perfectly correlated data, the correlation coefficient is 1.0. As the tables indicate for Table D - 1 through Table D - 3, most of the instruments have a value very nearly one to four or five decimal places. The *SEE* is a measure of the standard deviation and is in the same physical units as the instrument. For perfectly correlated data, *SEE* will be zero. It is also a measure of the uncertainty. Typically, 3×*SEE* is near the estimated uncertainty in the 95 % prediction limit from calibration theory. The next to the last column of the table, Spec., is the manufacturer's specification on instrument accuracy. The column with the heading CH is the channel number on the data acquisition card.

In general, the most critical items in the tables are the slopes. The intercepts should be corrected on the basis of zero measurements in calm water at zero model speed. Reproducibility during calibration requires that the tilt table be leveled with an instrument of lower uncertainty.

PCB Calibration Summary

The calibration constants for the PCB pressure transducers are summarized in Table D - 3. The analysis methods of this report were applied to the data in the PCB calibration sheets, where calibration values in mV were provided for five pressures from 1 to 5 psi. The pre- and post-test slopes and intercepts were compared by the hypothesis tests in Equations (D - 20) and (D - 24) for slope and intercept, respectively. The slopes failed in 3 of 13 transducers, but usually the Max Diff is within the largest uncertainty.

In Table D - 4, the slopes computed by the methods in this report are compared to the slope provided by PCB. The hypothesis test for the slope was applied via Equation (D - 30). The

results agreed in all case but one for transducer location P22 in post-test calibration. Apparently, the value computed by PCB from their data is in error, as the pre- and post-test values in Table D - 3 agree. The PCB pre-test values are acceptable and are in agreement with the values from the analysis for this report. However, some of the uncertainty estimates are large than manufacturer's specification. The larger maximum values for each transducer from Table D - 3 should be applied.

Table D - 4. Comparison of Computed Slope Calibration to PCB Value

Manufac.	Model #	Serial #	Function	Cal Date	Units	Computed	PCB	*t* - test
PCB	113B28	30629	P51	16-Sep-19	mV/psi	102.7	102.3	Pass
PCB	113B28	30629	P51	3-Jun-19	mV/psi	102.1	102.3	Pass
PCB	113B28	30630	P45	16-Sep-19	mV/psi	101.63	101.2	Pass
PCB	113B28	30630	P45	3-Jun-19	mV/psi	101.1	101.3	Pass
PCB	113B28	30631	P44	16-Sep-19	mV/psi	102.1	101.7	Pass
PCB	113B28	30631	P44	3-Jun-19	mV/psi	101.6	101.7	Pass
PCB	113B28	30632	P43	16-Sep-19	mV/psi	99.47	98.86	Pass
PCB	113B28	30632	P43	3-Jun-19	mV/psi	99.4	99.57	Pass
PCB	113B28	30633	P42	16-Sep-19	mV/psi	101.9	101.5	Pass
PCB	113B28	30633	P42	3-Jun-19	mV/psi	101.9	101.9	Pass
PCB	113B28	30640	P41	16-Sep-19	mV/psi	100.95	100.5	Pass
PCB	113B28	30640	P41	3-Jun-19	mV/psi	101.7	101.7	Pass
PCB	113B28	30641	P31	16-Sep-19	mV/psi	101.35	100.8	Pass

(Table Continued)

Manufac.	Model #	Serial #	Function	Cal Date	Units	Computed	PCB	*t* - test
PCB	113B28	30641	P31	3-Jun-19	mV/psi	101.5	101.6	Pass
PCB	113B28	30642	P23	16-Sep-19	mV/psi	102.7	102.5	Pass
PCB	113B28	30642	P23	3-Jun-19	mV/psi	102.9	102.9	Pass
PCB	113B28	30698	P22	16-Sep-19	mV/psi	100	99.36	Fail
PCB	113B28	30698	P22	3-Jun-19	mV/psi	100.09	99.94	Pass
PCB	113B28	30699	P21	16-Sep-19	mV/psi	99.2	98.89	Pass
PCB	113B28	30699	P21	3-Jun-19	mV/psi	99.92	99.81	Pass
PCB	113B28	30700	P13	16-Sep-19	mV/psi	97.49	97.49	Pass
PCB	113B28	30700	P13	3-Jun-19	mV/psi	100	100.6	Pass
PCB	113B28	30701	P12	16-Sep-19	mV/psi	94.33	94.24	Pass
PCB	113B28	30701	P12	3-Jun-19	mV/psi	98.77	99.17	Pass
PCB	113B28	30702	P11	16-Sep-19	mV/psi	98.4	98.38	Pass
PCB	113B28	30702	P11	3-Jun-19	mV/psi	97.65	98.05	Pass

Bold red indicates applied factory calibration for test

Wave Height

Wave height for this test series was measured with Senix model TSPC - 30S1 - 232 ToughSonic Distance Sensors. The manufacturer's specification on accuracy is ±0.1 % full-scale or ±0.030 inch (±0.76 mm) for a 30-inch (762 mm) traverse distance. The probes were bench calibrated on a Velmex BiSlide traverse. The estimated uncertainty of the Velmex is 0.0003 inch/inch.

Examples of the calibration curves for the CG and bow probes are presented in Figure D - 21 and Figure D - 22, respectively. The error bars in these figures include the combined uncertainty from the Type A and the position uncertainty from the Type B estimate. The Type B has a negligible contribution, while the largest contribution by the Type A method was ±0.0018 inch. As the figures indicate, the dominant uncertainty is from the curve fit.

Summaries of the calibration results for the wave height probes are presented in Table D - 2. The results are presented in a format similar to that of the model instrumentation. In this case, a post-test calibration was not available for a check on reproducibility. The maximum uncertainties in wave height for two probes from the table are ±0.0040 inch (±1.0 mm) for CG and ±0.12 inch (±3.1 mm) for the bow. The uncertainty for the bow appears to be excessive, but the cause is unknown.

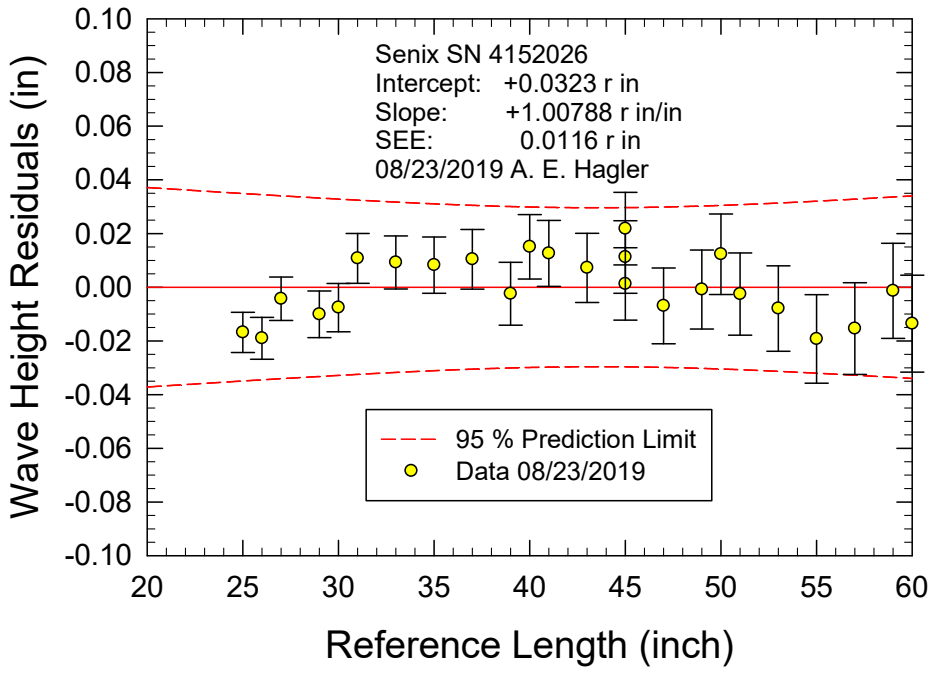

Figure D - 21. CG Wave Height Probe Calibration

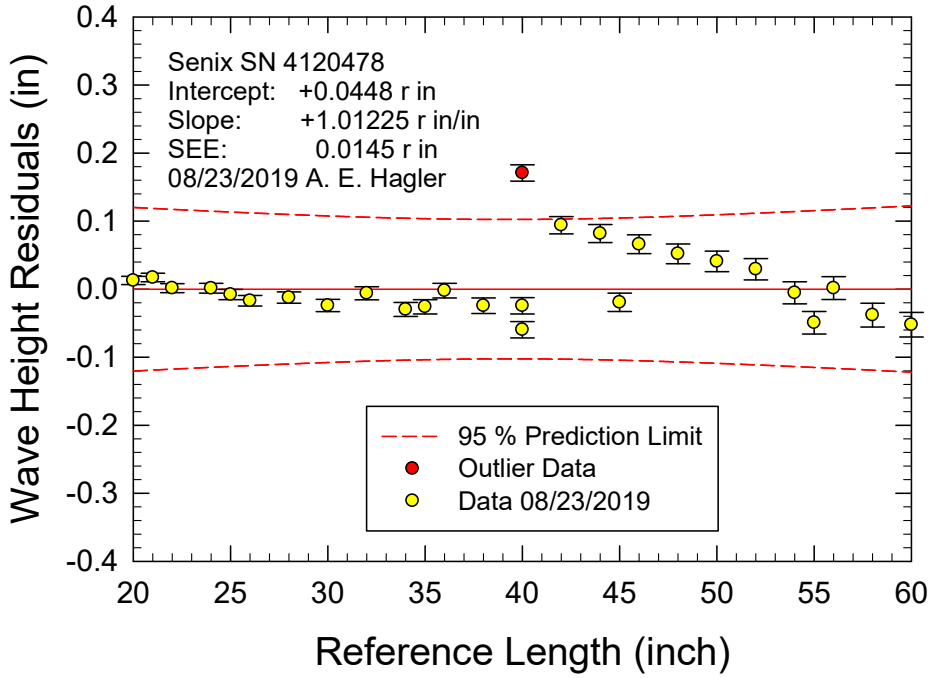

Figure D - 22. Bow Wave Height Probe Calibration

The calibration constants for the wave height transducers appear to be the directly measured values. In that case, the slopes should be one and the intercepts zero. The hypothesis tests from Equations (D - 29) and (D - 30) have been applied with $\alpha = 0.0$ and $\beta = 1.0$. The slope fails for both probes. In that case, either the wave height slopes should be corrected with the values from Table D - 2, or the estimated uncertainty increased.

Model Zeroes

Since the model instruments are not typically installed so that the output is zero in calm water conditions, the data must be corrected for offset with the averages with the model instrument readings at zero speed. During the test, the results of instrumentation sensitive to offset can be influenced by instrument drift. Any changes in the zeroes during the test series is a measure of the reproducibility of the data as defined in the JCGM GUM [D-1] and an indicator of the uncertainty in the results. Furthermore, correction of the experimental results with the zero reading is correlated data; consequently, the contribution to the uncertainty in the measurement of the Type B uncertainty from calibration is then zero. Correlated measurements with the same instrument are being differenced, which results in zero contribution from the Type B method. Thus, the uncertainty in the measurement becomes the uncertainty in the zero value as computed by the Type A method in Equation (D - 1) from the standard deviation.

CONCLUSIONS

This appendix describes the model instrument calibrations and related uncertainty estimates. Gains and offsets derived from the pre-calibration data were used for this test effort. The following is a summary of the important results:

- Accelerometers. The accelerometers were calibrated over the range of 1.0 g. Over this range, the uncertainty is nearly constant in physical units. The total range of the transducers was either ±10 or ±25 g. Outside the calibration range, the uncertainty increases linearly. Uncertainty estimates should be applied from the 95 % prediction limit in the calibration residual plots in this report.
- Pitch. The maximum uncertainty in pitch for the Schaevitz R30D was ±0.24° from Figure D - 15 and is within the manufacturer's specification of ±0.30° over the calibration range of ±26°.
- Heave. The maximum uncertainty in heave from the calibration of the Celsco PT1DC - 50 string potentiometer was ±0.20 inch over the calibration range and exceeds the manufacturer's specification of ±0.075 inch.
- Drag. Drag was measured with a stainless steel block gage. The maximum uncertainty was ±0.38 lbf over a range of 200 lbf or ±0.19 %.
- Side Force. Side force was also measured with a stainless steel block gage. The gage was linear from - 20 to +50 lbf with a maximum estimated uncertainty of ±0.23 lbf or ±0.46 % at +50 lbf. Side force was a non-critical channel and its purpose was to ensure proper alignment of the model during setup. If the side force channel data is used in the future for other purposes, the data should be reprocessed with the slope over the linear range from Figure D - 13a. Only test data for loads of - 20 to +50 lbf should be considered reliable.
- PCB Pressure Transducers. The slopes from the analysis in this report are in agreement with the manufacturer's calibration by a hypothesis test with one exception in post - test calibration as indicated in Table D - 4. The calibration constants currently applied from the manufacturer's pre - test calibration is acceptable; however, the uncertainty estimates from this document should be applied. From Table D - 3, uncertainty estimates from 12 of 26 calibrations or 46 % exceed manufacturer's specification of ±0.050 psi.

RECOMMENDATIONS

From the conclusions, the following are recommended:

- Accelerometers. Currently, calibration of the accelerometers is limited to the range of ±1.0 g on a tilt table. In the future, the accelerometers should be sent to a calibration laboratory with a capability of calibration to 25 g or the maximum acceleration observed during testing. The calibrations should be NIST traceable with a statement in the uncertainty estimate to 95 % confidence limit and data listed with nominally 10 equal increments over the calibration range. The suggested range is the maximum measured during the current test program.
- Single Axis Kistler Accelerometers. If single axis accelerometers are assembled for three-dimensional accelerations, the assembly should be calibrated in the same manner as

the tri-axial accelerometers. That is, the assembly should be calibrated not the individual accelerometers.

- Side Force. The side-force block gage should be replaced or repaired.
- PCB Pressure Transducers. In the future, the PCB pressure transducers should be calibrated in 0.1 psi increments from 0 to 5 psi.
- Pre - Test Calibrations. Pre - test calibrations should be completed prior to test with sufficient time for checking the calibrations for the proper slopes and intercepts, non-linearity, and outlier data and repeating calibrations or replacing transducers prior to testing if a problem is observed.

REFERENCES

[D-1] JCGM. 2008, "Evaluation of measurement data – Guide to the expression of uncertainty in measurement," JCGM 100:2008 GUM 1995 with minor corrections, Joint Committee for Guides in Metrology, Bureau International des Poids Mesures (BIPM**),** Sèvres**,** France.

[D-2] ITTC. 2014. "Guide to the Expression of Uncertainty in Experimental Hydrodynamics", ITTC Procedure 7.5 - 02 - 01 - 01, Revision 02, 27th International Towing Tank Conference.

[D-3] ITTC. 2017. "Uncertainty Analysis - Instrument Calibration," ITTC Procedure 7.5 - 01 - 03 - 01, Revision 02, 28th International Towing Tank Conference.

[D-4] Scheffe, H. 1973. "A Statistical Theory of Calibration," *The Annals of Statistics*, 1(1), pp. 1 - 37.

[D-5] Carroll, R. J. Spiegelman, C. H., and Sacks, J. 1988. "A Quick and Easy Multiple - Use Calibration - Curve Procedure," *Technometrics*, 30(2), pp. 137 - 141.

[D-6] Ross, S. M. 2004. *Introduction to Probability and Statistics for Engineers and Scientists*, Third Edition, Amsterdam, Elsevier Academic Press.

[D-7] NIST Handbook 105-1. 2019. "Specifications and Tolerances for Reference Standards and Field Standards and Measures," National Institute of Standards and Technology, Gaithersburg, Maryland.

[D-8] ASTM E74-18. 2018. "Standard Practice of Force - Measuring Instruments for Verifying the Force Indication of Testing Machines," American Society for Testing and Materials, West Conshohocken, PA.

[D-9] Moose, R. E. 1986. "The National Geodetic Survey Gravity Network," NOAA Technical Report NOS 121 NGS 39, U.S. Department of Commerce, National Oceanic and Atmospheric Administration, Washington, D.C.

[D-10] Kleinbaum, David G., Kupper, Lawrence L., and Muller, Keith E. 1988. *Applied Regression Analysis and Other Multivariable Methods*, Second Edition, PWS - Kent Publishing Company. Boston. pp. 266 - 269.

[D-11] Armitage, P. 1971. *Statistical Methods in Medical Research*, Blackwell Scientific Publications. Oxford. pp. 289 - 291.

[D-12] Devore, Jay L. 2008. *Probability and Statistics for Engineering and the Sciences*, Seventh Edition, Thomson Brooks/Cole. Belmont CA. pp. 274 - 275.

APPENDIX E: STATISTICAL ESTIMATORS AND CONFIDENCE INTERVALS

The methods and confidence interval based uncertainty calculations mentioned in the body of the technical report are further described in this appendix.

AUTOCOVARIANCE METHOD FOR PRIMARY VARIABLES

Diez et al. [E-1] described an autocovariance matrix method, which was applied to a single time series record or primary variable. Their autocovariance matrix method used Equation (E-1) to calculate the variance of the mean, $Var(EV)$, where Equation (E-2) was used to calculate the weighted autocovariance function, $R(\tau_i)$. For data acquired with multiple runs, the autocovariance term in Equation (E-1) can be eliminated with the incorporation of the ensemble variables when there are a sufficient number of repeats per Belenky et al. [E-2] and ITTC 7.5-02-01-08 [E-3]; ITTC 7.5-02-01-08 [E-3] states the number of repeats be equal to 30 runs or more, but V. Belenky states this requirement to be 7-15 runs (personal communication). Therefore, the variance of the mean of one record, $Var(EV_j)$, was calculated with Equation (E-3), and the variance of the ensemble mean, $Var(EV_a)$, was calculated with Equation (E-4). Similarly, the variance of the variance of one record, $Var((SD_j)^2)$, was calculated with Equation (E-5), and the variance of the ensemble standard deviation, $Var((SD_a)^2)$, was calculated with Equation (E-6).

$$Var(EV) = \frac{(SD)^2}{N} + \frac{2}{N}\sum_{i}^{N-1}\left(1 - \frac{i}{N}\right)R(\tau_i) \quad \text{(E - 1)}$$

$$R(\tau_i) = \frac{1}{N}\sum_{j=1}^{N-i}\left[x_j - EV(x)\right]\left[x_{j+i} - EV(x)\right] \quad \text{(E - 2)}$$

$$Var(EV_j) = \frac{(SD_j)^2}{N_j} \quad \text{(E - 3)}$$

$$Var(EV_a) = \sum_{j}^{N_r}(W_j)^2(EV_j - EV_a)^2 \quad \text{for } j = 1, \dots, N_r \quad \text{(E - 4)}$$

$$Var((SD_j)^2) = \frac{2(SD_j)^4}{N_j} \quad \text{(E - 5)}$$

$$Var((SD_a)^2) = \sum_{j}^{N_r}(W_j)^2((SD_j)^2 - (SD_a)^2)^2 \text{ for } j = 1, \dots, N_r \quad \text{(E - 6)}$$

The confidence intervals for EV_a are given by Equation (E-7) if a normal distribution is assumed in accordance with Belenky et al. [E-2]. Here $EV_{low,a}$ is the AC method lower confidence interval, $EV_{up,a}$ is the AC method upper confidence interval, and K_β is the $0.5(1 + P_\beta)$ quantile of a standard normal distribution with zero mean and unity variance, see Equation (E-8). The 95 % confidence intervals for EV_a, and all statistics variable, were evaluated using $K_\beta(0.95) \approx 2$. The AC method precision uncertainty for the ensemble mean, $P_{EV_a,AC}$, is then calculated with Equation (E-9). Confidence intervals for the mean of one run can be evaluated similarly via the AC method, and the AC method precision uncertainty for the mean of one run, $P_{EV_j,AC}$, is then calculated with Equation (E-10).

$$EV_{low,a} = EV_a - K_\beta\sqrt{Var(EV_a)}$$

$$EV_{up,a} = EV_a + K_\beta\sqrt{Var(EV_a)} \quad \text{(E - 7)}$$

$$K_\beta(\ P_\beta\ ) = Q_N\left(\frac{1+P_\beta}{2}\right) \quad \text{(E - 8)}$$

$$P_{EV_a} = \frac{1}{2}\left(EV_{up,a} - EV_{low,a}\right) = K_\beta\sqrt{Var(EV_a)} \quad \text{(E - 9)}$$

$$P_{EV_j} = K_\beta\sqrt{Var(EV_j)} \quad \text{(E - 10)}$$

Again, the confidence intervals for $\left(SD_j\right)^2$ and $(SD_a)^2$ are similar to Equation (E-7). However, the 95 % precision uncertainty for the standard deviation of one run, $P_{SD_j,AC}$, and the 95 % precision uncertainty for the ensemble standard deviation is evaluated with the central-limit theorem with Equations (E-11) and (E-12), respectively, see Diez et al. [E-1].

$$P_{SD_j} = SD_j\left(\sqrt{1 + \frac{K_\beta\sqrt{Var((SD_j)^2))}}{\left(SD_j\right)^2}} - 1\right) \quad \text{(E - 11)}$$

$$P_{SD_a} = SD_a\left(\sqrt{1 + \frac{K_\beta\sqrt{Var((SD_a)^2))}}{(SD_a)^2}} - 1\right) \quad \text{(E - 12)}$$

NON-OVERLAPPING BOOTSTRAPPING METHOD FOR PRIMARY VARIABLES

Bootstrapping analysis methods apply a statistical estimator to a data set repeatedly using random sampling with replacement to compute the validation values. The non-overlapping bootstrap method divides a time series record, or primary variable, into smaller segments for random sampling with replacement to compute the validation values. The NBB method is typically applied by dividing a time series of length N into $C = N/l$ blocks, where the optimal block length, l, is given by Equations (E-13), (E-14), and (E-15) as stated in Diez et al. [E-1].

$$l = (2\phi/c)^{2/3}N^{1/3} \quad \text{(E - 13)}$$

$$\text{c}=(1-\phi)(1+\phi) \quad \text{(E - 14)}$$

$$\phi = \frac{N\sum_i^{N-1}[x_{i+1}-EV][x_i-EV]}{(N-1)\sum_i^N[x_i-EV]2} \quad \text{(E - 15)}$$

As formulated, Equations (E-13), (E-14), and (E-15) will produce a different length block for each run in a multi-run data set. Therefore, these equations were used on several JUL 2019 GPPH runs from each test speed to determine a fixed NBB block size for analysis. The fixed block size used for data analysis was $l = 3T_e$, where T_e is the wave encounter period; this ensured the block size would not vary spot to spot. The number of non-overlapping bootstraps, B_{NBB}, was selected to be 1000.

The NBB method was implemented by first dividing each run into segments of length l. Since the run lengths, N_j, were not exact multiples of the block length (i.e. $N_j = C_j l + N_{j,rem}$), a small number of data points in each time series were discarded. To generate validation values for one run, this process provided a data set of $i = 1, \ldots, C_j$ time series segments. To generate

validation values for the ensemble data set, this process provided a total data set of $i = 1, \ldots, \sum_j^{N_r} C_j$ time series segments (i.e. all time series segments from all the runs).

Next, a random number generator was used to generate the specified number of bootstraps, B_{NBB}, for either data set length (i.e. C_j for one run or $N_r C_j$ for the ensemble). Then a "new" time series was generated B_{NBB}-times, and the statistical estimators were applied to each time series with the results tabulated. This produced B_{NBB}-values of each statistical estimator, which were then sorted lowest to highest. For example, the sorted mean values for one run, where $B_{NBB} = 1000$, were $EV_{j,[0.001B_{NBB}]}, \ldots, EV_{j,[1.000B_{NBB}]}$. Following the implementation of this process, Equations (E-16) and (E-18) were used to compute mean value for one run, EV_j, and the 95 % uncertainty value for the mean of one run via NBB, P_{EV_j}, respectively. Equations (E-17) and (E-19) were used to compute the standard deviation value for one run, SD_j, and the 95 % uncertainty value for the standard deviation of one run via NBB, P_{SD_j}, respectively. Equations (E-20) and (E-22) were used to compute ensemble mean value, EV_a, and the 95 % uncertainty value for the ensemble mean via NBB, P_{EV_a}, respectively. Equations (E-23) and (E-21) were used to compute the ensemble standard deviation value, SD_a, and the 95 % uncertainty value for the ensemble standard deviation via NBB, P_{SD_a}, respectively.

$$EV_j = EV_{j,[0.500B_{NBB}]} \quad \text{for } j = 1, \ldots, N_r \tag{E - 16}$$

$$SD_j = SD_{j,[0.500B_{NBB}]} \quad \text{for } j = 1, \ldots, N_r \tag{E - 17}$$

$$P_{EV_j} = \frac{1}{2}(EV_{j,[0.975B_{NBB}]} - EV_{j,[0.025B_{NBB}]}) \quad \text{for } j = 1, \ldots, N_r \tag{E - 18}$$

$$P_{SD_j} = \frac{1}{2}(SD_{j,[0.975B_{NBB}]} - SD_{j,[0.025B_{NBB}]}) \quad \text{for } j = 1, \ldots, N_r \tag{E - 19}$$

$$EV_a = EV_{a,[0.500B_{NBB}]} \tag{E - 20}$$

$$SD_a = SD_{a,[0.500B_{NBB}]} \tag{E - 21}$$

$$P_{EV_a} = \frac{1}{2}(EV_{a,[0.975B_{NBB}]} - EV_{a,[0.025B_{NBB}]}) \tag{E - 22}$$

$$P_{SD_a} = \frac{1}{2}(SD_{a,[0.975B_{NBB}]} - SD_{a,[0.025B_{NBB}]}) \tag{E - 23}$$

BOOTSTRAPPING METHOD FOR SECONDARY VARIABLES

The standard bootstrapping method was applied to the secondary variables that were derived via the peak identification method, see previous sections. Similar to the NBB method, the number of bootstraps, B_B, was selected to be 1000. For this bootstrap method, the peak identification process determined the number of validation values for one run of $j = 1, \ldots, N_j$ amplitude values/height values. To generate the validation values for the ensemble data set, the amplitude values/height values from all runs were combined to generate the total data set of $i = 1, \ldots, N_a$ amplitude values/height values.

Next, a random number generator was used to generate the specified number of bootstraps, B_B, for either data set length (i.e. N_j for one run or N_a for the ensemble). Then a "new" ordered data set was generated B_{NBB}-times, and the statistical estimators were applied to each data set

with the results tabulated. As stated above, for bootstrapping the statistical estimators include the mean values, standard deviation values, and the averages of the 1/3rd 1/10th, and 1/100th largest values in the data sets. This produced B_B-values of each statistical estimator, which were then sorted lowest to highest. For example, the sorted mean values for one run, where $B_B = 1000$, were $EV_{j,[0.001B_B]}, \ldots, EV_{j,[1.000B_B]}$. Following the implementation of this process, Equations (E-24) and (E-27) were used to compute mean value for one run, EV_j, and the 95 % uncertainty value for the mean of one run via bootstrapping, P_{EV_j}, respectively. Equations (E-25) and (E-28) were used to compute the standard deviation value for one run, SD_j, and the 95 % uncertainty value for the standard deviation of one run via bootstrapping, P_{SD_j}, respectively. Equations (E-26) and (E-29) were used to compute the average of the largest 1/n-th amplitude values/height values for one run, $EV_{\frac{1}{n},j}$, and the 95 % uncertainty value for the average of the largest 1/n-th amplitude values/height values of one run via bootstrapping, $P_{EV_{\frac{1}{n},j}}$, respectively. Equations (E-30) and (E-33) were used to compute ensemble mean value, EV_a, and the 95 % uncertainty value for the ensemble mean via bootstrapping, P_{EV_a}, respectively. Equations (E-31) and (E-34) were used to compute the ensemble standard deviation value, SD_a, and the 95 % uncertainty value for the ensemble standard deviation via bootstrapping, P_{SD_a}, respectively. Equations (E-32) and (E-35) were used to compute the ensemble average of the largest 1/n-th amplitude values/height values, $EV_{\frac{1}{n},a}$, and the 95 % uncertainty value for the ensemble average of the largest 1/n-th amplitude values/height values via bootstrapping, $P_{EV_{\frac{1}{n},a}}$, respectively.

$$EV_j = EV_{j,[0.500B_B]} \quad \text{for } j = 1, \ldots, N_r \tag{E - 24}$$

$$SD_j = SD_{j,[0.500B_B]} \quad \text{for } j = 1, \ldots, N_r \tag{E - 25}$$

$$EV_{\frac{1}{n},j} = EV_{\frac{1}{n},j,[0.500B_B]} \quad \text{for } j = 1, \ldots, N_r \tag{E - 26}$$

$$P_{EV_j} = \frac{1}{2}(EV_{j,[0.975B_B]} - EV_{j,[0.025B_B]}) \text{ for } j = 1, \ldots, N_r \tag{E - 27}$$

$$P_{SD_j} = \frac{1}{2}(SD_{j,[0.975B_B]} - SD_{j,[0.025B_B]}) \text{ for } j = 1, \ldots, N_r \tag{E - 28}$$

$$P_{EV_{\frac{1}{n},j}} = \frac{1}{2}(EV_{\frac{1}{n},j,[0.975B_B]} - EV_{\frac{1}{n},j,[0.025B_B]}) \quad \text{for } j = 1, \ldots, N_r \tag{E - 29}$$

$$EV_a = EV_{a,[0.500B_B]} \tag{E - 30}$$

$$SD_a = SD_{a,[0.500B_B]} \tag{E - 31}$$

$$EV_{\frac{1}{n},a} = EV_{\frac{1}{n},a,[0.500B_B]} \tag{E - 32}$$

$$P_{EV_a} = \frac{1}{2}(EV_{a,[0.975B_B]} - EV_{a,[0.025B_B]}) \tag{E - 33}$$

$$P_{SD_a} = \frac{1}{2}(SD_{a,[0.975B_B]} - SD_{a,[0.02 \quad B]}) \tag{E - 34}$$

$$P_{EV_{\frac{1}{n},a}} = \frac{1}{2}(EV_{\frac{1}{n},a,[0.975B_B]} - EV_{\frac{1}{n},a,[0.025B_B]}) \tag{E - 35}$$

REFERENCES

[E-1]. *Statistical Assessment and Validation of Experimental and Computational Ship Response in Irregular Waves.* Diez, Matteo, et al. 021004, s.l. : Journal of Verification, Validation and Uncertainty Qualification , Jne 2018, Vol. Vol. 3.

[E-2]. *Statistical Uncertainty of Ship Motion Data.* Belenky, V., V., Pipiras and Weems, K. Glasgow, UK : International Conference on the Stability of Ships and Ocean Vehicles, 2015, Vol. 12.

[E-3]. *Single Significant Amplitude and Confidence Intervals for Stochastic Processes.* pp. 1-16, s.l. : International Towing Tank Conference (ITTC), 2017. ITTC 7.5-02-01-08.

THIS PAGE INTENTIONALLY LEFT BLANK

APPENDIX F: ANALYSIS OF GRILLAGE AND PRESSURE EVENTS

CONTENTS

Appendix F: Analysis of Grillage and Pressure Events F-1
Maximum Events by Channel F-6
Traditional Grillage F-6
Optimized Grillage F-10
Maximum Events on Center Stiffener Channels by Condition F-13
Traditional Grillage F-13
Optimized Grillage F-17
Maximum Events and Responses on Each Stiffener Channel F-20
Traditional Grillage F-20
Optimized Grillage F-25
Severity F-30
Traditional Grillage F-30
Optimized Grillage F-35
References F-38

FIGURES

Figure F - 1. Maximum Event on Channel G7 (Traditional Grillage) F-8
Figure F - 2. Maximum Event on Channel G18 (Traditional Grillage) F-9
Figure F - 3. Maximum Event on Channel P11 (Traditional Grillage) F-9
Figure F - 4. Maximum Event on Channel 3 (Optimized Grillage) F-12
Figure F - 5. Maximum Event on Channel 24 (Optimized Grillage) F-13
Figure F - 6. Maximum Event on Channel P21 (Optimized Grillage) F-13
Figure F - 7. Largest Event on a Stiffener, Condition ID: 15 (Traditional Grillage) F-15
Figure F - 8. Second Largest Event on a Stiffener, Condition ID: 15 (Traditional Grillage) F-15
Figure F - 9. Third Largest Event on a Stiffener, Condition ID: 15 (Traditional Grillage) F-16
Figure F - 10. Fourth Largest Event on a Stiffener, Condition ID: 15 (Traditional Grillage) F-16

Figure F - 11. Largest Event on a Stiffener, Condition ID: 23 (Optimized Grillage) F-18
Figure F - 12. Second Largest Event on a Stiffener, Condition ID: 22 (Optimized Grillage) F-18
Figure F - 13. Third Largest Event on a Stiffener, Condition ID: 23 (Optimized Grillage)..... F-19
Figure F - 14. Fourth Largest Event on a Stiffener, Condition ID: 24 (Optimized Grillage) F-19
Figure F - 15. Time History of Largest Event of Traditional Grillage (Left) and Layout of Channels 16 - 20 on Grillage (Right)..... F-21
Figure F - 16. Strains along Stiffener Length of Traditional Grillage During Largest Event F-21
Figure F - 17. Time History of Second Largest Event of Traditional Grillage (Left) and Layout of Channels 21-25 on Grillage (Right) F-22
Figure F - 18. Strains along Stiffener Length of Traditional Grillage during Second Largest Event F-22
Figure F - 19. Time History of Third Largest Event of Traditional Grillage (Left) and Layout of Channels 16 - 20 on Grillage (Right) F-23
Figure F - 20. Strains along Stiffener Length of Traditional Grillage during Third Largest Event 23
Figure F - 21. Time history of Fourth Largest Event of Traditional Grillage (Left) and Layout of Channels 21 - 25 on Grillage (Right) F-24
Figure F - 22. Strains along Stiffener Length of Traditional Grillage during Fourth Largest Event F-24
Figure F - 23. Time History of Largest Event of Optimized Grillage (Left) and Layout of Channels 11 - 15 on Grillage (Right)..... F-26
Figure F - 24. Strains along Stiffener Length of Optimized Grillage during Largest Event F-26
Figure F - 25. Time History of Second Largest Event of Optimized Grillage (Left) and Layout of Channels 21 - 25 on Grillage (Right) F-27
Figure F - 26. Strains along Stiffener Length of Optimized Grillage during Second Largest Event F-27
Figure F - 27. Time History of Third Largest Event of Optimized Grillage (Left) and Layout of Channels 21 - 25 on Grillage (Right) F-28
Figure F - 28. Strains along Stiffener Length of Optimized Grillage during Third Largest Event F-28
Figure F - 29. Time History of Fourth Largest Event of Optimized Grillage (Left) and Layout of Channels 21 - 25 on Grillage (Right) F-29
Figure F - 30. Strains along Stiffener Length of Optimized Grillage during Fourth Largest Event F-29

TABLES

Table F - 1. Summary Table of Extrema on Differential Bending Channels (Traditional Grillage) F-6

Table F - 2. Summary Table of Positive Extrema on Single Strain Channels (Traditional Grillage) F-7

Table F - 3. Summary Table of Negative Extrema on Single Strain Channels (Traditional Grillage) F-7

Table F - 4. Summary Table of Extrema on Pressure Transducer Channels (Traditional Grillage) F-8

Table F - 5. Summary Table of Extrema on Differential Bending Channels (Optimized Grillage) F-10

Table F - 6. Summary Table of Positive Extrema on Single Strain Channels (Optimized Grillage) F-11

Table F - 7. Summary Table of Negative Extrema on Single Strain Channels (Optimized Grillage) F-11

Table F - 8. Summary Table of Extrema on Pressure Transducer Channels (Optimized Grillage) F-12

Table F - 9. Maximum Strain on Channel 18 and Corresponding Stiffener Gage Strains (Traditional Grillage) F-14

Table F - 10. Maximum Strain on Channel 25 and Corresponding Stiffener Gage Strains (Traditional Grillage) F-14

Table F - 11. Maximum Strain on Channel 13 and Corresponding Stiffener Gage Strains (Optimized Grillage) F-17

Table F - 12. Maximum Strain on Channel 18 and Corresponding Stiffener Gage Strains (Optimized Grillage) F-17

Table F - 13. Maximum Strain on Channel 23 and Corresponding Stiffener Gage Strains (Optimized Grillage) F-17

Table F - 14. Maximum Strains on Each Channel for Largest Event (Traditional Grillage) F-21

Table F - 15. Maximum Strains on Each Channel for Second Largest Event (Traditional Grillage) F-22

Table F - 16. Maximum Strains on Each Channel for Third Largest Event (Traditional Grillage) F-23

Table F - 17. Maximum Strains on Each Channel for Fourth Largest Event (Traditional Grillage) F-24

Table F - 18. Maximum Strains on Each Channel for Largest Event (Optimized Grillage) F-26

Table F - 19. Maximum Strains on Each Channel for Second Largest Event (Optimized Grillage) F-27

Table F - 20. Maximum Strains on Each Channel for Third Largest Event (Optimized Grillage) F-28

Table F - 21. Maximum Strains on Each Channel for Fourth Largest Event (Optimized Grillage) F-29

Table F - 22. Number of Events on Differential Bending Channels (Traditional Grillage) F-30

Table F - 23. Number of Severe Events on Differential Bending Channels (Traditional Grillage) F-30

Table F - 24. Rate of Severe Events on Differential Bending Channels (Traditional Grillage) F-31

Table F - 25. Number of Events on Single Strain Channels G11 - G18 (Traditional Grillage) F-32

Table F - 26. Number of Severe Events on Single Strain Channels G11 - G18 (Traditional Grillage) F-32

Table F - 27. Rate of Severe Events on Single Strain Channels G11 - G18 (Traditional Grillage) F-32

Table F - 28. Number of Events on Single Strain Channels G18 - G25 (Traditional Grillage) F-33

Table F - 29. Number of Severe Events on Single Strain Channels G18 - G25 (Traditional Grillage) F-33

Table F - 30. Rate of Severe Events on Single Strain Channels G18 - G25 (Traditional Grillage) F-33

Table F - 31. Number of Events of Pressure Transducer Channels (Traditional Grillage) F-34

Table F - 32. Number of Severe Events on Pressure Transducer Channels (Traditional Grillage) F-34

Table F - 33. Rate of Severe Events on Pressure Transducer Channels (Traditional Grillage) F-34

Table F - 34. Number of Events on Differential Bending Channels (Optimized Grillage) F-35

Table F - 35. Number of Severe Events on Differential Bending Channels (Optimized Grillage) F-35

Table F - 36. Rate of Severe Events on Differential Bending Channels (Optimized Grillage) F-35

Table F - 37. Number of Events on Single Strain Channels G11 - G18 (Optimized Grillage) F-36

Table F - 38. Number of Severe Events on Single Strain Channels G11 - G18 (Optimized Grillage) F-36

Table F - 39. Rate of Severe Events on Single Strain Channels G11 - G18 (Optimized Grillage) F-36

Table F - 40. Number of Events on Single Strain Channels G18 - G25 (Optimized Grillage) F-37
Table F - 41. Number of Severe Events on Single Strain Channels G18 - G25 (Optimized Grillage) F-37
Table F - 42. Rate of Severe Events on Single Strain Channels G18 - G25 (Optimized Grillage) F-37
Table F - 43. Number of Events of Pressure Transducer Channels (Optimized Grillage) F-38
Table F - 44. Number of Severe Events on Pressure Transducer Channels (Optimized Grillage) F-38
Table F - 45. Rate of Severe Events on Pressure Transducer Channels (Optimized Grillage) F-38

The body of the technical report discusses the procedure used to analyze grillage and pressure measurements. Data associated only with matrix IDs 14 and 15 are presented in the body. This appendix presents grillage and pressure analysis data for other conditions of interest. Matrix IDs 14 and 15 are repeated in this appendix in the interest of completeness.

MAXIMUM EVENTS BY CHANNEL

Table F - 1 to Table F - 4 provide summaries of the maximum event on each channel of the traditional grillage, and Table F - 5 to Table F - 8 provide summaries of the maximum event on each channel of the optimized grillage. The largest event for each type of channel are shown in Figure F - 1 to Figure F - 3 for the traditional grillage and in Figure F - 4 to Figure F - 6 for the optimized grillage.

Traditional Grillage

Table F - 1. Summary Table of Extrema on Differential Bending Channels (Traditional Grillage)

		Extrema									
		Differential Bending Channels (MS PSI)									
Matrix ID	Test Time (MS sec)	G1 (+)	G2 (+)	G3 (+)	G4 (+)	G5 (+)	G6 (+)	G7 (+)	G8 (+)	G9 (+)	G10 (+)
14 & 15	761	5	2	11	5	5	6	17	4	--	6
16 & 17	535	4	2	9	4	4	5	14	4	--	6

Table F - 2. Summary Table of Positive Extrema on Single Strain Channels (Traditional Grillage)

		Extrema														
		Single Strain Channels (microstrain)														
Matrix ID	**Test Time (MS sec)**	**G11 (+)**	**G12 (+)**	**G13 (+)**	**G14 (+)**	**G15 (+)**	**G16 (+)**	**G17 (+)**	**G18 (+)**	**G19 (+)**	**G20* (+)**	**G21 (+)**	**G22 (+)**	**G23 (+)**	**G24 (+)**	**G25* (+)**
14 & 15	761	471	1052	1279	1214	506	140	1266	1327	1153	115	168	1164	1241	1173	95
16 & 17	535	448	865	1221	1008	446	117	1021	1093	987	101	209	1004	1084	1044	91

*Results are presented for full disclosure, but the response of this channel was unreliable and it is recommended that these results are not used for comparison with CFD.

Table F - 3. Summary Table of Negative Extrema on Single Strain Channels (Traditional Grillage)

		Extrema														
		Single Strain Channels (microstrain)														
Matrix ID	**Test Time (MS sec)**	**G11 (-)**	**G12 (-)**	**G13 (-)**	**G14 (-)**	**G15 (-)**	**G16 (-)**	**G17 (-)**	**G18 (-)**	**G19 (-)**	**G20* (-)**	**G21 (-)**	**G22 (-)**	**G23 (-)**	**G24 (-)**	**G25* (-)**
14 & 15	761	-188	-335	-320	-464	-437	-910	-191	-198	-186	-603	-254	-137	-158	-173	-352
16 & 17	535	-111	-347	-254	-388	-343	-683	-159	-164	-155	-510	-272	-100	-109	-116	-325

*Results are presented for full disclosure, but the response of this channel was unreliable and it is recommended that these results are not used for comparison with CFD.

Table F - 4. Summary Table of Extrema on Pressure Transducer Channels (Traditional Grillage)

		Extrema					
		Pressure Transducers (MS PSI)					
Matrix ID	Test Time (MS sec)	P11 (+)	P12 (+)	P13 (+)	P21 (+)	P22 (+)	P23 (+)
14 & 15	761	12	11	7	10	7	11
16 & 17	535	9	6	4	9	6	4

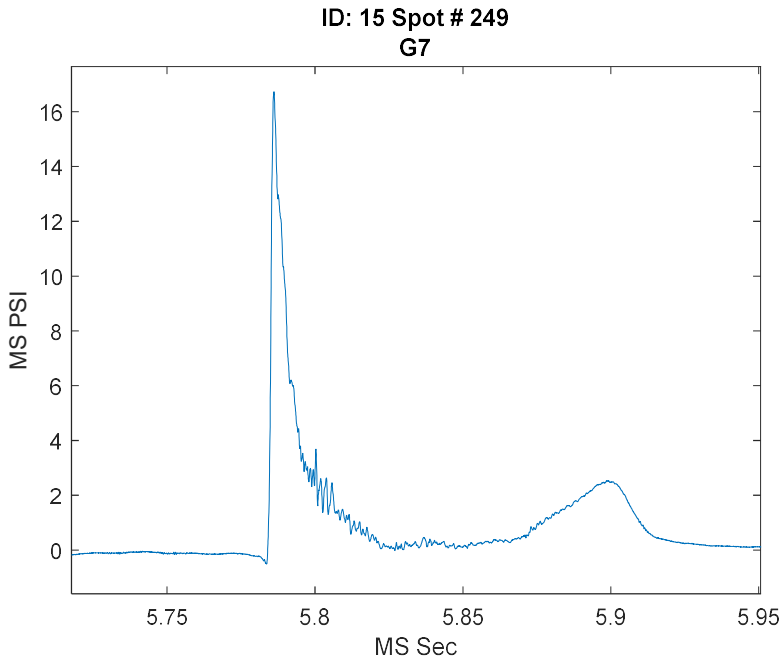

Figure F - 1. Maximum Event on Channel G7 (Traditional Grillage)

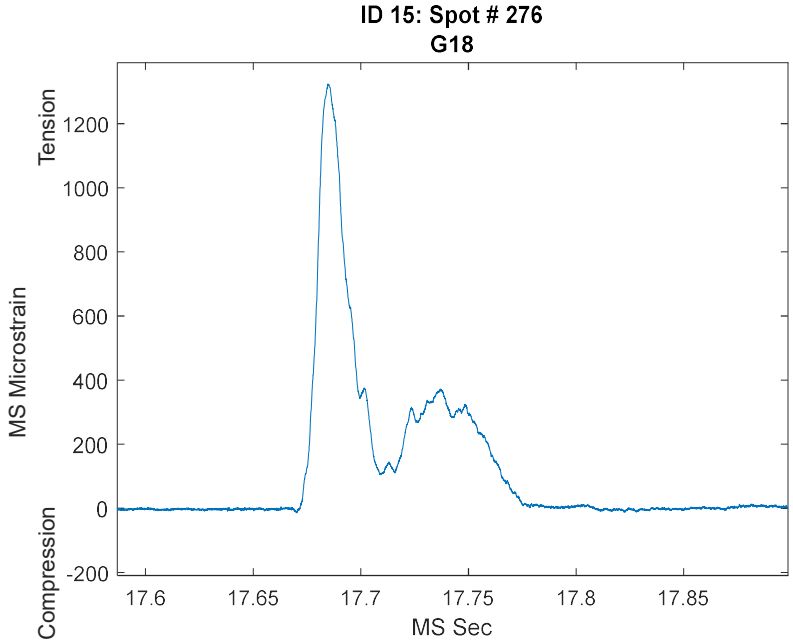

Figure F - 2. Maximum Event on Channel G18 (Traditional Grillage)

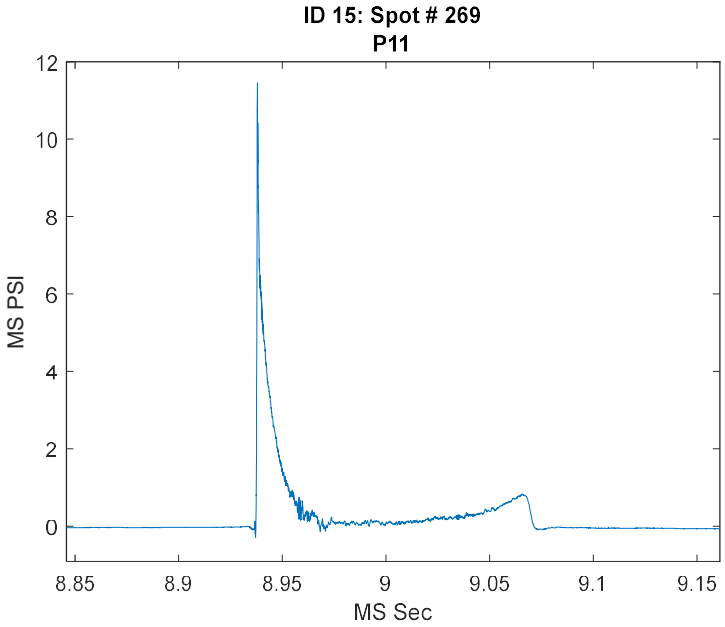

Figure F - 3. Maximum Event on Channel P11 (Traditional Grillage)

Optimized Grillage

Table F - 5. Summary Table of Extrema on Differential Bending Channels (Optimized Grillage)

		Extrema									
		Differential Bending Channels (MS PSI)									
Matrix ID	Test Time (MS sec)	G1 (+)	G2* (+)	G3 (+)	G4 (+)	G5 (+)	G6* (+)	G7* (+)	G8 (+)	G9 (+)	G10 (+)
22 & 23	1224	9	--	9	8	6	--	10	5	4	7
24 & 25	498	6	--	6	5	3	--	5	4	2	5

*Results are presented for full disclosure, but the response of this channel was unreliable and it is recommended that these results are not used for comparison with CFD.

Table F - 6. Summary Table of Positive Extrema on Single Strain Channels (Optimized Grillage)

	Extrema															
	Single Strain Channels (microstrain)															
Matrix ID	Test Time (MS s)	G11 (+)	G12 (+)	G13 (+)	G14 (+)	G15 (+)	G16 (+)	G17 (+)	G18 (+)	G19 (+)	G20* (+)	G21 (+)	G22 (+)	G23 (+)	G24 (+)	G25 (+)
22 & 23	1,224	173	2771	3868	3488	408	221	1798	1786	1166	127	327	3433	3706	4690	171
24 & 25	498	114	1948	2522	2126	304	149	1214	1119	777	141	193	2250	2470	1826	140

*Results are presented for full disclosure, but the response of this channel was unreliable and it is recommended that these results are not used for comparison with CFD.

Table F - 7. Summary Table of Negative Extrema on Single Strain Channels (Optimized Grillage)

	Extrema															
	Single Strain Channels (microstrain)															
Matrix ID	Test Time (MS s)	G11 (-)	G12 (-)	G13 (-)	G14 (-)	G15 (-)	G16 (-)	G17 (-)	G18 (-)	G19 (-)	G20* (-)	G21 (-)	G22 (-)	G23 (-)	G24 (-)	G25 (-)
22 & 23	1,224	-3601	-669	-633	-688	-1539	-910	-437	-458	-422	-1794	-1471	-833	-865	-696	-2313
24 & 25	-498	-2486	-514	-591	-639	-1019	-567	-268	-278	-283	-1134	-951	-464	-479	-380	-1388

*Results are presented for full disclosure, but the response of this channel was unreliable and it is recommended that these results are not used for comparison with CFD.

Table F - 8. Summary Table of Extrema on Pressure Transducer Channels (Optimized Grillage)

		Extrema					
		Pressure Transducers (MS PSI)					
Matrix ID	Test Time (MS sec)	P11 (+)	P12 (+)	P13 (+)	P21 (+)	P22 (+)	P23 (+)
22 & 23	1224	13	8	6	13	9	6
24 & 25	498	7	6	4	7	5	5

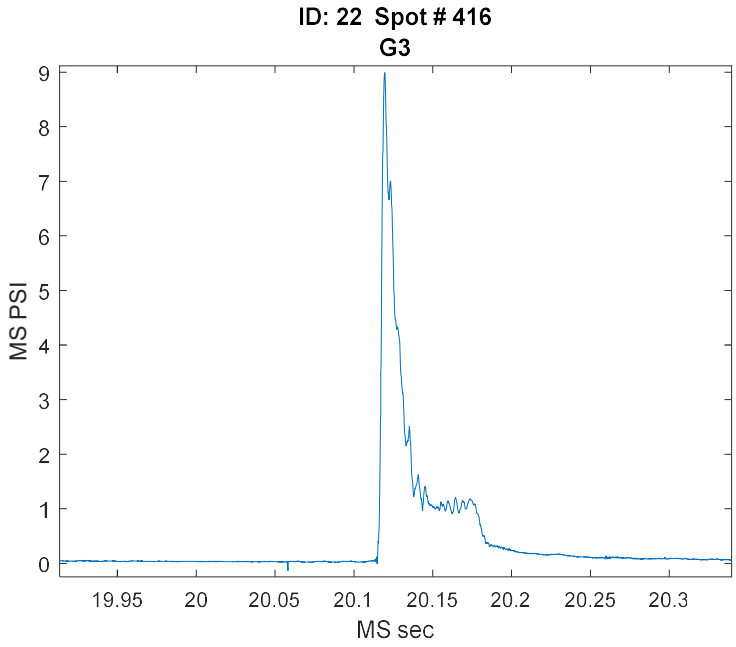

Figure F - 4. Maximum Event on Channel 3 (Optimized Grillage)

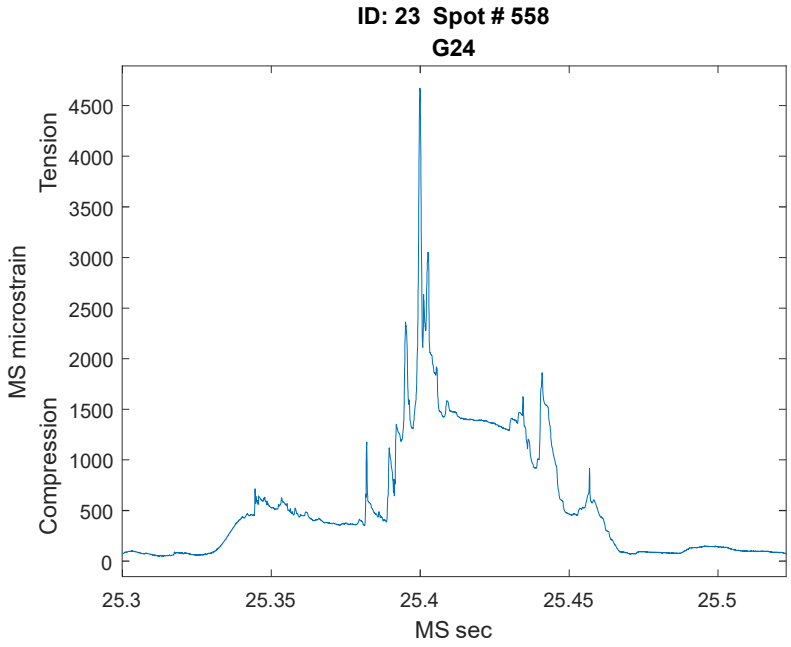

Figure F - 5. Maximum Event on Channel 24 (Optimized Grillage)

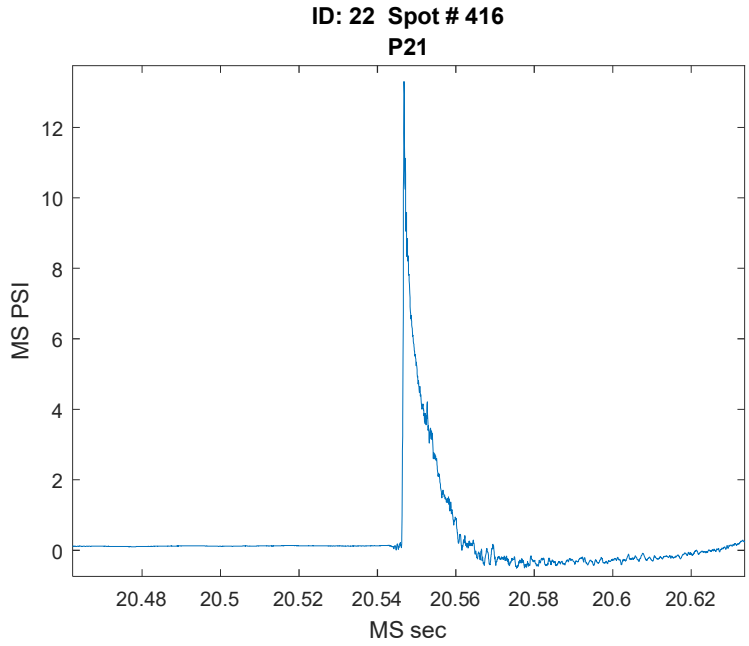

Figure F - 6. Maximum Event on Channel P21 (Optimized Grillage)

MAXIMUM EVENTS ON CENTER STIFFENER CHANNELS BY CONDITION

Traditional Grillage

For the single strain channels, the traditional grillage experienced the largest strains at the center of the stiffeners (at channels G18, and G23). Table F - 9 and Table F - 10 list the maximum strains on the center stiffener gages as well as the strains on the other four stiffener gages of the traditional grillage at the time the center gage reached its maximum for each condition. Figure F - 7 to Figure F - 10 show

the time histories of a selection of the largest events on the center stiffener gages. Maximum strains on gages G11 - G15 were not compiled, as the majority of data in channel G13 was distorted by noise and not considered for this analysis. The strains in matrix condition 14 and 15 are seen to have higher strains than matrix condition 16 and 17. This is expected given the higher speed at matrix condition 14 and 15. A more detailed list of the maximum strains on the center gages for each run can be found in Appendix G.

Table F - 9. Maximum Strain on Channel 18 and Corresponding Stiffener Gage Strains (Traditional Grillage)

		Stiffener Channels G16-G20					
Matrix ID	Run #	Time of Max Strain on Center Stiffener (sec)	Magnitude of Strain on G16 (microstrain)	Magnitude of Strain on G17 (microstrain)	Magnitude of Strain on G18 (microstrain)	Magnitude of Strain on G19 (microstrain)	Magnitude of Strain on G20 (microstrain)
14-15	276	17.6848	0	1253	**1324**	1142	0
16-17	296	30.7043	0	1012	**1087**	979	0

Table F - 10. Maximum Strain on Channel 25 and Corresponding Stiffener Gage Strains (Traditional Grillage)

		Stiffener Channels G21-25					
Matrix ID	Run #	Time of Max Strain on Center Stiffener (sec)	Magnitude of Strain on G21 (microstrain)	Magnitude of Strain on G22 (microstrain)	Magnitude of Strain on G23 (microstrain)	Magnitude of Strain on G24 (microstrain)	Magnitude of Strain on G25 (microstrain)
14-15	249	5.7888	0	1145	**1239**	1170	0
16-17	305	22.7342	0	987	**1079**	1029	0

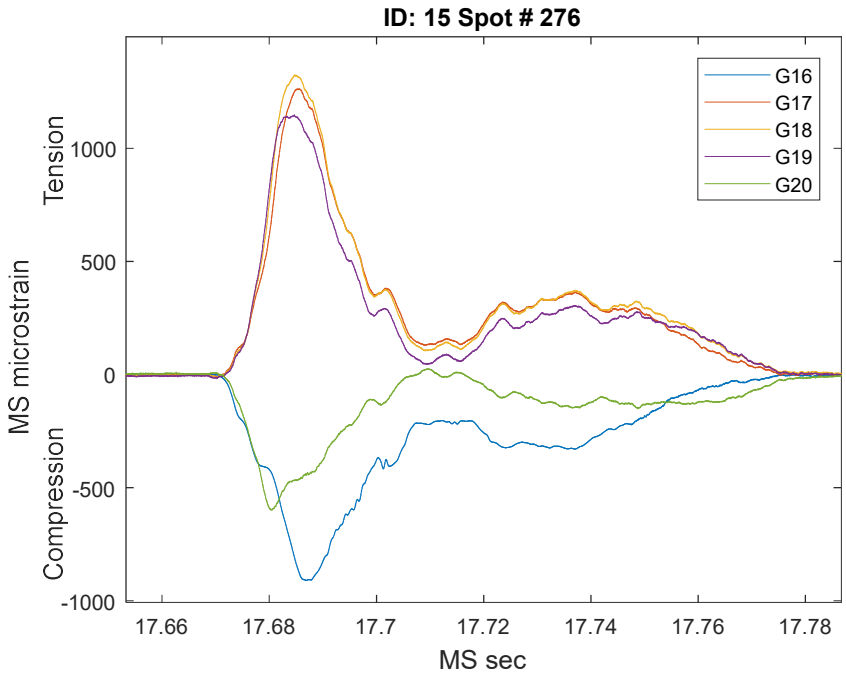

Figure F - 7. Largest Event on a Stiffener, Condition ID: 15 (Traditional Grillage)

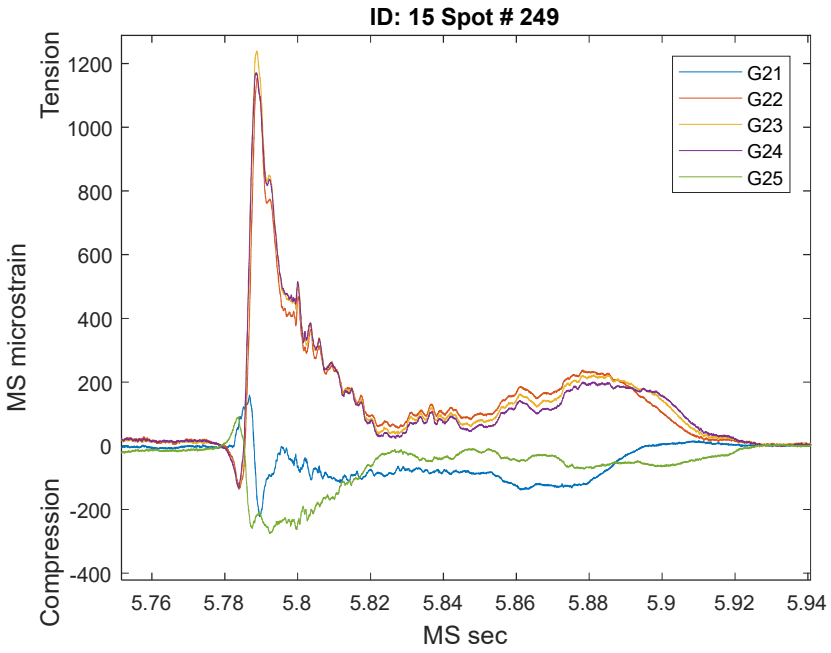

Figure F - 8. Second Largest Event on a Stiffener, Condition ID: 15 (Traditional Grillage)

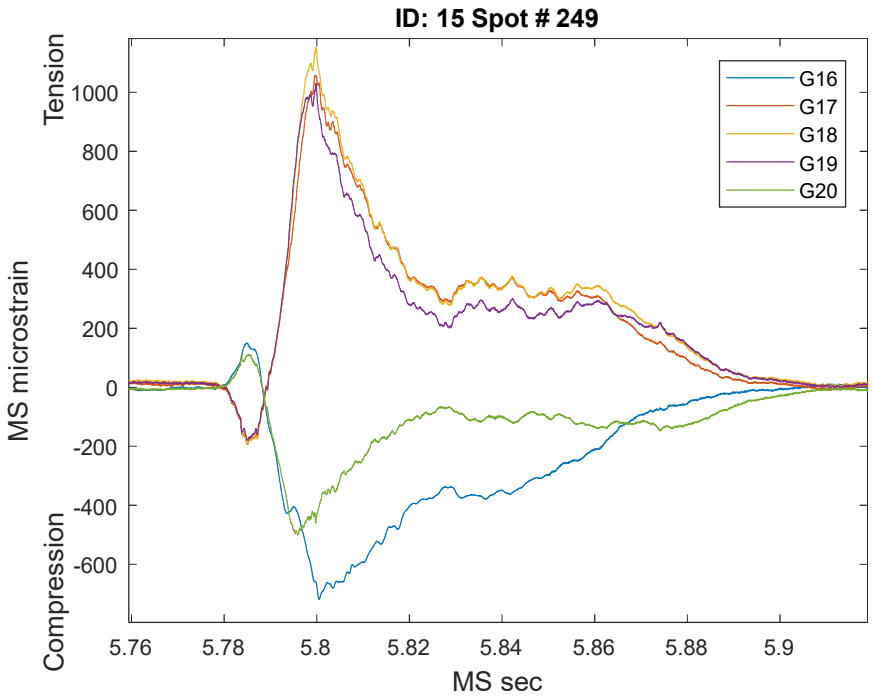

Figure F - 9. Third Largest Event on a Stiffener, Condition ID: 15 (Traditional Grillage)

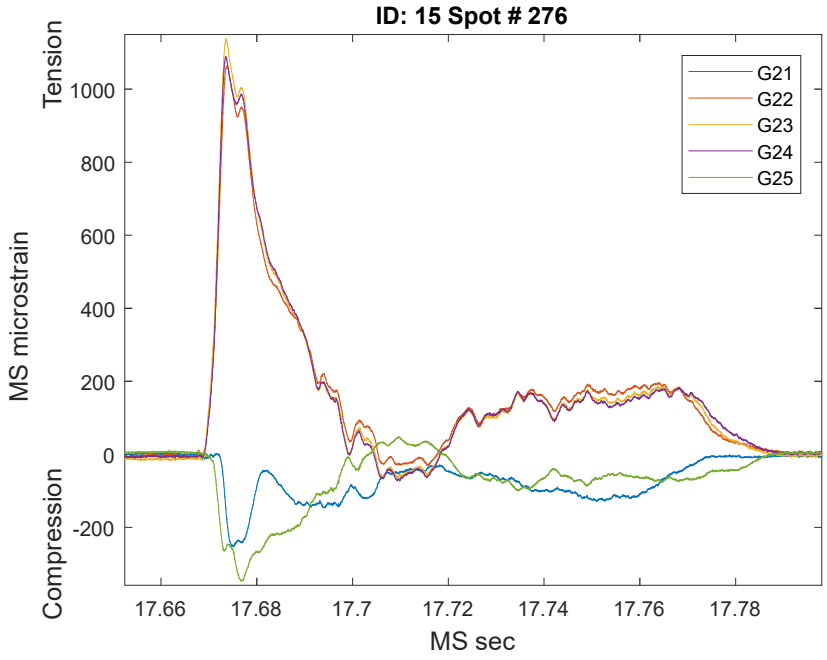

Figure F - 10. Fourth Largest Event on a Stiffener, Condition ID: 15 (Traditional Grillage)

Optimized Grillage

Like the traditional grillage, the optimized grillage experience the highest strains at the center of the stiffeners under matrix conditions 22 and 23. This is expected given by the higher run speeds in comparison to matrix conditions 24 and 25. Table F - 11 to Table F - 13 list the maximum strains on the center stiffener gages as well as the strains on the other four stiffener gages at the time the center gage reached its maximum for each condition. Figure F - 11 to Figure F - 14 show the time histories of a selection of the largest events on the center stiffener gages.

A more detailed list of the maximum strains on the center gages for each run of the optimized grillage can be found in Appendix G.

Table F - 11. Maximum Strain on Channel 13 and Corresponding Stiffener Gage Strains (Optimized Grillage)

		Stiffener Channels G11-G15					
Matrix ID	Run #	Time of Max Strain on Center Stiffener (sec)	Magnitude of Strain on G11 (microstrain)	Magnitude of Strain on G12 (microstrain)	Magnitude of Strain on G13 (microstrain)	Magnitude of Strain on G14 (microstrain)	Magnitude of Strain on G15 (microstrain)
22-23	446	27.4249	0	2637	**3868**	3348	0
24-25	468	19.8447	0	1797	**2522**	2054	0

Table F - 12. Maximum Strain on Channel 18 and Corresponding Stiffener Gage Strains (Optimized Grillage)

		Stiffener Channels G16-G20					
Matrix ID	Run #	Time of Max Strain on Center Stiffener (sec)	Magnitude of Strain on G16 (microstrain)	Magnitude of Strain on G17 (microstrain)	Magnitude of Strain on G18 (microstrain)	Magnitude of Strain on G19 (microstrain)	Magnitude of Strain on G20 (microstrain)
22-23	446	27.4300	198	1791	**1786**	1162	0
24-25	486	28.8606	325	1211	**1119**	669	0

Table F - 13. Maximum Strain on Channel 23 and Corresponding Stiffener Gage Strains (Optimized Grillage)

		Stiffener Channels G21-25					
Matrix ID	Run #	Time of Max Strain on Center Stiffener (sec)	Magnitude of Strain on G21 (microstrain)	Magnitude of Strain on G22 (microstrain)	Magnitude of Strain on G23 (microstrain)	Magnitude of Strain on G24 (microstrain)	Magnitude of Strain on G25 (microstrain)
22-23	416	20.1168	0	3373	**3706**	2677	0
24-25	489	18.4445	0	2172	**2470**	1822	0

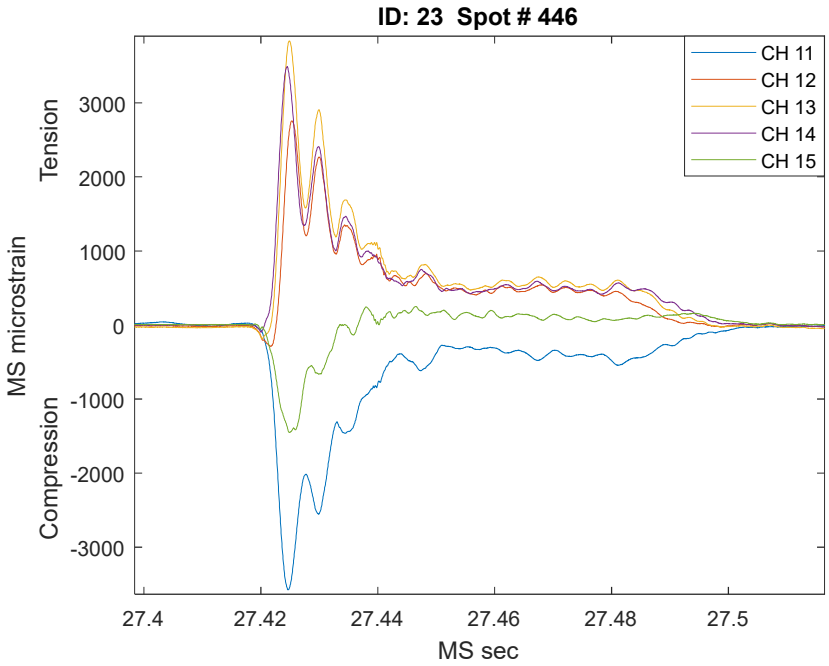

Figure F - 11. Largest Event on a Stiffener, Condition ID: 23 (Optimized Grillage)

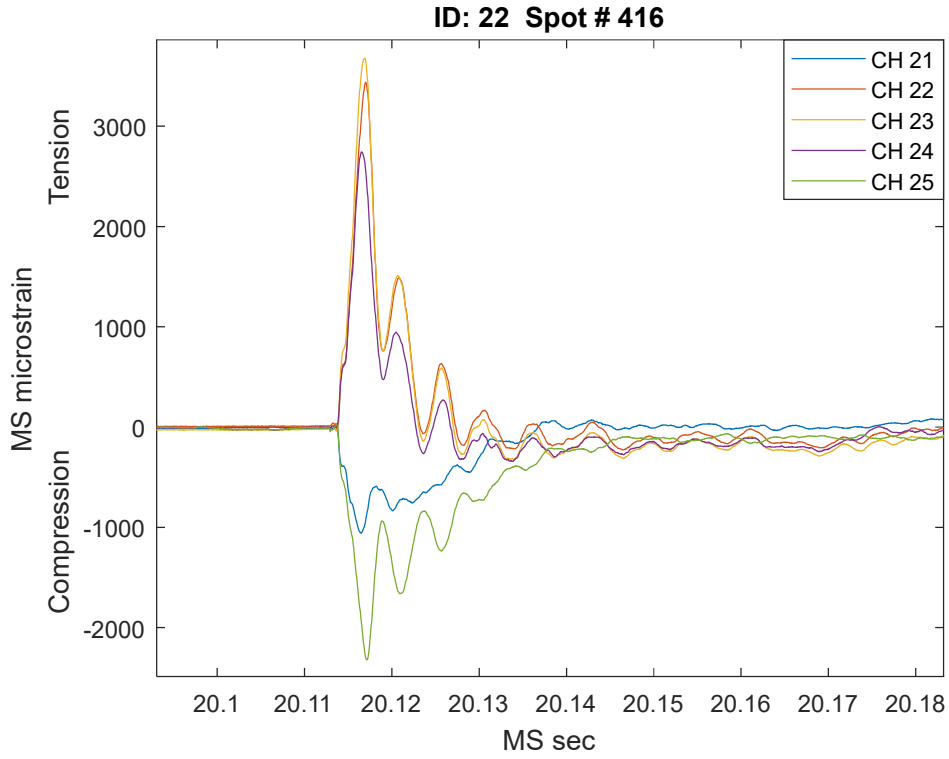

Figure F - 12. Second Largest Event on a Stiffener, Condition ID: 22 (Optimized Grillage)

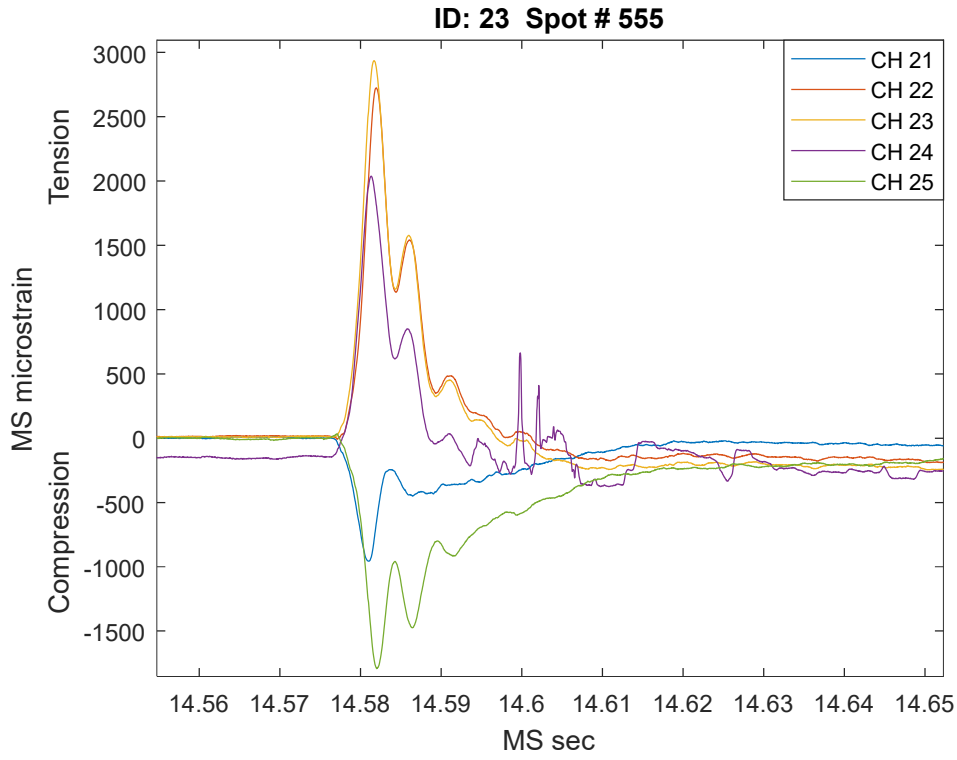

Figure F - 13. Third Largest Event on a Stiffener, Condition ID: 23 (Optimized Grillage)

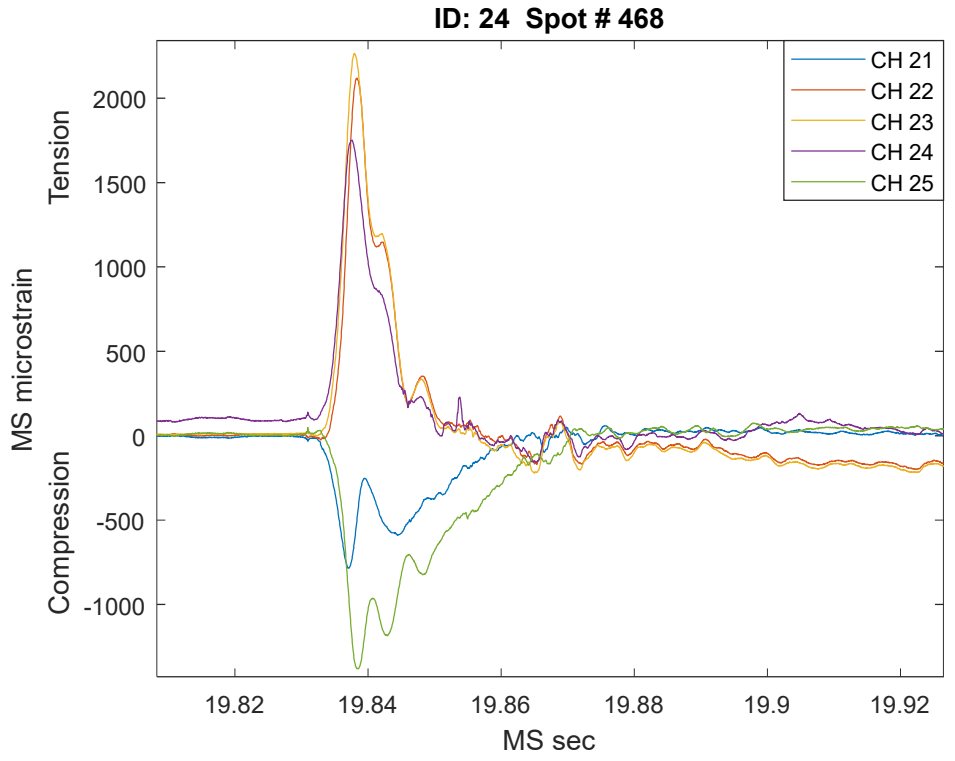

Figure F - 14. Fourth Largest Event on a Stiffener, Condition ID: 24 (Optimized Grillage)

MAXIMUM EVENTS AND RESPONSES ON EACH STIFFENER CHANNEL

Traditional Grillage

Below are the maximum strains at each stiffener channel, as well as the strain values on the other four stiffener channels at the exact time their peak value is reached. These maximum values are tabulated inTable F - 14 to Table F - 17 and the events are plotted in Figure F - 15 to Figure F - 22. For the spot runs shown, the maximum strain on each stiffener channel is shown to approximately occur at the same point in time, with the exception of second highest extrema (spot run 249).

Table F - 14. Maximum Strains on Each Channel for Largest Event (Traditional Grillage)

Extrema	Matrix ID	Run #	Max Channel	Time of Max Strain (sec)	Magnitude of Strain on G16 (microstrain)	Magnitude of Strain on G17 (microstrain)	Magnitude of Strain on G18 (microstrain)	Magnitude of Strain on G19 (microstrain)	Magnitude of Strain on G20 (microstrain)
1st	15	276	G16	17.6869	-909	1211	1251	1062	-441
			G17	17.6855	-873	1263	1315	1128	-461
			G18	17.6848	-815	1253	1324	1142	-467
			G19	17.6847	-807	1249	1322	1147	-468
			G20	17.6804	-436	695	856	907	-599

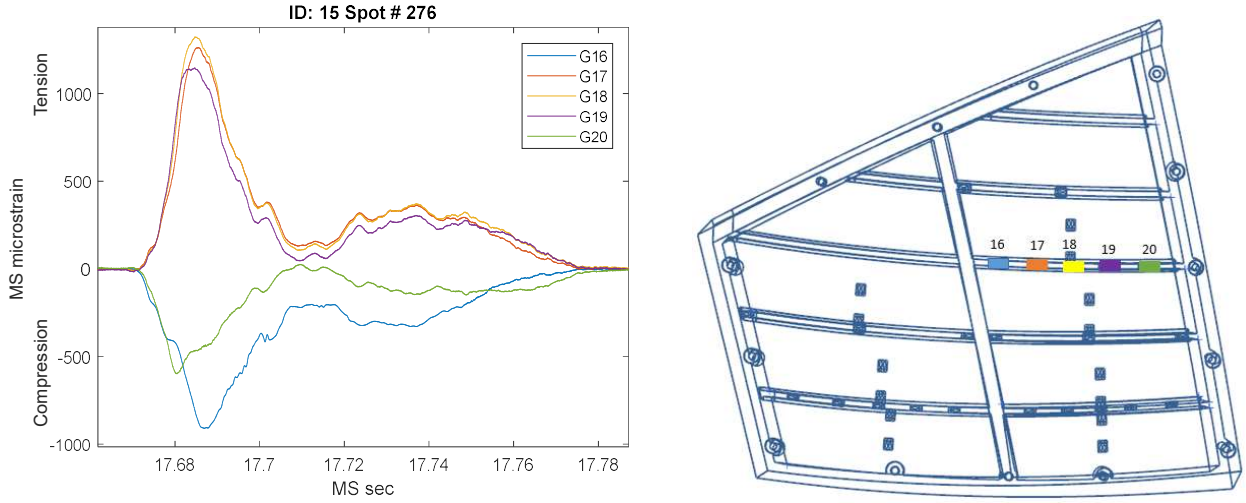

Figure F - 15. Time History of Largest Event of Traditional Grillage (Left) and Layout of Channels 16 - 20 on Grillage (Right)

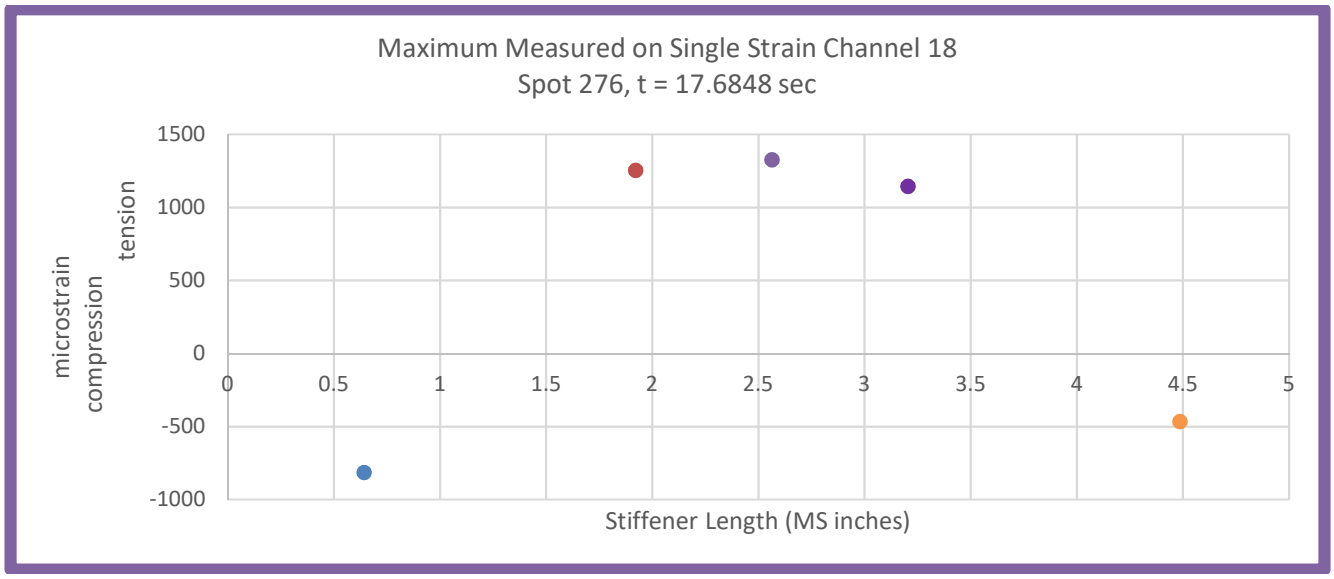

Figure F - 16. Strains along Stiffener Length of Traditional Grillage During Largest Event

Table F - 15. Maximum Strains on Each Channel for Second Largest Event (Traditional Grillage)

Extrema	Matrix ID	Run #	Max Channel	Time of Max Strain (sec)	Magnitude of Strain on G16 (microstrain)	Magnitude of Strain on G17 (microstrain)	Magnitude of Strain on G18 (microstrain)	Magnitude of Strain on G19 (microstrain)	Magnitude of Strain on G20 (microstrain)
3rd	15	249	G21	3.5539	-224	549	538	500	-150
			G22	5.7889	-174	1158	1235	1163	-219
			G23	5.7888	-150	1145	1239	1170	-220
			G24	5.7887	-137	1134	1234	1171	-221
			G25	13.7640	-218	869	920	890	-281

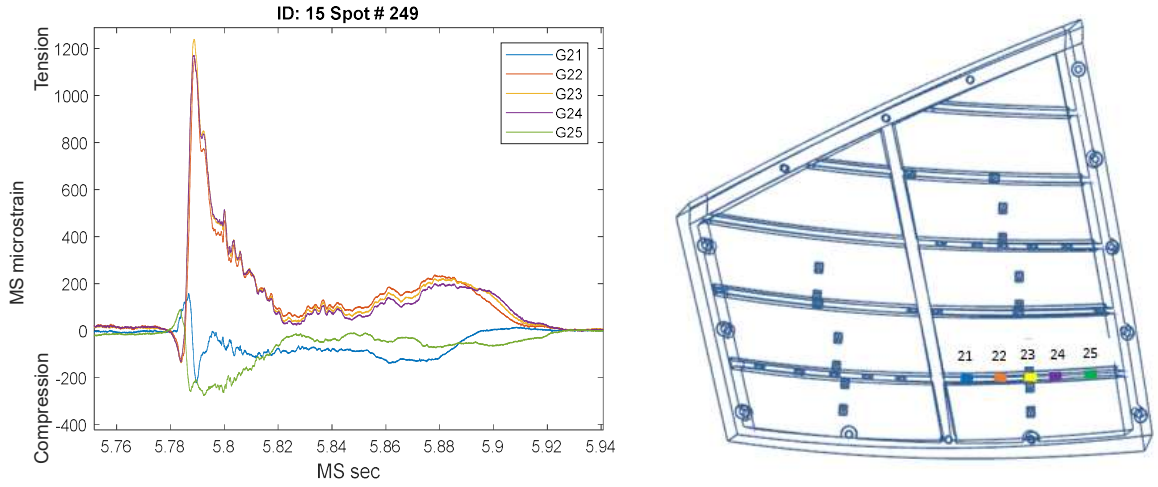

Figure F - 17. Time History of Second Largest Event of Traditional Grillage (Left) and Layout of Channels 21-25 on Grillage (Right)

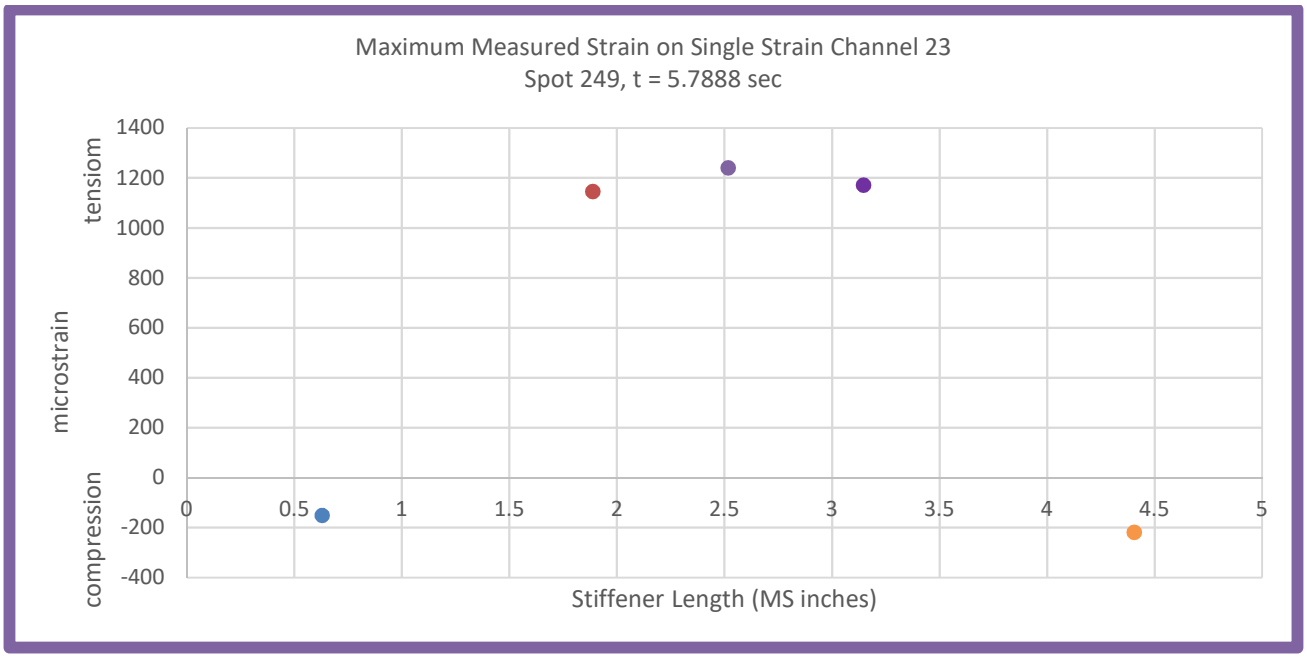

Figure F - 18. Strains along Stiffener Length of Traditional Grillage during Second Largest Event

Table F - 16. Maximum Strains on Each Channel for Third Largest Event (Traditional Grillage)

Extrema	Matrix ID	Run #	Max Channel	Time of Max Strain (sec)	Magnitude of Strain on G21 (microstrain)	Magnitude of Strain on G22 (microstrain)	Magnitude of Strain on G23 (microstrain)	Magnitude of Strain on G24 (microstrain)	Magnitude of Strain on G25 (microstrain)
4th	15	249	G16	5.8005	-719	1026	1071	922	-405
			G17	5.7996	-659	1057	1135	1005	-433
			G18	5.7998	-661	1056	1153	1030	-459
			G19	5.7998	-662	1055	1152	1030	-454
			G20	5.7959	-427	696	829	835	-500

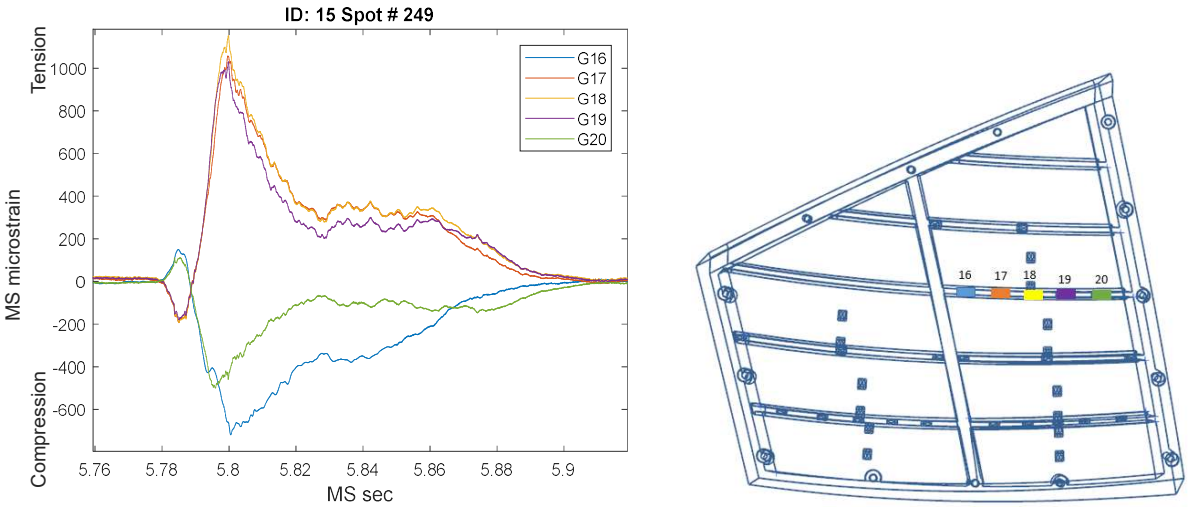

Figure F - 19. Time History of Third Largest Event of Traditional Grillage (Left) and Layout of Channels 16 - 20 on Grillage (Right)

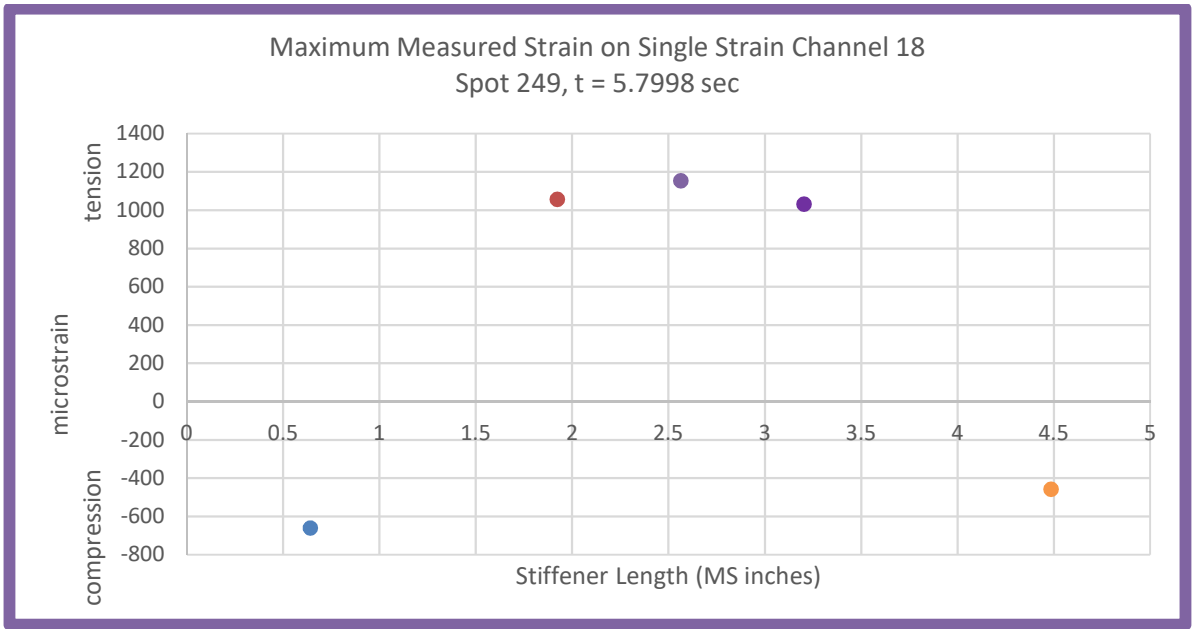

Figure F - 20. Strains along Stiffener Length of Traditional Grillage during Third Largest Event

Table F - 17. Maximum Strains on Each Channel for Fourth Largest Event (Traditional Grillage)

Extrema	Matrix ID	Run #	Max Channel	Time of Max Strain (sec)	Magnitude of Strain on G21 (microstrain)	Magnitude of Strain on G22 (microstrain)	Magnitude of Strain at G23 (microstrain)	Magnitude of Strain at G24 (microstrain)	Magnitude of Strain at G25 (microstrain)
5th	15	276	G21	17.6751	-253	979	1023	977	-269
			G22	17.6737	-176	1063	1132	1081	-251
			G23	17.6736	-153	1058	1138	1086	-260
			G24	17.6735	-146	1056	1135	1090	-258
			G25	17.6768	-241	951	1002	986	-347

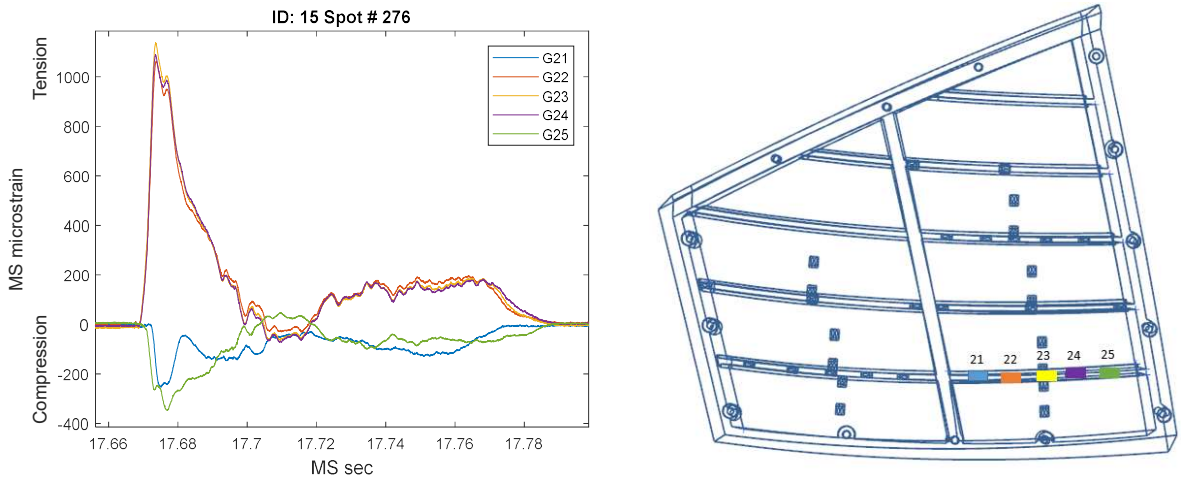

Figure F - 21. Time history of Fourth Largest Event of Traditional Grillage (Left) and Layout of Channels 21 - 25 on Grillage (Right)

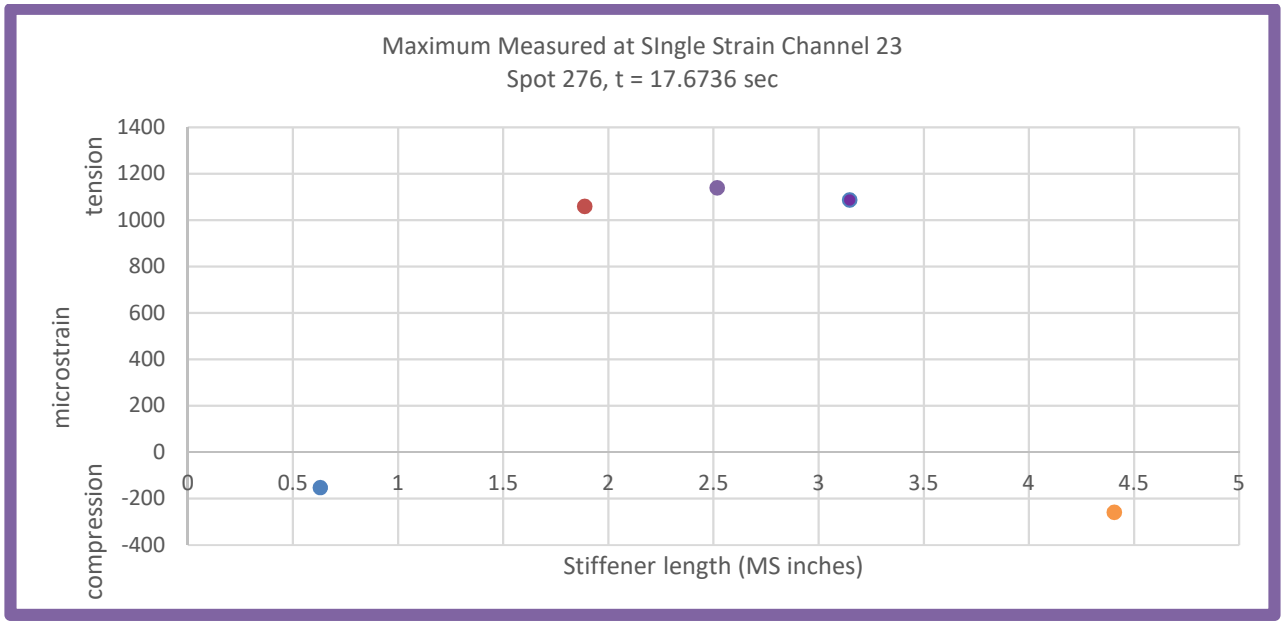

Figure F - 22. Strains along Stiffener Length of Traditional Grillage during Fourth Largest Event

Optimized Grillage

Below are the maximum strains at each stiffener channel, as well as the strain values on the other four stiffener channels at the exact time their peak value is reached. These maximum values are tabulated in Table F - 18 to Table F - 21 and the events are plotted in Figure F - 23 to Figure F - 30. Like the traditional grillage, the maximum strains on each stiffener channel is shown to approximately occur at the same point in time.

Table F - 18. Maximum Strains on Each Channel for Largest Event (Optimized Grillage)

Extrema	Matrix ID	Run #	Max Channel	Time of Max Strain (sec)	Magnitude of Strain on G11 (microstrain)	Magnitude of Strain on G12 (microstrain)	Magnitude of Strain on G13 (microstrain)	Magnitude of Strain on G14 (microstrain)	Magnitude of Strain on G15 (microstrain)
1st	23	446	G11	27.4247	-3604	2491	3831	3450	-1435
			G12	27.4253	-3406	2774	3708	3015	-1431
			G13	27.4249	-3579	2639	3867	3348	-1457
			G14	27.4245	-3588	2330	3746	3488	-1387
			G15	27.4249	-3579	2639	3867	3348	-1457

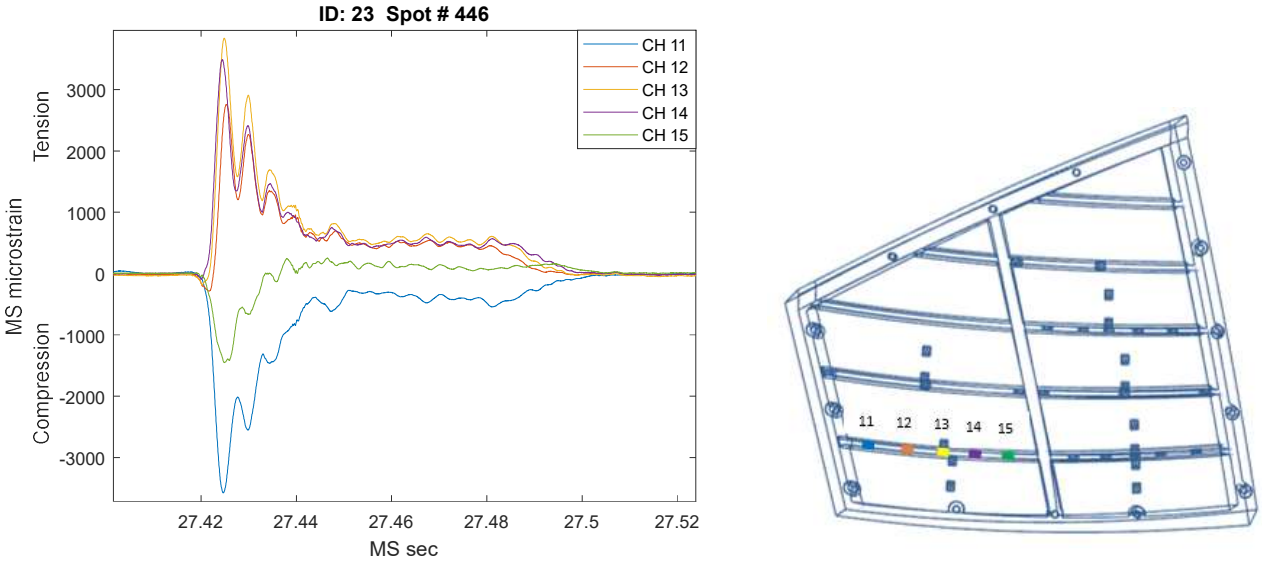

Figure F - 23. Time History of Largest Event of Optimized Grillage (Left) and Layout of Channels 11 - 15 on Grillage (Right)

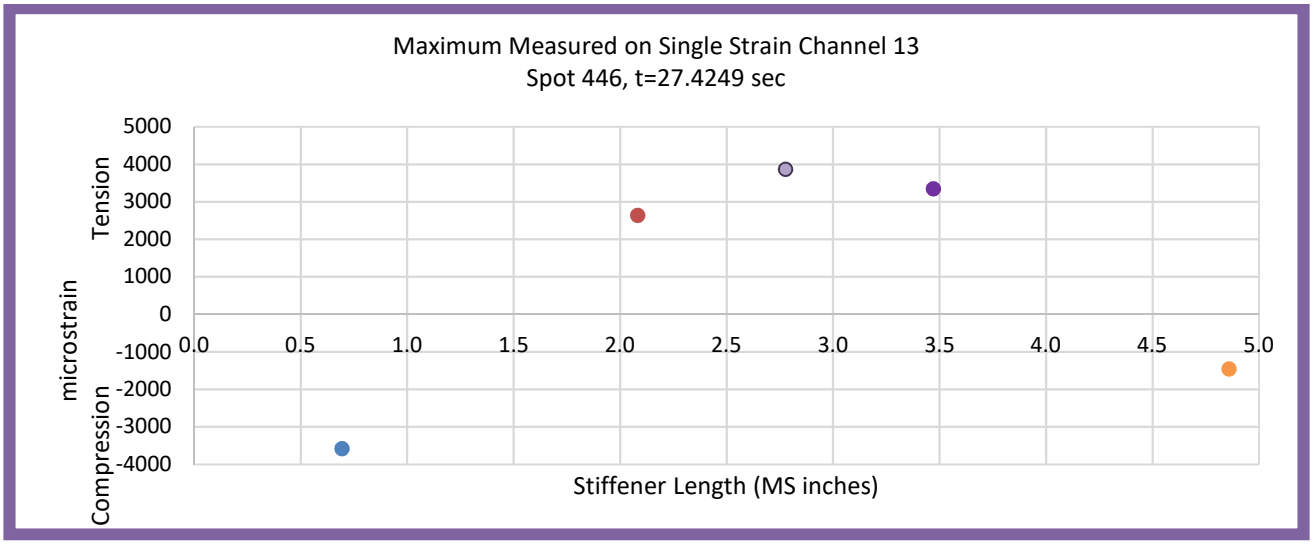

Figure F - 24. Strains along Stiffener Length of Optimized Grillage during Largest Event

Table F - 19. Maximum Strains on Each Channel for Second Largest Event (Optimized Grillage)

Extrema	Matrix ID	Run #	Max Channel	Time of Max Strain (sec)	Magnitude of Strain on G21 (microstrain)	Magnitude of Strain on G22 (microstrain)	Magnitude of Strain on G23 (microstrain)	Magnitude of Strain on G24 (microstrain)	Magnitude of Strain on G25 (microstrain)
2nd	22	416	G21	20.1164	-1048	3007	3502	2752	-1874
			G22	20.1170	-921	3433	3679	2583	-2278
			G23	20.1168	-985	3373	3707	2690	-2194
			G24	20.1165	-1045	3094	3570	2766	-1937
			G25	20.1172	-847	3384	3556	2421	-2303

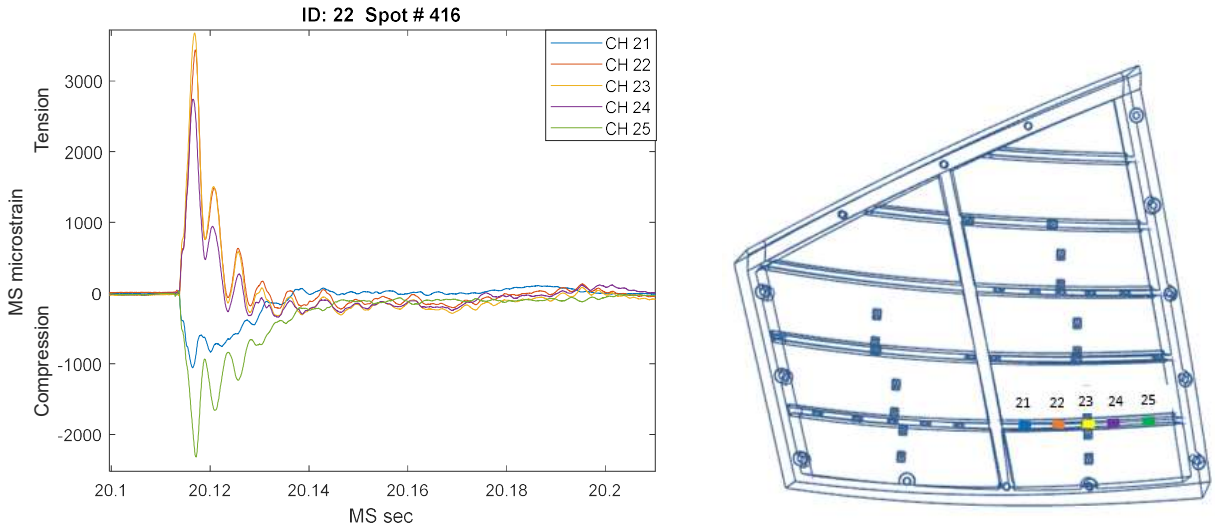

Figure F - 25. Time History of Second Largest Event of Optimized Grillage (Left) and Layout of Channels 21 - 25 on Grillage (Right)

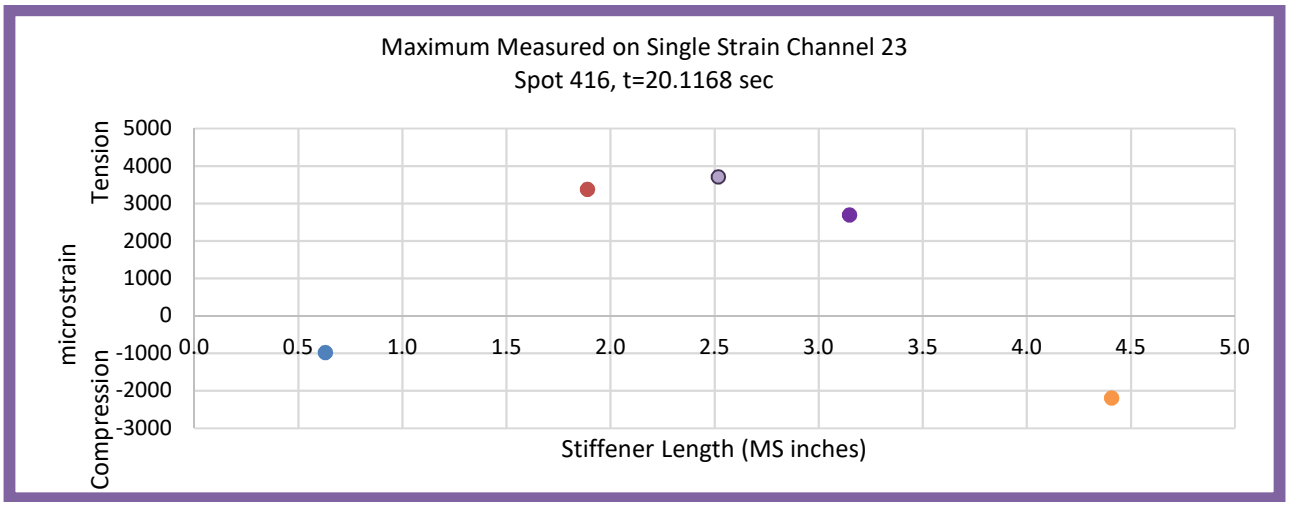

Figure F - 26. Strains along Stiffener Length of Optimized Grillage during Second Largest Event

Table F - 20. Maximum Strains on Each Channel for Third Largest Event (Optimized Grillage)

Extrema	Matrix ID	Run #	Max Channel	Time of Max Strain (sec)	Magnitude of Strain on G21 (microstrain)	Magnitude of Strain on G22 (microstrain)	Magnitude of Strain on G23 (microstrain)	Magnitude of Strain on G24 (microstrain)	Magnitude of Strain on G25 (microstrain)
3rd	23	555	G21	14.5810	-960	2043	2568	2124	-1298
			G22	14.5819	-669	2711	2876	1969	-1779
			G23	14.5817	-782	2660	2927	2082	-1722
			G24	14.5813	-923	2395	2832	2187	-1532
			G25	14.5820	-634	2705	2840	1929	-1785

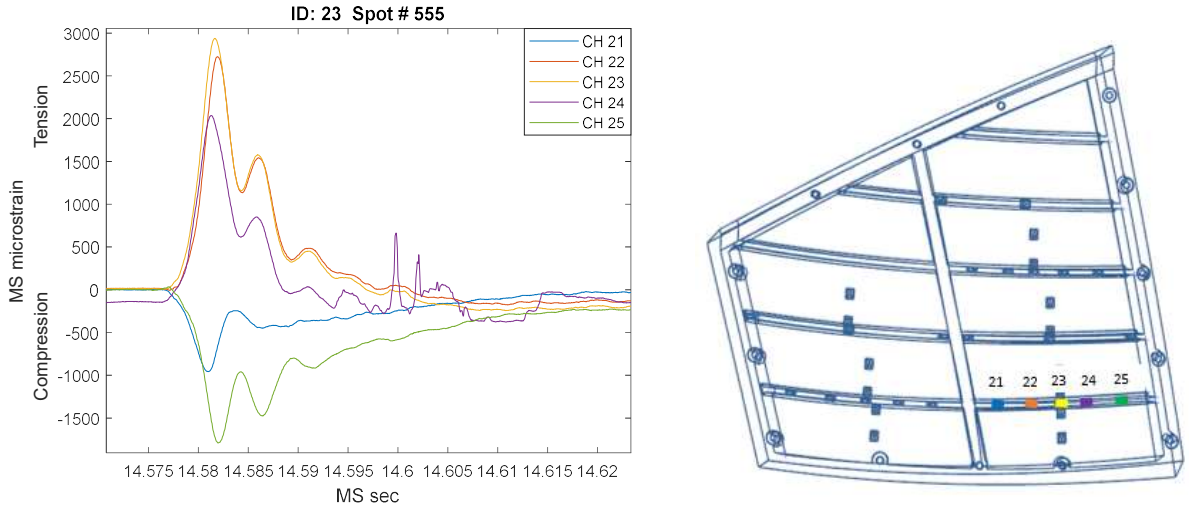

Figure F - 27. Time History of Third Largest Event of Optimized Grillage (Left) and Layout of Channels 21 - 25 on Grillage (Right)

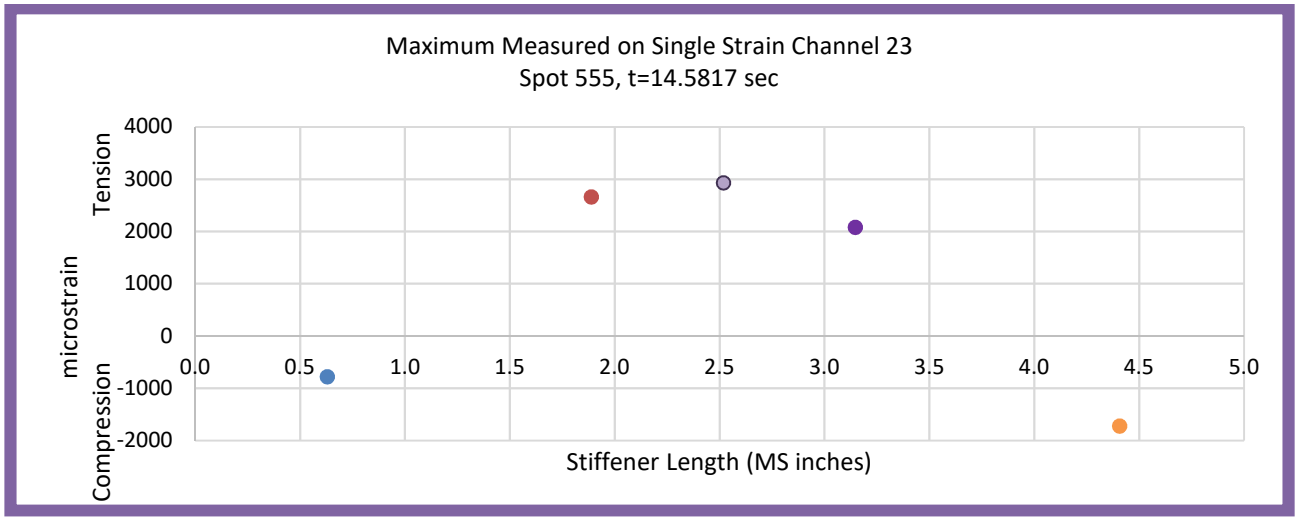

Figure F - 28. Strains along Stiffener Length of Optimized Grillage during Third Largest Event

Table F - 21. Maximum Strains on Each Channel for Fourth Largest Event (Optimized Grillage)

Extrema	Matrix ID	Run #	Max Channel	Time of Max Strain (sec)	Magnitude of Strain on G11 (microstrain)	Magnitude of Strain on G12 (microstrain)	Magnitude of Strain on G13 (microstrain)	Magnitude of Strain on G14 (microstrain)	Magnitude of Strain on G15 (microstrain)
4th	23	446	G11	7.0036	-2665	2246	2915	2264	-1445
			G12	7.0043	-2565	2374	2820	2078	-1451
			G13	7.0037	-2662	2264	2915	2247	-1452
			G14	7.0026	-2458	1481	2536	2452	-995
			G15	7.0040	-2629	2346	2887	2153	-1480

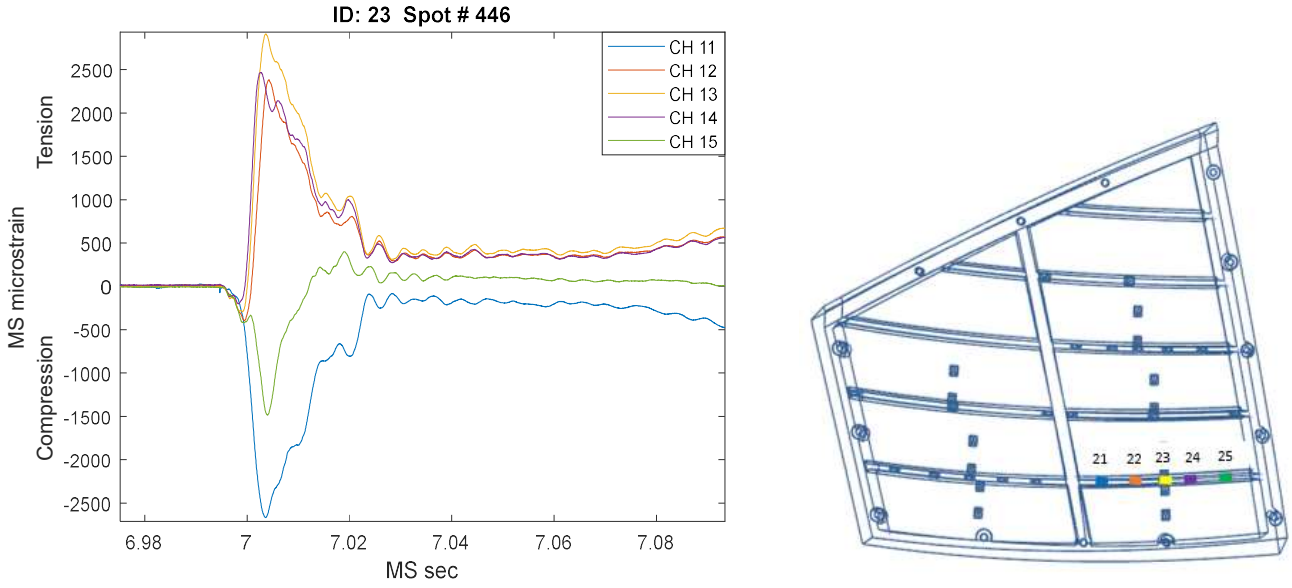

Figure F - 29. Time History of Fourth Largest Event of Optimized Grillage (Left) and Layout of Channels 21 - 25 on Grillage (Right)

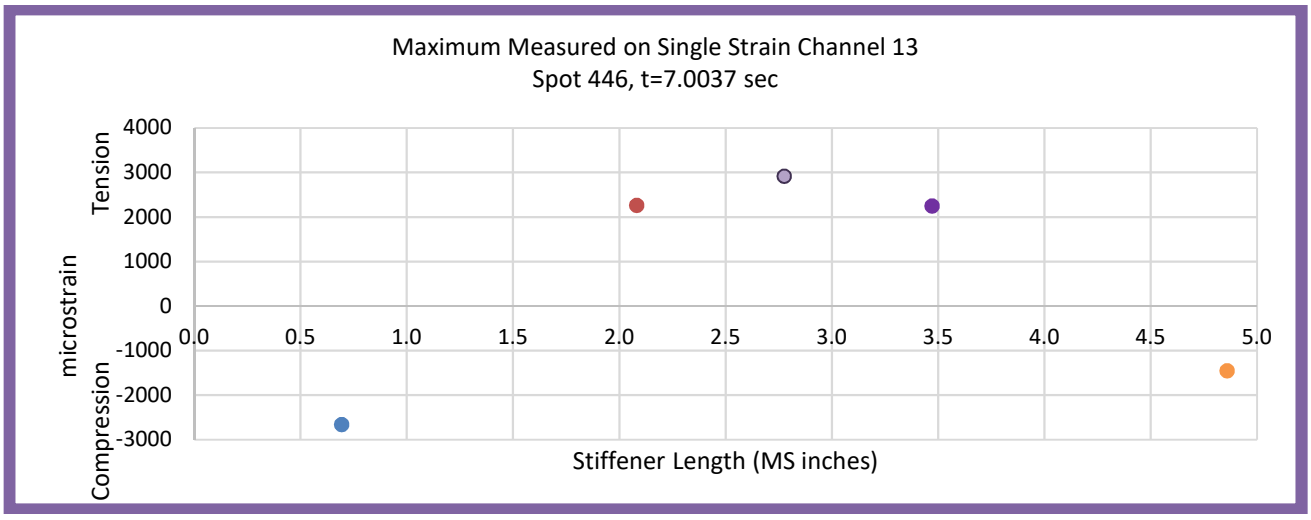

Figure F - 30. Strains along Stiffener Length of Optimized Grillage during Fourth Largest Event

SEVERITY

As defined by Judge et al. [F-1], a severe event is one that has a Z greater than 1.5, as shown by:

$$Z = \frac{P - \mu_p}{\sigma}$$

Where P is the event magnitude, μ_p is the population mean, and σ is the standard deviation.

Severity was calculated for all measured events for both grillages as a metric for comparison with past tests as well as future CFD tests.

The number of severe events and rate of severe events for both the traditional and optimized grillages are tabulated below. The events are summarized in Table F - 22 through Table F - 33 for the Traditional Grillage and Table F - 34 through Table F - 45 for the Optimized Grillage. Note that in the tables below, the (+) notation indicates tension on the sensor, while (-) indicates compression.

The rate of severe events was determined by taking the total number of severe events calculated in a given condition divided by the total time in the condition. The quotient, or rate, is expressed as number of severe events per model scale second.

Events were indentified using the methodology described in the subsection of this technical report titled “Pressure and Grillage Peak Identification Method for Irregular Waves”.

Traditional Grillage

Table F - 22. Number of Events on Differential Bending Channels (Traditional Grillage)

		Number of Events									
		Differential Bending Channels									
Matrix ID	Test Time (MS sec)	G1 (+)	G2 (+)	G3 (+)	G4 (+)	G5 (+)	G6 (+)	G7 (+)	G8 (+)	G9 (+)	G10 (+)
14 & 15	761	535	739	485	813	958	960	970	324	--	846
16 & 17	535	497	659	467	726	840	823	880	285	--	739

Table F - 23. Number of Severe Events on Differential Bending Channels (Traditional Grillage)

		Number of Severe Events									
		Differential Bending Channels									
Matrix ID	Test Time (MS sec)	G1 (+)	G2 (+)	G3 (+)	G4 (+)	G5 (+)	G6 (+)	G7 (+)	G8 (+)	G9 (+)	G10 (+)
14 & 15	761	39	36	36	55	69	71	80	27	--	67
16 & 17	535	42	44	40	55	55	58	76	22	--	53

Table F - 24. Rate of Severe Events on Differential Bending Channels (Traditional Grillage)

		Rate of Severe Events (Number of Severe Events / Model Scale Seconds)									
		Differential Bending Channels									
Matrix ID	Test Time (MS sec)	G1 (+)	G2 (+)	G3 (+)	G4 (+)	G5 (+)	G6 (+)	G7 (+)	G8 (+)	G9 (+)	G10 (+)
14 & 15	761	0.05	0.05	0.05	0.07	0.09	0.09	0.11	0.04	--	0.09
16 & 17	535	0.08	0.08	0.07	0.10	0.10	0.11	0.14	0.04	--	0.10

Table F - 25. Number of Events on Single Strain Channels G11 - G18 (Traditional Grillage)

		Number of Events														
		Single Strain Channels														
Matrix ID	Test Time (MS sec)	G11 (+)	G11 (-)	G12 (+)	G12 (-)	G13 (+)	G13 (-)	G14 (+)	G14 (-)	G15 (+)	G15 (-)	G16 (+)	G16 (-)	G17 (+)	G17 (-)	G18 (+)
14 & 15	761	416	187	383	508	115	136	850	590	975	669	186	720	766	300	793
16 & 17	535	534	129	423	611	56	70	529	706	830	592	107	629	674	185	695

Table F - 26. Number of Severe Events on Single Strain Channels G11 - G18 (Traditional Grillage)

		Number of Severe Events														
		Single Strain Channels														
Matrix ID	Test Time (MS sec)	G11 (+)	G11 (-)	G12 (+)	G12 (-)	G13 (+)	G13 (-)	G14 (+)	G14 (-)	G15 (+)	G15 (-)	G16 (+)	G16 (-)	G17 (+)	G17 (-)	G18 (+)
14 & 15	761	33	15	26	4	8	4	49	3	77	37	17	1	44	0	47
16 & 17	535	44	6	30	3	5	1	37	4	65	11	10	1	50	0	52

Table F - 27. Rate of Severe Events on Single Strain Channels G11 - G18 (Traditional Grillage)

		Rate of Severe Events (Number of Severe Events / Model Scale Seconds)														
		Single Strain Channels														
Matrix ID	Test Time (MS sec)	G11 (+)	G11 (-)	G12 (+)	G12 (-)	G13 (+)	G13 (-)	G14 (+)	G14 (-)	G15 (+)	G15 (-)	G16 (+)	G16 (-)	G17 (+)	G17 (-)	G18 (+)
14 & 15	761	0.04	0.02	0.03	0.01	0.01	0.01	0.06	0.00	0.10	0.05	0.02	0.00	0.06	0.00	0.06
16 & 17	535	0.08	0.01	0.06	0.01	0.01	0.00	0.07	0.01	0.12	0.02	0.02	0.00	0.09	0.00	0.10

Table F - 28. Number of Events on Single Strain Channels G18 - G25 (Traditional Grillage)

		Number of Events														
		Single Strain Channels														
Matrix ID	Test Time (MS sec)	G18 (-)	G19 (+)	G19 (-)	G20* (+)	G20* (-)	G21 (+)	G21 (-)	G22 (+)	G22 (-)	G23 (+)	G23 (-)	G24 (+)	G24 (-)	G25* (+)	G25* (-)
14 & 15	761	326	812	250	66	876	579	878	1033	112	1037	181	1082	182	82	998
16 & 17	535	240	727	181	30	758	384	800	945	46	986	65	1012	95	24	864

*Results are presented for full disclosure, but the response of this channel was unreliable and it is recommended that these results are not used for comparison with CFD.

Table F - 29. Number of Severe Events on Single Strain Channels G18 - G25 (Traditional Grillage)

		Number of Severe Events														
		Single Strain Channels														
Matrix ID	Test Time (MS sec)	G18 (-)	G19 (+)	G19 (-)	G20* (+)	G20* (-)	G21 (+)	G21 (-)	G22 (+)	G22 (-)	G23 (+)	G23 (-)	G24 (+)	G24 (-)	G25* (+)	G25* (-)
14 & 15	761	1	54	0	5	57	49	43	79	0	79	7	80	1	11	12
16 & 17	535	0	51	0	3	23	28	15	61	1	66	0	70	0	3	8

*Results are presented for full disclosure, but the response of this channel was unreliable and it is recommended that these results are not used for comparison with CFD.

Table F - 30. Rate of Severe Events on Single Strain Channels G18 - G25 (Traditional Grillage)

		Rate of Severe Events (Number of Severe Events / Model Scale Seconds)														
		Single Strain Channels														
Matrix ID	Test Time (MS sec)	G18 (-)	G19 (+)	G19 (-)	G20* (+)	G20* (-)	G21 (+)	G21 (-)	G22 (+)	G22 (-)	G23 (+)	G23 (-)	G24 (+)	G24 (-)	G25* (+)	G25* (-)
14 & 15	761	0.00	0.07	0.00	0.01	0.07	0.06	0.06	0.10	0.00	0.10	0.01	0.11	0.00	0.01	0.02
16 & 17	535	0.00	0.10	0.00	0.01	0.04	0.05	0.03	0.11	0.00	0.12	0.00	0.13	0.00	0.01	0.01

*Results are presented for full disclosure, but the response of this channel was unreliable and it is recommended that these results are not used for comparison with CFD.

Table F - 31. Number of Events of Pressure Transducer Channels (Traditional Grillage)

		Number of Events					
		Pressure Transducers					
Matrix ID	Test Time (MS sec)	P11 (+)	P12 (+)	P13 (+)	P21 (+)	P22 (+)	P23 (+)
14 & 15	761	722	636	414	942	787	706
16 & 17	535	650	585	400	820	697	664

Table F - 32. Number of Severe Events on Pressure Transducer Channels (Traditional Grillage)

		Number of Severe Events					
		Pressure Transducers					
Matrix ID	Test Time (MS sec)	P11 (+)	P12 (+)	P13 (+)	P21 (+)	P22 (+)	P23 (+)
14 & 15	761	51	44	23	70	60	34
16 & 17	535	49	48	33	72	51	45

Table F - 33. Rate of Severe Events on Pressure Transducer Channels (Traditional Grillage)

		Rate of Severe Events (Number of Severe Events / Model Scale Seconds)					
		Pressure Transducers					
Matrix ID	Test Time (MS sec)	P11 (+)	P12 (+)	P13 (+)	P21 (+)	P22 (+)	P23 (+)
14 & 15	761	0.07	0.06	0.03	0.09	0.08	0.04
16 & 17	535	0.09	0.09	0.06	0.13	0.10	0.08

Optimized Grillage

Table F - 34. Number of Events on Differential Bending Channels (Optimized Grillage)

		Number of Events									
		Differential Bending Channels									
Matrix ID	Test Time (MS s)	G1 (+)	G2* (+)	G3 (+)	G4 (+)	G5 (+)	G6* (+)	G7* (+)	G8 (+)	G9 (+)	G10 (+)
22 & 23	1,224	1142	--	1196	1794	2128	--	2180	775	857	1839
24 & 25	498	408	--	409	645	798	--	807	289	328	661

*Results are presented for full disclosure, but the response of this channel was unreliable and it is recommended that these results are not used for comparison with CFD.

Table F - 35. Number of Severe Events on Differential Bending Channels (Optimized Grillage)

		Number of Severe Events									
		Differential Bending Channels									
Matrix ID	Test Time (MS s)	G1 (+)	G2* (+)	G3 (+)	G4 (+)	G5 (+)	G6* (+)	G7* (+)	G8 (+)	G9 (+)	G10 (+)
22 & 23	1,224	83	--	93	142	156	--	167	49	55	138
24 & 25	498	30	--	35	52	60	--	64	15	17	51

*Results are presented for full disclosure, but the response of this channel was unreliable and it is recommended that these results are not used for comparison with CFD.

Table F - 36. Rate of Severe Events on Differential Bending Channels (Optimized Grillage)

		Rate of Severe Events (Number of Severe Events / Model Scale Seconds)									
		Differential Bending Channels									
Matrix ID	Test Time (MS s)	G1 (+)	G2* (+)	G3 (+)	G4 (+)	G5 (+)	G6* (+)	G7* (+)	G8 (+)	G9 (+)	G10 (+)
22 & 23	1,224	0.07	--	0.08	0.12	0.13	--	0.14	0.04	0.04	0.11
24 & 25	498	0.06	--	0.07	0.10	0.12	--	0.13	0.03	0.03	0.10

*Results are presented for full disclosure, but the response of this channel was unreliable and it is recommended that these results are not used for comparison with CFD.

Table F - 37. Number of Events on Single Strain Channels G11 - G18 (Optimized Grillage)

		Number of Events														
		Single Strain Channels														
Matrix ID	Test Time (MS s)	G11 (+)	G11 (-)	G12 (+)	G12 (-)	G13 (+)	G13 (-)	G14 (+)	G14 (-)	G15 (+)	G15 (-)	G16 (+)	G16 (-)	G17 (+)	G17 (-)	G18 (+)
22 & 23	1,224	96	1675	1169	2090	1362	2039	1463	2090	1546	2479	731	1854	1797	1781	1792
24 & 25	498	15	561	403	720	475	711	521	773	495	846	193	647	635	570	644

Table F - 38. Number of Severe Events on Single Strain Channels G11 - G18 (Optimized Grillage)

		Number of Severe Events														
		Single Strain Channels														
Matrix ID	Test Time (MS s)	G11 (+)	G11 (-)	G12 (+)	G12 (-)	G13 (+)	G13 (-)	G14 (+)	G14 (-)	G15 (+)	G15 (-)	G16 (+)	G16 (-)	G17 (+)	G17 (-)	G18 (+)
22 & 23	1,224	8	92	56	172	68	175	77	177	81	153	63	113	110	155	117
24 & 25	498	2	37	21	60	25	59	33	66	43	60	18	46	44	46	48

Table F - 39. Rate of Severe Events on Single Strain Channels G11 - G18 (Optimized Grillage)

		Rate of Severe Events (Number of Severe Events / Model Scale Seconds)														
		Single Strain Channels														
Matrix ID	Test Time (MS s)	G11 (+)	G11 (-)	G12 (+)	G12 (-)	G13 (+)	G13 (-)	G14 (+)	G14 (-)	G15 (+)	G15 (-)	G16 (+)	G16 (-)	G17 (+)	G17 (-)	G18 (+)
22 & 23	1,224	0.01	0.08	0.05	0.14	0.06	0.14	0.06	0.14	0.07	0.13	0.05	0.09	0.09	0.13	0.10
24 & 25	498	0.00	0.07	0.04	0.12	0.05	0.12	0.07	0.13	0.09	0.12	0.04	0.09	0.09	0.09	0.10

Table F - 40. Number of Events on Single Strain Channels G18 - G25 (Optimized Grillage)

		Number of Events														
		Single Strain Channels														
Matrix ID	Test Time (MS s)	G18 (-)	G19 (+)	G19 (-)	G20* (+)	G20* (-)	G21 (+)	G21 (-)	G22 (+)	G22 (-)	G23 (+)	G23 (-)	G24 (+)	G24 (-)	G25 (+)	G25 (-)
22 & 23	1,224	1909	1845	1891	286	1894	1690	2682	2629	1787	2739	1874	2451	1669	84	2261
24 & 25	498	616	672	591	51	616	510	915	1007	577	1044	609	877	520	11	815

*Results are presented for full disclosure, but the response of this channel was unreliable and it is recommended that these results are not used for comparison with CFD.

Table F - 41. Number of Severe Events on Single Strain Channels G18 - G25 (Optimized Grillage)

		Number of Severe Events														
		Single Strain Channels														
Matrix ID	Test Time (MS s)	G18 (-)	G19 (+)	G19 (-)	G20* (+)	G20* (-)	G21 (+)	G21 (-)	G22 (+)	G22 (-)	G23 (+)	G23 (-)	G24 (+)	G24 (-)	G25 (+)	G25 (-)
22 & 23	1,224	161	127	180	24	117	51	216	185	154	195	170	161	150	6	158
24 & 25	498	51	45	53	6	45	15	79	79	48	82	61	71	35	1	64

*Results are presented for full disclosure, but the response of this channel was unreliable and it is recommended that these results are not used for comparison with CFD.

Table F - 42. Rate of Severe Events on Single Strain Channels G18 - G25 (Optimized Grillage)

		Rate of Severe Events (Number of Severe Events / Model Scale Seconds)														
		Single Strain Channels														
Matrix ID	Test Time (MS s)	G18 (-)	G19 (+)	G19 (-)	G20* (+)	G20* (-)	G21 (+)	G21 (-)	G22 (+)	G22 (-)	G23 (+)	G23 (-)	G24 (+)	G24 (-)	G25 (+)	G25 (-)
22 & 23	1224	0.13	0.10	0.15	0.02	0.10	0.04	0.18	0.15	0.13	0.16	0.14	0.13	0.12	0.00	0.13
24 & 25	498	0.10	0.09	0.11	0.01	0.09	0.03	0.16	0.16	0.10	0.16	0.12	0.14	0.07	0.00	0.13

*Results are presented for full disclosure, but the response of this channel was unreliable and it is recommended that these results are not used for comparison with CFD.

Table F - 43. Number of Events of Pressure Transducer Channels (Optimized Grillage)

		Number of Events					
		Pressure Transducers					
Matrix ID	Test Time (MS s)	P11 (+)	P12 (+)	P13 (+)	P21 (+)	P22 (+)	P23 (+)
22 & 23	1,224	1648	1468	998	2134	1816	1645
24 & 25	498	593	538	374	786	646	601

Table F - 44. Number of Severe Events on Pressure Transducer Channels (Optimized Grillage)

		Number of Severe Events					
		Pressure Transducers					
Matrix ID	Test Time (MS s)	P11 (+)	P1 (+)	P13 (+)	P21 (+)	P22 (+)	P23 (+)
22 & 23	1,224	129	119	69	165	160	122
24 & 25	498	50	44	31	63	57	41

Table F - 45. Rate of Severe Events on Pressure Transducer Channels (Optimized Grillage)

		Rate of Severe Events (Number of Severe Events / Model Scale S.)					
		Pressure Transducers					
Matrix ID	Test Time (MS s)	P11 (+)	P12 (+)	P13 (+)	P21 (+)	P22 (+)	P23 (+)
22 & 23	1,224	0.11	0.10	0.06	0.13	0.13	0.10
24 & 25	498	0.10	0.09	0.06	0.13	0.11	0.08

REFERENCES

[F-1]. Experiments and CFD of high-speed deep-V planing hull - part II: Slamming in waves. Judge, Carolyn, et al. Applied Ocean Research 97 (2020) 102059, s.l. : Applied Ocean Research, 2019.

APPENDIX G: MAXIMUM STRAINS ON SINGLE STRAIN CHANNELS

This appendix presents the maximum observed strains per individual spot (or "run") in tabulated form and arranged by Matrix ID number.

Table G - 1 to Table G - 8 list the maximum strain on the center stiffener gages as well as the strains on the other four stiffener gages at the time the center gage reached its maximum for each run of the traditional grillage. Note that the stiffener containing channels 11 - 15 is not displayed due to bad data in channel 13.

Matrix ID: 14

Table G - 1. Maximum Strain on Channel 18 and Corresponding Stiffener Gage Strains on the Traditional Grillage, Condition ID: 14, All Runs

	Condition ID 14, Stiffener Channels G16-G20					
Run #	Time of Max Strain of Center Stiffener (sec)	Magnitude of Strain on G16 (microstrain)	Magnitude of Strain on G17 (microstrain)	Magnitude of Strain on G18 (microstrain)	Magnitude of Strain on G19 (microstrain)	Magnitude of Strain on G20 (microstrain)
184	21.3085	-557	730	**753**	636	-237
187	10.8916	-485	734	**786**	699	-300
190	7.4955	-630	894	**937**	809	-313
193	10.5991	-686	1001	**1049**	917	-338
196	19.9918	-627	867	**901**	776	-295
199	10.8084	-469	661	**697**	599	-221
202	13.3206	-582	927	**1008**	909	-383
205	6.6828	-626	817	**827**	690	-234
208	12.5628	-570	813	**843**	723	-263
237	25.3816	-620	964	**1019**	901	-357
240	19.8182	-538	742	**765**	650	-240
243	18.3222	-610	827	**856**	725	-243
246	15.3762	-627	932	**973**	849	-323

Table G - 2. Maximum Strain on Channel 23 and Corresponding Stiffener Gage Strains on the Traditional Grillage, Condition ID: 14, All Runs

	Condition ID 14, Stiffener Channels G21-G25					
Run #	Time of Max Strain of Center Stiffener (sec)	Magnitude of Strain on G21 (microstrain)	Magnitude of Strain on G22 (microstrain)	Magnitude of Strain on G23 (microstrain)	Magnitude of Strain on G24 (microstrain)	Magnitude of Strain on G25 (microstrain)
184	9.8778	-40	689	**746**	714	-173
187	10.8783	-140	786	**843**	783	-173
190	13.6903	-58	770	**846**	804	-187
193	10.5896	-92	901	**973**	917	-181
196	20.5757	-57	814	**873**	822	-163
199	17.3947	-99	718	**761**	712	-142
202	13.3104	-122	929	**1011**	958	-207
205	2.2650	-119	799	**852**	805	-171
208	13.8236	-25	762	**848**	819	-194
237	25.3711	-126	982	**1060**	991	-186
240	25.9941	-103	682	**740**	693	-154
243	18.8330	-108	856	**915**	849	-170
246	4.8336	-127	836	**897**	845	-179

Matrix ID: 15

Table G - 3. Maximum Strain on Channel 18 and Corresponding Stiffener Gage Strains on the Traditional Grillage, Condition ID: 15, All Runs

	Condition ID 15, Stiffener Channels G16-G20					
Run #	Time of Max Strain of Center Stiffener (sec)	Magnitude of Strain on G16 (microstrain)	Magnitude of Strain on G17 (microstrain)	Magnitude of Strain on G18 (microstrain)	Magnitude of Strain on G19 (microstrain)	Magnitude of Strain on G20 (microstrain)
249	5.7998	-661	1056	**1153**	1030	-459
257	9.0376	-523	736	**761**	641	-229
260	5.2449	-564	793	**820**	705	-264
263	25.8950	-703	993	**1036**	896	-352
266	6.3285	-597	885	**941**	819	-345
269	8.9494	-599	934	**999**	885	-339
273	25.7585	-421	765	**858**	789	-384
276	17.6848	-815	1253	**1324**	1142	-467

Table G - 4. Maximum Strain on Channel 23 and Corresponding Stiffener Gage Strains on the Traditional Grillage, Condition ID: 15, All Runs

	Condition ID 15, Stiffener Channels G21-G25					
Run #	Time of Max Strain of Center Stiffener (sec)	Magnitude of Strain on G21 (microstrain)	Magnitude of Strain on G22 (microstrain)	Magnitude of Strain on G23 (microstrain)	Magnitude of Strain on G24 (microstrain)	Magnitude of Strain on G25 (microstrain)
249	5.7888	-150	1145	**1239**	1170	-220
257	19.7743	-17	745	**864**	803	-215
260	5.2314	-142	691	**718**	661	-122
263	25.8832	-133	834	**883**	835	-167
266	14.8630	-142	921	**985**	922	-200
269	8.9389	-96	859	**931**	884	-188
273	25.7464	-167	980	**1054**	1006	-255
276	17.6736	-153	1058	**1138**	1086	-260

Matrix ID: 16

Table G - 5. Maximum Train on Channel 18 and Corresponding Stiffener Gage Strains on the Traditional Grillage, Condition ID: 16, All Runs

	Condition ID 16, Stiffener Channels G16-G20					
Run #	Time of Max Strain of Center Stiffener (sec)	Magnitude of Strain on G16 (microstrain)	Magnitude of Strain on G17 (microstrain)	Magnitude of Strain on G18 (microstrain)	Magnitude of Strain on G19 (microstrain)	Magnitude of Strain on G20 (microstrain)
174	15.1708	-489	771	**822**	745	-300
181	21.7739	-390	599	**636**	564	-236
279	23.4688	-506	698	**722**	617	-250
282	19.0163	-437	704	**765**	684	-296
285	24.4958	-507	928	**1016**	913	-388
290	34.0867	-360	582	**626**	559	-232
293	33.1726	-569	862	**924**	814	-339
296	30.7043	-604	1012	**1087**	979	-406
299	10.7476	-537	829	**883**	792	-327

Table G - 6. Maximum Strain on Channel 23 and Corresponding Stiffener Gage Strains on the Traditional Grillage, Condition ID: 16, All Runs

	Condition ID 16, Stiffener Channels G21-G25					
Run #	Time of Max Strain of Center Stiffener (sec)	Magnitude of Strain on G21 (microstrain)	Magnitude of Strain on G22 (microstrain)	Magnitude of Strain on G23 (microstrain)	Magnitude of Strain on G24 (microstrain)	Magnitude of Strain on G25 (microstrain)
174	25.2586	-72	771	**841**	793	-166
181	31.8414	-75	637	**695**	647	-138
279	28.0728	4	706	**806**	772	-185
282	19.0062	-195	999	**1052**	984	-198
285	29.5475	-170	905	**962**	896	-189
290	30.2321	-5	728	**823**	801	-194
293	33.1608	-107	957	**1041**	991	-221
296	30.6947	-117	965	**1040**	987	-219
299	26.8373	-115	879	**940**	895	-215

Matrix ID: 17

Table G - 7. Maximum Strain on Channel 18 and Corresponding Stiffener Gage Strains on the Traditional Grillage, Condition ID: 17, All Runs

	Condition ID 17, Stiffener Channels G16-G20					
Run #	Time of Max Strain of Center Stiffener (sec)	Magnitude of Strain on G16 (microstrain)	Magnitude of Strain on G17 (microstrain)	Magnitude of Strain on G18 (microstrain)	Magnitude of Strain on G19 (microstrain)	Magnitude of Strain on G20 (microstrain)
302	23.8572	-578	908	**968**	858	-339
305	22.7464	-282	528	**589**	536	-265
308	3.2756	-539	813	**865**	767	-318
310	9.5343	-411	599	**638**	568	-250
313	11.5357	-407	603	**636**	552	-236
317	21.3976	-421	768	**853**	783	-357

Table G - 8. Maximum Strain on Channel 23 and Corresponding Stiffener Gage Strains on the Traditional Grillage, Condition ID: 17, All Runs

	Condition ID 17, Stiffener Channels G21-G25					
Run #	Time of Max Strain of Center Stiffener (sec)	Magnitude of Strain on G21 (microstrain)	Magnitude of Strain on G22 (microstrain)	Magnitude of Strain on G23 (microstrain)	Magnitude of Strain on G24 (microstrain)	Magnitude of Strain on G25 (microstrain)
302	23.8468	-105	814	880	833	-170
305	22.7342	-72	987	1079	1029	-254
308	3.2643	-115	869	941	882	-192
310	9.5171	-43	673	745	707	-171
313	20.2359	-77	611	659	615	-127
317	21.3878	-130	920	1003	960	-210

Table G - 9 - Table G - 20 list the maximum strain on the center stiffener gages as well as the strains on the other four stiffener gages at the time the center gage reached its maximum for each run of the optimized grillage.

Matrix ID: 22

Table G - 9. Maximum Strain on Channel 13 and Corresponding Stiffener Gage Strains on the Optimized Grillage, Condition ID: 22, All Runs

	Condition ID 22, Stiffener Channels G11-G15					
Run #	Time of Max Strain on Center Stiffener (sec)	Magnitude of Strain on G11 (microstrain)	Magnitude of Strain on G12 (microstrain)	Magnitude of Strain on G13 (microstrain)	Magnitude of Strain on G14 (microstrain)	Magnitude of Strain on G15 (microstrain)
386	11.6294	-1910	1561	**2033**	1655	-797
389	12.4973	-1707	1153	**1708**	1469	-605
392	19.2402	-2412	2062	**2613**	2102	-962
395	9.6279	-2458	1956	**2556**	2084	-1010
398	22.4666	-2021	1685	**2159**	1761	-775
404	23.7653	-1965	1278	**1969**	1694	-683
407	17.7545	-1845	1087	**1808**	1655	-557
410	25.6178	-2510	2049	**2657**	2186	-785
413	11.3887	-1906	1621	**2066**	1651	-671
416	20.1233	-2879	2464	**3086**	2495	-938
419	2.3042	-1709	1387	**1832**	1500	-670
422	12.6251	-2351	1961	**2512**	2052	-776
425	9.6218	-1592	1043	**1584**	1388	-436

Table G - 10. Maximum Strain on Channel 18 and Corresponding Stiffener Gage Strains on the Optimized Grillage, Condition ID: 22, All Runs

	Condition ID 22, Stiffener Channels G16-G20					
Run #	Time of Max Strain on Center Stiffener (sec)	Magnitude of Strain on G16 (microstrain)	Magnitude of Strain on G17 (microstrain)	Magnitude of Strain on G18 (microstrain)	Magnitude of Strain on G19 (microstrain)	Magnitude of Strain on G20 (microstrain)
386	16.9512	180	815	**829**	562	-648
389	12.4999	202	798	**758**	453	-779
392	19.2437	375	1271	**1123**	582	-1351
395	9.6309	323	1312	**1243**	750	-1226
398	22.4703	361	1075	**985**	578	-986
404	23.7688	267	993	**931**	559	-925
407	17.7564	295	1009	**976**	658	-777
410	25.6198	379	1341	**1251**	754	-1296
413	11.3894	249	882	**842**	507	-820
416	20.5576	373	1723	**1633**	1002	-1527
419	21.8320	236	796	**767**	489	-645
422	12.6270	333	1360	**1289**	792	-1237
425	9.6228	236	805	**776**	500	-661

Table G - 11. Maximum Strain on Channel 23 and Corresponding Stiffener Gage Strains on the Optimized Grillage, Condition ID: 22, All Runs

	Condition ID 22, Stiffener Channels G21-G25					
Run #	Time of Max Strain on Center Stiffener (sec)	Magnitude of Strain on G21 (microstrain)	Magnitude of Strain on G22 (microstrain)	Magnitude of Strain on G23 (microstrain)	Magnitude of Strain on G24 (microstrain)	Magnitude of Strain on G25 (microstrain)
386	11.6224	-622	1832	**2017**	1450	-1301
389	12.4872	-548	1650	**1826**	1312	-1138
392	21.4623	-557	1551	**1704**	1205	-1169
395	9.6203	-558	1708	**1886**	1356	-1126
398	22.4573	-628	1711	**1898**	1339	-1206
404	23.7564	-438	1547	**1674**	1178	-1046
407	17.7441	-756	1889	**2171**	1605	-1330
410	25.6109	-626	2172	**2336**	1631	-1526
413	19.6228	-539	1612	**1792**	1303	-1119
416	20.1168	-986	3373	**3706**	2677	-2204
419	6.2864	-579	1359	**1558**	1133	-914
422	12.6183	-907	2582	**2831**	2019	-1888
425	9.6107	-626	2046	**2276**	1659	-1339

Matrix ID: 23

Table G - 12. Maximum Strain on Channel 13 and Corresponding Stiffener Gage Strains on the Optimized Grillage, Condition ID: 23, All Runs

	Condition ID 23, Stiffener Channels G11-G15					
Run #	Time of Max Strain on Center Stiffener (sec)	Magnitude of Strain on G11 (microstrain)	Magnitude of Strain on G12 (microstrain)	Magnitude of Strain on G13 (microstrain)	Magnitude of Strain on G14 (microstrain)	Magnitude of Strain on G15 (microstrain)
428	25.7976	-2217	1814	**2368**	1920	-887
431	14.9402	-1832	1322	**1854**	1560	-540
434	23.8093	-2244	2087	**2604**	2018	-1242
437	20.2392	-1682	1431	**1833**	1479	-642
440	13.1340	-1666	1370	**1789**	1449	-592
443	5.0346	-1972	1705	**2164**	1717	-789
446	27.4249	-3577	2637	**3868**	3348	-1458
449	11.2531	-1754	1507	**1901**	1501	-617
452	13.4185	-1710	1534	**1928**	1531	-706
504	20.4186	-2405	2109	**2629**	2064	-890
507	8.6232	-1474	1191	**1580**	1280	-432
511	1.8718	-2025	1582	**2129**	1718	-712
518	25.4792	-1410	1246	**1585**	1268	-363
521	14.3526	-2001	1572	**2092**	1664	-727
524	25.2772	-2613	1933	**2637**	2049	-1080
527	23.3573	-2063	1658	**2169**	1765	-550
530	26.4874	-2231	1726	**2338**	1864	-791
533	15.1874	-2181	1745	**2312**	1855	-706
536	26.2557	-2156	1893	**2398**	1884	-762
539	21.6984	-2213	1842	**2387**	1877	-765
542	4.0217	-1767	1522	**1941**	1532	-623
545	8.6264	-1869	1614	**2050**	1594	-670
548	2.4248	-1620	1213	**1706**	1383	-442
551	25.1062	-1622	1403	**1825**	1474	-464
555	14.5890	-2235	1203	**2220**	2021	-641
558	18.8426	-1882	1462	**1971**	1577	-675
561	19.5746	-1959	1235	**1980**	1689	-670
564	9.0661	-1719	1382	**1822**	1433	-614
567	14.3349	-2194	1778	**2269**	1788	-707
570	21.0832	-2128	1693	**2339**	1886	-1072

Table G - 13. Maximum Strain on Channel 18 and Corresponding Stiffener Gage Strains on the Optimized Grillage, Condition ID: 23, All Runs

	Condition ID 23, Stiffener Channels G16-G20					
Run #	Time of Max Strain on Center Stiffener (sec)	Magnitude of Strain on G16 (microstrain)	Magnitude of Strain on G17 (microstrain)	Magnitude of Strain on G18 (microstrain)	Magnitude of Strain on G19 (microstrain)	Magnitude of Strain on G20 (microstrain)
428	25.8017	388	1173	**1056**	591	-1107
431	14.9425	318	1065	**987**	591	-892
434	23.8148	254	1223	**1131**	640	-1360
437	20.2436	300	876	**794**	456	-835
440	22.5636	206	840	**828**	545	-581
443	5.0388	308	985	**911**	534	-955
446	27.4300	198	1791	**1786**	1162	-1753
449	11.2566	300	866	**784**	444	-842
452	13.4225	309	854	**781**	453	-824
504	20.4212	415	1218	**1106**	632	-1201
507	18.5861	310	826	**794**	530	-588
511	1.8750	334	1084	**1024**	643	-993
518	15.3265	241	783	**766**	523	-513
521	17.8046	312	976	**916**	574	-791
524	25.2812	390	1273	**1128**	615	-1330
527	23.3567	352	1097	**1056**	674	-946
530	26.4900	339	1173	**1106**	676	-1130
533	15.1901	329	1287	**1231**	788	-1109
536	26.2586	363	1217	**1149**	709	-1117
539	21.7014	373	1187	**1087**	639	-1120
542	4.0254	299	865	**799**	486	-838
545	8.6300	287	985	**901**	526	-945
548	14.9298	280	847	**807**	508	-714
551	25.1066	279	804	**781**	523	-649
555	14.5914	390	1301	**1216**	739	-1137
558	17.5566	292	1239	**1229**	819	-965
561	12.3996	291	991	**927**	570	-785
564	9.0704	307	863	**789**	466	-851
567	14.3353	259	1109	**1113**	751	-980
570	21.0893	330	1098	**1008**	602	-1098

Table G - 14. Maximum Strain on Channel 23 and Corresponding Stiffener Gage Strains on the Optimized Grillage, Condition ID: 23, All Runs

	Condition ID 23, Stiffener Channels G21-G25					
Run #	Time of Max Strain on Center Stiffener (sec)	Magnitude of Strain on G21 (microstrain)	Magnitude of Strain on G22 (microstrain)	Magnitude of Strain on G23 (microstrain)	Magnitude of Strain on G24 (microstrain)	Magnitude of Strain on G25 (microstrain)
428	25.7881	-632	1456	**1735**	1332	-941
431	14.9266	-418	1216	**1329**	942	-773
434	0.6475	-629	1525	**1773**	1319	-1044
437	16.0716	-553	1416	**1616**	1171	-925
440	7.3706	-493	1595	**1746**	1239	-1070
443	21.1766	-623	1794	**1990**	1418	-1258
446	27.4231	-1465	2404	**2761**	1988	-2036
449	6.3281	-612	1171	**1489**	1133	-744
452	17.3765	-677	2053	**2276**	1627	-1327
504	20.4111	-491	1971	**2107**	1457	-1296
507	18.5705	-542	1493	**1682**	1251	-947
511	1.8635	-481	1611	**1755**	1213	-1088
518	15.3064	-760	1476	**1765**	2033	-1112
521	0.9075	-555	1695	**1878**	1308	-1170
524	25.2711	-611	2045	**2224**	1586	-1417
527	23.3454	-774	2025	**2265**	1593	-1379
530	26.4794	-591	1959	**2128**	1482	-1351
533	15.1802	-526	1966	**2109**	1462	-1354
536	26.2482	-597	1965	**2114**	1441	-1410
539	21.6907	-532	1924	**2087**	1464	-1294
542	14.0204	-572	1197	**1445**	1081	-831
545	12.9012	-440	1219	**1375**	982	-848
548	14.9148	-639	1540	**1765**	1263	-1047
551	20.3367	-438	1485	**1609**	1121	-1104
555	14.5817	-779	2658	**2925**	2095	-1723
558	17.5473	-606	2541	**2765**	1954	-1631
561	19.5662	-615	2084	**2273**	1592	-1376
564	9.0575	-457	1429	**1590**	1144	-987
567	8.8920	1714	2717	**2697**	-3132	-568
570	21.0792	-595	1684	**1847**	1311	-1235

Matrix ID: 24

Table G - 15. Maximum Strain on Channel 13 and Corresponding Stiffener Gage Strains on the Optimized Grillage, Condition ID: 24, All Runs

	Condition ID 24, Stiffener Channels G11-G15					
Run #	Time of Max Strain on Center Stiffener (sec)	Magnitude of Strain on G11 (microstrain)	Magnitude of Strain on G12 (microstrain)	Magnitude of Strain on G13 (microstrain)	Magnitude of Strain on G14 (microstrain)	Magnitude of Strain on G15 (microstrain)
455	34.5568	-1274	1026	**1344**	1098	-333
458	22.5593	-1356	1139	**1474**	1166	-575
465	25.9784	-1620	1166	**1649**	1333	-709
468	19.8447	-2456	1797	**2522**	2054	-964
474	26.8005	-1344	1087	**1460**	1166	-484
477	13.3338	-1452	1122	**1516**	1222	-603
480	4.6798	-1249	836	**1244**	1056	-292
483	34.2547	-1715	1243	**1726**	1424	-579

Table G - 16. Maximum Strain on Channel 18 and Corresponding Stiffener Gage Strains on the Optimized Grillage, Condition ID: 24, All Runs

	Condition ID 24, Stiffener Channels G16-G20					
Run #	Time of Max Strain on Center Stiffener (sec)	Magnitude of Strain on G16 (microstrain)	Magnitude of Strain on G17 (microstrain)	Magnitude of Strain on G18 (microstrain)	Magnitude of Strain on G19 (microstrain)	Magnitude of Strain on G20 (microstrain)
455	30.2114	196	632	**603**	382	-542
458	21.8433	117	639	**681**	487	-444
465	25.9840	250	826	**761**	456	-782
468	19.8476	307	1091	**1021**	603	-1096
474	26.8046	195	556	**514**	301	-547
477	22.3900	128	688	**708**	493	-472
480	4.6788	188	673	**646**	409	-569
483	34.2574	252	937	**900**	581	-842

Table G - 17. Maximum Strain on Channel 23 and Corresponding Stiffener Gage Strains on the Optimized Grillage, Condition ID: 24, All Runs

	Condition ID 24, Stiffener Channels G21-G25					
Run #	Time of Max Strain on Center Stiffener (sec)	Magnitude of Strain on G21 (microstrain)	Magnitude of Strain on G22 (microstrain)	Magnitude of Strain on G23 (microstrain)	Magnitude of Strain on G24 (microstrain)	Magnitude of Strain on G25 (microstrain)
455	35.9550	-395	1190	**1322**	942	-739
458	16.9768	-507	1187	**1389**	1042	-796
465	0.7911	-502	1443	**1612**	1162	-973
468	19.8380	-621	2054	**2254**	1592	-1341
474	25.1848	-424	927	**1116**	847	-594
477	22.3730	-468	1194	**1365**	1000	-769
480	26.1864	-453	1268	**1426**	1069	-841
483	34.2466	-481	1613	**1781**	1289	-1075

Matrix ID: 25

Table G - 18. Maximum Strain on Channel 13 and Corresponding Stiffener Gage Strains on the Optimized Grillage, Condition ID: 25, All Runs

	Condition ID 25, Stiffener Channels G11-G15					
Run #	Time of Max Strain on Center Stiffener (sec)	Magnitude of Strain on G11 (microstrain)	Magnitude of Strain on G12 (microstrain)	Magnitude of Strain on G13 (microstrain)	Magnitude of Strain on G14 (microstrain)	Magnitude of Strain on G15 (microstrain)
486	28.8577	-1646	1086	**1615**	1366	-529
489	18.4566	-1834	1012	**1743**	1544	-452
492	24.9185	-1879	1371	**1926**	1555	-713
495	34.8900	-1219	1057	**1341**	1071	-402
498	31.6409	-1516	1061	**1534**	1272	-578
501	14.8301	-1476	1141	**1512**	1246	-362

Table G - 19. Maximum Strain on Channel 18 and Corresponding Stiffener Gage Strains on the Optimized Grillage, Condition ID: 25, All Runs

	Condition ID 25, Stiffener Channels G16-G20					
Run #	Time of Max Strain on Center Stiffener (sec)	Magnitude of Strain on G16 (microstrain)	Magnitude of Strain on G17 (microstrain)	Magnitude of Strain on G18 (microstrain)	Magnitude of Strain on G19 (microstrain)	Magnitude of Strain on G20 (microstrain)
486	28.8606	325	1211	**1119**	669	-986
489	18.4540	169	935	**1008**	729	-752
492	24.9228	314	1000	**904**	519	-953
495	9.9624	246	653	**597**	354	-597
498	17.5771	208	795	**751**	477	-650
501	14.8271	236	775	**741**	470	-643

Table G - 20. Maximum Strain on Channel 23 and Corresponding Stiffener Gage Strains on the Optimized Grillage, Condition ID: 25, All Runs

	Condition ID 25, Stiffener Channels G21-G25					
Run #	Time of Max Strain on Center Stiffener (sec)	Magnitude of Strain on G21 (microstrain)	Magnitude of Strain on G22 (microstrain)	Magnitude of Strain on G23 (microstrain)	Magnitude of Strain on G24 (microstrain)	Magnitude of Strain on G25 (microstrain)
486	28.8495	-484	1643	**1813**	1305	-1094
489	18.4445	-826	2172	**2470**	1822	-1264
492	24.9108	-487	1532	**1694**	1196	-1046
495	18.0778	-519	1177	**1379**	1031	-788
498	31.6322	-472	1435	**1594**	1180	-977
501	23.4854	-777	1676	**1979**	1446	-1103

THIS PAGE INTENTIONALLY LEFT BLANK

APPENDIX H: TABULATED RESULTS

A dataset of tabulated results has been compiled and has been included on compact disk (CD) to accompany the technical report. The purpose of this appendix is to document how the dataset is structured to support future use of the data.

OVERVIEW

The tabulated data is associated with the irregular wave condition which was the focus of the test effort. Most of the testing was conducted at this condition and at two speeds of interest: 14.8 and 17.5 knots. An advantage of this data set is that the precision uncertainty was minimized by obtaining a large number of wave encounters in the target wave condition.

The grillage data presented is for traditional and optimized grillages. The optimized grillage data should be used when exercising caution due to the distortions in shape observed during testing. Data from both the traditional and optimized grillages must be used carefully and with mindfulness given to the shortfalls and caveats presented in this technical report.

FILE STRUCTURE

The top level file structure shows two files. The first folder contains the pressure and grillage data, and the next contains the motion data. The preceding numbering indicates the date of creation. “20201130” represents 30 November 2020.

Pressure and Grillage Data

Within the upper level folder, there are three additional subfolders nested. One is for the pressure gages; the other two are for the traditional grillage. The later are separated by channel number: G1 through G10 are separated from G11 through G25.

Within each of these folders are additional subfolders showing statistics. Those statistics were calculated for each run, and for each configuration. The bootstrapping methodology further discussed in the Statistical Estimator and Confidence Intervals subsection of the technical report.

Motion Data

Within the upper level folder, there are seven additional subfolders nested. The first three relate to the identification of peaks within the data. Two different methodologies were used. The Standard G method was compared against the zero crossing method. There are folders for each as well as a folders comparing images (*.tif) comparing the two peak identification methods.

Next, two (of the seven) subfolders are for time series analysis. These folders use the autocovariance and non-overlapping bootstrap methods respectively. Additional detail can be found in the Statistical Estimator and Confidence Intervals subsection of the technical report.

The final two (of seven) subfolders are for the waves analysis. The first folder shows the comparisons between target values and measured values, broken out by condition of interest. And the second shows the wave statistics as measured.

APPENDIX I: WEIBULL ANALYSIS OF PRESSURES AND STRAINS

In this appendix, the Weibull results for each test condition are presented. A Weibull analysis was performed on measured events for both grillages as a metric for comparison with future Computational Fluid Dynamics (CFD) studies. The goal for the Weibull analysis is to estimate maximum pressures and strains that the local structure is expected to experience throughout the ship's operation. This is accomplished by creating a cumulative distribution of the measured peak events and fitting a straight line to the distribution in the Weibull space (modified-log-log space). The Weibull fit can then be used to estimate the extreme lifetime values given a particular probability of non-exceedance (PNE) and exposure time.

The Weibull cumulative density function (CDF) is the governing equation for the Weibull analysis and is as follows:

$$\boldsymbol{P(x) = \left[1 - e^{-\left(\frac{x-x_0}{\eta-x_0}\right)^{\beta}}\right]} \tag{I-1}$$

Rearranging **(I-1)** above to solve for x results in

$$\boldsymbol{x_n = (\eta - x_0)\left(ln\left(\frac{1}{1-P(x_n)}\right)^{\frac{1}{\beta}}\right) + x_0} \tag{I-2}$$

The Weibull fit parameters are as follows:

- Magnitude of the n^{th} event, x_n
- Shape parameter, β: Slope of the Weibull fit. The shape parameter identifies the distribution of the data sample.
- Threshold value, x_0: Analogous to the y-intercept of the fit, and is the value for which no event magnitudes fall below.
- Characteristic value, η: corresponds to a cumulative probability of 0.632. For multiple - point methods, the characteristic value is determined by computing a local fit between 0.5 and 0.764, to estimate the characteristic value corresponding to a 0.632 cumulative probability.
- Cumulative probability, P(x): When x is equal to the extreme value, the probability of non - exceedance (PNE) of the extreme value is *P(x)*. This is used to characterize the probability that an event of a certain magnitude is not exceeded.

Two methods were used to fit a linear trend to the distribution in Weibull space: three-parameter linear regression (LR3) and three-parameter moment method (MM3). The Weibull analysis was performed on events from Matrix IDs corresponding to the same conditions. These were matrix IDs 14 and 15 (17.5 knots, Hs = 7.4 in., Tp = 2.4 sec) and matrix IDs 16 and 17 (14.8 knots, Hs = 7.4 in., Tp = 2.4 sec) for the traditional grillage and matrix IDs 22 and 23 (17.5 knots, Hs = 7.4 in., Tp = 2.4 sec) and matrix IDs 24 and 25 (14.8 knots, Hs = 7.4 in., Tp = 2.4

sec) for the optimized grillage. The Weibull fit parameters and PNE calculations for the method which fit the data best (LR3 or MM3) are tabulated in Table 1 to Table I - 21 for the traditional grillage and in Table I - 22 to Table I - 41 for the optimized grillage. Representative Weibull plots for each type of channel are shown in Figure I - 1 to Figure I - 10 for the traditional grillage, and in Figure I - 11 to Figure I - 20 for the optimized grillage.

For cases where the Weibull distribution did not fit the data well, a multiplier was applied to the largest measured values to approximate the 36.8 % PNE. The multipliers are shown in Table 1, and were calculated as the averages of multipliers derived from 36.8 % PNE predictions for data that fit the distribution well.

Table 1. Multipliers to Estimate 36.8 % PNE Predictions

Multipliers for Traditional and Optimized Grillages to Estimate 36.8 % PNE Predictions	
100 hr	1.28
500 hr	1.36
1000 hr	1.40

Traditional Grillage: Matrix ID 14 and 15

Table I - 2. Weibull Shape Parameters for Differential Bending Channels in Matrix ID 14 and 15

Channel	Number of Events	Best Fit Method	σ (PSI)	Best Fit Parameters			
				β	η (PSI)	x_0 (PSI)	R^2
G1 (+)	535	MM3	0.8	2.3	2.1	0.0	--
G2 (+)	739	MM3	0.4	2.7	1.1	0.0	--
G3 (+)	485	MM3	1.5	2.4	5.0	1.2	--
G4 (+)	813	MM3	0.9	2.5	2.4	0.1	--
G5 (+)	958	MM3	0.6	2.5	1.8	0.2	--
G6 (+)	960	Multiplier	0.8	--	--	--	--
G7 (+)	970	Multiplier	2.2	--	--	--	--
G8 (+)	324	MM3	0.9	2.1	2.1	0.0	--
G10 (+)	846	LR3	0.9	2.6	2.4	0.0	0.9178

Table I - 3. Lifetime Extreme Estimates for Differential Bending Channels in Matrix ID 14 and 15

Channel	Number of Events	Best Fit Method	PNE @ 100 hr (PSI)			PNE @ 500 hr (PSI)			PNE @ 1000 hr (PSI)		
			36.8 %	90.0 %	99.0 %	36.8 %	90.0 %	99.0 %	36.8 %	90.0 %	99.0 %
G1 (+)	535	MM3	6	7	7	6	7	7	7	7	7
G2 (+)	739	MM3	3	3	3	3	3	3	3	3	3
G3 (+)	485	MM3	12	13	14	13	13	14	13	14	14
G4 (+)	813	MM3	6	7	7	7	7	7	7	7	8
G5 (+)	958	MM3	5	5	5	5	5	6	5	5	6
G6 (+)	960	Multiplier	9	--	--	10	--	--	10	--	--
G7 (+)	970	Multiplier	22	--	--	23	--	--	24	--	--
G8 (+)	324	MM3	7	7	8	7	8	8	7	8	8
G10 (+)	846	LR3	6	7	7	7	7	8	7	7	8

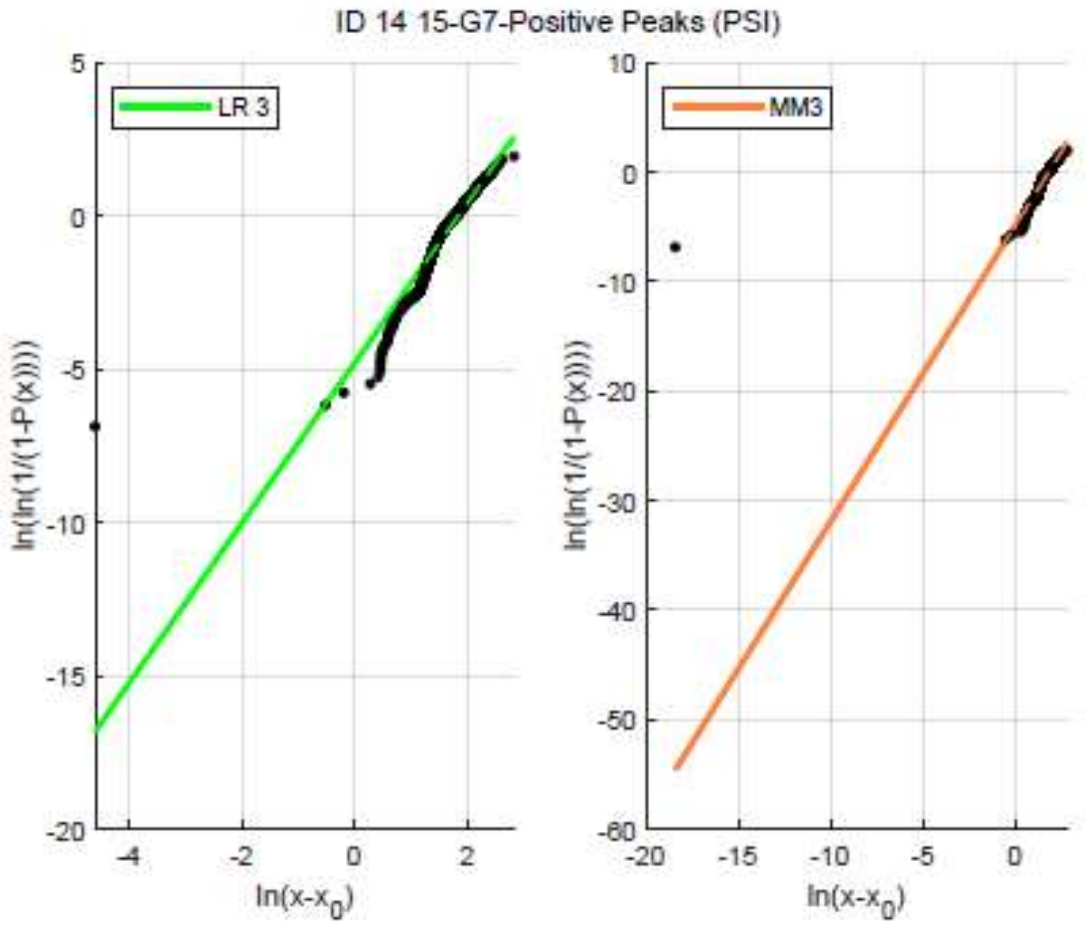

Figure I - 1. LR3 and MM3 Weibull Plots of Channel G7 for Matrix ID 14 and 15

Table I - 4. Weibull Shape Parameters for Single Strain Channels G11 - G15 in Matrix ID 14 and 15

Channel	Number of Events	Best Fit Method	σ (microstrain)	Best Fit Parameters			
				β	η (microstrain)	x_0 (microstrain)	R^2
G11 (+)	416	MM3	82	1.7	192	42	--
G11 (-)	187	MM3	36	2.9	107	0	--
G12 (+)	383	Multiplier	238	--	--	--	--
G12 (-)	508	MM3	58	2.0	144	17	--
G13 (+)	115	MM3	249	2.2	583	0	--
G13 (-)	136	MM3	57	2.2	164	31	--
G14 (+)	590	MM3	254	2.0	541	0	--
G14 (-)	895	Multiplier	52	--	--	--	--
G15 (+)	975	Multiplier	62	--	--	--	--
G15 (-)	669	MM3	75	2.5	201	5	--

Table I - 5. Lifetime Extreme Estimates for Single Strain Channels G11 - G15 in Matrix ID 14 and 15

Channel	Number of Events	Best Fit Method	PNE @ 100 hr (microstrain)			PNE @ 500 hr (microstrain)			PNE @ 1000 hr (microstrain)		
			36.8 %	90.0 %	99.0 %	36.8 %	90.0 %	99.0 %	36.8 %	90.0 %	99.0 %
G11 (+)	416	MM3	723	793	861	773	840	906	794	860	925
G11 (-)	187	MM3	-253	-268	-283	-264	-279	-292	-269	-283	-296
G12 (+)	383	Multiplier	1347	--	--	1431	--	--	1473	--	--
G12 (-)	508	MM3	-465	-502	-538	-492	-527	-561	-503	-537	-571
G13 (+)	115	MM3	1866	2010	2149	1970	2106	2238	2013	2146	2275
G13 (-)	136	MM3	-464	-498	-530	-488	-520	-551	-498	-529	-559
G14 (+)	590	MM3	1951	2121	2286	2074	2235	2392	2125	2283	2437
G14 (-)	895	Multiplier	-594	--	--	-631	--	--	-650	--	--
G15 (+)	975	Multiplier	648	--	--	689	--	--	709	--	--
G15 (-)	669	MM3	-549	-586	-621	-575	-610	-643	-586	-620	-652

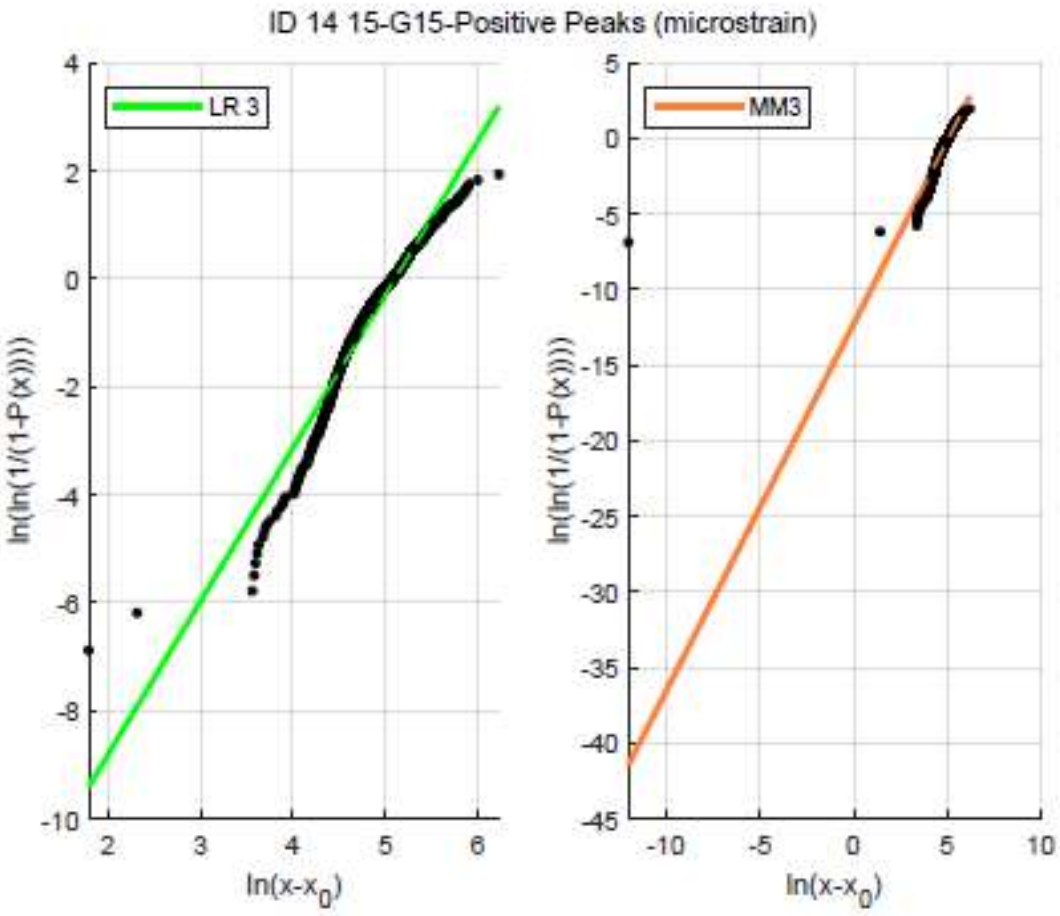

Figure I - 2. LR3 and MM3 Weibull Plots of Channel G15 for Matrix ID 14 and 15

Table I - 6. Weibull Shape Parameters for Single Strain Channels G16 - G20 in Matrix ID 14 and 15

Channel	Number of Events	Best Fit Method	σ (microstrain)	Best Fit Parameters			
				β	η (microstrain)	x_0 (microstrain)	R^2
G16 (+)	186	MM3	16	1.6	64	37	--
G16 (-)	720	MM3	163	1.7	305	0	--
G17 (+)	766	MM3	210	1.8	404	0	--
G17 (-)	300	MM3	20	1.3	71	44	--
G18 (+)	793	MM3	217	1.8	429	0	--
G18 (-)	326	MM3	21	1.6	75	40	--
G19 (+)	812	MM3	185	1.9	386	0	--
G19 (-)	250	MM3	20	1.5	73	42	--
G20 (+)*	66	MM3	15	1.3	66	45	--
G20 (-)*	876	Multiplier	80	--	--	--	--

*Results are presented for full disclosure, but the response of this channel was unreliable and it is recommended that these results are not used for comparison with CFD.

Table I - 7. Lifetime Extreme Estimates for Single Strain Channels G16 - G20 in Matrix ID 14 and 15

Channel	Number of Events	Best Fit Method	PNE @ 100 hr (microstrain)			PNE @ 500 hr (microstrain)			PNE @ 1000 hr (microstrain)		
			36.8 %	90.0 %	99.0 %	36.8 %	90.0 %	99.0 %	36.8 %	90.0 %	99.0 %
G16 (+)	186	MM3	161	176	191	172	186	200	177	190	204
G16 (-)	720	MM3	-1342	-1476	-1606	-1439	-1566	-1692	-1479	-1604	-1727
G17 (+)	766	MM3	1710	1874	2034	1828	1985	2139	1877	2031	2182
G17 (-)	300	MM3	-218	-243	-267	-236	-260	-284	-243	-267	-290
G18 (+)	793	MM3	1749	1912	2070	1866	2021	2173	1915	2067	2217
G18 (-)	326	MM3	-207	-226	-245	-221	-239	-257	-227	-245	-262
G19 (+)	812	MM3	1449	1575	1697	1540	1660	1777	1578	1695	1810
G19 (-)	250	MM3	-197	-216	-234	-210	-228	-246	-216	-234	-251
G20 (+)*	66	MM3	170	191	211	185	205	224	191	210	230
G20 (-)*	876	Multiplier	-771	--	--	-820	--	--	-844	--	--

*Results are presented for full disclosure, but the response of this channel was unreliable and it is recommended that these results are not used for comparison with CFD.

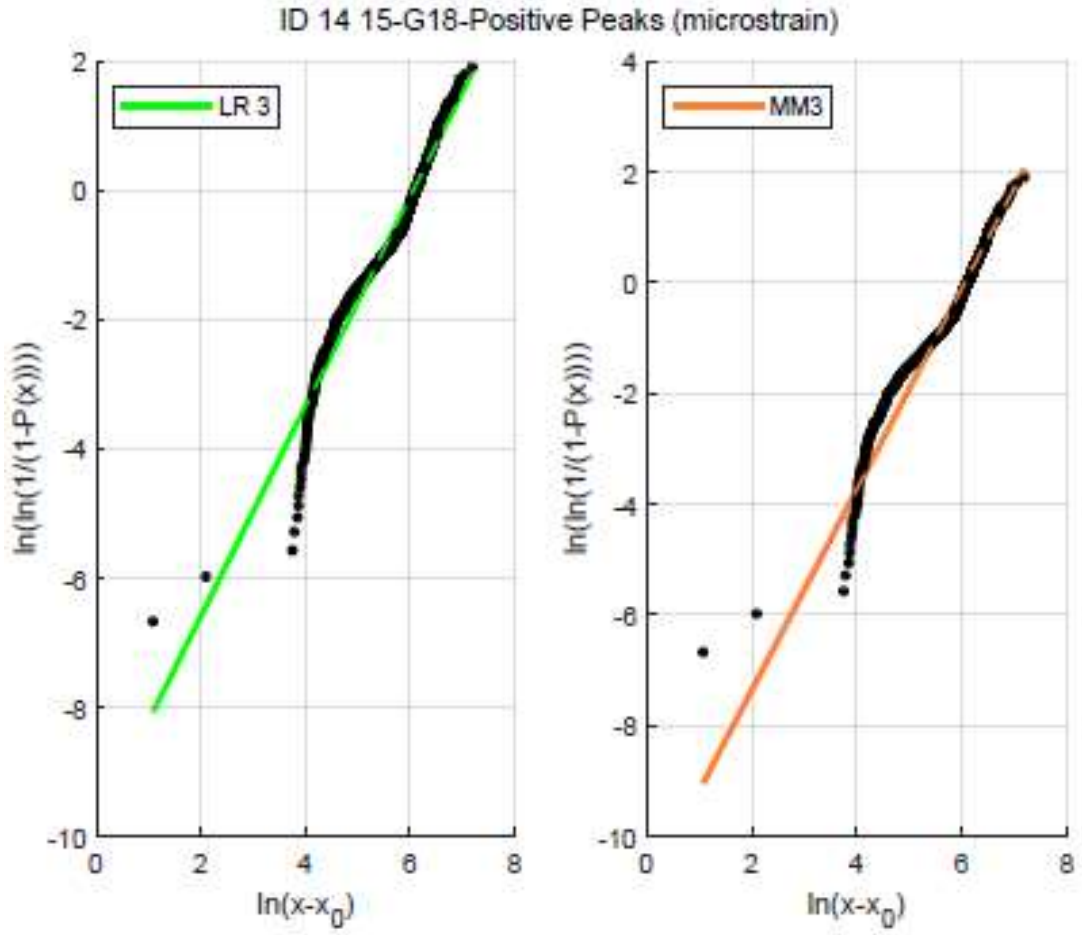

Figure I - 3. LR3 and MM3 Weibull Plots of Channel G18 for Matrix ID 14 and 15

Table I - 8. Weibull Shape Parameters for Single Strain Channels G21 - G25 in Matrix ID 14 and 15

Channel	Number of Events	Best Fit Method	σ (microstrain)	Best Fit Parameters			
				β	η (microstrain)	x_0 (microstrain)	R^2
G21 (+)	579	MM3	22	1.8	80	37	--
G21 (-)	878	LR3	33	3.8	138	0	0.8936
G22 (+)	1033	MM3	177	2.3	432	7	--
G22 (-)	112	MM3	19	1.4	72	42	--
G23 (+)	1037	MM3	190	2.2	448	8	--
G23 (-)	181	MM3	23	2.6	70	7	--
G24 (+)	1081	MM3	181	2.1	421	7	--
G24 (-)	182	MM3	23	1.7	76	34	--
G25 (+)*	82	MM3	11	1.6	65	45	--
G25 (-)*	998	Multiplier	44	--	--	--	--

*Results are presented for full disclosure, but the response of this channel was unreliable and it is recommended that these results are not used for comparison with CFD.

Table I - 9. Lifetime Extreme Estimates for Single Strain Channels G21 - G25 in Matrix ID 14 and 15

Channel	Number of Events	Best Fit Method	PNE @ 100 hr (microstrain)			PNE @ 500 hr (microstrain)			PNE @ 1000 hr (microstrain)		
			36.8 %	90.0 %	99.0 %	36.8 %	90.0 %	99.0 %	36.8 %	90.0 %	99.0 %
G21 (+)	579	MM3	215	233	250	228	244	261	233	249	265
G21 (-)	878	LR3	-269	-280	-291	-277	-288	-298	-280	-291	-300
G22 (+)	1033	MM3	1333	1430	1522	1403	1494	1582	1432	1520	1607
G22 (-)	112	MM3	-195	-216	-237	-210	-231	-251	-217	-237	-257
G23 (+)	1037	MM3	1459	1570	1677	1539	1644	1745	1573	1675	1774
G23 (-)	181	MM3	-166	-177	-188	-174	-185	-195	-177	-188	-197
G24 (+)	1081	MM3	1386	1492	1594	1463	1563	1660	1494	1592	1687
G24 (-)	182	MM3	-211	-231	-251	-226	-245	-263	-232	-250	-269
G25 (+)*	82	MM3	134	145	157	142	153	164	146	157	167
G25 (-)*	998	Multiplier	-451	--	--	-479	--	--	-493	--	--

*Results are presented for full disclosure, but the response of this channel was unreliable and it is recommended that these results are not used for comparison with CFD.

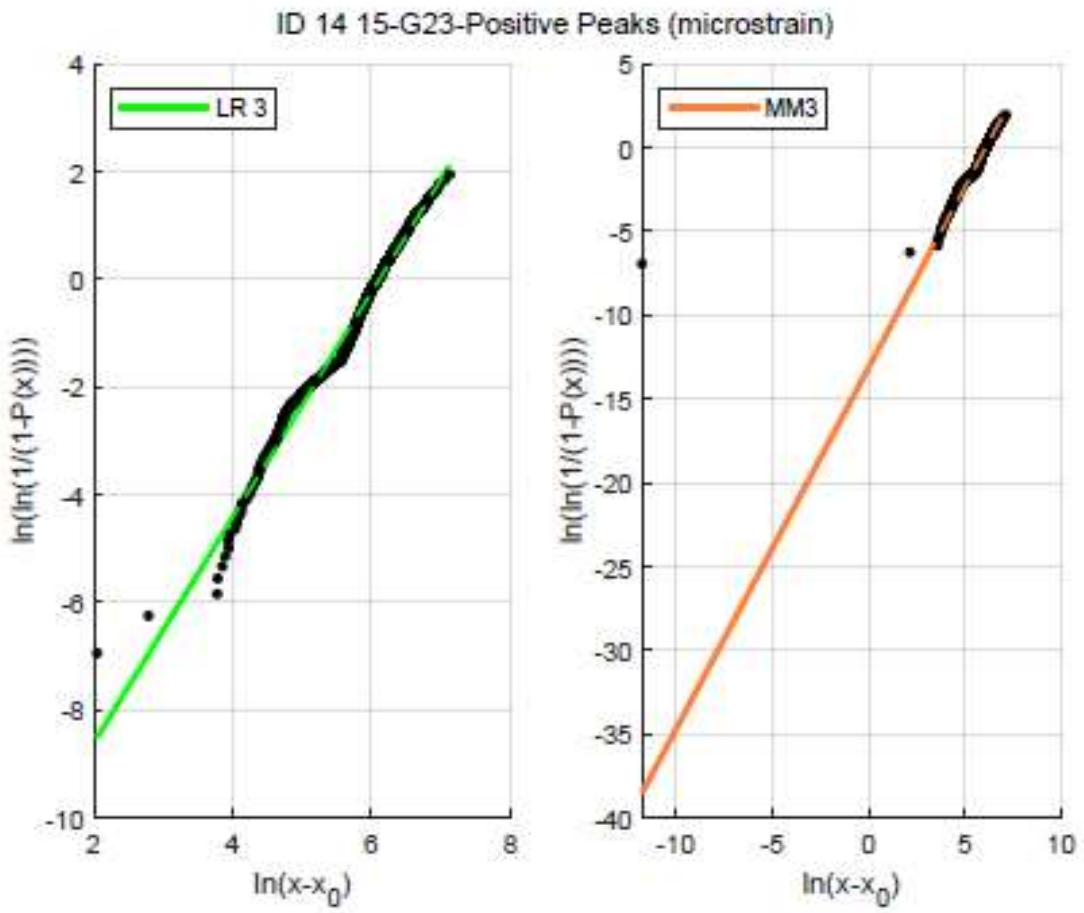

Figure I - 4. LR3 and MM3 Weibull Plots of Channel G23 for Matrix ID 14 and 15

Table I - 10. Weibull Shape Parameters for Pressure Transducer Channels in Matrix ID 14 and 15

Channel	Number of Events	Best Fit Method	σ (PSI)	Best Fit Parameters			
				β	η (PSI)	x_0 (PSI)	R^2
P11 (+)	722	Multiplier	1.0	--	--	--	--
P12 (+)	636	Multiplier	1.0	--	--	--	--
P13 (+)	414	Multiplier	0.8	--	--	--	--
P21 (+)	942	Multiplier	1.3	--	--	--	--
P22 (+)	787	MM3	0.9	1.7	2.1	0.4	--
P23 (+)	706	Multiplier	0.8	--	--	--	--

Table I - 11. Lifetime Extreme Estimates for Pressure Transducer Channels in Matrix ID 14 and 15

Channel	Number of Events	Best Fit Method	PNE @ 100 hr (PSI)			PNE @ 500 hr (PSI)			PNE @ 1000 hr (PSI)		
			36.8 %	90.0 %	99.0 %	36.8 %	90.0 %	99.0 %	36.8 %	90.0 %	99.0 %
P11 (+)	722	Multiplier	15	--	--	16	--	--	16	--	--
P12 (+)	636	Multiplier	14	--	--	15	--	--	15	--	--
P13 (+)	414	Multiplier	9	--	--	9	--	--	10	--	--
P21 (+)	942	Multiplier	13	--	--	13	--	--	14	--	--
P22 (+)	787	MM3	8	9	9	9	9	10	9	9	10
P23 (+)	706	Multiplier	14	--	--	14	--	--	15	--	--

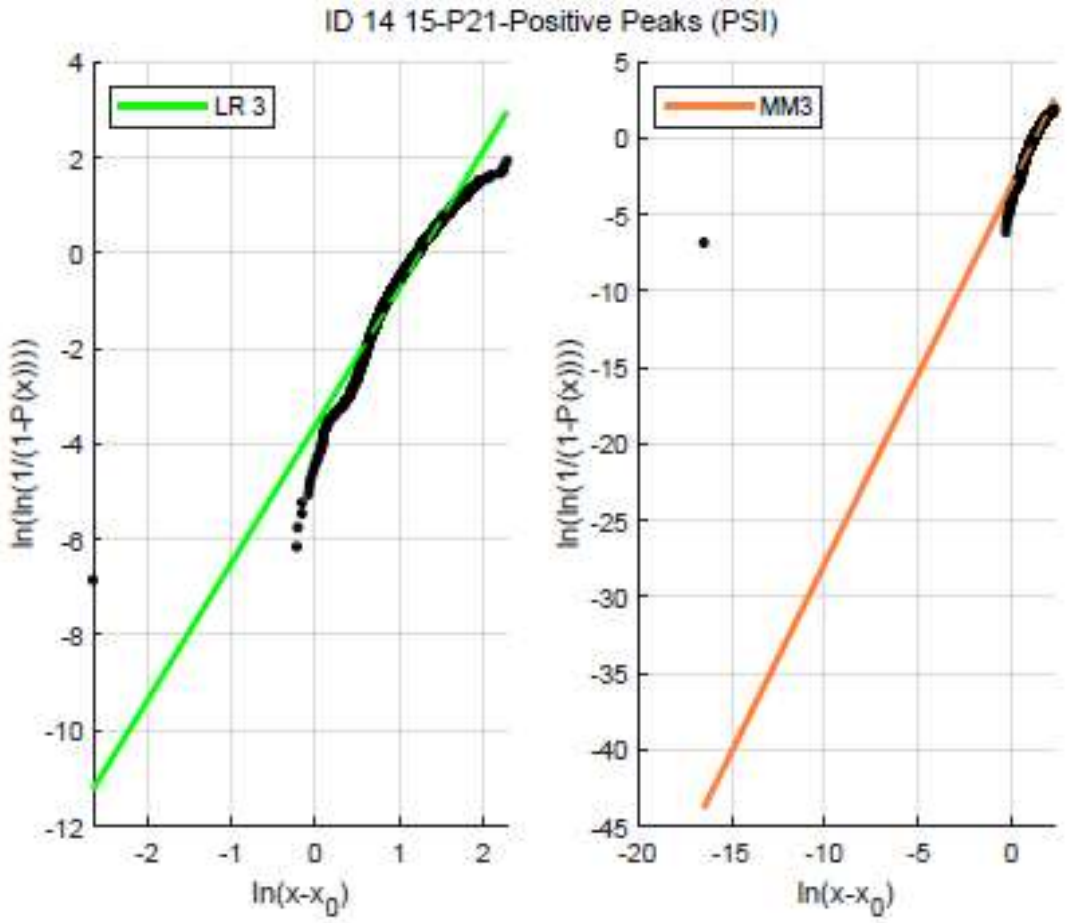

Figure I - 5. LR3 and MM3 Weibull Plots of Channel P21 for Matrix ID 14 and 15

Traditional Grillage: Matrix ID 16 and17

Table I - 12. Weibull Shape Parameters for Differential Bending Channels in Matrix ID 16 and 17

Channel	Number of Events	Best Fit Method	σ (PSI)	Best Fit Parameters			
				β	η (PSI)	x_0 (PSI)	R^2
G1 (+)	497	MM3	0.7	2.2	1.6	0.0	--
G2 (+)	659	Multiplier	0.3	--	--	--	--
G3 (+)	467	MM3	1.3	2.5	3.8	0.4	--
G4 (+)	726	MM3	0.7	2.6	1.9	0.0	--
G5 (+)	840	Multiplier	0.5	--	--	--	--
G6 (+)	823	Multiplier	0.7	--	--	--	--
G7 (+)	880	MM3	1.9	2.2	4.9	0.3	--
G8 (+)	285	MM3	0.7	2.2	1.7	0.0	--
G10 (+)	739	Multiplier	0.8	--	--	--	--

Table I - 13. Lifetime Extreme Estimates for Differential Bending Channels in Matrix ID 16 and 17

Channel	Number of Events	Best Fit Method	PNE @ 100 hr (PSI)			PNE @ 500 hr (PSI)			PNE @ 1000 hr (PSI)		
			36.8 %	90.0 %	99.0 %	36.8 %	90.0 %	99.0 %	36.8 %	90.0 %	99.0 %
G1 (+)	497	MM3	5	5	6	5	6	6	5	6	6
G2 (+)	659	Multiplier	3	--	--	3	--	--	3	--	--
G3 (+)	467	MM3	10	10	11	10	11	11	10	11	12
G4 (+)	726	MM3	5	5	6	5	6	6	5	6	6
G5 (+)	840	Multiplier	5	--	--	5	--	--	5	--	--
G6 (+)	823	Multiplier	7	--	--	7	--	--	8	--	--
G7 (+)	880	MM3	15	16	17	16	17	18	16	17	18
G8 (+)	285	MM3	5	5	6	5	6	6	5	6	6
G10 (+)	739	Multiplier	7	--	--	8	--	--	8	--	--

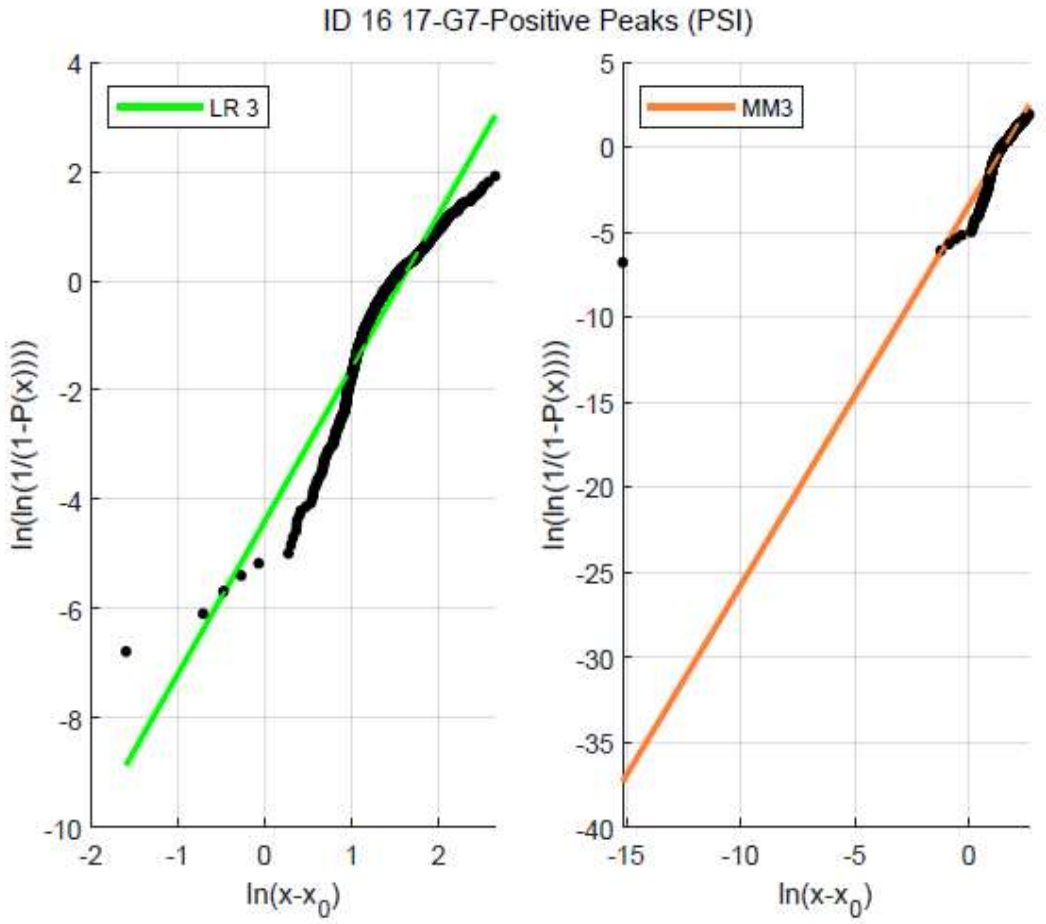

Figure I - 6. LR3 and MM3 Weibull Plots of Channel G17 for Matrix ID 16 and 17

Table I - 14. Weibull Shape Parameters for Single Strain Channels G11 - G15 in Matrix ID 16 and 17

Channel	Number of Events	Best Fit Method	σ (microstrain)	Best Fit Parameters			
				β	η (microstrain)	x_0 (microstrain)	R^2
G11 (+)	534	MM3	63	2.0	154	16	--
G11 (-)	129	LR3	14	2.6	81	42	0.9949
G12 (+)	423	MM3	173	1.9	364	0	--
G12 (-)	611	Multiplier	45	--	--	--	--
G13 (+)	56	MM3	237	1.7	450	3	--
G13 (-)	70	MM3	53	1.8	134	30	--
G14 (+)	529	MM3	192	2.0	423	0	--
G14 (-)	706	Multiplier	50	--	--	--	--
G15 (+)	830	Multiplier	57	--	--	--	--
G15 (-)	592	MM3	58	2.4	157	9	--

Table I - 15. Lifetime Extreme Estimates for Single Strain Channels G11 - G15 in Matrix ID 16 and 17

Channel	Number of Events	Best Fit Method	PNE @ 100 hr (microstrain)			PNE @ 500 hr (microstrain)			PNE @ 1000 hr (microstrain)		
			36.8 %	90.0 %	99.0 %	36.8 %	90.0 %	99.0 %	36.8 %	90.0 %	99.0 %
G11 (+)	534	MM3	505	546	585	534	573	610	547	584	621
G11 (-)	129	LR3	-142	-149	-155	-147	-153	-160	-149	-155	-161
G12 (+)	423	MM3	1343	1460	1574	1428	1539	1648	1463	1572	1679
G12 (-)	611	Multiplier	-444	--	--	-471	--	--	-485	--	--
G13 (+)	56	MM3	1940	2133	2321	2079	2263	2443	2137	2317	2495
G13 (-)	70	MM3	-453	-492	-531	-482	-519	-555	-493	-530	-566
G14 (+)	529	MM3	1474	1596	1714	1562	1677	1790	1599	1711	1821
G14 (-)	706	Multiplier	-496	--	--	-528	--	--	-543	--	--
G15 (+)	830	Multiplier	571	--	--	607	--	--	625	--	--
G15 (-)	592	MM3	-432	-461	-489	-453	-480	-506	-462	-488	-514

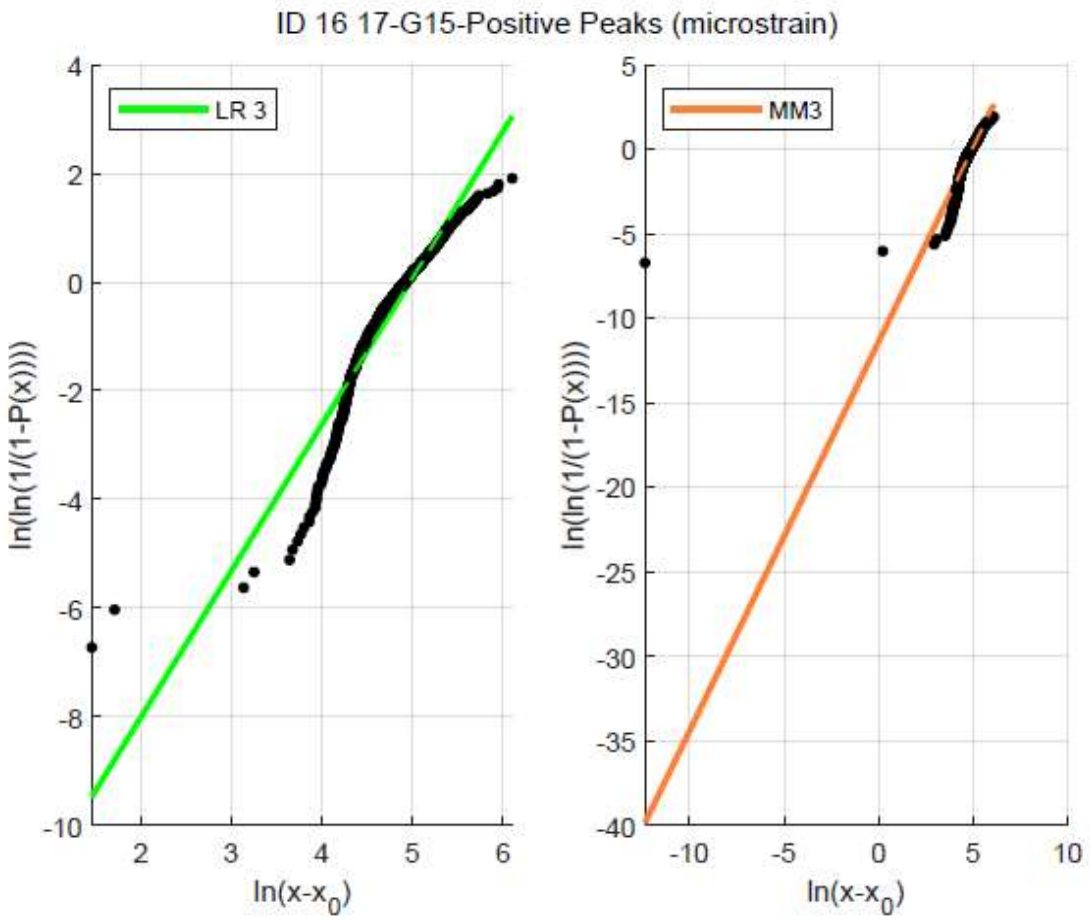

Figure I - 7. LR3 and MM3 Weibull Plots of Channel G15 for Matrix ID 16 and 17

Table I - 16. Weibull Shape Parameters for Single Strain Channels G16 - G20 in Matrix ID 16 and 17

Channel	Number of Events	Best Fit Method	σ (microstrain)	Best Fit Parameters			
				β	η (microstrain)	x_0 (microstrain)	R^2
G16 (+)	107	MM3	16	1.4	59	35	--
G16 (-)	629	MM3	128	1.8	245	0	--
G17 (+)	674	LR3	167	1.6	329	18	0.9805
G17 (-)	185	MM3	17	1.4	70	44	--
G18 (+)	695	LR3	173	1.6	354	21	0.9790
G18 (-)	240	MM3	18	1.5	70	41	--
G19 (+)	727	MM3	152	1.9	317	0	--
G19 (-)	181	MM3	17	1.4	68	44	--
G20 (+)*	30	MM3	13	1.2	63	47	--
G20 (-)*	758	MM3	69	2.3	181	14	--

*Results are presented for full disclosure, but the response of this channel was unreliable and it is recommended that these results are not used for comparison with CFD.

Table I - 17. Lifetime Extreme Estimates for Single Strain Channels G16 - G20 in Matrix ID 16 and 17

Channel	Number of Events	Best Fit Method	PNE @ 100 hr (microstrain)			PNE @ 500 hr (microstrain)			PNE @ 1000 hr (microstrain)		
			36.8 %	90.0 %	99.0 %	36.8 %	90.0 %	99.0 %	36.8 %	90.0 %	99.0 %
G16 (+)	107	MM3	175	195	216	190	209	229	196	215	235
G16 (-)	629	MM3	-1056	-1158	-1256	-1129	-1226	-1321	-1160	-1255	-1348
G17 (+)	674	LR3	1591	1757	1921	1711	1870	2029	1761	1918	2075
G17 (-)	185	MM3	-192	-212	-231	-206	-225	-244	-212	-231	-249
G18 (+)	695	LR3	1658	1828	1995	1780	1943	2105	1832	1992	2151
G18 (-)	240	MM3	-192	-210	-228	-205	-222	-239	-210	-227	-244
G19 (+)	727	MM3	1207	1311	1412	1282	1381	1477	1313	1410	1505
G19 (-)	181	MM3	-191	-211	-231	-205	-225	-245	-212	-231	-250
G20 (+)*	30	MM3	159	181	202	175	196	217	181	202	223
G20 (-)*	758	MM3	-530	-567	-602	-557	-591	-625	-568	-602	-635

*Results are presented for full disclosure, but the response of this channel was unreliable and it is recommended that these results are not used for comparison with CFD.

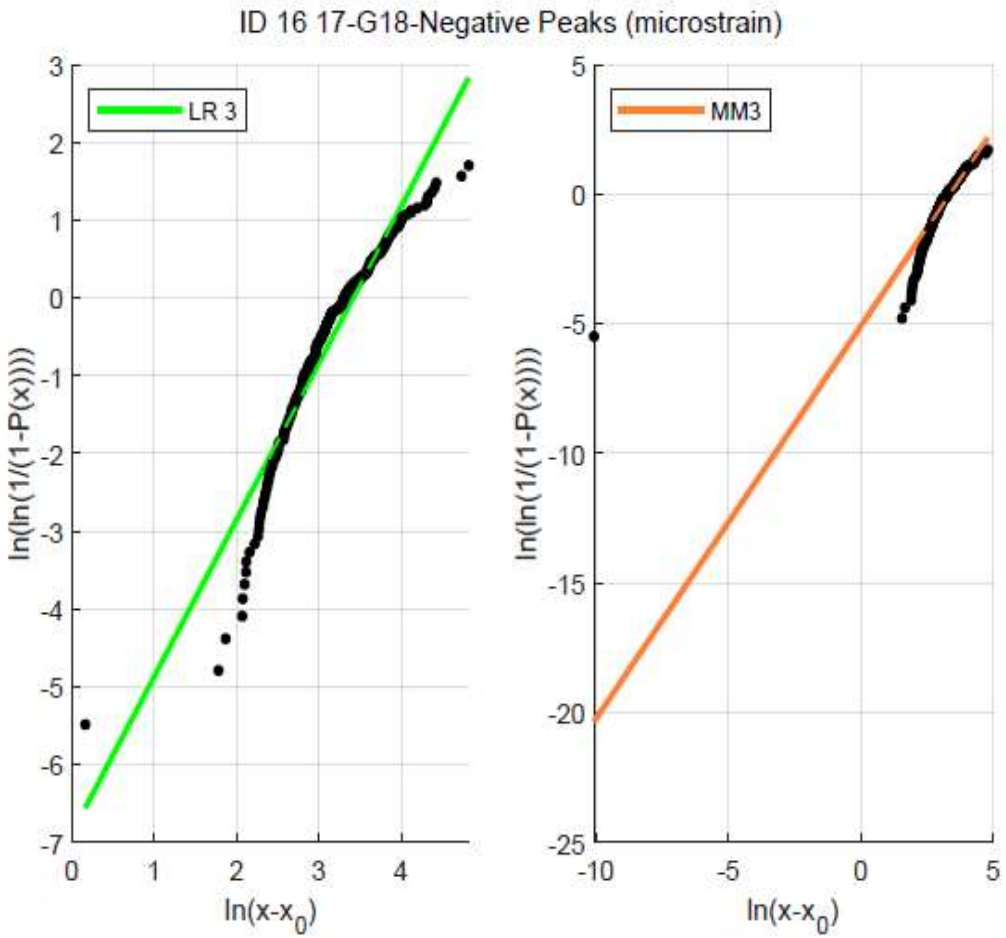

Figure I - 8. LR3 and MM3 Weibull Plots of Channel G18 for Matrix ID 16 and 17

Table I - 18. Weibull Shape Parameters for Single Strain Channels G21 - G25 in Matrix ID 16 and 17

Channel	Number of Events	Best Fit Method	σ (microstrain)	Best Fit Parameters			
				β	η (microstrain)	x_0 (microstrain)	R^2
G21 (+)	384	MM3	20	1.2	73	47	--
G21 (-)	800	Multiplier	28	--	--	--	--
G22 (+)	945	MM3	161	1.9	342	8	--
G22 (-)	46	MM3	14	1.7	66	40	--
G23 (+)	986	MM3	173	1.9	356	4	--
G23 (-)	65	MM3	14	1.4	67	45	--
G24 (+)	1011	MM3	165	1.9	334	3	--
G24 (-)	95	MM3	16	1.4	67	42	--
G25 (+)*	24	MM3	11	1.5	62	45	--
G25 (-)*	864	Multiplier	40	--	--	--	--

*Results are presented for full disclosure, but the response of this channel was unreliable and it is recommended that these results are not used for comparison with CFD.

Table I - 19. Lifetime Extreme Estimates for Single Strain Channels G21 - G25 in Matrix ID 16 and 17

Channel	Number of Events	Best Fit Method	PNE @ 100 hr (microstrain)			PNE @ 500 hr (microstrain)			PNE @ 1000 hr (microstrain)		
			36.8 %	90.0 %	99.0 %	36.8 %	90.0 %	99.0 %	36.8 %	90.0 %	99.0 %
G21 (+)	384	MM3	257	288	319	279	310	340	289	319	349
G21 (-)	800	Multiplier	-349	--	--	-370	--	--	-381	--	--
G22 (+)	945	MM3	1297	1406	1512	1376	1479	1580	1408	1509	1609
G22 (-)	46	MM3	-146	-159	-172	-155	-168	-180	-159	-172	-184
G23 (+)	986	MM3	1406	1526	1644	1493	1608	1720	1529	1642	1753
G23 (-)	65	MM3	-166	-185	-203	-180	-197	-215	-185	-203	-220
G24 (+)	1011	MM3	1343	1460	1574	1428	1539	1648	1463	1571	1678
G24 (-)	95	MM3	-176	-195	-213	-190	-207	-225	-195	-213	-230
G25 (+)*	24	MM3	126	139	151	135	147	159	139	150	162
G25 (-)*	864	Multiplier	-416	--	--	-442	--	--	-455	--	--

*Results are presented for full disclosure, but the response of this channel was unreliable and it is recommended that these results are not used for comparison with CFD.

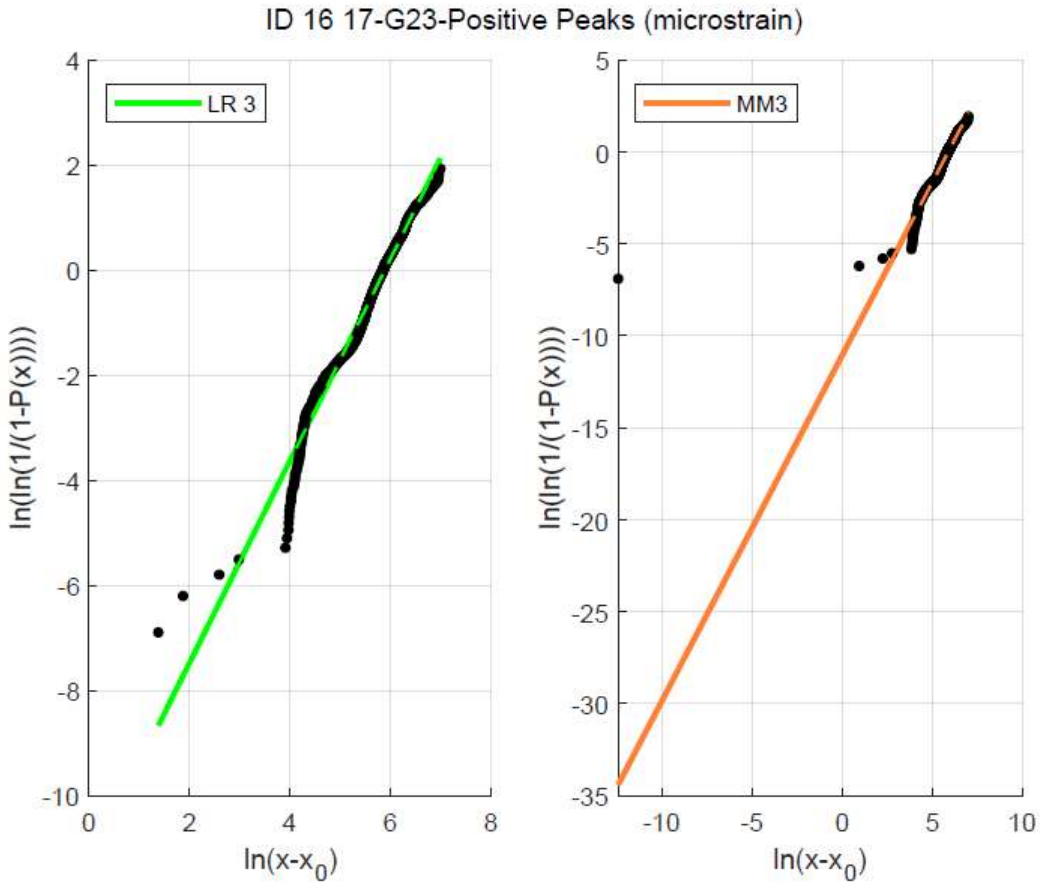

Figure I - 9. LR3 and MM3 Weibull Plots of Channel G23 for Matrix ID 16 and 17

Table I - 20. Weibull Shape Parameters for Pressure Transducer Channels in Matrix ID 16 and 17

Channel	Number of Events	Best Fit Method	σ (PSI)	Best Fit Parameters			
				β	η (PSI)	x_0 (PSI)	R^2
P11 (+)	650	Multiplier	1.0	--	--	--	--
P12 (+)	585	MM3	0.9	2.6	2.4	0.1	--
P13 (+)	400	MM3	0.7	1.9	1.7	0.4	--
P21 (+)	820	Multiplier	1.1	--	--	--	--
P22 (+)	697	MM3	0.8	1.9	1.7	0.1	--
P23 (+)	664	Multiplier	0.6	--	--	--	--

Table I - 21. Lifetime Extreme Estimates for Pressure Transducer Channels in Matrix ID 16 and 17

Channel	Number of Events	Best Fit Method	PNE @ 100 hr (PSI)			PNE @ 500 hr (PSI)			PNE @ 1000 hr (PSI)		
			36.8 %	90.0 %	99.0 %	36.8 %	90.0 %	99.0 %	36.8 %	90.0 %	99.0 %
P11 (+)	650	Multiplier	11	--	--	12	--	--	12	--	--
P12 (+)	585	MM3	6	7	7	7	7	7	7	7	7
P13 (+)	400	MM3	6	6	6	6	6	7	6	6	7
P21 (+)	820	Multiplier	11	--	--	12	--	--	12	--	--
P22 (+)	697	MM3	6	7	7	7	7	8	7	7	8
P23 (+)	664	Multiplier	6	--	--	6	--	--	6	--	--

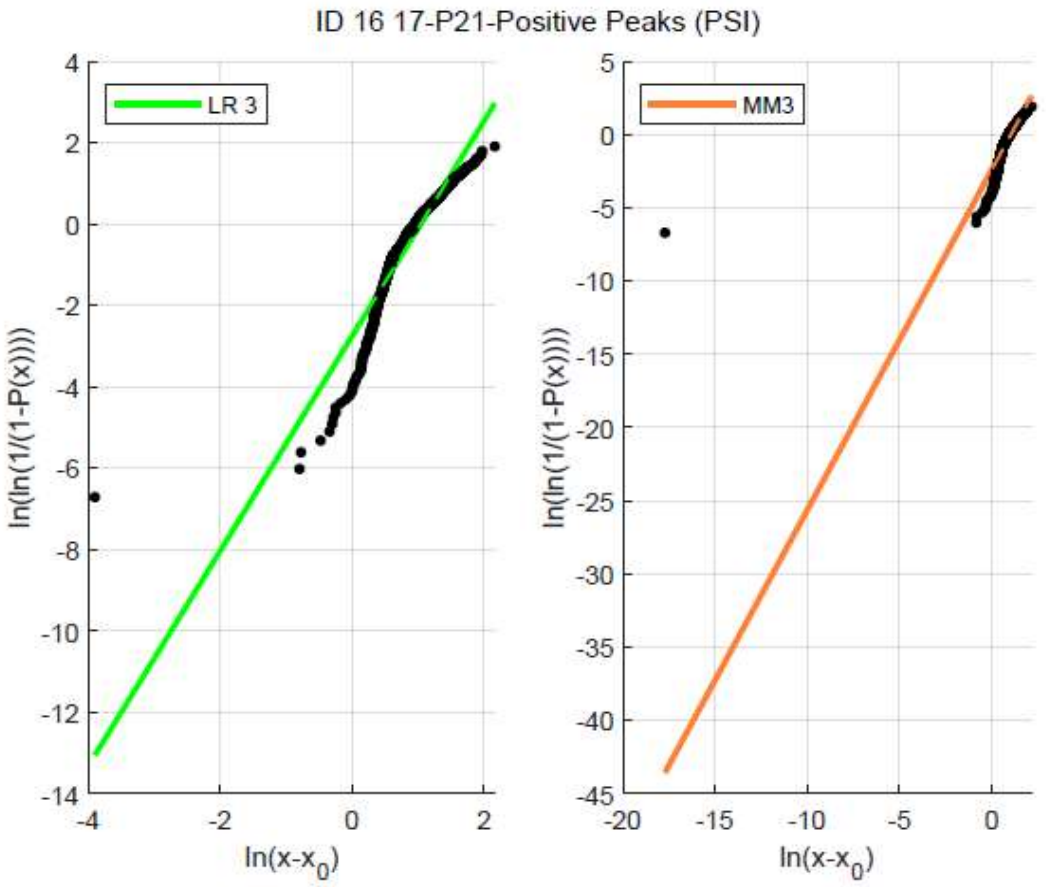

Figure I - 10. LR3 and MM3 Weibull Plots of Channel P21 for Matrix ID 16 and 17

Table I - 22. Weibull Shape Parameters for Differential Bending Channels in Matrix ID 22 and 23

Channel	Number of Events	Best Fit Method	σ (PSI)	Best Fit Parameters			
				β	η (PSI)	x_0 (PSI)	R^2
G1 (+)	1142	MM3	1.4	2.3	3.7	0.2	--
G3 (+)	1196	Multiplier	1.2	--	--	--	--
G4 (+)	1794	LR3	1.1	2.7	3.1	0.0	0.9580
G5 (+)	2128	Multiplier	0.6	--	--	--	--
G7* (+)	2180	Multiplier	0.7	--	--	--	--
G8 (+)	775	Multiplier	0.7	--	--	--	--
G9 (+)	857	Multiplier	0.4	--	--	--	--
G10 (+)	1839	Multiplier	0.8	--	--	--	--

*Results are presented for full disclosure, but the response of this channel was unreliable and it is recommended that these results are not used for comparison with CFD.

Table I - 23. Lifetime Extreme Estimates for Differential Bending Channels in Matrix ID 22 and 23

Channel	Number of Events	Best Fit Method	PNE @ 100 hr (PSI)			PNE @ 500 hr (PSI)			PNE @ 1000 hr (PSI)		
			36.8 %	90.0 %	99.0 %	36.8 %	90.0 %	99.0 %	36.8 %	90.0 %	99.0 %
G1 (+)	1142	MM3	11	12	12	11	12	13	12	12	13
G3 (+)	1196	Multiplier	11	--	--	12	--	--	13	--	--
G4 (+)	1794	LR3	8	9	9	9	9	10	9	9	10
G5 (+)	2128	Multiplier	7	--	--	8	--	--	8	--	--
G7* (+)	2180	Multiplier	12	--	--	13	--	--	13	--	--
G8 (+)	775	Multiplier	7	--	--	7	--	--	7	--	--
G9 (+)	857	Multiplier	5	--	--	5	--	--	6	--	--
G10 (+)	1839	Multiplier	9	--	--	10	--	--	10	--	--

*Results are presented for full disclosure, but the response of this channel was unreliable and it is recommended that these results are not used for comparison with CFD.

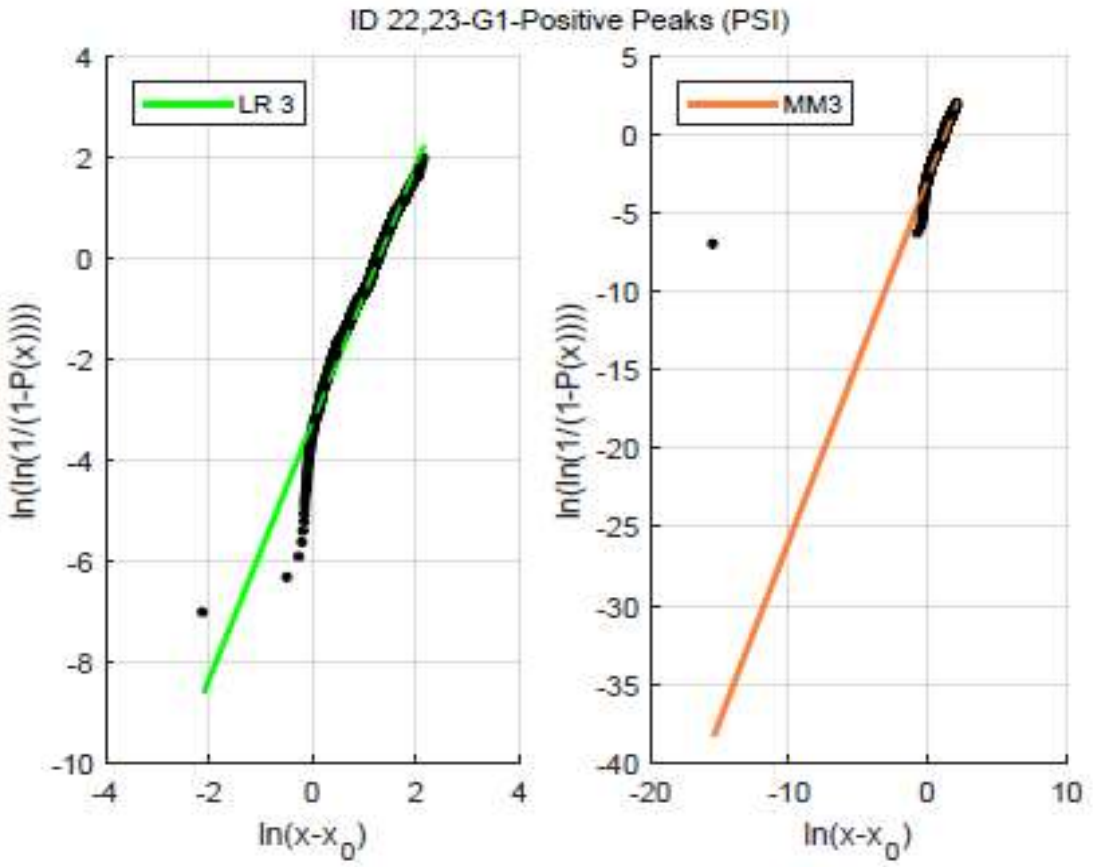

Figure I - 11. LR3 and MM3 Weibull Plots of Channel G1 for Matrix ID 22 and 23

Table I - 24. Weibull Shape Parameters for Single Strain Channels G11 - G15 in Matrix ID 22 and 23

Channel	Number of Events	Best Fit Method	σ (microstrain)	Best Fit Parameters			
				β	η (microstrain)	x_0 (microstrain)	R^2
G11 (+)	96	LR3	27	1.3	47	12	0.9854
G11 (-)	1675	MM3	526	1.6	905	0	--
G12 (+)	1169	LR3	418	1.6	944	0	0.9479
G12 (-)	2090	Multiplier	83	--	--	--	--
G13 (+)	1362	LR3	521	1.5	1184	0	0.9406
G13 (-)	2039	MM3	93	2.2	221	3	--
G14 (+)	1463	LR3	412	1.7	1031	0	0.9270
G14 (-)	2090	MM3	99	2.2	239	5	--
G15 (+)	1546	Multiplier	35	--	--	--	--
G15 (-)	2479	Multiplier	156	--	--	--	--

Table I - 25. Lifetime Extreme Estimates for Single Strain Channels G11 - G15 in Matrix ID 22 and 23

Channel	Number of Events	Best Fit Method	PNE @ 100 hr (microstrain)			PNE @ 500 hr (microstrain)			PNE @ 1000 hr (microstrain)		
			36.8 %	90.0 %	99.0 %	36.8 %	90.0 %	99.0 %	36.8 %	90.0 %	99.0 %
G11 (+)	96	LR3	227	263	300	253	288	324	264	299	334
G11 (-)	1675	MM3	-4619	-5107	-5589	-4971	-5440	-5905	-5118	-5579	-6039
G12 (+)	1169	LR3	4830	5361	5886	5213	5723	6230	5373	5875	6375
G12 (-)	2090	Multiplier	-856	--	--	-910	--	--	-937	--	--
G13 (+)	1362	LR3	6579	7328	8072	7119	7841	8562	7345	8057	8769
G13 (-)	2039	MM3	-714	-767	-817	-752	-802	-850	-768	-816	-864
G14 (+)	1463	LR3	4871	5366	5854	5228	5703	6173	5377	5844	6307
G14 (-)	2090	MM3	-763	-818	-872	-803	-855	-906	-819	-871	-920
G15 (+)	1546	Multiplier	522	--	--	554	--	--	571	--	--
G15 (-)	2479	Multiplier	-1970	--	--	-2093	--	--	-2155	--	--

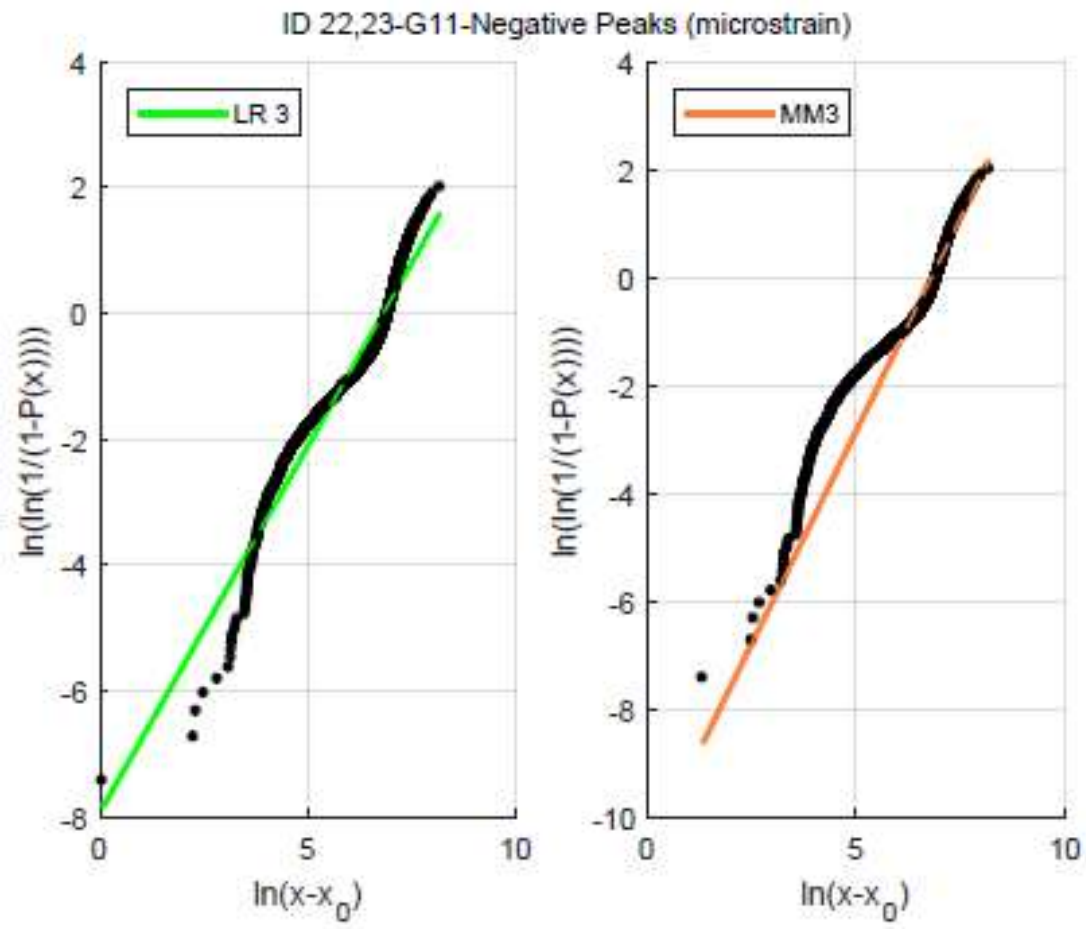

Figure I - 12. LR3 and MM3 Weibull Plots of Channel G11 for Matrix ID 22 and 23

Table I - 26. Weibull Shape Parameters for Single Strain Channels G16 - G20 in Matrix ID 22 and 23

Channel	Number of Events	Best Fit Method	σ (microstrain)	Best Fit Parameters			
				β	η (microstrain)	x_0 (microstrain)	R^2
G16 (+)	731	MM3	24	1.5	78	37	--
G16 (-)	1854	Multiplier	109	--	--	--	--
G17 (+)	1797	MM3	256	1.7	481	0	--
G17 (-)	1781	Multiplier	45	--	--	--	--
G18 (+)	1792	LR3	225	1.7	463	5	0.9627
G18 (-)	1909	Multiplier	49	--	--	--	--
G19 (+)	1845	Multiplier	137	--	--	--	--
G19 (-)	1891	MM3	52	1.8	119	18	--
G20 (+)*	286	LR3	18	3.7	70	0	0.8495
G20 (-)*	1894	MM3	253	1.4	391	0	--

*Results are presented for full disclosure, but the response of this channel was unreliable and it is recommended that these results are not used for comparison with CFD.

Table I - 27. Lifetime Extreme Estimates for Single Strain Channels G16 - G20 in Matrix ID 22 and 23

Channel	Number of Events	Best Fit Method	PNE @ 100 hr (microstrain)			PNE @ 500 hr (microstrain)			PNE @ 1000 hr (microstrain)		
			36.8 %	90.0 %	99.0 %	36.8 %	90.0 %	99.0 %	36.8 %	90.0 %	99.0 %
G16 (+)	731	MM3	246	270	294	263	287	310	271	294	316
G16 (-)	1854	Multiplier	-1165	--	--	-1238	--	--	-1274	--	--
G17 (+)	1797	MM3	2147	2353	2554	2295	2492	2686	2357	2550	2741
G17 (-)	1781	Multiplier	-559	--	--	-594	--	--	-611	--	--
G18 (+)	1792	LR3	2173	2389	2602	2329	2536	2741	2394	2597	2799
G18 (-)	1909	Multiplier	-587	--	--	-624	--	--	-642	--	--
G19 (+)	1845	Multiplier	1492	--	--	1585	--	--	1632	--	--
G19 (-)	1891	MM3	-448	-488	-527	-477	-515	-552	-489	-526	-563
G20 (+)*	286	LR3	136	143	149	141	147	153	143	149	155
G20 (-)*	1894	MM3	-2388	-2665	-2942	-2587	-2856	-3126	-2671	-2937	-3204

*Results are presented for full disclosure, but the response of this channel was unreliable and it is recommended that these results are not used for comparison with CFD.

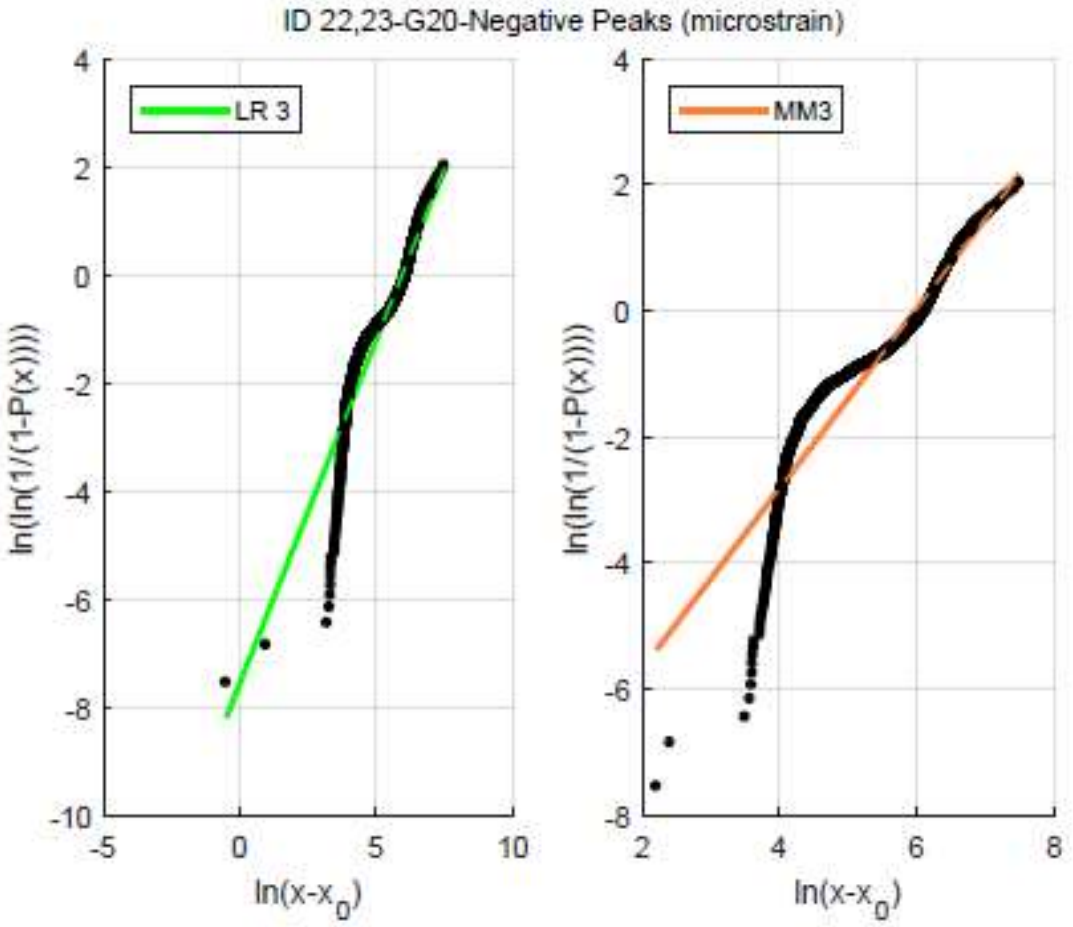

Figure I - 13. LR3 and MM3 Weibull Plots of Channel G20 for Matrix ID 22 and 23

Table I - 28. Weibull Shape Parameters for Single Strain Channels G21 - G25 in Matrix ID 22 and 23

Channel	Number of Events	Best Fit Method	σ (microstrain)	Best Fit Parameters			
				β	η (microstrain)	x_0 (microstrain)	R^2
G21 (+)	1690	Multiplier	22	--	--	--	--
G21 (-)	2682	Multiplier	162	--	--	--	--
G22 (+)	2629	Multiplier	381	--	--	--	--
G22 (-)	1787	Multiplier	68	--	--	--	--
G23 (+)	2738	Multiplier	418	--	--	--	--
G23 (-)	1874	Multiplier	80	--	--	--	--
G24 (+)	2451	Multiplier	339	--	--	--	--
G24 (-)	1669	Multiplier	80	--	--	--	--
G25 (+)	84	MM3	24	1.4	67	29	--
G25 (-)	2261	Multiplier	249	--	--	--	--

Table I - 29. Lifetime Extreme Estimates for Single Strain Channels G21 - G25 in Matrix ID 22 and 23

Channel	Number of Events	Best Fit Method	PNE @ 100 hr (microstrain)			PNE @ 500 hr (microstrain)			PNE @ 1000 hr (microstrain)		
			36.8 %	90.0 %	99.0 %	36.8 %	90.0 %	99.0 %	36.8 %	90.0 %	99.0 %
G21 (+)	1690	Multiplier	418	--	--	445	--	--	458	--	--
G21 (-)	2682	Multiplier	-1883	--	--	-2001	--	--	-2060	--	--
G22 (+)	2629	Multiplier	4394	--	--	4668	--	--	4806	--	--
G22 (-)	1787	Multiplier	-1066	--	--	-1133	--	--	-1166	--	--
G23 (+)	2738	Multiplier	4743	--	--	5040	--	--	5188	--	--
G23 (-)	1874	Multiplier	-1107	--	--	-1176	--	--	-1211	--	--
G24 (+)	2451	Multiplier	6003	--	--	6378	--	--	6566	--	--
G24 (-)	1669	Multiplier	-891	--	--	-947	--	--	-975	--	--
G25 (+)	84	MM3	222	251	280	243	271	299	252	280	307
G25 (-)	2261	Multiplier	-2961	--	--	-3146	--	--	-3238	--	--

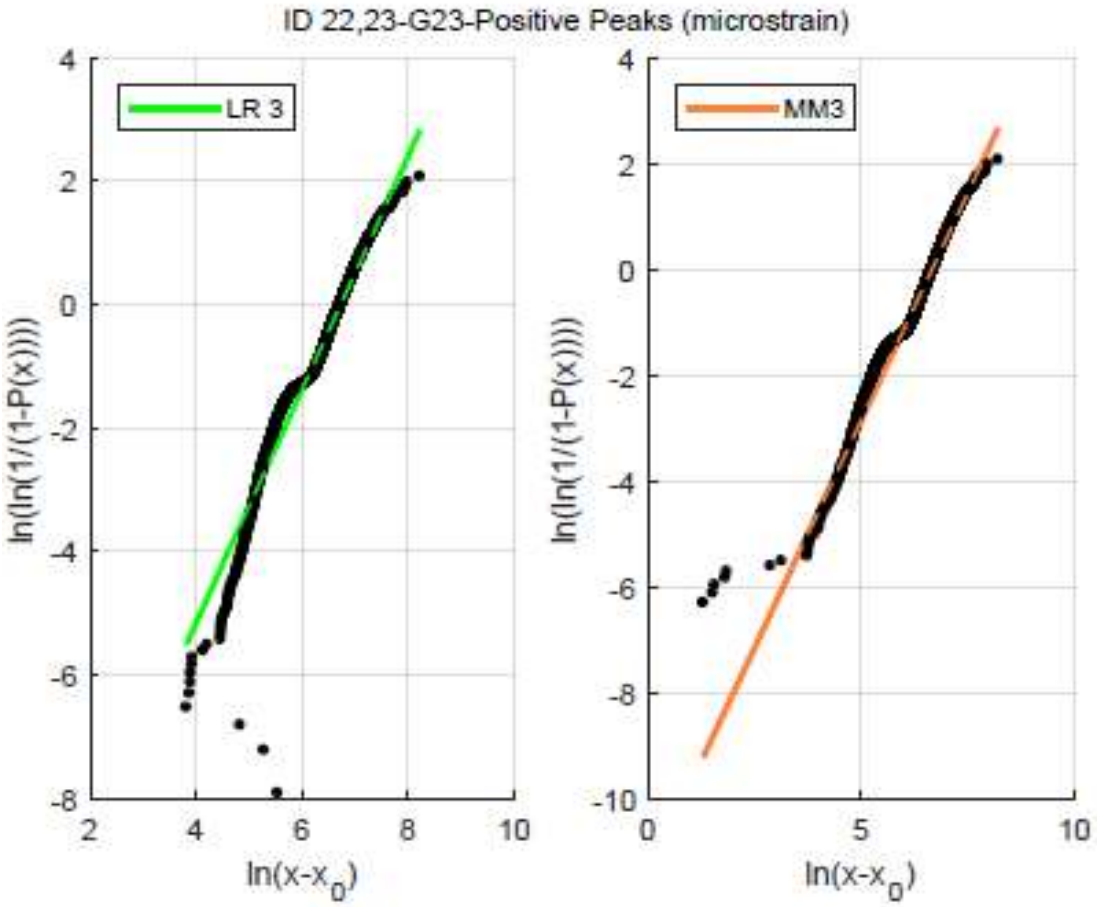

Figure I - 14. LR3 and MM3 Weibull Plots of Channel G23 for Matrix ID 22 and 23

Table I - 30. Weibull Shape Parameters for Pressure Transducer Channels in Matrix ID 22 and 23

Channel	Number of Events	Best Fit Method	σ (PSI)	Best Fit Parameters			
				β	η (PSI)	x_0 (PSI)	R^2
P11 (+)	1648	Multiplier	1.1	--	--	--	--
P12 (+)	1468	MM3	1.0	2.3	3.1	0.7	--
P13 (+)	998	MM3	0.8	2.4	2.3	0.3	--
P21 (+)	2134	Multiplier	1.3	--	--	--	--
P22 (+)	1816	Multiplier	0.9	--	--	--	--
P23 (+)	1645	Multiplier	0.7	--	--	--	--

Table I - 31. Lifetime Extreme Estimates for Pressure Transducer Channels in Matrix ID 22 and 23

Channel	Number of Events	Best Fit Method	PNE @ 100 hr (PSI)			PNE @ 500 hr (PSI)			PNE @ 1000 hr (PSI)		
			36.8 %	90.0 %	99.0 %	36.8 %	90.0 %	99.0 %	36.8 %	90.0 %	99.0 %
P11 (+)	1648	Multiplier	16	--	--	17	--	--	18	--	--
P12 (+)	1468	MM3	8	9	9	9	9	10	9	9	10
P13 (+)	998	MM3	6	6	7	6	7	7	6	7	7
P21 (+)	2134	Multiplier	17	--	--	18	--	--	18	--	--
P22 (+)	1816	Multiplier	11	--	--	12	--	--	12	--	--
P23 (+)	1645	Multiplier	8	--	--	9	--	--	9	--	--

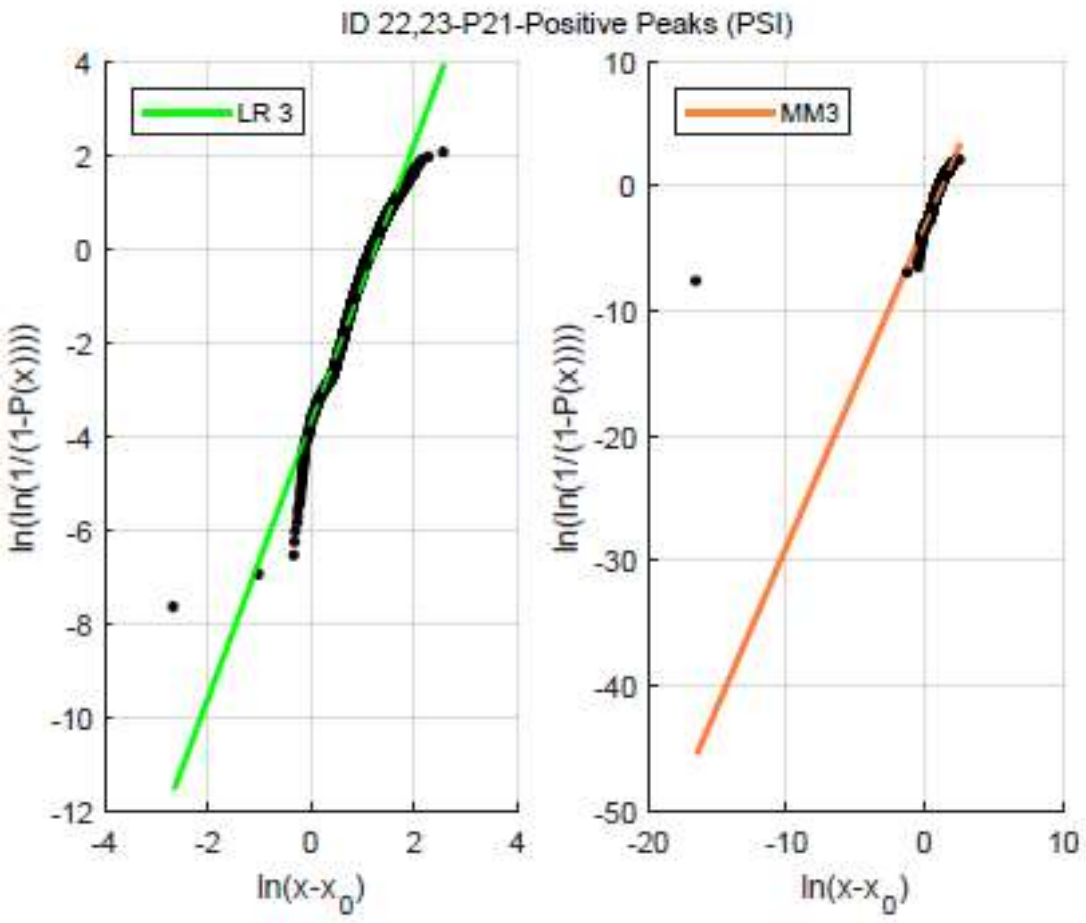

Figure I - 15. LR3 and MM3 Weibull Plots of Channel P21 for Matrix ID 22 and 23

Optimized Grillage: Matrix ID 24 and 25

Table I - 32. Weibull Shape Parameters for Differential Bending Channels in Matrix ID 24 and 25

Channel	Number of Events	Best Fit Method	σ (PSI)	Best Fit Parameters			
				β	η (PSI)	x_0 (PSI)	R^2
G1 (+)	408	LR3	1.1	2.1	2.9	0.3	0.9923
G3 (+)	409	MM3	0.8	2.4	2.7	0.6	--
G4 (+)	645	MM3	0.9	2.0	2.3	0.4	--
G5 (+)	798	MM3	0.5	2.6	1.4	0.0	--
G7 (+)*	807	Multiplier	0.6	--	--	--	--
G8 (+)	289	LR3	0.6	1.7	1.4	0.2	0.9879
G9 (+)	328	Multiplier	0.3	--	--	--	--
G10 (+)	661	Multiplier	0.7	--	--	--	--

*Results are presented for full disclosure, but the response of this channel was unreliable and it is recommended that these results are not used for comparison with CFD.

Table I - 33. Lifetime Extreme Estimates for Differential Bending Channels in Matrix ID 24 and 25

Channel	Number of Events	Best Fit Method	PNE @ 100 hr (PSI)			PNE @ 500 hr (PSI)			PNE @ 1000 hr (PSI)		
			36.8 %	90.0 %	99.0 %	36.8 %	90.0 %	99.0 %	36.8 %	90.0 %	99.0 %
G1 (+)	408	LR3	9	9	10	9	10	11	9	10	11
G3 (+)	409	MM3	7	7	7	7	7	8	7	7	8
G4 (+)	645	MM3	7	8	8	8	8	9	8	8	9
G5 (+)	798	MM3	4	4	4	4	4	4	4	4	4
G7 (+)*	807	Multiplier	6	--	--	7	--	--	7	--	--
G8 (+)	289	LR3	5	6	6	6	6	6	6	6	7
G9 (+)	328	Multiplier	3	--	--	3	--	--	3	--	--
G10 (+)	661	Multiplier	7	--	--	7	--	--	7	--	--

*Results are presented for full disclosure, but the response of this channel was unreliable and it is recommended that these results are not used for comparison with CFD.

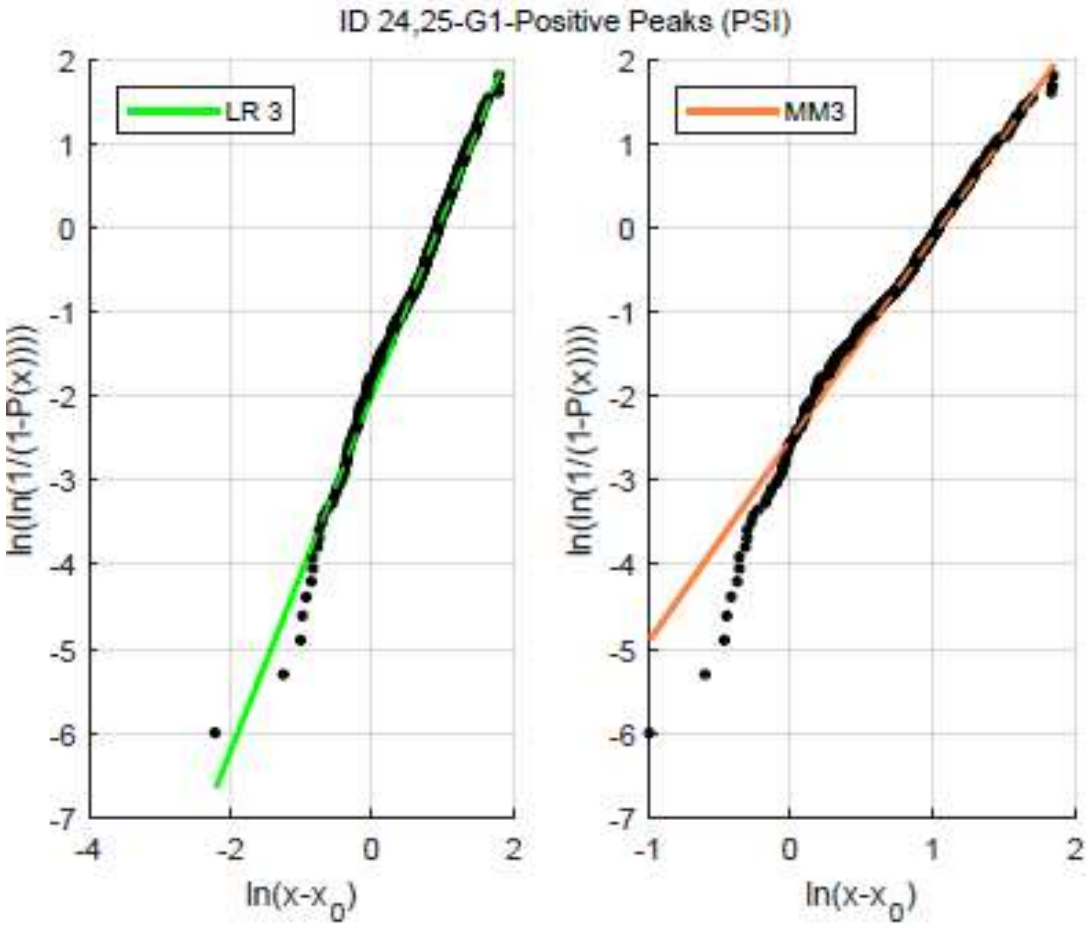

Figure I - 16. LR3 and MM3 Weibull Plots of Channel G1 for Matrix ID 24 and 25

Table I - 34. Weibull Shape Parameters for Single Strain Channels G11 - G15 in Matrix ID 24 and 25

Channel	Number of Events	Best Fit Method	σ (microstrain)	Best Fit Parameters			
				β	η (microstrain)	x_0 (microstrain)	R^2
G11 (+)	15	Multiplier	31	--	--	--	--
G11 (-)	561	MM3	406	1.7	760	0	--
G12 (+)	403	LR3	303	1.8	736	0	0.9590
G12 (-)	720	MM3	76	1.8	162	17	--
G13 (+)	475	MM3	401	2.1	888	0	--
G13 (-)	711	MM3	86	2.1	193	1	--
G14 (+)	521	MM3	325	2.2	760	0	--
G14 (-)	773	MM3	92	1.8	202	25	--
G15 (+)	495	MM3	32	1.4	86	37	--
G15 (-)	846	MM3	125	1.6	231	18	--

Table I - 35. Lifetime Extreme Estimates for Single Strain Channels G11 - G15 in Matrix ID 24 and 25

Channel	Number of Events	Best Fit Method	PNE @ 100 hr (microstrain)			PNE @ 500 hr (microstrain)			PNE @ 1000 hr (microstrain)		
			36.8 %	90.0 %	99.0 %	36.8 %	90.0 %	99.0 %	36.8 %	90.0 %	99.0 %
G11 (+)	15	Multiplier	146	--	--	155	--	--	159	--	--
G11 (-)	561	MM3	-3362	-3691	-4013	-3599	-3914	-4224	-3698	-4007	-4312
G12 (+)	403	LR3	3006	3294	3574	3214	3488	3757	3300	3569	3833
G12 (-)	720	MM3	-644	-703	-761	-687	-743	-798	-704	-760	-814
G13 (+)	475	MM3	3056	3307	3549	3238	3475	3705	3313	3544	3770
G13 (-)	711	MM3	-671	-724	-776	-709	-760	-809	-725	-775	-823
G14 (+)	521	MM3	2442	2630	2810	2578	2754	2925	2634	2806	2973
G14 (-)	773	MM3	-793	-864	-935	-845	-913	-981	-866	-933	-1000
G15 (+)	495	MM3	333	369	405	359	394	429	370	404	439
G15 (-)	846	MM3	-1134	-1251	-1366	-1218	-1331	-1443	-1253	-1364	-1475

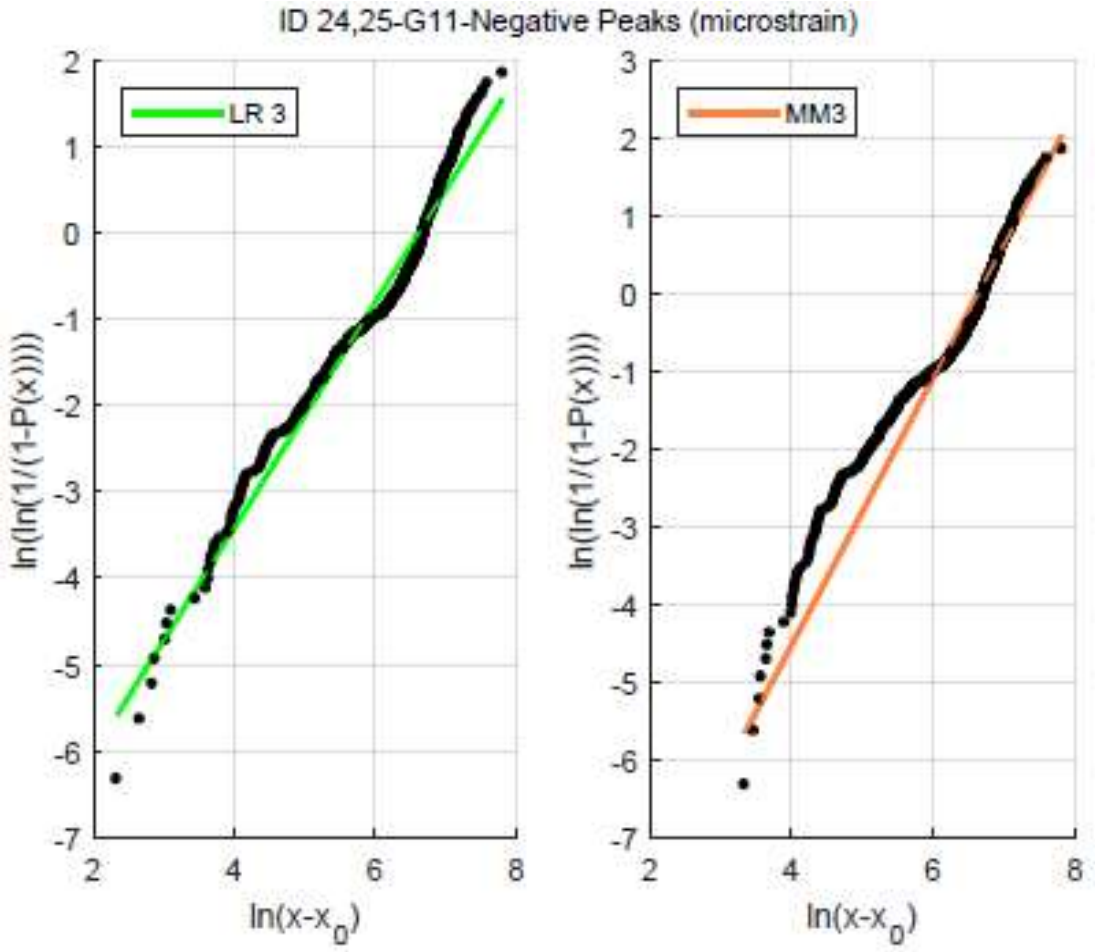

Figure I - 17. LR3 and MM3 Weibull Plots of Channel G11 for Matrix ID 24 and 25

Table I - 36. Weibull Shape Parameters for Single Strain Channels G16 - G20 in Matrix ID 24 and 25

Channel	Number of Events	Best Fit Method	σ (microstrain)	Best Fit Parameters			
				β	η (microstrain)	x_0 (microstrain)	R^2
G16 (+)	193	MM3	22	1.3	76	43	--
G16 (-)	647	LR3	83	1.5	176	36	0.9840
G17 (+)	635	MM3	206	1.8	404	0	--
G17 (-)	570	MM3	38	1.6	100	32	--
G18 (+)	644	MM3	183	1.9	381	0	--
G18 (-)	616	MM3	40	1.6	104	32	--
G19 (+)	672	LR3	114	1.8	258	21	0.9868
G19 (-)	591	MM3	40	1.9	107	22	--
G20 (+)*	51	MM3	24	1.3	69	37	--
G20 (-)*	616	MM3	193	1.7	347	0	--

*Results are presented for full disclosure, but the response of this channel was unreliable and it is recommended that these results are not used for comparison with CFD.

Table I - 37. Lifetime Extreme Estimates for Single Strain Channels G16 - G20 in Matrix ID 24 and 25

Channel	Number of Events	Best Fit Method	PNE @ 100 hr (microstrain)			PNE @ 500 hr (microstrain)			PNE @ 1000 hr (microstrain)		
			36.8 %	90.0 %	99.0 %	36.8 %	90.0 %	99.0 %	36.8 %	90.0 %	99.0 %
G16 (+)	193	MM3	249	277	306	269	297	325	278	306	333
G16 (-)	647	LR3	-774	-854	-933	-831	-908	-985	-856	-931	-1007
G17 (+)	635	MM3	1671	1824	1974	1782	1928	2072	1828	1972	2113
G17 (-)	570	MM3	-354	-388	-420	-378	-410	-442	-388	-420	-450
G18 (+)	644	MM3	1449	1573	1695	1539	1657	1773	1576	1692	1806
G18 (-)	616	MM3	-378	-414	-449	-404	-438	-472	-414	-448	-481
G19 (+)	672	LR3	1001	1091	1178	1066	1151	1235	1093	1177	1259
G19 (-)	591	MM3	-337	-364	-391	-357	-383	-408	-365	-390	-415
G20 (+)*	51	MM3	240	273	307	264	296	329	274	306	339
G20 (-)*	616	MM3	-1642	-1809	-1972	-1762	-1922	-2080	-1812	-1969	-2125

*Results are presented for full disclosure, but the response of this channel was unreliable and it is recommended that these results are not used for comparison with CFD.

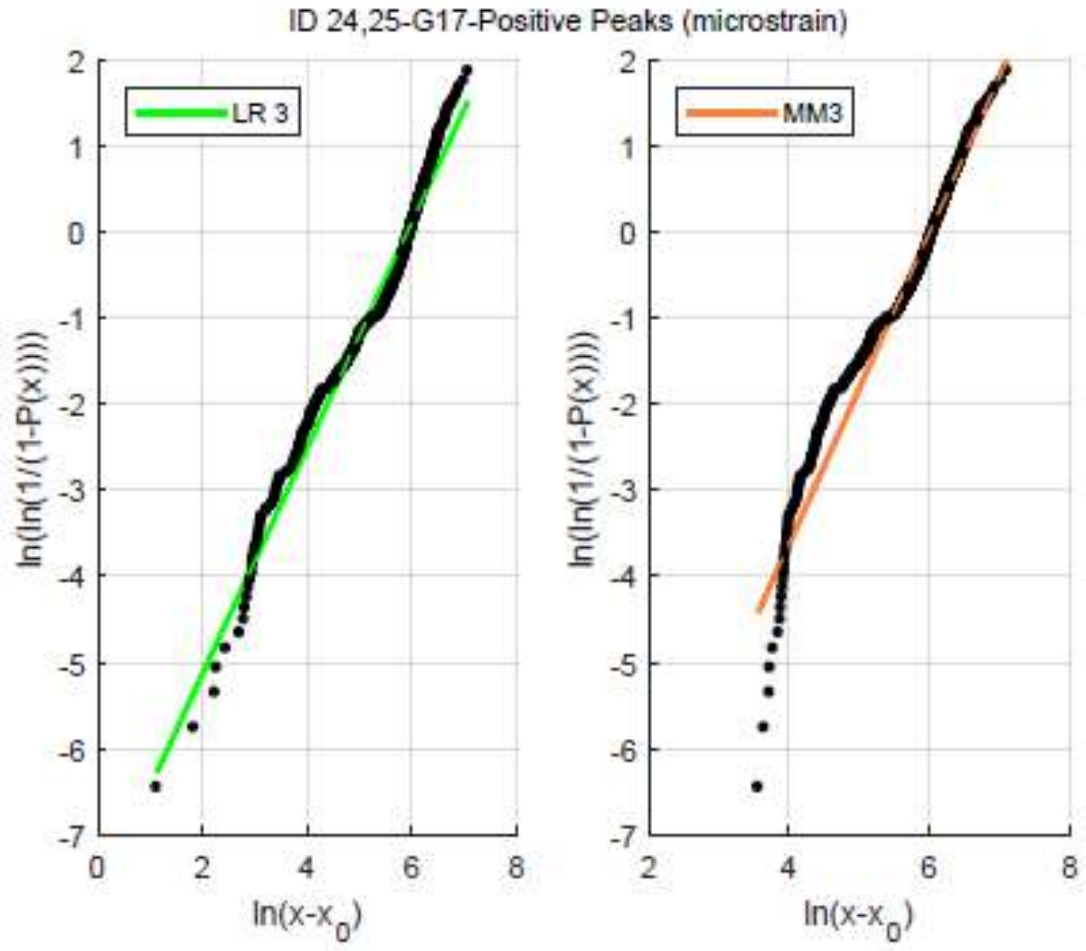

Figure I - 18. LR3 and MM3 Weibull Plots of Channel G17 for Matrix ID 24 and 25

Table I - 38. Weibull Shape Parameters for Single Strain Channels G21 - G25 in Matrix ID 24 and 25

Channel	Number of Events	Best Fit Method	σ (microstrain)	Best Fit Parameters			
				β	η (microstrain)	x_0 (microstrain)	R^2
G21 (+)	510	Multiplier	13	--	--	--	--
G21 (-)	915	MM3	140	1.8	279	6	--
G22 (+)	1007	LR3	314	1.8	580	2	0.9605
G22 (-)	577	Multiplier	45	--	--	--	--
G23 (+)	1043	LR3	348	1.6	611	0	0.9611
G23 (-)	609	Multiplier	50	--	--	--	--
G24 (+)	877	MM3	299	1.6	523	3	--
G24 (-)	520	LR3	53	2.1	120	0	0.9895
G25 (+)	11	Multiplier	24	--	--	--	--
G25 (-)	815	MM3	203	1.7	426	45	--

Table I - 39. Lifetime Extreme Estimates for Single Strain Channels G21 - G25 in Matrix ID 24 and 25

Channel	Number of Events	Best Fit Method	PNE @ 100 hr (microstrain)			PNE @ 500 hr (microstrain)			PNE @ 1000 hr (microstrain)		
			36.8 %	90.0 %	99.0 %	36.8 %	90.0 %	99.0 %	36.8 %	90.0 %	99.0 %
G21 (+)	510	Multiplier	247	--	--	262	--	--	270	--	--
G21 (-)	915	MM3	-1169	-1275	-1378	-1246	-1346	-1445	-1277	-1376	-1473
G22 (+)	1007	LR3	2484	2708	2927	2646	2859	3070	2713	2923	3130
G22 (-)	577	Multiplier	-595	--	--	-632	--	--	-650	--	--
G23 (+)	1043	LR3	3087	3397	3703	3311	3608	3904	3404	3697	3989
G23 (-)	609	Multiplier	-613	--	--	-652	--	--	-671	--	--
G24 (+)	877	MM3	2654	2924	3191	2848	3108	3367	2930	3186	3440
G24 (-)	520	LR3	-399	-431	-461	-422	-452	-481	-432	-461	-489
G25 (+)	11	Multiplier	179	--	--	191	--	--	196	--	--
G25 (-)	815	MM3	-1751	-1913	-2072	-1868	-2023	-2176	-1917	-2069	-2220

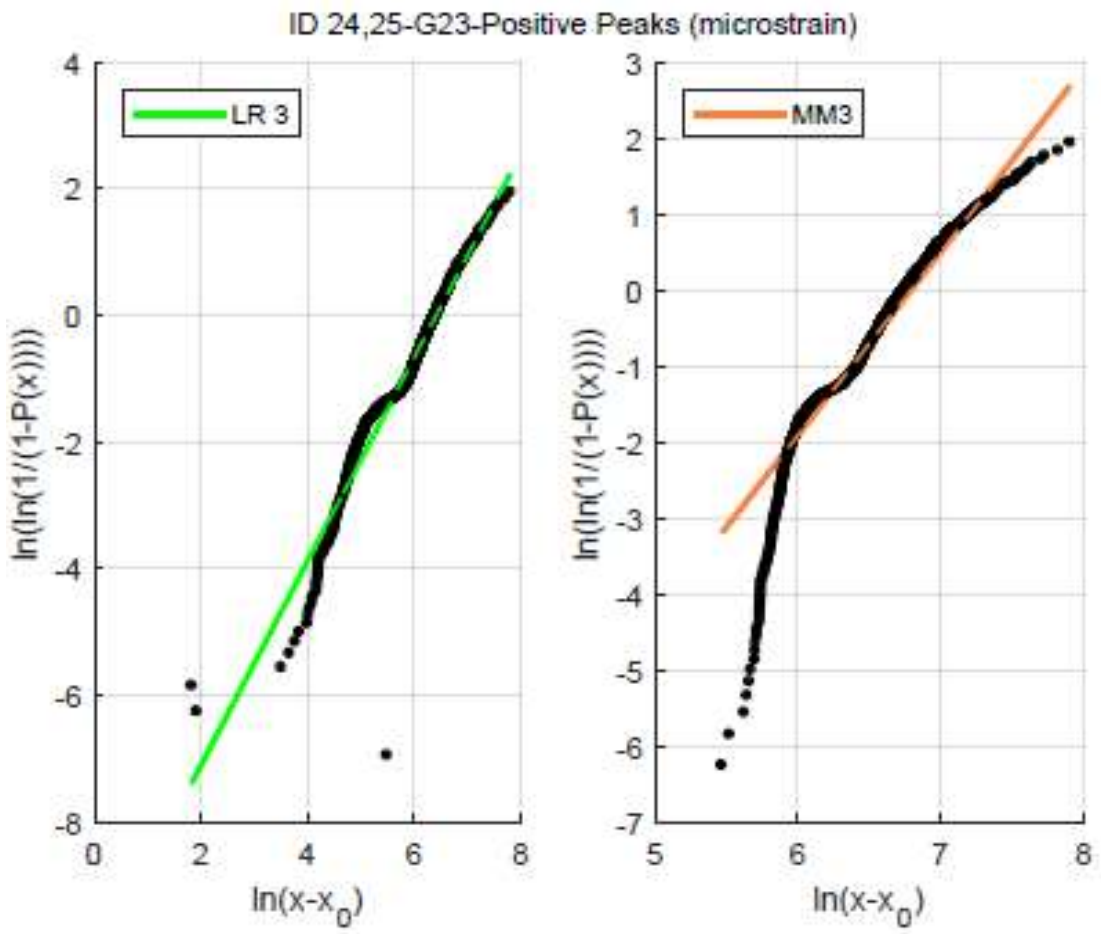

Figure I - 19. LR3 and MM3 Weibull Plots of Channel G23 for Matrix ID 24 and 25

Table I - 40. Weibull Shape Parameters for Pressure Transducer Channels in Matrix ID 24 and 25

Channel	Number of Events	Best Fit Method	σ (PSI)	Best Fit Parameters			
				β	η (PSI)	x_0 (PSI)	R^2
P11 (+)	593	MM3	0.9	1.6	2.3	0.7	--
P12 (+)	538	MM3	0.9	2.0	2.5	0.5	--
P13 (+)	374	MM3	0.6	2.3	1.7	0.2	--
P21 (+)	786	MM3	1.0	1.7	2.6	0.7	--
P22 (+)	646	MM3	0.9	1.6	1.8	0.3	--
P23 (+)	601	MM3	0.6	2.1	1.7	0.4	--

Table I - 41. Lifetime Extreme Estimates for Pressure Transducer Channels in Matrix ID 24 and 25

Channel	Number of Events	Best Fit Method	PNE @ 100 hr (PSI)			PNE @ 500 hr (PSI)			PNE @ 1000 hr (PSI)		
			36.8 %	90.0 %	99.0 %	36.8 %	90.0 %	99.0 %	36.8 %	90.0 %	99.0 %
P11 (+)	593	MM3	9	10	10	9	10	11	10	10	11
P12 (+)	538	MM3	7	8	9	8	8	9	8	9	9
P13 (+)	374	MM3	5	5	6	5	5	6	5	6	6
P21 (+)	786	MM3	9	10	11	10	11	12	10	11	12
P22 (+)	646	MM3	8	8	9	8	9	10	8	9	10
P23 (+)	601	MM3	5	5	6	5	5	6	5	6	6

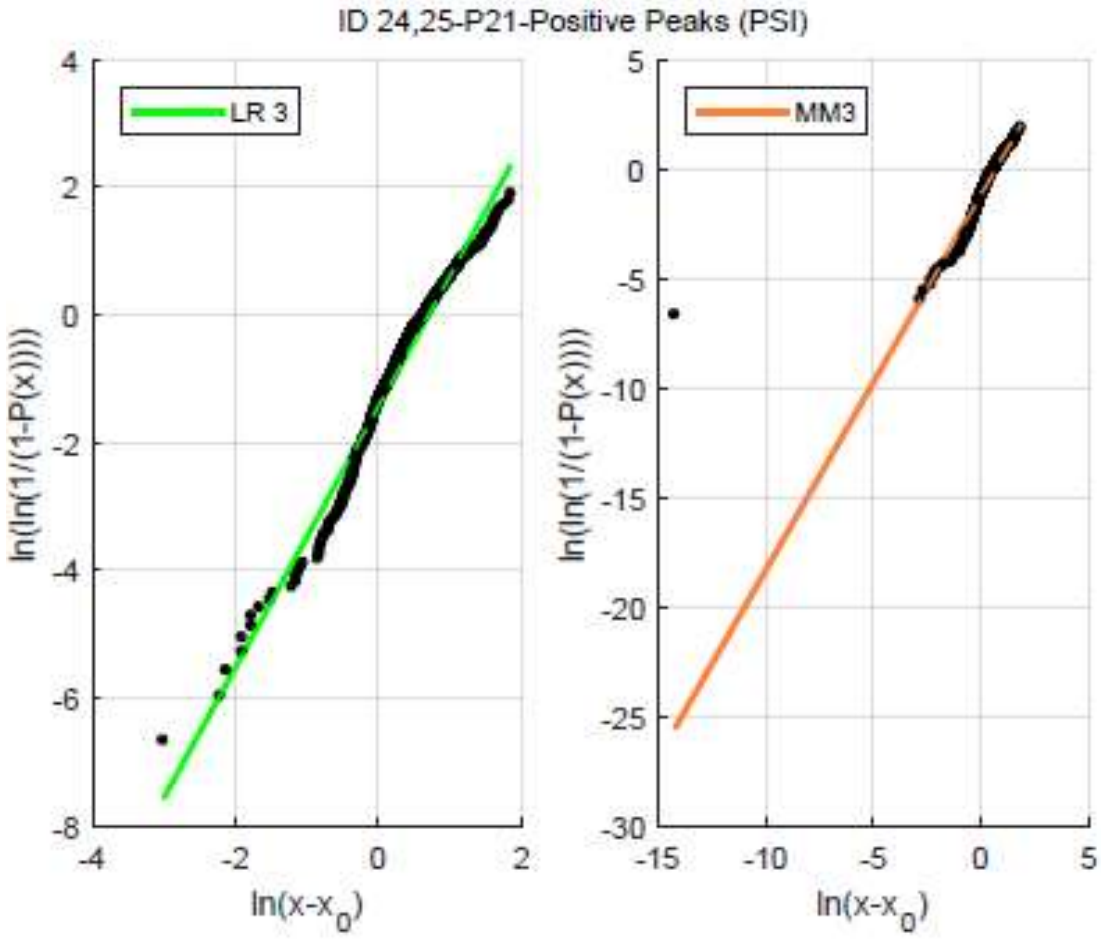

Figure I - 20. LR3 and MM3 Weibull Plots of Channel P21 for Matrix ID 24 and 25

Distribution

SPONSOR	Hard Copies #	Digital Copies #	NSWC, CARDEROCK DIVISION INTERNAL DISTRIBUTION Code	Name	Hard Copies	Digital Copies #
Office of Naval Research Division 331 Dr. Robert Brizzolara Program Officer 875 North Randolph Street Suite 1425 Arlington, VA, 22203		1	809	D. Intolubbe		1
			83	Technical Data Repository		1
			8321	E. Kubina		1
			85	M. Donnelly		1
			852	J. Turner		1
			852	L. Snyder		1
Defense Technical Information Center (DTIC) 8725 John Kingman Road Fort Belvoir, VA 22000-6218		1	852	A. McCoy		1
			852	J. Park		1
			871	M. Jiang		1
			872	E. Harrison		1
			653	S. Nesson		1
			654	T. Wright		1
			656	A. Powers		1
			744	A. Fullerton		1
			1033	TIC-SCRIBE		1


NAVSEA
WARFARE CENTERS
Carderock